Tesis Doctoral

Programa de Doctorado Ingeniería Energética, Química y Ambiental

# Technological challenges of seawater desalination: analysis of future opportunities

Autor: Arturo Buenaventura Pouyfaucon

Directora: Lourdes García Rodríguez

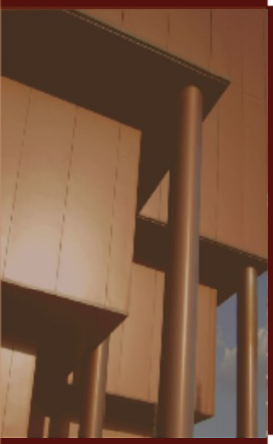

**Departamento de Ingeniería Energética**
**Escuela Técnica Superior de Ingeniería**
**Universidad de Sevilla**

Sevilla, 2018

*Technological challenges of seawater desalination: analysis of future opportunities*

**Table of contents** **Page**

***Technological challenges of seawater desalination: analysis of future opportunities***

# 1. Introduction

Close to 1/3 of the world´s population live in water scarce areas. Over 780 M people are still without access to improved sources of drinking water.

Seawater desalination is part of the solution to these water challenges and has been used now for decades to generate alternative water resources.

In order to make affordable drinking water obtained from seawater desalination, there has been a continuous optimisation of the process looking for more efficient solutions in terms of energy consumption.

In this regard, the use of thermal desalination technologies, such as Multi-Stage Flash distillation (MSF) and Multi-Effect Distillation (MED), has been changed in the last decades to Reverse Osmosis (RO) membrane technology because it requires less energy to desalinate seawater.

However, at the same time there has been a general trend of reviewing all industrial processes under sustainability criteria, that is, looking for more environmental friendly solutions, reducing the energy consumption and $CO_2$ emissions.

In this context, thermal desalination technologies have been considered again because of their conceptual advantage to be coupled with solar thermal energy, thus allowing for solar thermal-powered seawater desalination solutions.

Therefore, assessing the viability of coupling solar thermal energy with seawater thermal desalination technologies has been the first objective of this thesis, analysed in Chapter 1. A key factor in the analysis was the size of the plant, that is, the water production capacity (market opportunities) and the corresponding required power (the size of the solar plant). On top of that, thermal desalination technologies were also compared with reverse osmosis when both coupled with solar thermal-power.

Based on Chapter 1, for coupling with solar thermal energy all thermal desalination technologies where discarded except for very small-capacity seawater desalination systems.

Membrane Distillation (MD) technology may be potentially used in small-capacity systems due to the compactness, ability of dealing with highly concentrated saline solutions and its feasibility for operating at partial and variable loads. Seawater desalination based on MD was then analysed in Chapter 2 considering its current trends and future prospects.

The basic concepts of seawater desalination based on MD have been analysed. The existing MD configurations and pre-commercial and commercial MD systems have been reviewed. The performance of those systems have also been studied based on experimental data from tests performed by independent researchers. Having in mind other existing and well proven technologies, such as MED and RO, potential applications of MD technology in seawater desalination have been assessed. While the limited production capacity could be improved by advanced MD configurations, the low energy efficiency of the process may be a real barrier for MD technology. The most promising application of MD technology seems to be in brine concentration systems.

The use of conventional distillation systems (MED, MSF) have been rejected for seawater desalination (Chapter 1) and MD systems have inherent limitations such as low energy efficiency and small production capacity (Chapter 2). Therefore, RO systems are the reference technology for desalination processes in general and, in particular, when considering its combination with solar thermal power.

Having a deep understanding of RO technology is then important (Chapters 3 and 4) and is the technology in which to focus (Chapter 5) in order to improve seawater desalination. For RO Technology, the minimum theoretical Specific Energy Consumption (SEC) required for solvent extraction from standard seawater salt concentration, at recovery rates of 50% and the absolute minimum theoretical SEC required for recovery rate of 0% that is, obtaining only a drop of product water. Besides that, inefficiencies attributable to the status of membrane technology, to pumping inefficiencies, to plant configurations, etc, are calculated. Finally, the option of adopting innovative configurations reported in the literature is assessed in Chapter 3.

The core of the RO technology is the RO membrane, therefore the RO membrane modules are the key components. The design of SWRO membranes have been improved during the last decades coming to a standard design consisting in a module of typically 8 inches diameter and 1 meter long with spiral wounded flat sheets RO membranes. These RO membrane modules are placed inside a Pressure Vessel (PV) where a number of these modules can be installed in series. There are a number of phenomena, such as water and salt permeabilities, scaling, bio-fouling and concentration polarization that are inherent to the RO technology and to the fact that is based on the flow of the dissolvent through a membrane.

These phenomena depend on the membrane characteristics, module configuration, operating conditions (pressure and temperature) and the system configuration (recovery rate, number of membranes in serial), and have a direct impact on water production, product quality and energy consumption.

A thorough membrane performance model has been implemented (Chapter 4), including effects of pressure losses and concentration polarization at the feed-blowdown channel. This software calculates the water permeability and salts permeability from experimental data. Alternatively, this calculates salt concentration and flow of permeate from given design parameters of a specific membrane module.

Concerning a membrane serial, criteria of selecting the best membrane type for each position in the pressure vessel, depending on their permeability, have been reviewed. Membrane permeability should increase along the serial of membrane elements, having high rejection low energy elements in the first positions. In Canary Islands, two of those elements are enough to comply the required permeate quality. Besides that, the SEC reduces as the length of the series increases. The limiting factor is the product quality.

Finally, chapter 5 deals with a thorough analysis of innovative configurations with high prospects to achieve SEC decreasing. Not only configuration proposed in the literature are analysed, but also a patent pending innovation is proposed.

# Chapter 1. SOLAR THERMAL-POWERED DESALINATION: A VIABLE SOLUTION FOR A POTENTIAL MARKET

This chapter has been published in the international journal *Desalination*, in a special issue on "Desalination using renewable energy" – volume 435 (June, 2018), pp. 60-69 – with the following title, authors and abstract:

Title: *Solar Thermal-Powered Desalination: A Viable Solution for a Potential Market*

**Authors:** Arturo Buenaventura Pouyfaucon[(1)] and Lourdes García-Rodríguez[(2)]

[(1)]Abengoa – Spain. C/ Energía Solar, nº1. 41014- Sevilla. abuenaventura@abengoa.com

[(2)]Dpto. Ingeniería Energética. Universidad de Sevilla. ETSI, Camino de Los Descubrimientos, s/n. 41092-Sevilla. mgarcia17@us.es

**Abstract:**

This paper deals with an assessment of solar thermal-powered desalination technologies in order to identify key issues for developing market opportunities. The topic of selecting the best solar desalination solution is analysed, case by case, considering different scenes: i) Rural communities with limited fresh water demand; ii) Regions with high demands of both, water and electricity and iii) Intermediate water demands. Detailed analyses of solar thermal-driven desalination – i.e. distillation and Reverse Osmosis (RO) - in comparison to solar PV/RO are presented. The quantitative assessment performed highlights that membrane distillation systems, when fully developed, will have market opportunities at very small-capacity seawater desalination systems. Besides that, dish concentrators coupled to micro gas turbines in case of limited water demand is a promising option. A single unit could produce about 10 m3/h of fresh water from seawater and several units could be coupled to drive the same desalination plant. Moreover, the only stand-alone systems with market opportunities for intermediate water production are based on reverse osmosis driven by parabolic troughs or linear Fresnel concentrators by means of organic Rankine Cycles. Finally, water demands over 25,000 $m^3$/d require both, a solar power plant and a reverse osmosis desalination plant.

# 1. INTRODUCTION

This paper deals with an assessment of solar thermal-powered desalination technologies in order to identify key issues for developing market opportunities. Not only to overcome some technical bottlenecks is necessary, but also to point out that energy and water production are concepts that should be considered as a whole.

The topic of selecting the best solar desalination solution is analysed, case by case, considering different scenes:

- Rural communities with limited fresh water demand. Literature reports intensive R&D activities focused on providing fresh water to small rural communities in developing countries. Many low-efficiency systems have been constructed, which integrates the solar thermal conversion and the desalination process in the same device. Nevertheless as plant capacity increases, the use of such devices makes no sense.
- Regions with high demands of both, water and electricity. This kind of systems have been scarcely analysed in the literature. A solar power plant can produce the energy needs of the desalination plant, based on reverse osmosis or any distillation process.
- Intermediate water demands. The solar distillation systems consist of a desalination unit and a solar field, directly connected or coupled by an energy storage system. In case of using a desalination process driven by electricity, a power cycle with relatively small power output is necessary. Several plants have been implemented, normally within the framework of R&D projects.

In the next sections detail analyses of solar thermal-driven desalination – i.e. distillation and Reverse Osmosis (RO) - in comparison to solar PhotoVoltaic (PV) RO are presented. Important aspects such as the energy efficiency and strategies for optimum desalination plant and solar field locations are analysed.

## 2. STATE OF THE ART OF SOLAR DESALINATION TECHNOLOGIES

There are many references in literature that deal with solar desalination as follows: Delyannis [1], Ajona [2], Delyannis and Belessiotis [3], Baltas and Perrakis [4], Subiela *et al* [5], Belessiotis and Delyannis [6-7], García-Rodríguez [8-10], Blanco *et al* [11] and Li *et al* [12].

Some specific designs of solar collectors for seawater desalination applications have been developed. Some of them are described by Rajvanshi [13], Hermann *et al* [14]; Ajona *et al* [15] and Quoilin *et al* [16]. At these days, stationary solar collectors and a wide variety of parabolic troughs are commercially available within the range of temperature suitable for solar desalination [17].

The most common solar thermal-driven desalination systems have been based on Multi-Stage Flash (MSF) distillation, Multi-Effect Distillation (MED) and Membrane Distillation (MD). Other solar desalination technology is Reverse Osmosis (RO) powered by a solar power cycle. Besides that, also freezing [18] and mechanical vapour compression [19] plants driven by solar-thermal power have been implemented.

In addition to conventional desalination technologies, it is remarkable that there are a few designs specifically developed for solar desalination applications:

- *Multi Stage Flash Distillation.* The company ATLANTIS developed an MSF unit referred to as 'Autoflash', which is able to match variable conditions of the heat input. Therefore, this can be coupled to a salinity-gradient solar pond [20].
- *Reverse Osmosis desalination.* Childs *et al* [21] present a system that permits to be connected to solar thermal collectors and a RO plant.

Finally, the direct solar desalination concept, which integrates within the same device the energy conversion and the distillation process, is limited to small-capacity systems. The development of this technology and cost analysis is reported by Tiwari [22], Fath [23] and Goosen *et al* [24], among others. Some other processes limited to small capacity are humidification-dehumidification [25], or the pilot system SMCEC (Solar Multiple Condensation Evaporation Cycle) described by Bacha *et al* [26].

### 2.1. Salinity-gradient solar ponds coupled to distillation plants

Salinity-gradient solar ponds are solar devices that integrate long-term thermal storage. This feature along with their low cost and scale economy make them especially suitable to be coupled to distillation units. This technology was thoroughly studied over the 80´s, attributable to the dominant distillation market of seawater desalination. Some related papers are the following, Bucher [27], Rajvanshi [13] and Tleimat and Howe [28].

Pilot plants consisting in a solar pond coupled to a MSF unit were erected at different places: Margarita de Savoya, Italia - plant capacity: 50-60 $m^3/d$ - [1]; Islands of Cape Verde - Atlantis "Autoflash" 300 $m^3/d$ - [20]; Tunisia, at the Laboratoire of Thermique Industrielle - an MSF prototype of $8.6 \cdot 10^{-3}$ $m^3/h$ and a solar pond of 1500 $m^2$ - [29]; El Paso, Texas - plant capacity: 19 $m^3/d$ - [30]. Besides that, pilot plants based on MED process were also installed. Examples can be found near Dead Sea - 3000 $m^3/d$ - [31] and at the University of Ancona, Italy [32]. The latter consists in a hybrid MED-thermocompressor plant with capacity of 30 $m^3/d$, which uses steam generated by conventional energy for driving thermocompressors.

It is remarkable the aforementioned test facility of El Paso (USA), described by Lu *et al* [33]. The solar pond not only drives thermal desalination processes, but also RO process by means of a low temperature Rankine cycle. Los Baños solar pond is another test facility in which solar RO was tested [34].

### 2.2. Solar distillation processes driven by solar collector fields

The development of experimental plants with capacities up to 100 $m^3/d$ shows the interest focused on the solar MSF technology over the XX century.

- Kuwait - 100 $m^3/d$ (MSF autoregulated); parabolic trough collectors - [1].
- La Paz, Méjico - 10 $m^3/d$; flat plate and parabolic trough collectors - [35].
- Safat, Kuwait - 10 $m^3/d$ - [31].
- Berken, Germany - 10 $m^3/d$ - [36].
- Gran Canaria, Spain - 10 $m^3/d$; low concentration solar collectors - [37].
- Lampedusa Island, Italy – 0.3 $m^3/d$; low concentration solar collectors - [38].
- Al Azhar University in Gaza - 0.2 $m^3/d$ (experimental system MSF with 4-stages); solar thermal collectors and PV-cells to drive the auxiliary equipment – [39].

Regarding the technology development, an important advance was achieved by Mabrouk and Fath [40]. They report on the experimental test campaign conducted with NanoFiltration (NF) pretreatment of the MSF feed, thus resulting in high top temperature and enhanced Performance Ratio (PR – ratio of 2300 kJ/kg and specific thermal consumption -) of 15. Nevertheless, the high auxiliary consumption of MSF process limits the commercial prospects of solar desalination based on MSF technology. It should be noted that NF pretreatment requires additional electric consumption and the use of NF does not reduce the great mass flow rate circulating through the plant. Therefore, auxiliary consumption dramatically increases.

Besides MSF plants, some Multi-Effect Distillation (MED) plants driven by solar collectors were installed at different locations:

- Arabian Gulf – 6,000 $m^3$/d; parabolic trough collectors - [1].
- Abu Dhabi, U.A.E – 120 $m^3$/d; evacuated tube collectors - [41].
- Almería, Spain a 14 effect-MED plant with capacity of 72 $m^3$/d [42] was installed at the solar research centre Plataforma Solar de Almería (PSA). Based on this distillation unit, different solar plants have been installed within the framework of different R&D projects:
    - MED plant driven by steam from a parabolic trough solar field.
    - MED-TC (ThermoCompressors) driven by the steam generated by a parabolic trough solar field.
    - MED plant driven by water heated by means of compound parabolic concentrators.
    - MED coupled to a Double-Effect Absorption Heat Pump (DEAHP) through two auxiliary water tanks. A new parabolic trough collector field and boiler produce the steam required by the DEAHP (saturated at 180ºC). The low temperature heat input of the absorption cycle is the steam generated within the last distillation effect. Besides that, the DEAHP provides the required heat consumption of the MED unit as hot water.
- La Desired Island, French Caribbean – 40 $m^3$/d; evacuated tube collectors - [43].
- Takami Island, Japan – 16 $m^3$/d; flat plate collectors - [1].
- Hzag, Tunisia - 0.1-0.35 $m^3$/d - [31].

Finally, Hanafi [41] reports on a solar distillation hybrid plant - MED-55 stages MSF-75 stages; 500 $m^3$/d - driven by parabolic trough collectors at Al-Ain, U.A.E.

More recently, there have been increasing interest of developing membrane distillation systems [45-52], which are especially suitable for solar desalination. Values of PR about 6 have been obtained [53].

### 2.3. Solar thermal-driven RO

One axis-tracking solar collectors, linear Fresnel concentrators or parabolic troughs are the most efficient technologies to drive an Organic Rankine Cycle (ORC) to produce the energy consumption of a RO system. Nevertheless, other systems have been implemented driven by stationary solar collectors [54-55].

The high costs required to install and operate parabolic trough collectors had resulted in the past years in the inexistence of experimental facilities of desalination. Due to the quite different collectors commercially available, three top temperature ranges are considered in order to assess the efficiencies of the ORC:

- *150ºC-200ºC:* Quoiling *et al* [56] report thermal efficiencies of the ORC of 13.1% for a heat source of 190ºC and working fluid SES36. The corresponding overall efficiency of the solar ORC Is about 8%. Besides that, in the analysis reported, R245fa exhibit slightly low efficiency. Wang *et al* [57] analysed different fluids, obtaining with top temperature 190ºC thermal performance below 15% for the R134a working fluid.
- *300ºC-350ºC:* The maximum value found by the authors in the literature survey is 28.2% [58].
- *350ºC-400ºC:* Values of 29.8-30.5% are the best reported by Maraver *et al* [58] for siloxanes.

### 2.4. Solar thermal energy for water and electricity production

An hybrid MSF-RO system driven by a dual-purpose solar plant was installed at Kuwait [1]. The desalination system consists of a 25 $m^3$/d-MSF plant and a 20 $m^3$/d–RO plant. In regards to analyses of cogeneration plants: Rheinländer and Lippke [59] studied a system coupling a MED plant to a solar tower power plant, and Glueckstern [60] presented a detailed analysis of dual-purpose solar plants. More recently, some thorough analyses are the following, Palenzuela *et al* [61-63].

## 3. SOLAR DESALINATION: THERMAL DESALINATION VS RO. A GLOBAL UNDERSTANDING OF THE ENERGY NEEDS

Solar desalination is an attractive concept since it allows for drinking water to be produced from seawater and brackish water using solar energy. Moreover, regions with water scarcity and water stress are typically arid regions thus with high solar radiation. Everything fits and is aligned with sustainability; therefore the challenge is to produce drinking water with solar desalination at an affordable cost.

The first step and essential is to look for energy efficiency in solar desalination. Thinking in terms of required solar energy units per unit of drinking water produced is the only way to move forward and look for the solar desalination process that requires less energy.

Figure 1.1 shows the energy analysis for different seawater desalination processes from solar thermal energy. Firstly advanced distillation, consisting in a Multieffect Distillation (MED) unit coupled to a Double-Effect Absorption Heat Pump (DEAHP), which exhibits PR of 20 [64-69]. This is equivalent to a specific heat consumption of about 115 kJ/kg. The DEAHP requires one-axis solar concentrators, thus Parabolic Trough Collector (PTC) is the option shown is this figure. Secondly, MED driven by stationary solar collectors - Evacuated Tube Collector (ETC) within a range of thermal performance and Compound Parabolic Concentrator (CPC) – and PTC. Finally, Reverse Osmosis (RO) powered by a solar Organic Rankine Cycle (ORC). The first relevant conclusion is that distillation processes require at least in the order of four times the energy than the RO desalination process, being MED+DEAHP the most efficient among them.

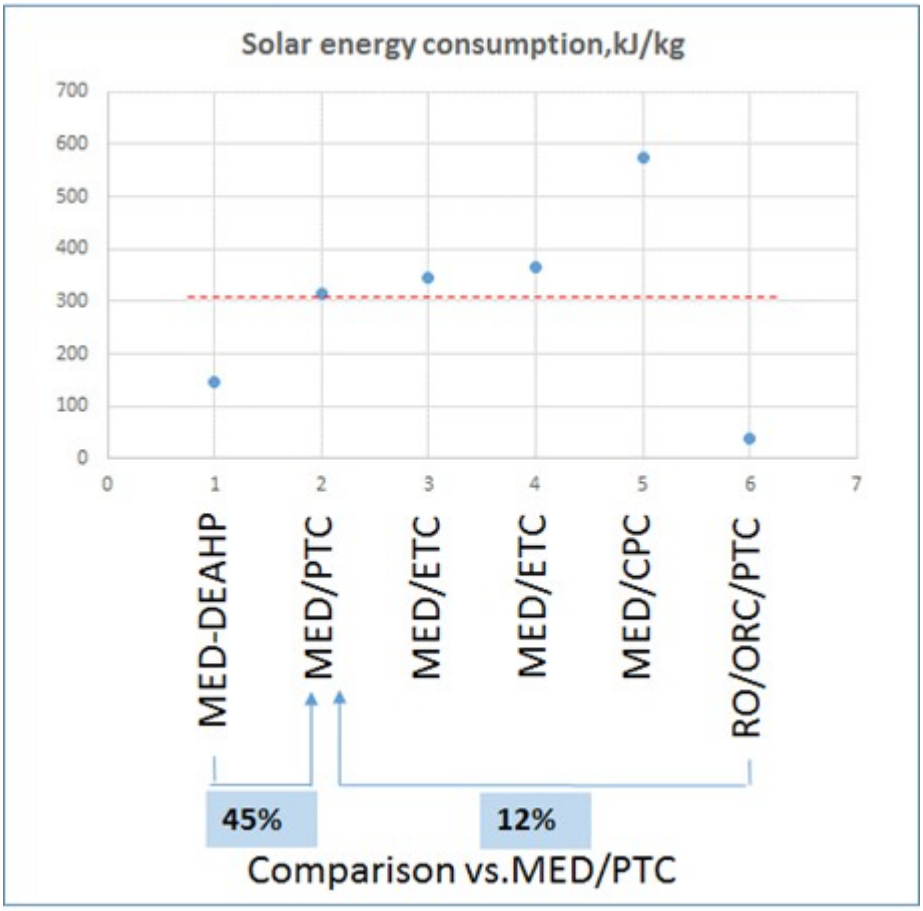


**Figure 1.1. Solar energy consumption of different solar desalination technologies: MED (Multi-Effect Distillation); DEAHP (Double-Effect Absorption Heat Pump); RO (Reverse Osmosis); ORC (Organic Rankine Cycle); PTC (Parabolic Trough Collector); ETC (Evacuated Tube Collector); CPC (Compound Parabolic Concentrator) -.**

RO desalination can be powered by solar photovoltaic and solar thermoelectric energy, being these two concepts of solar desalination the most efficient ones by far. In both concepts the efficiency of the solar collectors is less determining than in the case of the solar thermal desalination. Figure 1.2 shows the influence of solar thermal conversion on the solar energy required to produce a mass unit of fresh water from seawater. Values of OX-axis correspond to different solar thermal conversion systems namely, from salinity-gradient Solar Ponds (SP), Flat Plate Collectors (FPC), Compound Parabolic Concentrators (CPC), Evacuated Tube Collectors (ETC) and Parabolic Trough Collectors (PTC). Only MED and RO processes are included in the analysis, since other distillation processes, MSF and MD, are less efficient than MED. In this figure, some aspects can be analysed:

- The MED technology exhibits the highest energy consumption (PR= 10). The corresponding curve – on the top – shows the high influence on the required energy

of the solar thermal technology that could be used: solar ponds, stationary collectors (FPC and ETC), and PTC within a representative range of performance for this technology.

- The MED-DEAHP technology (PR= 20) results in solar energy requirement equivalent to solar ORC-RO in which the thermal performance of the ORC is 7% (this is a low value since even with stationary solar collectors higher performance of the ORC can be achieved). On the curve MED-DEAHP the range corresponding to PTC is marked.
- A set of curves represents the solar ORC-RO desalination with different values of thermal performance of the ORC: 10%, 15%, 20% and 25%. The required top temperature increases with the cycle performance. Therefore, solar pond and stationary solar collectors would be suitable with cycle performance as low as 10%. Thorough analyses of RO driven by solar ORC have been reported in the literature [70-80]. In this case, the specific energy consumption is obtained by multiplying the performances of the solar collector and that of the organic Rankine cycle.
- As a reference value for comparison to competitor technology, PV-RO, an horizontal black line is included in the figure considering energy efficiency of 14% for the solar photovoltaic conversion. In these days, efficiencies of PV conversion around 20% can be achieved. Efficiency values depend on the cost of the selected commercial product.

Figure 1.2 shows that PV/RO exhibits the lowest solar energy needs versus solar ORC/RO and solar distillation.

In addition, a comparison between RO driven by solar power plants and distillation is necessary. Moreover, in order to assess potential future prospects of a given technology, the influence of the historical evolution of main energy consumption of SeaWater Reverse Osmosis (SWRO) desalination should be analysed. Past evolution from 7 kWh/m$^3$ up to about 2 kWh/m$^3$ and future values, which might be lower. Then, a complementary analysis is presented in which solar-thermal RO systems are compared to the best solar distillation technology, MED-DEAHP (PR= 20).

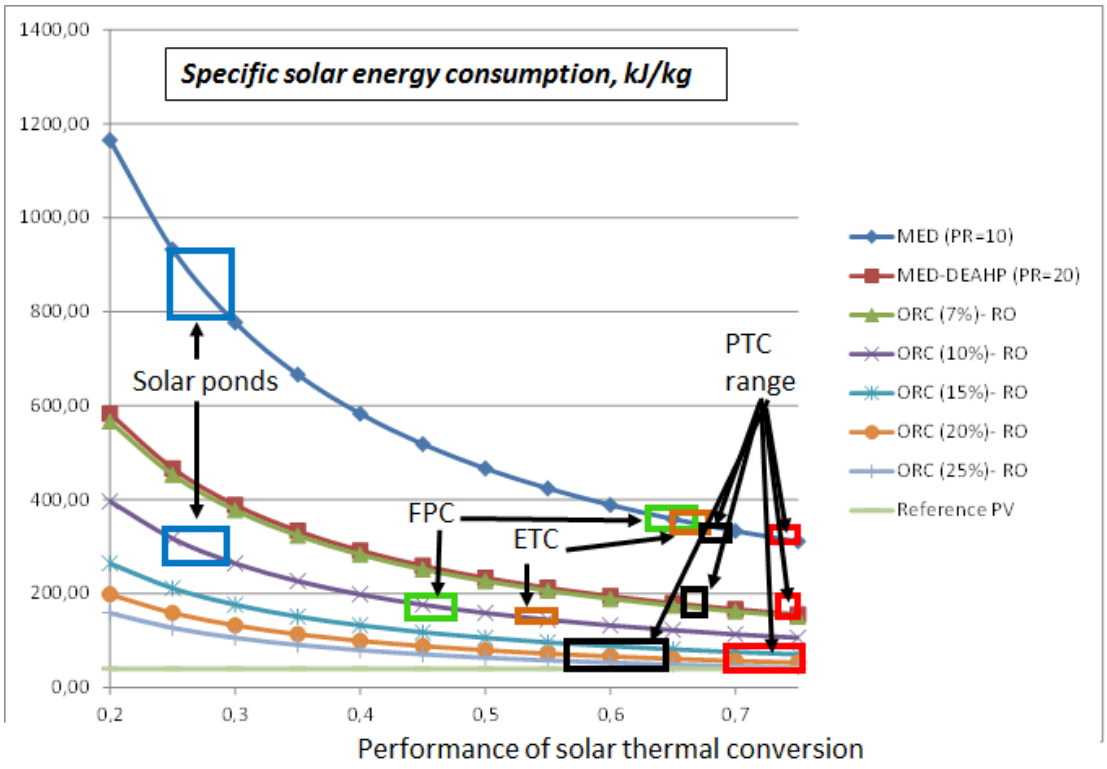


**Figure 1.2. Solar energy required for unit of fresh water production, in kJ/kg, vs solar thermal conversion efficiency - MED (Multi-Effect Distillation); DEAHP (Double-Effect Absorption Heat Pump); RO (Reverse Osmosis); ORC (Organic Rankine Cycle); PTC (Parabolic Trough Collector); ETC (Evacuated Tube Collector); CPC (Compound Parabolic Concentrator) -.**

As an example, with 115 kJ of solar energy consumed, a MED-DEAHP would produce 1 kg of fresh water. The corresponding production by means of solar SWRO depends on the performance of the solar collectors and the specific features of the Rankine cycle used. In figure 1.3, for a given unit of solar energy consumed, the ratio of production of SWRO and MED-DEAHP (PR=20) processes is shown. Reasonable ranges of thermal performance of the Rankine cycles are selected, between 10% and 25% for ORC, and 31-37% for conventional solar power

plants based on PTC. Figure 3 proves that solar-thermal RO desalination is superior versus distillation driven by solar thermal collectors.

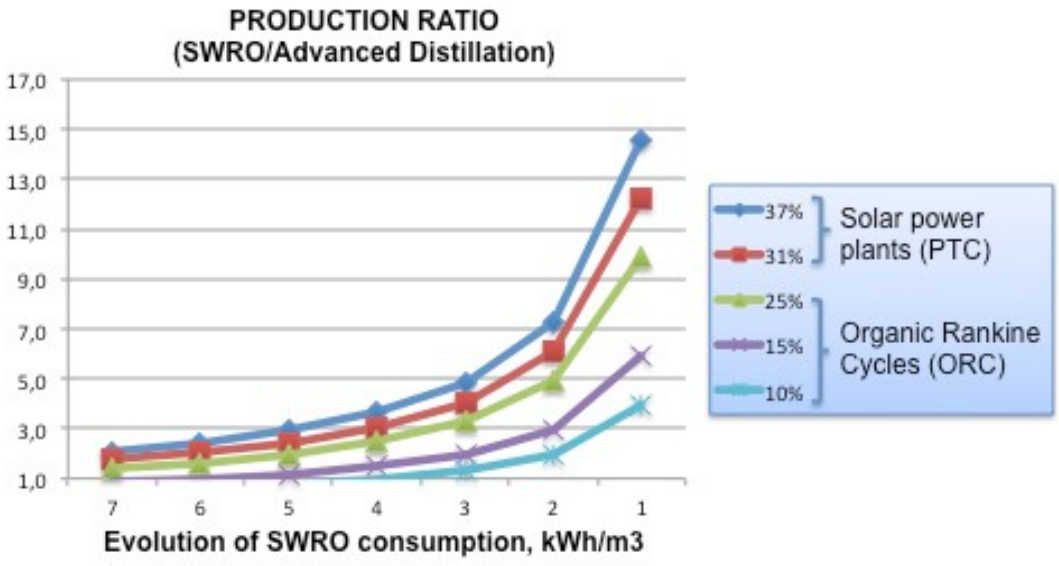


**Figure 1.3. Comparison between SWRO desalination and the most efficient distillation as a function of SWRO energy consumption, historical evolution and potential future. For a given value of solar energy consumed, OY-axis shows the ratio of water production by SWRO and distillation based on MED-DEAHP.**

## 4. COMPETITOR TECHNOLOGY: SOLAR PV DESALINATION

The photovoltaic technology connected to a RO system is commercial since the 90´s. As an example, the Canary Islands Technological Institute (ITC, Spain) developed a stand-alone system (DESSOL® [81]), available up to 100 $m^3$/d of nominal capacity. The PV energy could compete with conventional energy in specific cases due to long distance to the electric grid.

RO systems powered by PV field normally include batteries. Besides that, it is remarkable research conducted by the Instituto Tecnológico de Canarias (ITC) on gradual capacity systems [82-83], applicable to PV and wind-powered RO, and by Thomson and Infield [84]. In order to validate the developed model and control, they simulate and implement a PV-driven RO system with variable flow without batteries. The system consists of a 3 $m^3$/d RO unit and a PV array of 2.4 kWp.

Besides that, the most suitable solar technology for brackish water desalination at the smallest scale of fresh water demand is solar PV electrodialysis (ED). An example of a small-capacity plant is described by Adiga *et al* [85]. This was installed at Thar dessert, India, consisting in a 0.120 $m^3$/h brackish water desalination unit based on ED and a 450 Wp PV field.

Several pilot plants of ED systems connected to photovoltaic cells by means of batteries have been implemented. Moreover, this kind of plants could be even operated in batches, thus permitting a simple operation without batteries. This is an important advantage in comparison to brackish water RO in case of small fresh water demands. As water demand increases, brackish water composition as much as capital and O&M costs are the main parameters to assess for an adequate selection of the desalination technology. In addition, in remote areas maintenance requirements and chemical supply should be taking into account at the first stage of process selection. Some of the earlier PV-ED systems reported in the literature were installed at Ohsima island, Nagasaki [86]; the Spencer Valley, near Gallup (New Mexico) [87], and Fukue city, Nagasaki (8.33 $m^3$/h, brackish water) [88]. Besides that, it is also remarkable experimental research in PV-ED performed at Laboratory for Water Research, University of Miami - Miami, FL U.S.A. [89]. Finally, Husseiny and Hamester [90] report an hybrid RO-ED system with capacity of 6.000 $m^3$/d in which the ED unit is driven by a PV field and the RO system is powered by solar thermal energy by means of a Rankine cycle.

Finally, it should be highlighted that if wind resources are exploitable at the plant location, wind-powered RO is the best option [91].

# 5. VIABLE SOLUTIONS FOR A POTENTIAL MARKET

## 5.1. Scene of small water demands

The scene of small water demands is the best application of renewable energy-powered desalination, since the high investment required is not so big and an electric grid is frequently not available near the water demand. Plant capacities of up to 100 $m^3$/d are considered in this case, thus the simplicity of the system is a requirement. Therefore, the use of solar thermal energy is limited to stationary solar collectors: flat plate or compound parabolic concentrators. Given the corresponding values of solar energy consumption shown in figure 1.2, solar ORC/RO and conventional distillation processes (MED and MSF) are rejected in comparison to PV-RO.

Table 1.1 shows some PV-RO systems implemented over the XX century, thus showing the maturity of this technology. In these days, control and energy storage in such systems have achieved significant development [92-96].

With regard to operational problems, needs of chemicals supply, spare parts and skill workers for maintenance may be the most important problems of PV-RO. PV-ED should be also considered in case of brackish water with low salt concentration. Besides that, due to the intermittent energy supply, ED systems are interesting since they are able to operate in batches [97-98]. Only in case of seawater desalination, other candidate technology is MD. In spite of the low energy efficiency, a significant advantage might be that MD is able to operate with high-salinity brines up to saturation, thus resulting in a possible economic activity based on obtaining salts with high economic value. Stand-alone solar systems are suitable to this capacity range.

**Table.1.1. A few reverse osmosis plants driven by photovoltaic systems [10].**

| Plant location | Salt concentration | Plant capacity | PV system |
|---|---|---|---|
| Cituis West, Jawa, Indonesia[31] | Brackish water | 1.5 $m^3$/h | 25 kWp |
| Concepción del Oro, Mexico[2] | Brackish water | 1.5 $m^3$/d | 2.5 kW peak |
| Doha, Qatar [31] | Sea water | 5.7 $m^3$/d | 11.2 kWp |
| Eritrea[84] | - | 3 $m^3$/d | 2.4 kWp |
| Florida St. Lucie Inlet State Park, USA[31] | Sea water | 2x0.3 $m^3$/d | 2.7 kWp + diesel generator |
| Hassi-Khebi, Argelie [31,99] | Brackish water (3.2 g/l) | 0.95 $m^3$/h | 2.59 kWp |
| Heelat ar Rakah camp of Ministry of Water Resources, Oman[100] | Brackish water | 5 $m^3$/d (5 h/d operation) | 3250 kWp |
| INETI, Lisboa, Portugal[101] | brackish water about 5000 ppm. | 0.1-0.5 $m^3$/día | - |
| Jeddah, Saudi Arabia [31,1] | 42800 ppm. | 3.2 $m^3$/d | 8 kW peak |
| Lampedusa island, Italy[31] | Sea water | 3+2 $m^3$/h | 100 kWp |
| Lipari island, Italy[31] | Sea water | 2 $m^3$/h | 63 kWp |
| North of Jawa, Indonesia[1] | Brackish water | 12 $m^3$/d | 25.5 kW peak |
| North west of Sicily, Italy[31] | Sea water | - | 9.8 kWp + 30 kW diesel generator |
| Perth, Australia[31] | Brackish water | 0.5-0.1 $m^3$/h | 1.2 kWp |
| Pozo Izquierdo- ITC, Gran Canaria, Spain[102] | Sea water | 3 $m^3$/d | 4.8 kWp |
| Red Sea, Egypt [31,87] | Brackish water (4.4 g/l) | 50 $m^3$/d | 19.84 kW peak (pump) +0.64 kW peak (control) |
| Thar desert, India [31] | Brackish water | 1 $m^3$/d | 0.45 kWp |
| University of Almería, Almería, Spain[31] | Brackish water | 2.5 $m^3$/h | 23.5 kWp |
| Vancouver, Canada[31] | Sea water | 0.5-1 $m^3$/d | 4.8 kWp |
| Wanoo Roadhouse, Australia[31] | Brackish water | - | 6 kWp |

### 5.2. Scene of large fresh water demand: Concept of solar thermal energy for water and electricity production

Large capacity systems within the framework of renewable energy-powered desalination could be from around 25,000 $m^3$/d. Such water demands may require energy consumptions within the range of solar power plants. Due to scale economy, the oversize of the solar power plants in order to produce both, water and electricity is a key issue in market opportunities. Within this framework, regional and national authorities are the decision makers since the potential market is based on the global understanding of water and power supply as a whole.

To run a RO desalination plant with concentrated solar power (CSP) two possible concepts are considered, parabolic through collectors (PTC) and tower. In both concepts only areas with high solar radiation (>1800 kWh/$m^2$) are suitable, however an important surface is required for the solar field, being this requirement even larger for PTC concept. In the tower concept the effect of a reduction in the solar radiation will affect more the efficiency of the solar plant because of the distance from the mirrors to the solar receiver. Therefore, in both concepts placing the solar plant near the coast will result in an efficiency reduction due to the high level of humidity in the ambient.

The RO seawater desalination plants are typically placed by the sea, to reduce the energy costs of transporting the seawater to the desalination plant. Therefore the optimum location for a desalination plant is different than the optimum one for the corresponding solar power plant, being the solution to connect both from the electrical point of view, through a dedicated power line or connecting both to the electrical grid. Therefore, potential synergies of having both plants in the same location, such as using seawater cooling for the solar plant allowing preheating of the seawater for the desalination plant or using water produced from the desalination plant for the power cycle makeup water, are abandoned.

The solar power plant will operate during the day or during an extended period of time if energy storage is considered. However, these storage systems require significant CAPital EXpenses (CAPEX) and OPEration EXpenses (OPEX) that may be justified in solar power plants that are part of the power generation system and the grid.

When thinking in a RO plant powered by a solar plant, the power demand is then defined by the desalination plant. Desalination plants are typically designed to operate at 100% capacity 24 h a day and trying to maximize the plant availability in order to reduce the cost per $m^3$ of product water. Therefore the discontinuous energy production profile of a solar power plant does

not match the 24 h a day steady state optimum operation of a desalination plant. At this point a decision regarding the concept of solar desalination needs to be made.

Being straight forward, the optimum solar desalination concept is that for which the cost of the $m^3$ of desalinated water is the lowest considering both CAPEX and OPEX. This can only be possible by optimising the solar power plant and the desalination plant CAPEX and OPEX. Therefore, the optimum solar desalination concept requires that the desalination plant is by the sea, the solar power plant is located where the solar radiation is as higher as possible and both connected through the grid. The solar power plant is then dimensioned – at least - to produce accumulated in a year the required energy that the desalination plant will consume in that year based in a steady state 24 h operation. The water consumption of the solar power plant should be guarantee by the availability of surface or undergroud water, rainwater storage or even transport.

Other related concept is the distributed water production, which is inherent to the management of water supply. Sometimes the population is distributed along the coast with a pattern and orography that makes the most suitable option to implement two different desalination plants instead of one. In addition, note that sometimes the best location of the new RO plant will be next to the existing conventional power production plant.

To sum up, the integrated production of water and electricity based on solar power plant has no advantages. Therefore, this integrated production is only recommended to supply the water demand directly associated to the solar power plant equipment and staff. In this case, part of the demand requires fresh water with TDS in the order of ppb. The recommended option is SWRO to produce permeate with enough quality to human consumption. In addition, processes capable to provide permeate with TDS in the order of ppb as electrodialysis and electrodeionization, should be used as a treatment of SWRO permeate.

### 5.3. Scene of intermediate water demand

When the water demand is derived from an industrial activity near the sea, the desalination system could be integrated to the solar system but enough land area is required. In this case there will be market opportunities for the following options:

- Dish-Stirling concentrators to drive the RO plant. Although high maintenance of Stirling engines is a drawback.

- Dish concentrators coupled to micro gas turbines. A prototype with electricity production of 10 kW has been installed in the Italian research centre ENEA [103]. An adequate range for this developing technology is about 10-30 kWe, so up to about 10 $m^3$/h could be produced by a single unit. Besides, several solar micro gas turbines could work in parallel to drive a RO plant. No studies related to desalination have been conducted so far.
- Lineal Fresnel concentrators or parabolic troughs to drive a RO plant by means of an ORC. There are no technical limitations for the commercial development of this technology, except the availability of reliable commercial products of ORC within a wide range of power output. Turboden products of 1 MW for solar power production exhibit high efficiency with the only limitations attributable to organic fluids. In these days, the use of innovative thermal storages could promote the market development of such a technology.

The competitor solar technology is the PV-RO. Depending of the demand curve, the fresh water storage can minimize the use of batteries.

The final decision should be based on the CAPEX and OPEX of a specific project as well as the land availability and orography. These four technologies do not permit the continuous operation of the desalination plant, thus resulting in oversizing the RO plant to achieve a given water demand. Moreover, in order to expand the daily operation hours of the desalination plant, also the solar thermal or PV field must be oversized.

For solar thermal energy, in comparison to solar desalination plants with conventional energy backup, about double size of the solar field and double plant capacity is required for about 12 h/d of plant operation. Therefore, the design of the desalination plant based on stand-alone concept results in significant increase of capital cost. Moreover, operation and maintenance are also increased due to the discontinuous operation of the desalination plant.

Stand-alone solar desalination plants within this range of water demand are not recommended due to aforementioned reasons. The recommended design selection is the continuous operation of the desalination plant as combination of three operation modes:

- Mode 1: Desalination plant at its nominal working conditions driven by either, thermal or PV solar system.
- Mode 2: Desalination plant operated out of its nominal conditions (part load). This mode requires a specific modified design. Different concepts have been

developed in order to match the desalination plant consumption and the electricity production – see section 4 -.

- Mode 3: Plant operated at nominal conditions connected to the grid when mode 1 is not possible and mode 2 is not recommended.

In the case of the convenience of using mode 3 only over specific hours, the option of either, plant shut-down or using enough energy storage should be compared.

Note that the relatively low performance of the ORC makes the option of using a conventional gas fire-boiler rejected. The bottleneck of this technology is the availability of inexpensive and high capacity thermal storage in order to develop stand-alone desalination systems. Concerning solar micro gas turbines, they are able to be operated with fossil fuels, but this option is only recommended in cloudy days.

# 6. CANDIDATE TECHNOLOGIES FOR POTENTIAL MARKET

In order to assess candidate technologies for potential market of solar thermal desalination, analyses of CAPital EXpenses (CAPEX) are essential. Global comparison of solar technologies are normally based on design points. This approach is adopted in this section.

In addition to points discussed in sections 4 and 5, table 1.2 shows a comparative estimation of capital cost based on design point - 800 $W/m^2$ with incidence angle 0º - of the parabolic trough solar field. Since the curve of the thermal production of parabolic troughs is quite flat in clear days except at sunrise and sunset, the solar field size is set at the design point as that required to drive the desalination plant working at its nominal conditions. This assumption has only the purpose of easily comparing the different solar desalination technologies considered. Note that normally the solar field of a stand-alone system is significantly oversized in order to expand operational hours.

Table 1.2 compares PV/SWRO with the following solar desalination technologies driven by Parabolic Trough Collectors (PTC): ORC/SWRO, MED, MED-DEAHP and MD. Regarding MD process, it is not fully developed, so table 1.2 considers theoretical achievable values of PR and CAPEX. A PR around 9 and CAPEX around 800-1400 €/($m^3$/d) might be achieved in the near future.

**Table 1.2. Estimations of capital cost range for solar seawater desalination based on parabolic troughs in comparison to PV-RO at design point.Case study: seawater RO plant (2,500 $m^3$/d nominal, total energy consumption: 3 kWh/$m^3$ - 0.3 MW -).**

| Main items | PTC/Organic Rankine Cycle (ORC)/SWRO | | PTC/multi-effect distillation (MED) | | Hypohetical advanced membrane distillation | PV/ SWRO |
|---|---|---|---|---|---|---|
| | ORC (siloxanes) | ORC: cascade | MED/ DEAHP | MED | | |
| Main energy requirement | 210.9 kWe (High Presure and BOoster Pumps, HPP+BOP) | | 3,328 kWt (PR=20) | 6,655 kWt (PR=10) | 7,395-8,319 kWt (PR=9-8) | 210.9 kWe (HPP+BOP) |
| Feed water required (1) | 260 $m^3$/h (recovery rate 40%) | | | | | |
| Seawater cooling | 0 | 0 | 0 | 342 $m^3$/h | 375-455 $m^3$/h | 0 |
| Feed water pumping (2) | 88.4 kW | | | | | |
| Cooling water pumping | 0 | 0 | 0 | 116 kW | 216-243 kW | 0 |
| Minimum aperture area at design point (3) | 1,567 $m^2$ | 2,387 $m^2$ | 5,737 $m^2$ | 11,320 $m^2$ | 12,580 $m^2$ - 14,150 $m^2$ | 4,774 $m^2$ |
| Corresponding range of capital cost (300-500 €/$m^2$) | 0.47-0.78M€ | 0.72-1.2 M€ | 1.7-2.9 M€ | 3.4-5.7 M€ | 3.8-6.3 M€ 4.2-7.1 M€ | 0.7-1.3 M€ (1-2 €/Wp) |
| Other main items | ORC | | Boiler-DEAHP | Boiler | Heat exchanger | None |
| Estimated capital cost | 0.21-0.63 M€ | | n.a. | Negligible | Negligible | 0 |
| Estimated range of capital cost of distillation 1.000-1.400 €/($m^3$/d) | n.a. | | 2.5-3.5 M€ (Tentative for MD when fully developed) | | | n.a. |
| Estimated range of capital cost SWRO: 800-1.200 €/($m^3$/d) | 2-3 M€ | | n.a. | | | 2-3 M€ |
| Total capital cost | 2.7-4.4 M€ | 2.9-4.8 M€ | > 4.2-6.4 M€ | 5.9-9.2 M€ | 6.2-9.8 M€/ 6.7-10 M€ | 2.7-4.3 M€ |
| Specific capital cost, k€/($m^3$/d) | 1.07-1.77 | 1.17-1.93 | >1.69-2.55 | 2.36-3.66 | 2.5-3.9/2.7-4.0 | 1.07-1.72 |
| Production per unit of aperture area, L/($m^2$·h) | 66.5 | 43.6 | 18.2 | 9.2 | 8.3/7.4 | 21.8 |
| Specific auxiliary energy, kWhe/$m^3$ | 0.85 | 0.85 | 0.85 | 2.0 | 2.1-2.3 | 0.85 |

(1) Recovery rate is assumed to be 40% to make easier the technology comparison
(2) Selected for this case study (3) Auxiliary energy attributable to control, pretreatment, vacuum (only MED plants), etc. is not considered.

As table 1.2 shows, MD exhibits the highest CAPEX. However, MD is suitable for discontinuous operation, which is a significant advantage. Therefore, it could be useful for stand-alone plants with small capacity. In this case, both, the nominal plant capacity and the solar field should be oversized and thermal storage should be included in order to extend the plant operation.

Besides, conventional MED process or coupled to DEAHP exhibit CAPEX much higher than both, solar ORC/SWRO and PV/SWRO. Besides that, in these days the continuous operation without conventional energy backup is not reasonable by using parabolic troughs. In addition, SWRO is superior to conventional distillation processes in relation to discontinuous operation. Then, MED and MED-DEAHP are rejected. Moreover, the direct use of fossil fuels as backup of distillation processes makes no sense due to their high energy consumption.

To sum up, solar ORC/SWRO and PV/SWRO are the best technologies.

Finally, table 1.3 summarises the selection of candidate solar thermal-powered desalination and competitor technologies.

**Table 1.3. Proposed technology selection for different scenes.**

| **End user** | **Water demand ($m^3/d$)** | **Tentative range of electricity demand (MW)** | **Candidate technologies for solar production** | **Candidate technologies for water production** (Estimation of energy consumption of seawater desalination) |
|---|---|---|---|---|
| Rural communities | <100 | 0 | PV, stationary solar thermal fields | RO, ED, MD |
| | <1,000 | 0 | PV, solar ORC (linear Fresnel concentrators or PTC), Dish/micro gas turbines | RO (0.13 MW), ED |
| Local authorities and companies with industrial activities | 5,000-20,000 | 0 | PV, PTC-solar ORC, Dish/Stirling | RO (0.63-2.5 MW) |
| Regional/ National authorities | > 25,000 | >10 | PV | RO (>3.1 MW) |
| | | >20 | Power plants (Solar tower or PTC) | |
| | | >50 | Power plant (PTC) | |

# 7. CONCLUSIONS

The main conclusions with regard to viable solutions for a potential market of solar thermal-powered desalination are the following:

- Membrane distillation systems, when fully developed, will have market opportunities at very small-capacity seawater desalination systems. The main drawback is the cooling requirements as any other distillation technology. Otherwise, low recovery rate is obtained.
- Conventional distillation processes for seawater desalination, namely multi-effect distillation and multi-stage flash distillation, exhibit too high solar energy consumption to compete with solar thermal-driven reverse osmosis. Moreover, discontinuous operation is not suitable for such technologies. Therefore, the use of conventional distillation processes is rejected in all cases, in particular when integrated into the thermal-cycle of a conventional solar power plant.
- For market opportunities up to about 20.000 $m^3$/d, the only stand-alone solar thermal-powered desalination systems that may be considered are based on reverse osmosis driven by either:
    - Parabolic troughs or linear Fresnel concentrators by means of organic Rankine Cycles.
    - Dish concentrators coupled to micro gas turbines in case of limited water demand. A single unit could produce about 10 $m^3$/h of fresh water from seawater. Besides, several units could be coupled to drive the same desalination plant.

  The main advantage of first option in comparison to stand-alone PV-RO desalination is the possible use of thermal storage instead of batteries. Fire-boilers are not recommended as energy backup for solar organic Rankine Cycles due to the relatively low efficiency. Besides that, solar micro gas turbines have the advantage of the availability of heat rejection, which allow the Zero Liquid Discharge (ZLD) concept. Finally, they can be powered at night with conventional fossil if necessary. Anyhow, for stand-alone desalination systems with energy backup, PV-RO desalination would always be more competitive than solar thermal-powered desalination systems.
- Higher water demands require a large scale solar power plant and a reverse osmosis desalination plant. The concept of finding a global balance between consumption of electricity by the water production facility and the solar electricity generation is recommended, instead of the traditional concept of integrating both processes within the same plant. Besides that, the solar power plant technology, location and production should be adapted to the convenience of CAPEX and OPEX. In addition, distributed fresh water

production could also be considered if orography and distance between water demand locations make it necessary.

## 8. REFERENCES


1. Delyannis, E. E., (1987), *Status of Solar Assisted Desalination: a Review.* Desalination 67, 3-19.

2. Ajona, J. I., (1991), *Desalination with thermal Solar Systems: Technology Assessment and Perspectives.* Instituto de Energías Renovables CIEMAT. Madrid.

3. Delyannis, E. y Belessiotis, V. A Historical Overview of Renewable Energies. *Mediterranean Conference on Renewable Energy Sources for Water Production*. European Commission, EURORED Network, CRES; EDS. Santorini, Grecia, 10-12 de junio de 1996. pp. 3-19.

4. Baltas P., Perrakis K., y Tzen E. *Proceedings of Mediterranean Conference on Renewable Energy Sources for Water Production*. European Commission, EURORED Network, CRES; EDS. Santorini, Greece, 10-12 June 1996, pp. 31-35.

5. Subiela, V. J.; de la Fuente, J. A.; Piernavieja, G., and Peñate, B. *Canary Islands Institute of Technology (ITC) experiences in desalination with renewable energies (1996-2008).* Desalination and Water Treatment, 7, 2009, pp. 220-235.

6. Belessiotis, V., and Delyannis, E., (2001), *Water shortage and renewable energies (RE) desalination – possible technological applications.* Desalination, 139, pp.133-138.

7. Belessiotis, V., and Delyannis, E., (2000), *The story of renewable energies for water desalination*. Desalination, 128, 147-159.

8. García-Rodríguez, L. Assessment of most promising development in solar desalination. *En: Solar Desalination for the 21st Century*. Eds: Luzzio Rizzuti y Hisham Ettouney. Springer, 2007, pp. 355- 369. ISBN: 978-1-4020-5506-5.

9. García-Rodríguez, L. *Renewable energy applications in desalination. State of the Art.* Solar Energy, 2003, 75, pp. 381- 393.

10. García-Rodríguez, L., *Seawater Desalination Driven by Renewable Energies, a review.* Desalination, 143(2), 2002, pp. 103-113.

11. Blanco, J.; Malato, S.; , Fernández-Ibañez, P.; Alarcón, D.; Gernjak, W., and Maldonado, M. I.. *Review of feasible solar energy applications to water processes*. Renewable and Sustainable Energy Reviews, 13 (6-7), 2009, pp. 1437-1445.

12. Li, C.; Goswami, Y., and Stefanakos, E., *Solar assisted sea water desalination: A review.* Renewable and Sustainable Energy Reviews, 19, 2013, pp. 136-163.

13. Rajvanshi, A. K., (1980), *A scheme for large scale desalination of sea water by solar energy.* Solar Energy, 24, 551-560.

14. Rommel, M., Köhl, M., Graf, W.; Wellens, C.; Brucker, F.; Lustig, K., and Bahr, P., (1997), *Corrosion-free collectors with selectively coated plastic absorbers,* Desalination, 109(2), 149-155.

15. Ajona, J. I., (1992), *ACE-20 spanish parabolic trough collector.* In: Proceedings of the 6thInternational Symposium on Solar Thermal Concentrating Technologies. Vol, I, September, 28- October-2, 1992. CIEMAT. Ministerio de Industria y Energía, Madrid.

16. Quoilin, S.; Orosz, M.; Hemond, H., Lemort, V., (2011). *Performance and design optimization of a low-cost solar Organic Rankine Cycle for remote power generation.* Energy, 85, p. 955-966.

17. Fernández-García, A.; Zarza, E.; Valenzuela, L., and Pérez, M. *Parabolic-trough solar collectors and their applications*. Renewable and Sustainable Energy Reviews, 14 (7), 2010, p. 1695-1721.

18. Luft W., *Five Solar-Energy Desalination Systems.* Int. J. Solar Energy, 1, 1982, pp.21-32.

19. Rodríguez-Gironés M.A., Rodríguez M., Pérez, J. y Veza J. (1996) Proceedings of the Mediterranean Conference on Renewable Energy Sources for Water Production. European Commission, EURORED Network, CRES; EDS. Santorini, Grecia, 10-12 de junio de 1996. pp. 20-25.

20. Szacsvay, T.; Hofer-Noser, P.; y Posnansky, M., *Technical and economic aspects of small-scale solar-pond-powered seawater desalination systems.* Desalination, 122, 1999, pp. 185-193.

21. Childs, W. D., Dabiri,A.E., Al-Hinai, H. A., and Abdullah,H.A., (1999), *VARI-RO solar-powered desalting technology,* Desalination, 125, 155-166.

22. Tiwari, G. N.; Singh, H. N., y Tripathi, R. *Present status of solar distillation*. Solar Energy, 75, 2003, pp. 367-373.

23. Fath, E. S. H.; *Solar distillation: a promising alternative for water provision with free energy, simple technology and a clean environment*. Desalination, 116, 1998, pp. 45-56.

24. Goosen, M. F. A.; Sablani, S. S.; Shayya, W. H.; Paton, C., and Al-Hinai, H., (2000), Thermodynamic and economic considerations in solar desalination. Desalination, 129, 63-89.

25. Rommel, M.;,Hermann, M., and Koschikowski, J., (2000), The SODESA project: development of solar collectors with corrosion-free absorbers and first results of the desalination pilot plant. *Mediterranean Conference on Policies and Strategies for Desalination and Renewable Energies, 21-23 June 2000, Santorini Island, Greece.*

26. Bacha,H. B.; Maalej, A. Y.; Dhia, H. B.; Ulber, I.; Uchtmann, H., (1999), Martin Engelhardt and Jürgen Krelle, *Perspectives of solar-powered desalination with the "SMCEC" technique,* Desalination, 122(2-3) 177-183.

27. Bucher, W. (1998) Renewable Energy Sources and Seawater Desalination- an Assessment of Methods and Potential. In ASRE 89, International Conference on Applications of Solar & Renewable Energy. March 19-22, 1998, Cairo.

28. Tleimat, M. C.; and Howe, E. D., (1989), *Use of energy from salt-gradient solar ponds for reclamation of agricultural drainage water in California: analysis and cost prediction*, Solar Energy, 42 (4), 339-349.

29. Safi, M. J., *Performance of a flash desalination unit intended to be coupled to a solar pond.* Renewable Energy, 14(1-4), 1998, pp. 339-343.

30. Lu, H., Walton, J.C., and Swift, A. H. P., (2000), *Zero discharge desalination.* The Int. Desalination and water Reuse Quarterly, 10/3, 35-43.

31. European Commision. *Desalination Guide Using Renewable Energies*, 1998.

32. Caruso, G., and Naviglio, A., *A desalination plant using solar heat as heat supply, not affecting the environment with chemicals.* Desalination, 122, 1999, pp. 225-234.

33. Lu, H.; Walton, J. C., y Swift, A. H.P. *Desalination coupled with salinity-gradient solar ponds.* Desalination, 136, 2001, pp. 13-23.

34. Engdahl, D. D., 1987, Technical Information record on the Salt- Gradient solar Pond system at Los Baños Demonstration Desalting Facility. Diciembre.

35. Manjares, R. and Galván, M., *Solar multistage flash evaporation (SMSF) as a solar energy application on desalination processes. Description of one demonstration project.* Desalination, 31(1-3), 1979, pp. 545-554.

36. Krystsis, S., (1996), In proceedings of the Mediterranean Conference on Renewable Energy Sources for Water Production. *European Commission, EURORED Network, CRES; EDS. Santorini, Greece, 10-12 June, 1996, 265-270.*

37. Valverde Muela, V., (1982), (Centro de Estudios de la Energía). Planta Desaladora con Energía Solar de Arinaga (Las Palmas de Gran Canaria). Departamento de Investigación y Nuevas Fuentes. Abril- 1982.

38. Palma, F., *Photovoltaic Powered sea Water Desalination Unit. Seminar on New Technologies for the Use of Renewable Energies in Water Desalination.* Commission of the European Communities. DG XVII for Energy. CRES (Centre for Renewable Energy Sources. Atenas, 26-28 de septiembre de 1991.

39. Abu-Jabal, M. S.; Kamiya, I., and Narasaki, Y., *Proving test for a solar-powered desalination system in Gaza-Palestine.* Desalination, 137, 2001, pp. 1-6.

40. Mabrouk, A.N.A., Fath, H.E.S., *Experimental study of high-performance hybrid NF-MSF desalination pilot test unit driven by renewable energy.* Desalination and Water Treatment. (2013) 1-10.

41. El Nashar A. M., *Abu Dhabi Solar Distillation Plant.* Desalination, 52. 1985, pp. 217-234.

42. Zarza Moya, E., 1995, Solar Thermal Desalination Project, Phase II Results and Final Project Report. Ed. CIEMAT. Madrid.

43. Madani, A. A., *Economic of desalination systems*. Desalination, 78, 1990, pp. 187-200.

44. Hanafi, A., (1991), *Design and performence of solar MSF desalination system,* Desalination 82 (1-3), 165-174.

45. Alklaibi, A. M., and Lior, N., *Membrane-distillation desalination: status and potential*. Desalination, 171, 2004, pp. 111-113.

46. Hanemaaijer, J. H.; van Medevoort, J.; Jansen, A. E.; Dotremont, C.; van Sonsbeek, E.; Yuan, T., and De Ryck, L., *Memstill membrane distillation – a future desalination Technology.* Desalination 199 (2006) 175–176.

47. Xu, Y.; Zhu, B., and Xu, Y. *Pilot test of vacuum membrane distillation for seawater desalination on a ship.* Desalination 189 (2006) 165–169.

48. Meindersma, G.W.; Guijt, C.M., and de Haan, A.B.. *Desalination and water recycling by air gap membrane distillation.* Desalination 187 (2006) 291-301.

49. Fath, H. E. S. et al., *PV and thermally driven small-scale, stand-alone solar desalination systems with very low maintenance needs.* Desalination, 225, 2008, pp. 58-69.

50. Blanco Gálvez, J.; García-Rodríguez, L., and Martín-Mateos, I. *Stand-Alone Seawater Desalination by Innovative Solar-Powered Membrane-Thermal Distillation System: MEDESOL project*. Desalination, 246, 2009, pp. 567-576.

51. Vega-Beltrán, J. C.; García-Rodríguez, L.; Martín-Mateos, I., y Blanco Gálvez, J. *Solar membrane distillation: theoretical assessment of multi-stage concept.* Desalination and Water Reuse, 18, 2010, pp. 133-138.

52. Zaragoza, G.; Ruiz-Aguirre, A., and Guillén-Burrieza, E. *Efficiency in the use of solar thermal energy of small membrane desalination systems for decentralized water production.* Applied Energy, 130, 2014, pp. 491-499.

53. Ruiz Aguirre, A.; Alarcón-Padilla, D. C., and Zaragoza, G. *Productivity analysis of two spiral-wound Membrane distillation prototypes coupled with solar energy.* European Desalination Society Conference, Chipre, 2014.

54. Libert, J. J., y Maurel, A., Desalination, 39, 1981, pp. 363-372.

55. Manolakos D.; Kosmadakis, G.; Kyritsis, S.; Papadakis, G. *On Site Experimental Evaluation of a Low-Temperature Solar Organic Rankine Cycle System for RO Desalination.* Solar Energy, 83 (2009), p. 646-656.

56. Quoilin, S.; Declaye, S.; Tchanche, B. F., and Lemort, V., (2011). *Thermo-economic optimization of waste recovery organic Rankine cycles.* Applied Thermal Engineering, 31, p. 2885-2893.

57. Wang, H.; Peterson, R.; Harada, K.; Miller, E.; Ingram-Goble, R., and Fisher, L., 2011. *Performance of a combined organic Rankine cycle and vapor compression cycle for heat*

*activated cooling.* Energy, 36, p. 447-458.

58. Maraver, D.; Uche, J., and Royo, J., 2012. *Assessment of high temperature organic Rankine cycle engine for polygeneration with MED desalination: A preliminary approach*. Energy Conversion and Management, 53, p. 108-117.

59. Rheinländer, K., and Lippke, F., (1998), *Electricity and potable water from a solar tower power plant*. Renewable Energy, 14 (1-4), 23-28.

60. Glueckstern, P., 1995, *Potential uses of solar energy for seawater desalination*. Desalination, 101(1), pp. 11-20.

61. Palenzuela, P.; Alarcón-Padilla, D. C., and Zaragoza, G. *Large-scale solar desalination by combination with CSP: Techno-economic analysis of different options for the Mediterranean Sea and the Arabian Gulf.* Desalination, 2015, In press.

62. Palenzuela, P.; Zaragoza, G.; Alarcón-Padilla, D. C., and Blanco*, J. Simulation and evaluation of the coupling of desalination units to parabolic-trough solar power plants in the Mediterranean region.* Desalination, 281, 2011, p. 379-387.

63. Palenzuela, P.; Zaragoza, G.; Alarcón-Padilla, D. C., and Blanco*,* J. *Evaluation of cooling technologies of concentrated solar power plants and their combination with desalination in the mediterranean area*. Applied Thermal Engineering*,* 50 (2), 2013, pp. 1514-1521.

64. Alarcón-Padilla, Diego-César; García-Rodríguez, Lourdes; Blanco-Gálvez, Julián; (2010a). Design recomendations for a multi-effect distillation plant connected to a double-effect absortion heat pump: a solar desalination case-study. Desalination, 262 (1-3), 2010, pp.11-14.

65. Alarcón-Padilla, Diego-César; García-Rodríguez, Lourdes; Blanco-Gálvez, Julián; (2010b) Connection of absorption heat pumps to multi-effect distillation systems: pilot test facility at the Plataforma Solar de Almería (Spain). Desalination and Water Treatment, 18, 2010, pp.126-132.

66. Alarcón-Padilla, Diego-César; García-Rodríguez, Lourdes; Blanco-Gálvez, Julián; (2010c) Experimental assessment of connection of an absorption heat pump to a multi-effect distillation unit. Desalination, 250, 2010, pp. 500-505.

67. Alarcón-Padilla, D.-C.; Blanco-Gálvez, J.; García-Rodríguez, L.; Gernjak, W., y Malato-Rodríguez, S. First experimental results of a new hybrid solar/gas multi-effect distillation system: the AQUASOL Project. Desalination, 220(1), 2008, pp. 619-625.

68. Alarcón-Padilla, D. C. y García-Rodríguez, L.; (2007a) Application of absorption heat pumps to multi-effect distillation: a case study of solar desalination. Desalination, 212, 2007, pp. 294-302.

69. Alarcón-Padilla, D. C.; García-Rodríguez, L., y Blanco-Gálvez, J., (2007b) *Assessment of an absorption heat pump coupled to a multi-effect distillation unit within AQUASOL project.* Desalination, 212, 2007, pp. 303-310.

70. Buenaventura, A and García-Rodríguez, L. *Solar thermal-powered desalination: A viable solution for a potential market.* Desalination, 435, 2018, pp. 60-69.

71. Delgado-Torres, A., and García Rodríguez, L. *Design recommendations for solar organic Rankine cycle (ORC)-powered reverse osmosis (RO) desalination.* Renewable and Sustainable Energy Reviews, 16(1), 2012, pp.44-53.

72. Delgado-Torres, A., and García-Rodríguez, L., (2010a). *Preliminary design of seawater and brackish water desalination system driven by low-temperature solar organic rankine cycles.* Energy Conversion and Management, 51(12), 2010, pp.2913-2920.

73. Delgado-Torres, A. M., and García-Rodríguez, L. (2010b). *Analysis and optimization of the low-temperature solar organic Rankine cycle (ORC).* Energy Conversion and Management, 51(12), 2010, pp. 2846-2856.

74. Delgado-Torres, A., and García-Rodríguez, L., (2007a) *Double cascade organic Rankine cycles for solar-driven reverse osmosis desalination.* Desalination, 216, 2007, pp. 306-313.

75. Delgado-Torres, A., and García-Rodríguez, L., (2007b) *Comparison of solar technologies for driving a desalination system by means of an organic Rankine cycle.* Desalination, 216, 2007, pp. 276-291.

76. Delgado-Torres, A., and García-Rodríguez, L., (2007c) *Preliminary assessment of solar organic Rankine cycles for driving a desalination system.* Desalination, 216, 2007, pp. 252-275.

77. Delgado-Torres, A., and García-Rodríguez, L., (2007d) *Status of Solar thermal-driven reverse osmosis desalination*. Desalination, 216, 2007, pp. 242-251.

78. Delgado-Torres, A.; García-Rodríguez, L., and Roero Ternero, V. *Preliminary design of a solar thermal-powered seawater reverse osmosis system.* Desalination, 216, 2007, pp. 292-305.

79. García-Rodríguez, L., and Blanco-Gálvez, J.; Solar-heated Rankine cycles for water and electricity production: POWERSOL project. Desalination, 212, 2007, pp. 311-318.

80. García-Rodríguez, L., and Delgado-Torres, A., *Solar-powered Rankine cycles for fresh water production.* Desalination, 212, 2007, pp. 319- 327.

81. Peñate, B. and García-Rodríguez, L. *Seawater reverse osmosis desalination driven by a solar organic Rankine cycle: design and technology assessment for medium capacity range.* Desalination, 284, 2012, pp. 86-91.

82. DESSOL® http://www.itccanarias.org/web/tecnologias/agua/dessol.jsp?lang=es. Last visit 18/08/2017.

83. Carta, J. A.; González, J., and Subiela, V. (2004), *The SDAWES project: an ambitious R&D prototype for wind-powered desalination.* Desalination, 161, pp. 33-48.

84. Peñate, B.; García-Rodríguez, L.; Castellano, F., and Bello, A., *Assessment of a stand-alone gradual capacity reverse osmosis desalination plant to adapt to wind power availability: a case study.* Energy, 36(7), 2011, pp. 4372-4384.

85. Thomson, M., and Infield, D., *A photovoltaic-powered seawater reverse-osmosis system without batteries.* Desalination, 153 (1-3), 2003, pp. 1-8.

86. Adiga, M. R.; Adhikary, S. K.; Narayanan, P. K.; Harkare, W. P.; Gomkale, S. D., and Govindan, K. P., *Performance analysis of photovoltaic electrodialysis desalination plant at Tanote in Thar desert,* Desalination, 67, 1997, pp.59-66.

87. Kuroda, O.; Takahashi, S.; Kubota, S.; Kikuchi, K.; Eguchi, Y.; Ikenaga, Y.; Sohma, N.; Nishinoiri, K.; Wakamatsu, S., and Itoh, S., *An electrodialysis sea water desalination system powered by photovoltaic cells,* Desalination, 67, 1987, pp. 33-41.

88. Maurel, A., (1991), Desalination by Reverse Osmosis Using Renewable Energies (Solar-Wind) Cadarche Centre Experiment. Seminar on New Technologies for the Use of Renewable Energies in Water Desalination. Commission of the European Communities. DG XVII for Energy. CRES (Centre for Renewable Energy Sources. Athens, 26-28 September 1991.

89. Ishimaru, N., *Solar photovoltaic desalination of brackish water in remote areas by electrodialysis,* Desalination, 98(1-3), 1994, pp. 485-493.

90. Kvajic, G., (1981), Solar power desalination, PV- ED system, *Desalination, 39, 175.*

91. Husseiny, A. A., and Hamester, H. L., (1981), Engineering design of a 6000$m^3$/day seawater hybrid RO-ED helio-desalting plant, *Desalination, 39, 171-172.*

92. García Rodríguez, L.; *Desalination by Wind Power*. Wind Engineering, 28, 2004, pp. 453-466.

93. Spectra Water Makers, 2014 http://www.spectrawatermakers.com

94. Thomson, M., and Infield, D., 2002, A photovoltaic-powered seawater reverse-osmosis system without batteries. Desalination, 153: pp.1-8.

95. ERI: http://www.energyrecovery.com

96. Danfoss: http://www.danfoss.com

97. Peñate, B.; de la Fuente, J. A.; Barreto, M. Operation of the RO Kinetics® energy recovery system: description and real experiences. Desalination, 252, 2010, pp. 179-185.

98. Ortiz, J. M.; Sotoca, J. A.; Expósito, E.; Gallud, F.; García-García, V, and Montiel, A., Brackish water desalination by electrodyalisis: batch recirculation operation modelling. Journal of Membrane Science, 1-2, 2005, pp. 65-85.

99. Ortiz, J. M.; Expósito, E.; Gallud, F.; García-García, V.; Montiel, A., and Aldaz, A. Desalination of underground brackish waters using and electrodyalisis system powered directly by photovoltaic energy. Desalination, 208, 2007, pp. 89-100.

100. Kehal, S., (1991), Reverse Osmosis Unit of 0.85 m3/h Capacity Driven by Photovoltaic Generator in South Algeria. Seminar on New Technologies for the Use of Renewable Energies in Water Desalination. *Commission of the European Communities. DG XVII for Energy. CRES (Centre for Renewable Energy Sources. 26-28, Ahtens, September, 1991.*

101. Al Suleimani, Z., and Nair, N. R., *Desalination by solar-powered reverse osmosis in a remote area of Sultanate of Oman.* Applied Energy, 64, 2000, pp. 367-380.

102. Joyce, A.; Loureiro, D.; Rodrígues, C., and Rojas, S., (2001), *Small reverse osmosis units using PV systems for water purification in rural places.* Desalination, 137, 39-44.

103. Herold, D., and Neskakis, A., *A small PV- driven reverse osmosis desalination plant on the island of Gran Canaria.* Desalination, 137, 2001, pp. 285-292.

104. OMsop Project https://omsop.serverdata.net/Pages/Project%20Brochure.aspx.

# Chapter 2. SEAWATER DESALINATION BASED ON MEMBRANE DISTILLATION: CURRENT TRENDS AND FUTURE PROSPECTS

This chapter is a brief summary of the Master Thesis presented at the University of Seville in December, 2014. Main part of this chapter has been published (Buenaventura and García Rodríguez (2017).

## 1. INTRODUCTION

Close to 1/3 of the world´s population live in water scarce areas. Over 780 M people are still without access to improved sources of drinking water [WHO, 2012].

Seawater desalination is part of the solution to these water challenges and has been used now for decades to generate alternative water resources. The use of thermal desalination technologies, such as Multi-Stage Flash distillation (MSF) and Multi-Effect Distillation (MED), has been changed in the last decade to Reverse Osmosis (RO) membrane technology because of its reduction in the required energy to desalinate seawater.

The objective of this paper is to analyse the viability and competitiveness of Membrane Distillation (MD) desalination technology, that is a combination of thermal desalination and membrane technology.

What in principal makes MD technology of interest versus other thermal desalination processes is that it exhibits:

- Compactness.
- Ability of dealing with highly concentrated saline solutions. This is an exceptional feature versus conventional desalination processes, both, distillation and reverse osmosis.
- Flexibility of the system for operating at partial load and variable load.

Membrane Distillation (MD) desalination is normally based on generating a temperature gradient between the two sides of a hydrophobic membrane, where the saline solution is the higher temperature side. The vapor pressure difference due to the corresponding values at the given temperature in each of the membrane side generates vapor in the high temperature side and is the driving force of the process. That vapor crosses the hydrophobic membrane towards the cooler side where is condensed, thus generating the desalinated product water. The saline solution temperature decreases due to the released enthalpy of phase change and it also increases its saline concentration. Figure 2.1 shows a conceptual diagram of a section of the feed channel, limited by the membrane. Feed (F),

BlowDown (BD) - or concentrate - and Vapor mass flow rates - $q_F$, $q_{BD}$ and $q_V$, respectively -, and heat power losses, $P_{Q,L}$, are shown.

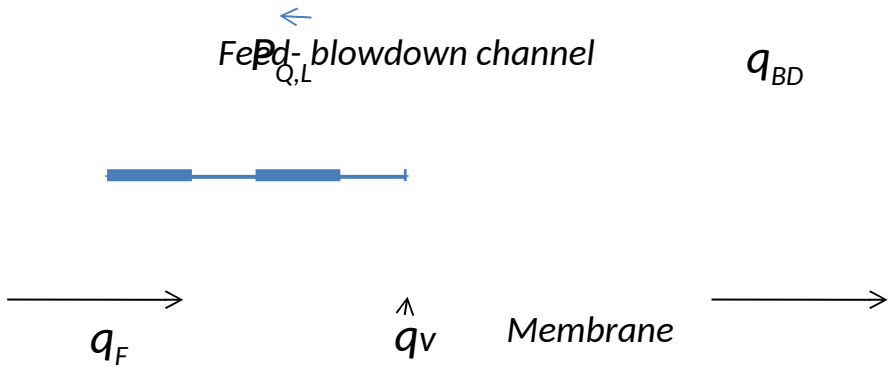


**Figure 2.1. Conceptual diagram of a portion of feed channel in a desalination process based on Membrane Distillation (MD).**

In comparison to conventional distillation, the MD desalination technology has been developed recently and available commercial products and prototypes exhibit limited efficiency. The basic concept of MD is named Direct Contact Membrane Distillation (DCMD) due to the steam generated passes through the membrane and condenses directly in the bulk of pure liquid water at lower temperature (coolant flow). Besides that, Air Gap Membrane Distillation (AGMD) incorporates an air chamber of few millimetres width between the membrane and a condensation surface on which the vapour condenses. This surface is cooled by a liquid flow, normally feed that is thus preheated. The air gap significantly reduces the heat transferred from the feed channel to the permeate channel in the DCMD process, which results in the corresponding losses of permeate production. If the channel between the membrane and the cooling surface is full by permeate, the process is called Liquid Gap Membrane Distillation (LGMD). This exhibits the advantage of lower heat losses than DCMD and lower mass resistance of AGMD process [Zaragoza *et al*, 2014]. Other process is Sweeping Gas Membrane Distillation (SGMD), in which a gas with forced circulation is in the opposite membrane side to the saline solution. The gas flow extracts the distillate from the membrane module and drives it to an external condensing device that could be used to preheat the saline water feed. Finally, another possibility is based on generate the vapour pressure difference by using the following processes, Vacuum Membrane Distillation (VMD). The opposite side of the membrane consists in a chamber under vacuum. The vapour condensation takes place out of the membrane module.

For seawater desalination applications DCMD, AGMD and LGMD are normally used. The feed water is seawater that has been previously heated with external thermal energy and

flows in one of the membrane sides. In the other side of the membrane a lower temperature flow circulates, generating in this way the required temperature gradient. The vapor crosses the membrane towards the cooler side where is then condensed, thus pre-heating the feed water. The produced pure water is named permeate, and the ratio between the feed water (kg) and the produced water (kg) is the system recovery, *r*.

Many experimental devices at lab scale are described in the literature. However, references become scarcer when we look for complete membrane distillation modules, that is, including membranes, spacers, condensation surface, inflow and product conduits and cooling. There were only few pre-commercial or commercial MD modules, as those manufactured by: SCARAB [Kullab *et al.,* 2005], Keppel-Seguers [Hanemaaijer *et al,* 2006] [Hanemaaijer, 2004][Meindersma *et al*., 2006], ISE Fraunhofer Institute [Wieghaus *et al*., 2008], and MEMSYS [memsys, 2017]. The latest developed modules are thoroughly described by Ruiz-Aguirre (2017).

# 2. BASIC CONCEPTS OF SEAWATER DESALINATION BASED ON MEMBRANE DISTILLATION

## 2.1. Driving force

Conceptually, the minimum required actual temperature gradient across the membrane is the Boiling Point Elevation (BPE) - see Fig. 2.2 -. It is important to note that the presence of salts in the saline water has the effect of reducing the vapor pressure at a given temperature, in respect to the vapor pressure of pure water at the same temperature. Therefore, the concentration of salts in the saline solution has a direct effect on the driving force of the process, being this effect significant if the temperature gradient between the two sides of the membrane is relatively small.

Another important aspect regarding the driving force of the process, besides the temperature gradient, is the temperature of the saline solution - see Fig. 2.3 -. For instance, for a temperature gradient of 10 K and reference seawater (mass fraction 0.035), the driving force will reduce to half of its value if the saline solution temperature is of 80ºC instead of 100ºC. This is a key aspect in order to select the better applications of MD technology, since applications where the thermal energy available is of limited temperature, that is, with relatively low exergy, will not be well recommended. It is also important to have this aspect in mind when extrapolating the results of experiments to conditions where the maximum temperature of the saline solution is lower.

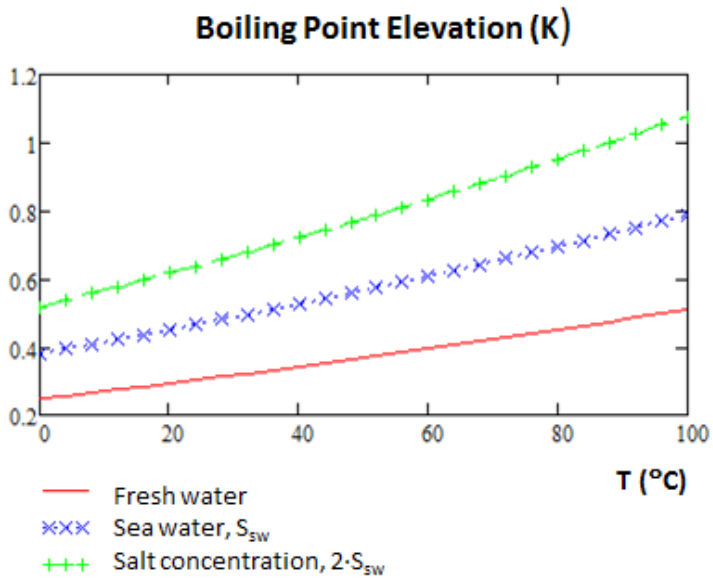


**Figure 2.2. Boiling Point Elevation (BPE) versus temperature of the saline solution, for concentrated and dilutions of the reference seawater (salinity $S_{sw}$= 0.035 kg/kg).**

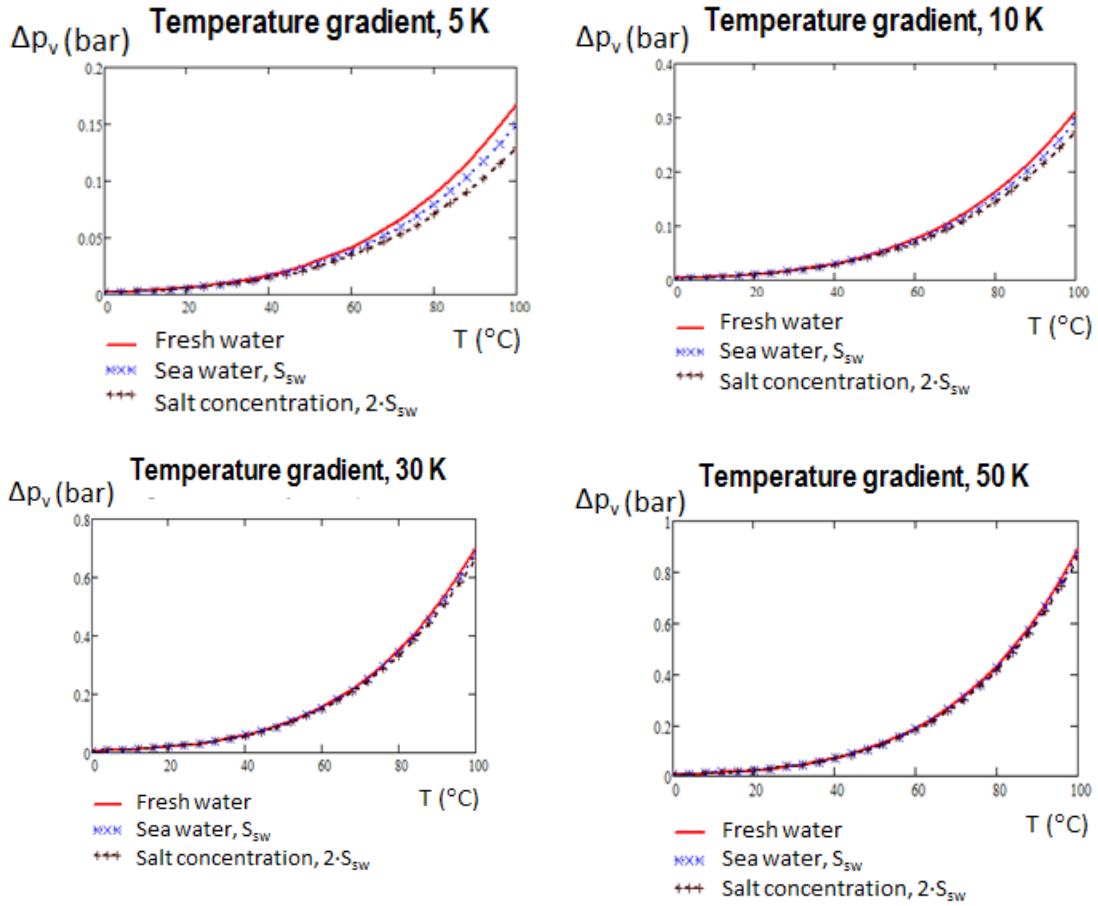


**Figure 2.3. Driving force of the Membrane Distillation (MD) process – vapour pressure difference, $\Delta p_v$ - for different temperature gradient across the membrane.**

## 2.2. Main energy consumption

All basic desalination processes that involve evaporation require the corresponding enthalpy of phase change to generate 1 kg of steam. In order to decrease the energy needs of the desalination process as a whole, energy recovery based on the reuse of the condensation heat released is required. Therefore, the condensation of the vapor generated releases heat that should be absorbed by the feed as industrial distillation processes. Nevertheless, the heat recovery is limited by the overall energy balance of the desalination process. Normally the seawater input of a conventional distillation plant – i.e. MED or MSF - only circulates through:

- The end condenser in a conventional MED plant, except if the steam generated within the last effect is used by a thermocompression process.
- The Heat Reject Section (HRS) in a conventional MSF plant, in which only part of the steam generated condenses.

Therefore, after this preheating, most of the seawater mass flow rate is discharged from the plant, and the rest continues the circulation for the rest of the plant. The existing MD desalination modules are conceptually based on the layout depicted in figure 2.4, thus resulting in the corresponding temperature profile shown. Note that the external heat input is supplied before starting the vapour generation, as in a conventional MSF. If recirculation of the blowdown is adopted, the configuration of conventional MSF plants, adapted to the case of MD desalination would be that given in figure 2.5. Configuration concepts related to the most efficient interconnection of MD modules based on multiple stages have been scarcely analysed in the literature [Hanbury and Hodgkiess, 1985][Blanco *et al*, 2009][Vega-Beltrán *et al*, 2010].

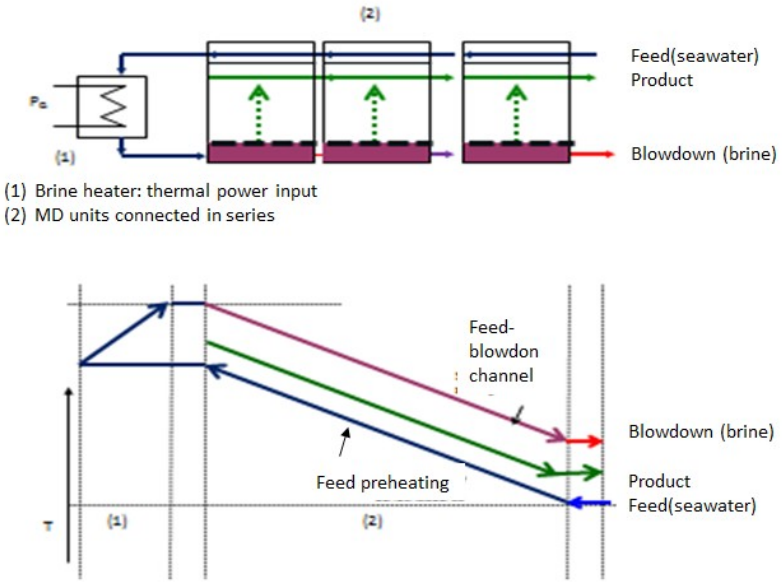


**Figure 2.4. Conceptual diagram and approximate temperature profile of a series of MD modules.**

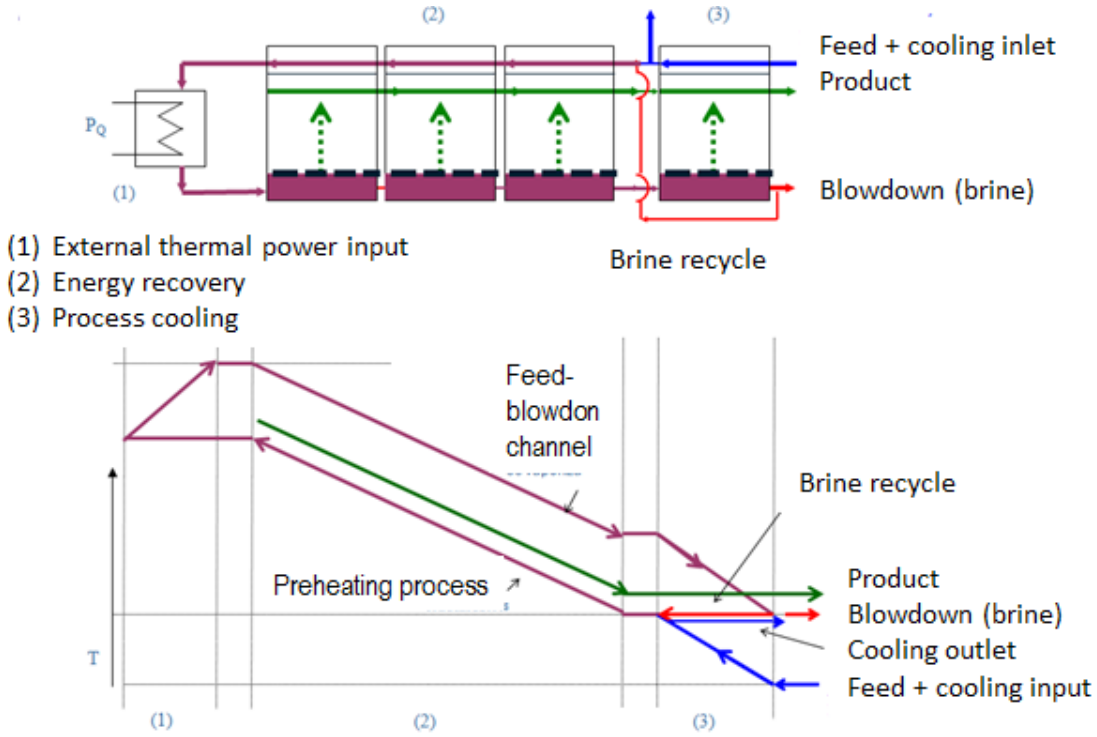


**Figure 2.5. Conceptual diagram and aproximate temperature profile of a serie of MD modules with brine recycle and cooling.**

Figure 2.6 shows the relation between main parameters of a generic distillation process. This results from combining the following equations related to the desalination process as a whole in which a mass flow rate ($q$) of feed (F) is separate on two steams, BlowDown (BD) and Product (P), due to a heat power consumption ($P_Q$), under the assumptions of steady state and no heat losses:

- Mass flow rate balances concerning desalination process, expressed as global and salts balances respectively:

$$q_F = q_P + q_{BD} \tag{2.1}$$

$$q_F \cdot S_F = q_{BD} \cdot S_{BD} \tag{2.2}$$

Where S is salinity – i.e. mass fraction of salts -.

- Mass flow rate balance on the cooling flow (cool) if any:

$$q_{cool,out} = q_{cool,\in ¿¿} \tag{2.3}$$

- Energy power balance:

$$0 = P_Q + q_F \cdot h_F - q_P \cdot h_P - q_{BD} \cdot h_{BD} + q_{cool} \cdot ¿¿ \tag{2.4}$$

- Definition of recovery rate:

$$r = q_P / q_F \tag{2.5}$$

Section 4 report on calculations of feasible sets of operating parameters.

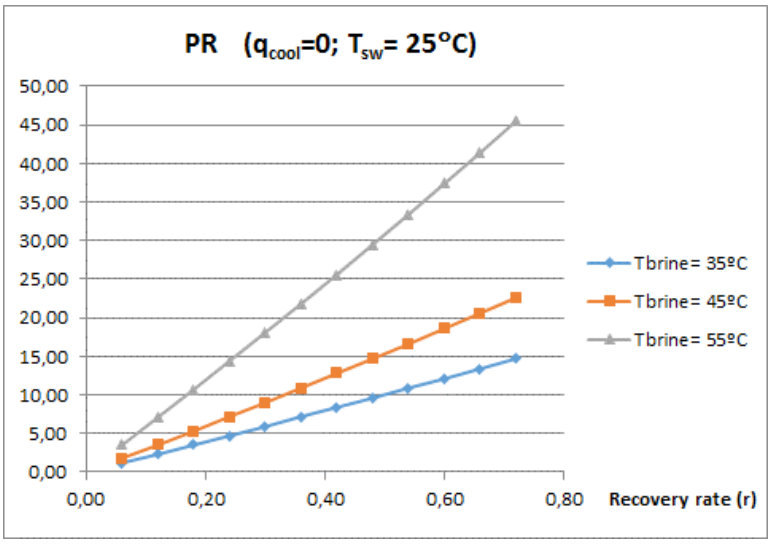


**Figure 2.6. Theoretical analysis of the influence of temperature of brine output if no cooling flow is available. This figure does not represent feasible points. Performance Ratio (PR) – ratio between 2330 kJ/ kg and specific thermal energy consumption -.**

## 2.3. Auxiliary consumption

Figure 2.7 shows the ratio of mass flow rate between cooling and product as function of the temperature difference from the seawater input and the PR assumed by hypothesis. Note that this is the main drawback of distillation processes in comparison the reverse osmosis, since the latter does not require cooling. All distillation processes are not able to achieve the PR assumed by hypothesis. Specific assessment of MD process is given in section 4 in order to calculate possible values of PR of MD process.

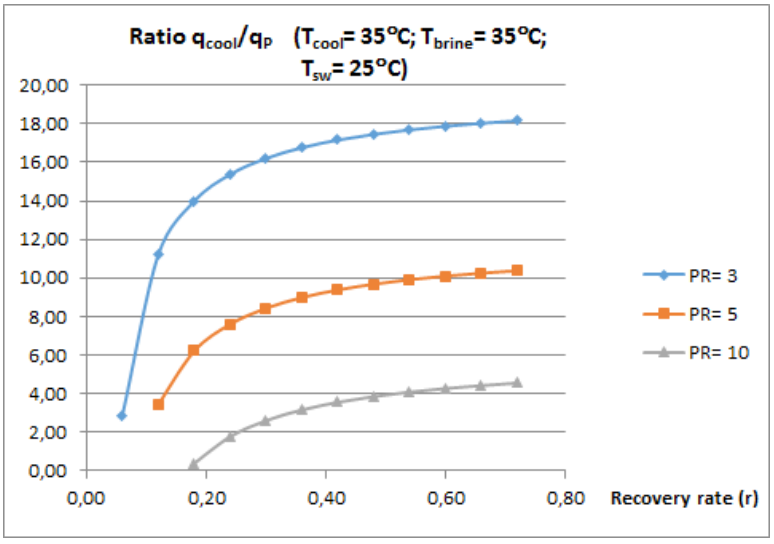


a) $T_{cool}$= 35ºC; $T_{brine}$= 35ºC.

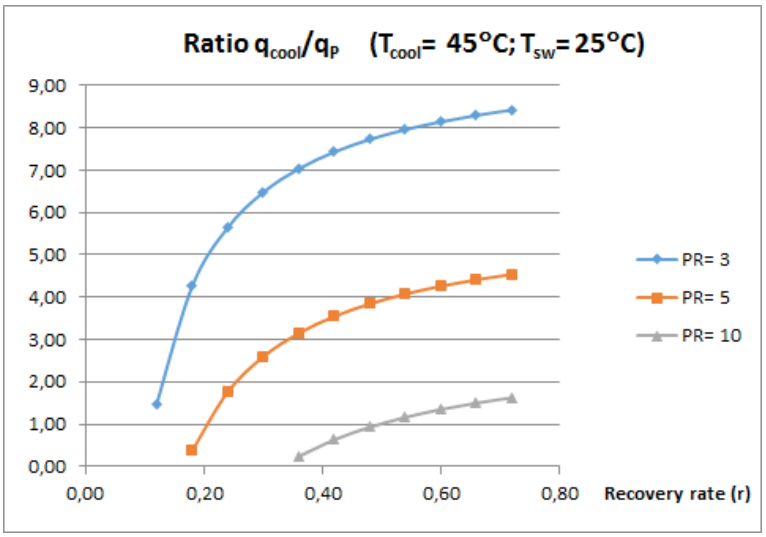


b) $T_{cool}$= 45ºC; $T_{brine}$= 45ºC.

**Figure 2.7. Ratio between cooling and product mass flow rate for different values of output temperature of the cooling flow, $T_{cool}$, $T_{sw}$=25ºC. This figure does not represent feasible points.**

### 2.4. Vapor transport mechanisms

The mechanisms of transport of the steam generated in the hot side across the membrane are thoroughly described in the literature Ding et al (2002). There are relevant research activities focused on improving membranes. Nevertheless, when areas of membrane and condensate surfaces are similar and metals are not used, the limiting factor of the vapor generation could be the conductivity of the condensing surface instead of the transmembrane flow permitted by the operating conditions.

## 3. OVERVIEW OF THE STATUS OF MD TECHNOLOGIES

In this section the existing MD pre-commercial or commercial technologies are described and the external experimental evaluations by independent research organisations presented. A brief descriptions of such MD modules is presented below, sorted by the manufacturer company:

- Scarab Development AB. The Swedish company Scarab Devlopment AB [SCARAB, 2015] developed MD modules. The application of these modules to seawater desalination has also been considered by the company. These products have been tested at the Plataforma Solar de Amería- CIEMAT within the framework of the EU project MEDESOL (FP6-2005-Global-4, FP6-036986, *Seawater Desalination by Innovative Solar-Powered Membrane- Distillation System*) [Blanco Galvez *et al*, 2009]. The technology is based on AGMD, using flat sheet membranes.

- Memstill technology. Memstill technology is attributable to the patents developed by a research organization in Holland, TNO, licensed by the company Keppel-Seghers (Singapur). Keppel-Seghers contracted the Plataforma Solar de Almería for testing two of the company´s prototype modules. Both prototypes, M33 and PT5, are based on LGMD process and have flat sheet membrane configuration and total membrane area of 9 $m^3$. The M33 prototype is manufactured as a single module, while the latter is composed by three serial modules [Zaragoza *et al*, 2014]. In addition, aforementioned company have developed other MD systems.

- Aquastill. The company Aquastill [Ruíz Aguirre, 2017] started its activities in 2008. Their MD modules are known as AQUA⎪FLEX 25; AQUA⎪FLEX 100 and AQUA⎪FLEX 150R.

- Solar Spring. The German Institute ISE-Fraunhofer has developed an MD module that today is being commercialized by their spin-off Solar Spring. There have been several

pilot units powered with solar thermal energy, one of the first ones in the Instituto Tecnológico de Canarias, another one at Plataforma Solar de Almería-CIEMAT. The Oryx 150 consists of a LGMD module with a spiral wound configuration and maximum temperature permitted 85ºC [Zaragoza *et al*, 2014l.

- Memsys. The German company Memsys has developed a MD module. Among pilot systems are those installed in the Plataforma Solar de Almería-CIEMAT and Singapur [Kui *et al*., 2011].

- Aquaver. The company Aquaver commercializes as WTS-40A a MD module based on Memsys modules, with flat sheet V-MEMD membranes (5.76 $m^2$). This uses a novel configuration of vacuum MD that uses the multi-effect distillation concept with 7 effects working at decreasing boiling point. Zaragoza *et al* (2014) describe this innovative configuration.

When analysing distillation systems, two parameters are essential to evaluate the performance of the process:

- The Performance Ratio, PR, that is the ratio between the water enthalphy of phase change (2330 kJ/kg) and the specific thermal energy consumption of the process itself (kJ/kg).

- The Gain Output Ratio, GOR, the ratio between the obtained product (kg of condensed vapor) and the required energy of the process (in terms of kg of condensed vapor of the thermal source).

GOR and PR have typically values very close one to each other because of their respective definitions.

In table 2.1 below, experimental results of tests carried out at PSA-CIEMAT are presented for the different MD technologies. Zaragoza *et al.* (2014) reports on experimental assessment of different MD modules. Experiments were performed for different conditions by controlling in each case the temperature of the hot and cold source, as well as the feed flow rate. Constant measuring was done and the results averaged during intervals in which the operational conditions were kept stationary. In all cases, the modules were supplied with thermal energy coming from the solar field at temperatures between 60ºC and 90ºC. For a full description of the test set-up, experiments and results, refer to Zaragoza *et al* (2014). In this paper we summarize some of those results for feed conductivities corresponding to salinities of about 35 g/L (similar to seawater salinity), and temperature difference between the hot inlet and the cold inlet in the order of 40ºC. The parameters reported are:

- the distillate flux, $J_p$, distillate flow rate per unit surface of membrane.

- the recovery ratio, *r*, is the percentage of the feed which is converted into distillate – ratio between corresponding mass flow rate -.

- the Specific Thermal Energy Consumption, STEC, that is the total thermal energy consumption weighted by the total production of distillate.

Table 2.1 summarises the best values obtained for the aforementioned MD modules based on experimental data obtained at the Plataforma Solar de Almería.

**Table 2.1. Summary of the best data obtained based on experimental results reported by [(1)]Zaragoza *et al.* (2014) and [(2)]Guillén Burrieza et al. (2011), Ruiz-Aguirre *et al* (2014).**

| | Aquastill[(2)] | SCARAB[(1)] | M33 Keppel-Sheghers[(1)] | PT5 Keppel-Sheghers[(1)] | Oryx 150 Solar Spring[(1)] | WST-40[a] Aquaver[(1)] |
|---|---|---|---|---|---|---|
| **Membrane surface, $m^2$** | | 8.4 | 9 | 9 | 10 | 5.75 |
| **Distillate Flux, Fd, L/h $m^2$** | <1.5 | 6.5 | 3.5 | 5 | <3.5 | 7.1 |
| **Recovery ratio, r %** | <5 | 2.5 | 3.23 | 5.08 | <6 | 59 |
| **STEC** | | 1000 | 1800 | 450 | | 175 |
| **PR** | <7 | 0.64 | 0.35 | 1.4 | <3.5 | 3.7 |

Besides that, a GOR value of 5.5 was achieved with the technology developed by Institute ISE Fraunhofer and was measured in the experimental facilities of the Instituto Tecnológico de Canarias. Moreover, Ruiz-Aguirre (2017) reports on a range of energy consumption of:

- 100-700 kWh/$m^3$ (PR= 6.5-0.92) obtained by connecting ten SCARAB´s modules in Sweden. This installation produces 1-2 $m^3$/d of fresh water.

- 350-2.000 MJ/ $m^3$ (PR= 6.7-1.17) achieved by several installations based on Memstill technology (modules M28, M32, M33 and K1).

- 90-95 kWh/$m^3$ (PR= 7.2-6.8) at maximum temperature of 70ºC with modules manufactured by Aquastill.

- 100-200 kWh/m$^3$ (PR=6.5-3.24) measured by using ISE Fraunhofer technology with top temperatures 85-60ºC. Besides, 117 kWh/m$^3$ (PR= 5.5) was reported with the first Oryx system.

Finally, González et al (2017) review the status of MD technology and report on energy consumption and transmembrane flux based on both, experimental and hypothesis assumed by different authors. Cost calculation reported by Al-Obaidani et al (2008) are interesting but they excluded the auxiliary pumping consumption, which is significant in MD system accordingly results obtained in this chapter.

## 4. ANALYSIS OF MD TECHNOLOGY

In this section the main aspects of MD technology are analysed, identifying the possible limitations of the technology and the current designs.

In order to assess the experimental values reported in the literature as much as potential of development of such MD modules, a thermodynamic analysis of MD modules connected in series without brine recirculation is conducted. The basic conceptual configuration is depicted in figure 2.8. Main role of components shown in this figure are as follows:

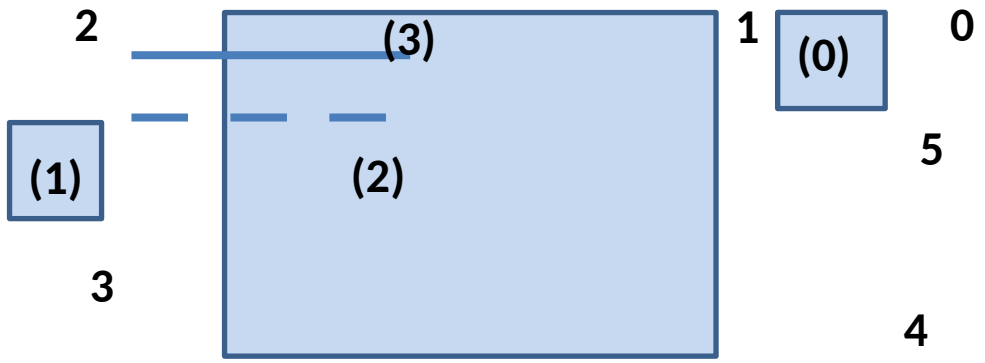


**Figure 2.8. Conceptual diagram of a serie connection of MD modules with no brine recycling.**

(1) Seawater intake, seawater pumping and pretreatment. The corresponding matter and energy balances are:

$$S_1 = S_0 \quad (2.6)$$

$$q_0 - q_1 = 0 \quad (2.7)$$

$$q_0 \cdot h_0 - q_1 \cdot h_1 + P_W = 0 \tag{2.8}$$

In above and following equations, subscripts corresponding to the numbered mass streams of figure 2.8. Besides that, quantities involved are: salinity (mass fraction of saltls), S; mass flow rate, q; mass enthalpy, h; thermal power, $P_Q$, and auxiliary power, $P_W$.

(1) The heating of the feed after being pre-heated, takes place within the brine heater by means of an external thermal energy source. The corresponding thermodynamic equations are the following:

$$S_3 = S_2 \tag{2.9}$$

$$q_2 - q_3 = 0 \tag{2.10}$$

$$q_2 \cdot h_2 - q_3 \cdot h_3 + P_Q = 0 \tag{2.11}$$

(2) Desalination process, in which the liquid feed increases its salt concentration and decreases its temperature due to the vapour generation and thermal losses thought the membrane, $P_{Q,L}$. The desalination process also includes the vapour condensation. The channel limited by the membrane through which the feed circulates is commonly called in desalination membrane technology the feed-blowdown channel. The following equations result, respectively from applying: definition of recovery rate, mass balance in component 2, and the energy balance to the feed-blowdown channel:

$$S_4 = \frac{S_0}{1-r} \tag{2.12}$$

$$q_3 - q_4 - q_5 = 0 \tag{2.13}$$

$$q_F \cdot h_F - q_v \cdot \acute{h}_v - q_{BD} \cdot h_{BD} - P_{Q,L} = 0 \tag{2.14}$$

(3) Heat recovery process, resulting in feed preheating, expressed by:

$$S_2 = S_1 \tag{2.15}$$

$$q_1 - q_2 = 0 \tag{2.16}$$

$$q_v \cdot \acute{h}_v + q_1 \cdot h_1 + P_{Q,L} - q_2 \cdot h_2 - q_P \cdot h_P = 0 \tag{2.17}$$

Besides that, an important issue is to set the thermodynamic maximum limit to obtain vapour generated by a previously heated feed flow at a given thermodynamic state. In this process of vapour generation, the enthalpy of the heated feed decreases up to the existing limit of the cooling flow input that is normally ambient temperature.

Table 2.2 gives main results of the thermodynamic analysis of an MD system with configuration shown in figure 2.8, for different operation conditions. The first two columns shows, respectively, the maximum temperature (T3) and the difference T4-T0, which is similar to the global temperature gradient between cooling and feed flows (T3-T2) generated by the brine heater. The last column, *Precal*, gives the increasing of temperature due to the feed preheating.

**Table 2.2. Results of thermodynamic analysis of the MD system shows in figure 2.6.**

| Tmax, ºC | T4-T0, ºC | T5-T1, ºC | PR | r, % | T3-T2, ºC | Precal, ºC |
|---|---|---|---|---|---|---|
| 95 | 25 | 3 | 2 | 8.1 | 23 | 51 |
| 85 | 25 | 3 | 1.6 | 6.5 | 23.4 | 40.6 |
| 75 | 25 | 3 | 1.2 | 4.8 | 23.8 | 30.2 |
| 65 | 25 | 3 | 0.8 | 3.7 | 24.2 | 19.8 |
| 55 | 25 | 3 | 0.3 | 1.5 | 24.6 | 24.6 |
| **Tmax, ºC** | **T4-T0, ºC** | **T5-T1, ºC** | **PR** | **r, %** | **T3-T2, ºC** | **Precal, ºC** |
| 95 | 15 | 3 | 4.1 | 9.6 | 13.7 | 60.3 |
| 85 | 15 | 3 | 3.3 | 8 | 13.9 | 50.1 |
| 75 | 15 | 3 | 2.6 | 2.6 | 14.1 | 39.9 |
| 65 | 15 | 3 | 1.9 | 4.8 | 14.3 | 29.7 |
| 55 | 15 | 3 | 1.3 | 3.1 | 14.6 | 19.4 |
| 45 | 15 | 3 | 0.6 | 1.5 | 14.8 | 9.2 |
| **Tmax, ºC** | **T4-T0, ºC** | **T5-T1, ºC** | **PR** | **r, %** | **T3-T2, ºC** | **Precal, ºC** |
| 95 | 10 | 2 | 6.6 | 10.4 | 9.1 | 65 |
| 85 | 10 | 2 | 5.5 | 8.7 | 9.2 | 54.8 |
| 75 | 10 | 2 | 4.4 | 7.2 | 9.3 | 44.7 |
| 65 | 10 | 2 | 3.3 | 5.6 | 9.4 | 34.5 |
| 55 | 10 | 2 | 2.4 | 3.9 | 9.6 | 24.3 |
| 45 | 10 | 2 | 1.4 | 2.3 | 9.8 | 14.2 |
| **Tmax, ºC** | **T4-T0, ºC** | **T5-T1, ºC** | **PR** | **r, %** | **T3-T2, ºC** | **Precal, ºC** |
| 95 | 5 | 2 | 13.8 | 11.1 | 4.6 | 69.3 |
| 85 | 5 | 2 | 11.8 | 9.5 | 4.7 | 59.3 |
| 75 | 5 | 2 | 9.7 | 7.9 | 4.7 | 49.2 |
| 65 | 5 | 2 | 7.6 | 6.3 | 4.8 | 39.2 |
| 55 | 5 | 2 | 5.7 | 4.7 | 4.8 | 29.1 |
| 45 | 5 | 2 | 3.7 | 3 | 4.9 | 19.1 |

The low recovery rate reported in table 2.2 results in high auxiliary pumping consumption. Besides, brine could be partially recycled, from point 4 to point 1 in figure 2.8. In this modified configuration, the ratio of mass flow rate between product and flow in the brine heater is the parameter *r* in table 2.2. Therefore, brine recycle does not improve the PR of the desalination process. To achieve the steady state in this configuration requires that temperature of product and brine output are high enough to comply the energy balance given in section 2.2 with no cooling seawater flow. This configuration is not adopted in

conventional distillation industry (MSF process) since the increase of temperature difference $T_4$-$T_0$ reduces the PR. Therefore, the author does not recommend this option. On the contrary, the conventional solution adopted in MSF distillation industry is that reported in figure 2.5.

# 5. DISCUSSION OF THERMODYNAMIC RESULTS AND IMPROVEMENT SUGGESTION

From experimental results published and the thermodynamic analysis performed, the following points should be highlighted:

- Low values of PR and GOR. Experimental PR of the Instituto Fraunhofer (Solarspring) module is remarkable, which is attributable to the low transmembrane gradient achieved. Note that there is a good agreement to maximum values of PR given in table 3.2 for temperature gradients of 10ºC and 5ºC, respectively. Also Aquastill module exhibits relatively high PR, which is consistent with the highest values obtained from the thermodynamic analysis carried out. Zaragoza *et al*. (2014) indicate the thermal energy consumption of between 60ºC and 90ºC delivered by a solar collector field, but they do not report on the transmembrane temperature gradient of the experimental test campaigns. It should be highlighted that results obtained at the Plataforma Solar de Almería – CIEMAT for Aquastill and Fraunhofer (Solarspring) modules exhibit extremely low values of recovery rate. They are consistent to tables 2.2.

- Low values of recovery rate, *r*. Having in mind that in SWRO the main energy consumption is around 2-2.5 kWh/m$^3$, the auxiliary electricity consumption of desalination based on MD is essential. Note that SWRO plants do not require cooling seawater but only feed water pumping with recovery rate of about 45-50%. Table 2.1 shows that the only high value of recovery rate, r, is that corresponding to the Aquaver module, which is discussed in the next point.

- Aquavert WTS-40A system. Since the system has been manufactured by using four effects in which vapor is generated by heat absorption in addition to the membrane distillation concept, the PR should be slightly lower than the number of effects as is in conventional MED units. This is consistent with the experimental assessment. In addition, there is no thermodynamic limit to the recovery rate of process based on vapour generation by heat absorption as experimental results proved. The recovery is only limited by the convenience of operating below salt precipitation limits. The high permeate flux is attributable to the use of the VMD process. This advantage is balanced by the drawback of increasing the auxiliary energy consumption due to the vacuum system. Finally, the so

high auxiliary consumption is attributable the vacuum system and the flow circulation through the system.

- Limited PR values. High temperature gradients across the membrane result in increasing the vapour flux but reducing the PR. For an exemplary case with top temperature of 95ºC, the following maximum PR may be obtained at different transmembrane gradients:

  PR= 2.0, $\Delta T \cong$ 25ºC

  PR= 4.1, $\Delta T \cong$ 15ºC

  PR= 6.6, $\Delta T \cong$ 10ºC

  PR= 13.8, $\Delta T \cong$ 5ºC

  Note that calculated performance ratios are maximum values since hypothesis of negligible heat losses across the membrane is assumed. In addition note that temperature gradients as low as 5ºC may result in excessive membrane area required for a commercial MD module.

Section 3 proves that the limited energy efficiency of MD systems in based on the thermodynamic concepts of generating vapor from a vapor pressure difference, thus inherent to the MD process. This energy efficiency can be improved by:

- Increasing the maximum temperature of operation up to the limits recommended by the membrane manufacturer. In addition, due to the existing chemical pretreatments, temperatures over 105ºC may require physical pretreatment on nanofiltration, as in conventional MSF plants. The main drawback of using nanofiltration is the increasing of auxiliary consumption of the overall desalination process. Therefore, the use of such high temperatures does not seem an opportunity of development in spite of the development of membrane technology might permit it.

- Reduction of transmembrane temperature gradients in DCMD, AGMD and LGMD. Literature reports on transmembrane gradients of 5 K, published by ISE-Fraunhofer [Wieghaus et al, 2008]. This value has low potential of improvement, attributable to the following reasons:
  - Temperature gradient is the sum of the gradients across the following components: feed channel, membrane, condenser plate and cooling channel.
  - The temperature gradient should also compensate the effect of the BPE.
  - Since the low temperature gradients the high the membrane area required, even if at laboratory scale gradients near the conceptual limits can be achieved, the cost effectiveness of the module would make recommendable designs based on higher gradients.

Finally, with regard to Memsys concept, the vapor generation is similar to a conventional MED process, which is able to operate with 2.5ºC of temperature difference between adjacent effects. Nevertheless, at such a low temperature gradients, membrane would not be able to operate. Therefore, at the same top temperature, conventional MED process is much more efficient than Aquavert systems, thus the latter only could compete only in low-capacity desalination applications.

# 6. MD TECHNOLOGY IN SEAWATER DESALINATION: OPPORTUNITIES VERSUS COMPETING TECHNOLOGIES

Having regard that MD is a developing technology, capital costs are assumed to be highly variable, and probably when fully developed, cost trends might reach that of other distillations systems. Therefore, the future prospect assessment emphatics other aspects.

In order to assess the future prospects of MD technology, let´s consider four ranges of fresh water demand. Based on the analysis reported in previous sections the opportunities of technology development are pointed out. Finally, the comparison to competitor technologies results in identifying future prospects.

### 6.1. Plant capacity greater than 20.000 $m^3/d$

The first capacity range considered corresponds to large plants with nominal capacity over 20.000 $m^3/d$. The most important feature of the technology in such large plants is capital cost as much as energy efficiency. The Sea Water Reverse Osmosis (SWRO) technology is consolidated nowadays as the dominant technology in new contracted plants, even in markets traditionally dominated by distillation technologies.

Even if MD systems adopt in future more efficient designs based on multistage concept or multieffect concept of Aquaver´s systems -, efficiency limitations of such designs are the same of current MSF or MED technologies. Besides that, although the superior ability of MD systems on treating high concentrated brines in comparison to MED and MSF units has been demonstrated, this do not compensate the much lower efficiency versus RO systems. Moreover, even if costs of MD would decrease below that of SWRO systems, the lack of maturity of MD technology would be a huge drawback in the large plant market.

### 6.2. Intermediate capacity, ranged between 20.000 $m^3/d$ and 1.000 $m^3/d$

Conventional distillation plants integrated in power cycles (dual purpose plants) are not able to compete with SWRO in these days. Differences in capital costs are even more favourable for SWRO than in higher capacities. Note that the demineralised water required in the power cycle can be obtained by apply further treatment to the SWRO permeate. Therefore, distillation does not offer any advantage. It should be also highlighted that the heat rejection of the power cycle avoided due to the integration of a distillation plant is similar to heat power rejection required for the distillation unit – see eq. 5-. Therefore, this issue is not a reason in favour of distillation integrated in power cycles.

In case of waste heat is available at temperatures around 70ºC, distillation may have an opportunity. It should be take into account that at the same top temperature MED process with current technology is able to achieve higher PR than MD or MSF processes. Therefore, in principle there would be no opportunity for MD technology.

Due to high capital costs, demands of solar thermal-driving systems in this capacity range are not probable since they are not able to compete with PV-SWRO systems – see chapter 1. Moreover, in coastal areas, frequently exploitable wind resources are available, thus resulting in the highest opportunities of wind-powered desalination.

### 6.3. Small capacity, ranged between 1.000 $m^3/d$ and 10 $m^3/d$

Since MED and MSF are no modular systems, their capital costs significantly increases as plant capacity decreases. Therefore, the range between 1.000 $m^3$/d and 10 $m^3$/d is even less favourable for conventional distillation in comparison to SWRO. This is the typical range of capacity of demanding renewable energy-driven systems. This is attributable to the lack of electrical grid or problems of fuel supply to electricity generation by means of combustion engines. If suitable for the plant location, wind-SWRO technology is the best option.

Near the upper limit MD has no opportunity versus solar thermal SWRO systems based on organic Rankine cycles or solar photovoltaic SWRO – see chapter 1. Both of them can be designed as autonomous solar system without conventional energy backup. On the other hand, the opportunities of MD increase as plant capacity decreases. This is due to the small demands typical of isolated regions with difficult access to chemicals or fuel supplies, and with no availability of skill workers. Next subsection highlights the benefits of MD in these kind of remote areas.

Within this capacity range, applications of MD to crystalize some salts with economic value could be important in order to promote socioeconomic development, in addition to achieve the Zero Liquid Discharge (ZLD) concept in the desalination process.

### 6.4. Very small plant capacities below 5-10 $m^3$/d

The lowest fresh water demands gives an excellent opportunity of developing MD systems, since the simplicity of operation and maintenance together with low chemical consumption are important features for a desalination system at such a low plant capacity. In this case, the efficiency of the systems is not so important issue. Therefore, the use of waste heat could be reasonable, even with low temperature of operation. In this case, the low efficiency of the system is balanced with the nil energy cost and low values of driving force should be compensated by higher membrane area in order to achieve the target mass flow rate.

Moreover, the simplicity of installing stationary solar collectors for driving an autonomous solar desalination system and the demonstrated ability of unattended operation of MD technology is important in remote locations. Finally, the experience of long-term operation acquired in the ITC during years of operation at variable working conditions with the existing solar autonomous MD system shows that MD could compete with mature technologies – i.e. solar photovoltaic-RO - at very small capacity. Solar-driving MD systems seem to be the most simple solar desalination systems in which the solar conversion and the

desalination processes are not integrated in the same device. Integrated devices as solar stills are not considered since their PR is extremely low, around 1.

# 7. PROSPECT ASSESSMENT OF MD TECHNOLOGY APPLIED TO BRINE CONCENTRATION

Ability of MD systems to treat high concentrated saline solutions has been demonstrated at laboratory scale in order to be coupled to a conventional seawater desalination plant. There is a potential interest of brine concentration in both, large and small capacity plants. In addition to achieving low auxiliary consumption by increase recovery rate, the economic value of some seawater component that could crystallize should be taking into account. Moreover, an MD system can be operated in batches, which could be an advantage in designing brine treatment systems.

Based on aforementioned expectative, a literature survey was carried out. Science Direct reports on around thirty documents, some of them focused on salt crystallization by using MD technology as part of the solvent extraction processes. They are summarised as follows.

It is remarkable research conducted by Drioli *et al*, Ge *et al* (2014), Chen and Fane (2014), Creusen *et al.* (2013, 2012), Edwie and Chung (2013), Macedonio *et al.* (2013), Ji *et al* (2010), Mariah *et al* (2006). Other authors proposed MD for crystallyzation in industrial water treatment [Wu *et al*, 1991][Tun and Groth, 2011].

Macedonio et al (2013) reports on the potential economic benefits of recovering specific components from brines and analyses the modelling of this process. Mariah *et al* (2006) analysed the driving force for precipitation of specific salts existing in sea salt solutions by means of experimental test campaigns of transmembrane flux and modelling. They used two concentrated solutions of mixed electrolytes, $MgSO_4$ and NaCl with concentrations of 225 - 225 g/L, and 275 - 137.5 g/L, respectively. Ji et al (2010) conducted experimental research with RO brines being treated by MD. They reported an overall recovery ratio of 90%. Besides that, Creusen et al (2013) analysed the total solvent extraction from seawater – see figure 2.9 -. They estimated a product cost of 1€/$m^3$. Besides that, Ge et al (2014) analysed $CaSO_4$ crystallisation, and the crystal formation on the membrane surface.

Figure 2.10 presents the experimental system described by Mariah *et al* (2006), in which the feed tank stores the crystals.

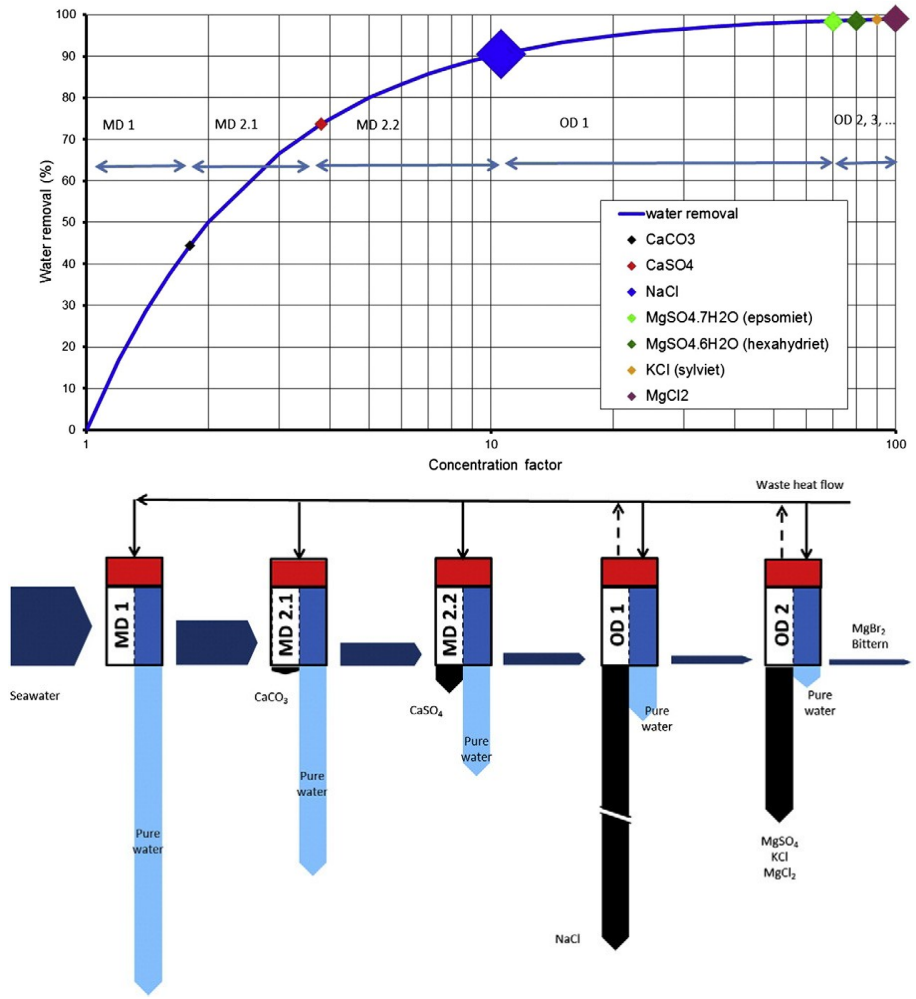


**Figure 2.9. Salt removal from seawater during evaporation. The symbols are placed at the concentration factor where crystallization starts and their size is an indication for the amount of salt that crystallizes [Creusen et al, 2013].**

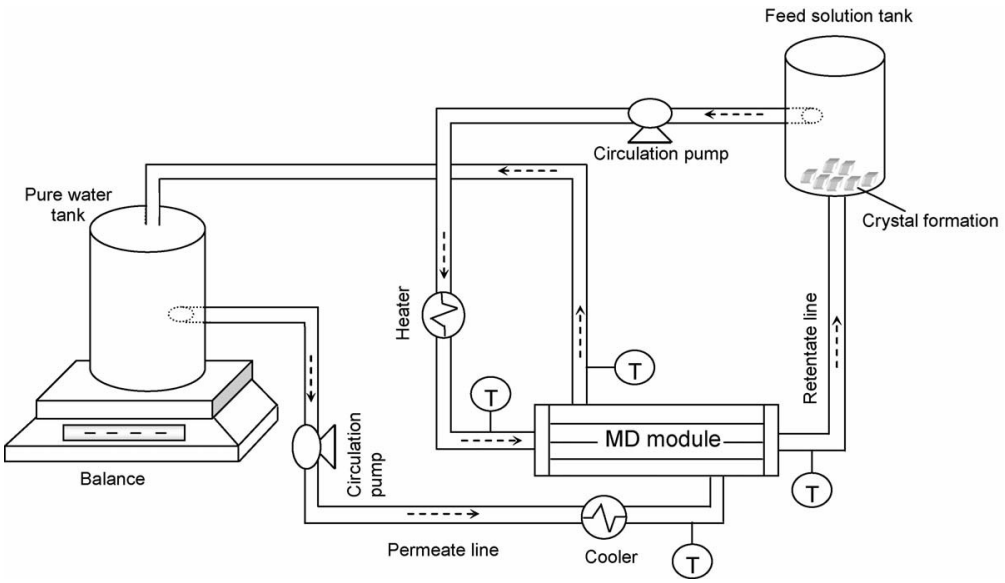


**Figure 2.10. Scheme of the experimental system described by Mariah *et al* (2006).**

Concerning transmembrane flux, values of around 6 L/($m^2$·h) were obtained by Creusen *et al* (2012) with almost saturated aqueous solution of NaCl. The flux exhibits a decreasing when salt crystallization starts. Therefore, crystallization on the membrane surface should be avoided. Besides that, Edwie and Chung (2012, 2013) proposed MD process to obtain the simultaneous production of both, pure water and crystals. Periods of 5000 min at stable membrane performance are achieved by keeping the transmembrane flux below a given limit (critical flux). Transmembrane flux between 2 and 9 kg/($m^2$·h) are reported.

Membranes were also analysed focused on salt crystallization. In order to improve the fouling resistance of membrane at operation conditions with high concentration feed, Meng et al (2014) tested nano-composite PVDF membranes in which the membrane surface was modified. The improving of antifouling membrane behaviour was demonstrated. Besides, Meng et al (2015) analysed superhydrophobic capillary membranes, in which the rate of deposition was found lower than that in hydrophobic membranes. Moreover, crystal removing is easy in superhydrophobic membranes. Advances in membranes based on using nano-materials in order to increase hydrophobicity [Prince *et al,* 2012] may result in reliable MD systems to treat brines from RO and conventional distillation processes.

# 8. CONCLUSIONS

The basic concepts of seawater desalination by means of MD have been studied. The existing MD configurations and pre-commercial and commercial MD systems have been reviewed. The performance of those systems have also been analysed based on experimental data from tests performed by independent researchers.

A detailed thermodynamic analysis of seawater desalination based on MD technology has been carried out to understand the physical phenomena, the driving forces of the process and to identify and quantify the theoretical limits of the technology. The main conclusions from this analysis are:

- Low energy efficiency of the conceptual process, since theoretical performance ratios (PR) at conventional operating conditions (T ≤85ºC) range from 6.5 to 8.7 (Table 2.2), in line to what has been tested for commercial available modules (Table 2.1), and far away from other thermal seawater desalination technologies such as MED, with actual PR> 8. If temperature gradient across the membrane as low as 5ºC is achieved, which is difficult due to the boiling point elevation (0.7ºC at 85ºC for seawater salinity – Fig.2.2 -), the theoretical limit is PR= 9.5.

- High potential of improving the existing MD systems, since it is a technology in development phase and most of the R&D efforts so far have been focused in the module design, but there is still a high potential of improving the system design. Temperature gradients across the membrane as low as 5ºC has been achieved, therefore increasing the efficiency up to PR of the order of 8-10 is possible.
- Limited production capacity of existing commercial products, as tested in commercial available modules with distillated fluxes in the range of 1 to 6.5 L/(h·m$^2$) (Table 2.1), far away from other membrane seawater desalination technologies such as RO (with average permeate fluxes in the range of 14 L/(h·m$^2$).
- High auxiliary energy consumption, as has been reported in literature and accordingly to high mass flow rate of seawater required to obtain unitary product flow.

While the limited production capacity could be improved by advanced MD configuration, the low energy efficiency of the process is a real barrier for MD technology.

Having in mind other existing and well proven technologies, such as MED and RO, potential applications of MD technology in seawater desalination have been assessed. The main conclusion is that for medium and large seawater desalination systems, the low energy efficiency and limited production capacity of MD technology make it not competitive at all. On the other hand, the technology may be applied for small seawater desalination systems where the two handicaps of MD technology may be irrelevant compared to other advantages it has, such as simple pretreatment and process control, low maintenance requirements and its conceptual ability to be coupled with solar thermal energy. Thus, a specific application of MD technology would be small autonomous solar thermal seawater desalination systems but competing with PV or wind powered RO seawater desalination systems.

For small and medium size seawater desalination systems where Zero Liquid Discharge (ZLD) is demanded, MD technology offers the possibility to concentrate the brine coming from the desalination plant to levels that other technologies can not simply reach. However, this application of MD technology is not recommended.

## 9. REFERENCES


1. Al-Obaidani, S.; Curcio, E.; Macedonio, F.; Di Profio, G.; Al-Hinai, H., and Drioli, E. Potential of membrane distillation in seawater desalination: Thermal efficiency sensitivity study and cost estimation. *Journal of Membrane Science*, 323, 2008, pp. 85-98.
2. Blanco Gálvez, J.; García-Rodríguez, L., and Martín-Mateos, I. *Stand-Alone Seawater Desalination by Innovative Solar-Powered Membrane-Thermal Distillation System:*

*MEDESOL project.* Desalination, 246, 2009, pp. 567-576.

3. Buenaventura, A and García-Rodríguez, L. *Solar thermal-powered desalination: A viable solution for a potential market.* Desalination, 435, 2018, pp. 60-69.
4. Creusen, R.; van Medevoort, J.; Roelands, M.; van Renesse van Duivenbode, A.; Hanemaaijer, J. H., and van Leerdam, R., Integrated membrane distillation–crystallization: Process design and cost estimations for seawater treatment and fluxes of single salt solutions, Desalination, 323, 2013, pp. 8-16, ISSN 0011-9164, http://dx.doi.org/10.1016/j.desal.2013.02.013.
5. Creusen, R. J. M.; van Medevoort, J.; Roelands, C.P.M.; van Renesse van Duivenbode, J.A.D. *Brine Treatment by a Membrane Distillation-crystallization (MDC) Process*, Procedia Engineering, 44, 2012, pp. 1756-1759, ISSN 1877-7058, http://dx.doi.org/10.1016/j.proeng.2012.08.937.
6. Chen, G.; Lu, Y.; Krantz, W. B.; Wang, R., and Fane, A. G., Optimization of operating conditions for a continuous membrane distillation crystallization process with zero salty water discharge, Journal of Membrane Science, 450, 2014, pp. 1-11. ISSN 0376-7388, http://dx.doi.org/10.1016/j.memsci.2013.08.034.
7. Ding, Z; Ma, R., and Faneb, A.G.. A new model for mass transfer in direct contact membrane distillation. Desalination 15l (2002) 2 17-227
8. Edwie, F., and Chung, T. S., Development of hollow fiber membranes for water and salt recovery from highly concentrated brine via direct contact membrane distillation and crystallization, Journal of Membrane Science, 421–422, 2012, pp. 111-123. ISSN 0376-7388, http://dx.doi.org/10.1016/j.memsci.2012.07.001.
9. Edwie, F., and Chung, T.-S., *Development of simultaneous membrane distillation–crystallization (SMDC) technology for treatment of saturated brine*, Chemical Engineering Science, 98, 2013, pp. 160-172, ISSN 0009-2509, http://dx.doi.org/10.1016/j.ces.2013.05.008.
10. García-Rodríguez, L., *"Destilación por membranas para tratamientos de agua de mar o concentrados de sales marinas"*, Informe personal: apuntes del Máster Universitario en Sistemas de Energía Térmica (Curso 2013-2014).
11. Ge, J.; Peng, Y.; Li, Z.; Chen, P., and Wang, S., *Membrane fouling and wetting in a DCMD process for RO brine concentration*, Desalination, 344, 2014, pp. 97-107. ISSN 0011-9164, http://dx.doi.org/10.1016/j.desal.2014.03.017.
12. González, D.; Amigo, J., and Suárez, F. Membrane distillation: Perspectives for sustainable and improved desalination. *Renewable and Sustainable Energy Reviews*, 80, 2017, pp. 238-259.
13. Guillén Burrieza, E.; Blanco, J.; Zaragoza, G.; Alarcón, D.C.; Palenzuela, P., and Ibarra, M. *Experimental analysis of an air-gap membrane distillation solar desalination pilot system.* Journal of Membrane

14. Hanbury, W. T., and Hodgkiess, T. *Membrane distillation- An assessment.* Desalination, 56, 1985, pp. 287-297.

15. Hanemaaijer, J. H.. van Medevoort, J.; Jansen, A. E. ; Dotremont, C.; van Sonsbeek, E.; Yuan, T., and De Ryck, L.. Memstill membrane distillation – a future desalination Technology. Desalination, 199, 2006, pp. 175–176.

16. Hanemaaijer, Jan H.. Memstill® low cost membrane distillation technology for seawater desalination. Desalination, 168, 2004, p. 355.

17. Ji, X.; Curcio, E.; Al Obaidani, S.; Di Profio, G.; Fontananova, E., and Drioli, E., *Membrane distillation-crystallization of seawater reverse osmosis brines*, Separation and Purification Technology, 71(1), 2010, pp. 76-82. ISSN 1383-5866, http://dx.doi.org/10.1016/j.seppur.2009.11.004.

18. Memsys http://www.memsys.eu/technology/membrane-distillation-technology.html (Last visit, 2017).

19. Kullab, A.; Liu, C., and Martin, A. Solar Desalination Using Membrane Distallation – Technical Evaluation Case Study, International Solar Energy Society Conference, Orlando, FL, August 2005.

20. Macedonio, F.; Quist-Jensen, C. A.; Al-Harbi, O.; Alromaih, H; Al-Jlil, S. A.; Al Shabouna, F, and Drioli, E. *Thermodynamic modeling of brine and its use in membrane crystallizer.* Desalination, 323, 2013, pp. 83-92.

21. Mariah, L.; Buckley, C. A.; Brouckaert, C. J.; Curcio, E.; Drioli, E., Jaganyi, D., and Ramjugernath, D., *Membrane distillation of concentrated brines—Role of water activities in the evaluation of driving force,* Journal of Membrane Science, 280(1–2), 2006, pp. 937-947. ISSN 0376-7388, http://dx.doi.org/10.1016/j.memsci.2006.03.014.

22. Meindersma, G. W.; Guijt, C. M., and de Haan, A. B. Desalination and water recycling by air gap membrane distillation. Desalination 187 (2006) 291–301.

23. Meng, S.; Ye, Y.; Mansouri, J., and Chen, V., Fouling and crystallisation behaviour of superhydrophobic nano-composite PVDF membranes in direct contact membrane distillation, Journal of Membrane Science, 463, 2014, pp. 102-112, ISSN 0376-7388, http://dx.doi.org/10.1016/j.memsci.2014.03.027.

24. Meng, S.; Ye, Y.; Mansouri, J., and Chen, V., Crystallization behavior of salts during membrane distillation with hydrophobic and superhydrophobic capillary membranes, Journal of Membrane Science, 473, 2015, pp. 165-176, ISSN 0376-7388, http://dx.doi.org/10.1016/j.memsci.2014.09.024.

25. Prince, J.A.; Singh, G.; Rana, D.; Matsuura, T.; Anbharasi, V., and Shanmugasundaram, T.S., Preparation and characterization of highly hydrophobic poly(vinylidene fluoride) – Clay nanocomposite nanofiber membranes (PVDF–clay NNMs) for desalination using direct contact membrane distillation, Journal of Membrane Science, 397–398, 2012, pp. 80-86, ISSN 0376-7388, http://dx.doi.org/10.1016/j.memsci.2012.01.012.

26. PSA (Plataforma Solar de Almería, CIEMAT). http://www.psa.es/projects/medesol.

27. Ruiz Aguirre, A.; Alarcón-Padilla, D. C., and Zaragoza, G. *Productivity analysis of two spiral-wound Membrane distillation prototypes coupled with solar energy* European Desalination Society Conference, Chipre, 2014.

28. Ruiz Aguirre, A.. *Evaluación de sistemas comerciales de espiral de destilación por membranas y su aplicación al tratamiento de aguas.*. University of Almería, Spain, 4/07/2017. Supervisors: G. Zaragoza y J.M. Fernández Sevilla.

29. SCARAB – www.scarab.se – (Last visit 01/2015).

30. Tun, C. M., and Groth, A. M. Sustainable integrated membrane contactor process for water reclamation, sodium sulfate salt and energy recovery from industrial effluent, Desalination, 283, 2011, pp. 187-192, ISSN 0011-9164, http://dx.doi.org/10.1016/j.desal.2011.03.054.

31. Vega-Beltrán, J. C.; García-Rodríguez, L.; Martín-Mateos, I., y Blanco Gálvez, J. *Solar membrane distillation: theoretical assessment of multi-stage concept.* Presented at the EDS (European desalination Society Conference, Baden-Baden, 17-20 may, 2009, and published in *Desalination and Water Reuse,* 18, 2010, pp. 133-138.

32. WHO/UNICEF 2012, Progress on drinking water and sanitation 2012 update.

33. Wieghaus, M.; Koschikowski, J., and Rommel, M., *Solar desalination for a water supply in remote areas with poor grid connection.* Proceedings of the 2nd International Conference on Renewable Energies and Water Technologies, CIERTA 2008, October, 2nd-3rd, 2008, Almería, Spain. pp.13-24.

34. Wu, Y.; Kong, Y.; Liu, J.; Zhang, J., and Xu, J., An experimental study on membrane distillation-crystallization for treating waste water in taurine production, Desalination, 80(2–3), 1991, pp. 235-242, ISSN 0011-9164, http://dx.doi.org/10.1016/0011-9164(91)85160-V.

35. Zaragoza, G.; Ruiz-Aguirre, A., and Guillén-Burrieza, E. *Efficiency in the use of solar thermal energy of small membrane desalination systems for decentralized water production.* Applied Energy, 130, 2014, pp. 491-499.

# Chapter 3. BASIC CONCEPTS ON SEAWATER REVERSE OSMOSIS DESALINATION

A summary of this chapter will be submitted for publication to the international journal *Desalination* with the following authors, title and abstract:

**Authors:** Arturo Buenaventura Pouyfaucon[(1)] and Lourdes García-Rodríguez[(2)]

[(1)]Abengoa– Spain. C/ Energía Solar, nº1. 41014- Sevilla. abuenaventura@abengoa.com

[(2)]Dpto. Ingeniería Energética. Universidad de Sevilla. ETSI, Camino de Los Descubrimientos, s/n. 41092-Sevilla. mgarcia17@us.es

Title: *Sea Water Reverse Osmosis: Towards 1 kWh/m$^3$ of Specific Energy Consumption*

# 1. INTRODUCTION

This chapter deals with the thermodynamic assessment of Sea Water Reverse Osmosis (SWRO) desalination with the main objective of assessing the milestone of Specific Energy Consumption (SEC) of 1 kWh/m$^3$ set by the H2020 [EC, 2015]. To this end, the minimum SEC inherent to the state-of-the-art of the SeaWater Reverse Osmosis (SWRO) desalination technology is analysed. Not only configurations normally used are considered, but also innovative proposals from the literature. The minimum SEC´s technically achievable by adopting different configurations are comparatively analysed in order to assess the actual prospects to achieve values as low as 1 kWh/m$^3$.

First of all, table 3.1 shows exemplary [Wilf, 2007] cases of seawater composition, pH and temperature in order to understand the influence of plant location. Reference Composition of seawater and apparent molar mass of solutes ($62.808 \cdot 10^{-3}$ kg/mol) are given in table 3.2. Besides that, the composition referred to as Standard Seawater corresponds to 0.03516504 kg/kg of mass fraction [Millero *et al*, 2008]. Finally, a few data on extreme seawater conditions are reported by Sharqawy *et al*, (2010) namely, the shores lines of Kuwait and Saudi Arabia, 50 g/kg - g (salts)/kg (seawater) -; Australian Shark Bay, 70 g/kg, or desiccating seas like Dead Sea with salt content approaching saturation concentration.

**Table 3.1 Exemplary cases of seawater composition in a number of plant locations [Wilf, 2007].**

| Constituent | Mediterra-nean | Persian Gulf | Read Sea | Caribbean | Pacific | Atlantic | Canary Islands |
|---|---|---|---|---|---|---|---|
| Temperature | 14ºC, 28ºC | 16ºC, 34ºC | 16ºC, 26ºC | 26ºC | 20ºC | 20ºC | 22ºC |
| pH | 8.1 | 7.0 | 7.8 | 8.2 | 8.0 | 8.0 | 7.8 |
| $Ca^+$, ppm | 483 | 478 | 500 | 477 | 440 | 410 | 464 |
| $Mg^+$, ppm | 1557 | 1672 | 1540 | 1160 | 1300 | 1302 | 1526 |
| $Na^+$, ppm | 12200 | 14099 | 13300 | 11322 | 10200 | 10812 | 11700 |
| $K^-$, ppm | 481 | 530 | 490 | 386 | 380 | 389 | 429 |
| $CO_3^-$, ppm | 5 | 4.2 | 2.3 | 2.3 | 2.0 | 2.0 | 3.2 |
| $HCO_3^-$, ppm | 162 | 154 | 126.8 | 137 | 170 | 143 | 204 |
| $SO_4^{2-}$, ppm | 3186 | 3314 | 3240 | 2600 | 3000 | 2713 | 3059 |
| $Cl^-$, ppm | 22599 | 24927 | 23180 | 20034 | 18500 | 19441 | 21344 |
| $F^-$, ppm | 1.4 | - | - | - | - | - | - |
| $NO_3^-$, ppm | - | - | - | - | - | - | - |
| $B^+$, ppm | 5 | 5 | 5.3 | 5.3 | 4.5 | 4.5 | 4.5 |
| $SiO_2$, ppm | 1.6 | - | - | - | - | - | - |
| **TDS, ppm** | **40686** | **45199** | **42389** | **36149** | **34000** | **35240** | **38739** |

**Table 3.2 Reference Composition of seawater [Millero *et al*, 2008].**

| Solute, $i$ | $10^7\ X_i$ (Definition) | $X_i\ A_i$ | $W_i$ |
|---|---|---|---|
| | Properties of sea salt of Reference Composition | | |
| $Na^+$ | 4 188 071 | 9.6282786 | 0.3065958 |
| $Mg^{2+}$ | 471 678 | 1.1464134 | 0.0365055 |
| $Ca^{2+}$ | 91 823 | 0.3680082 | 0.0117186 |
| $K^+$ | 91 159 | 0.3564162 | 0.0113495 |
| $Sr^{2+}$ | 810 | 0.0070972 | 0.0002260 |
| $Cl^-$ | 4 874 839 | 17.2827667 | 0.5503396 |
| $SO_4^{2-}$ | 252 152 | 2.4222377 | 0.0771319 |
| $HCO_3^-$ | 15 340 | 0.0935998 | 0.0029805 |
| $Br^-$ | 7520 | 0.0600878 | 0.0019134 |
| $CO_3^{2-}$ | 2134 | 0.0128059 | 0.0004078 |
| $B(OH)_4^-$ | 900 | 0.0070956 | 0.0002259 |
| $F^-$ | 610 | 0.0011589 | 0.0000369 |
| $OH^-$ | 71 | 0.0001208 | 0.0000038 |
| $B(OH)_3$ | 2807 | 0.0173565 | 0.0005527 |
| $CO_2$ | 86 | 0.0003785 | 0.0000121 |
| Sum | 10 000 000 | 31.4038218 | 1.0000000 |
| $H_2O$ | | | |
| Sum | | | |

$10^7\ X_i$ (Definition)—$10^7$ times the mole fractions of the Reference Composition (from Table 3).
$X_iA_i$—the atomic weight of each component weighted by its mole fraction. Note the sum of this column is the average atomic weight of sea salt, $\langle A \rangle$, 31.4038218… $g\,mol^{-1}$.
$W_i$—mass fractions of sea salt (grams of a particular solute/grams of total solute).

After this brief introduction, section 2 focuses on the thermodynamic analysis of a basic desalination process at given temperature and pressure. The absolute minimum energy consumption of the process is calculated in section 3. Also the case study of SWRO desalination is analysed in section 4, to obtain its actual minimum work required. Based on the aforementioned analyses, future prospects of reducing energy consumption in SWRO desalination plants are discussed in section 5. In section 6 a recap of the results obtained and a comparison with the target of 1 kWh/m$^3$ is presented.

## 2. THERMODYNAMIC ANALYSIS OF A DESALINATION PROCESS

Figure 1.1 depicts the diagram of a basic desalination process within a control volume at steady state. There is a single inlet flow of saline solution (Feed, F) and two outlet flows, a low concentration solution (Product, P) and a high concentration solution (Blowdown, BD). The control volume consumes useful power, $P_W$, from a work source and interchanges thermal power,

$P_Q$, with the ambient. If the product of the process is approximately pure water, desalination becomes a solvent extraction process.

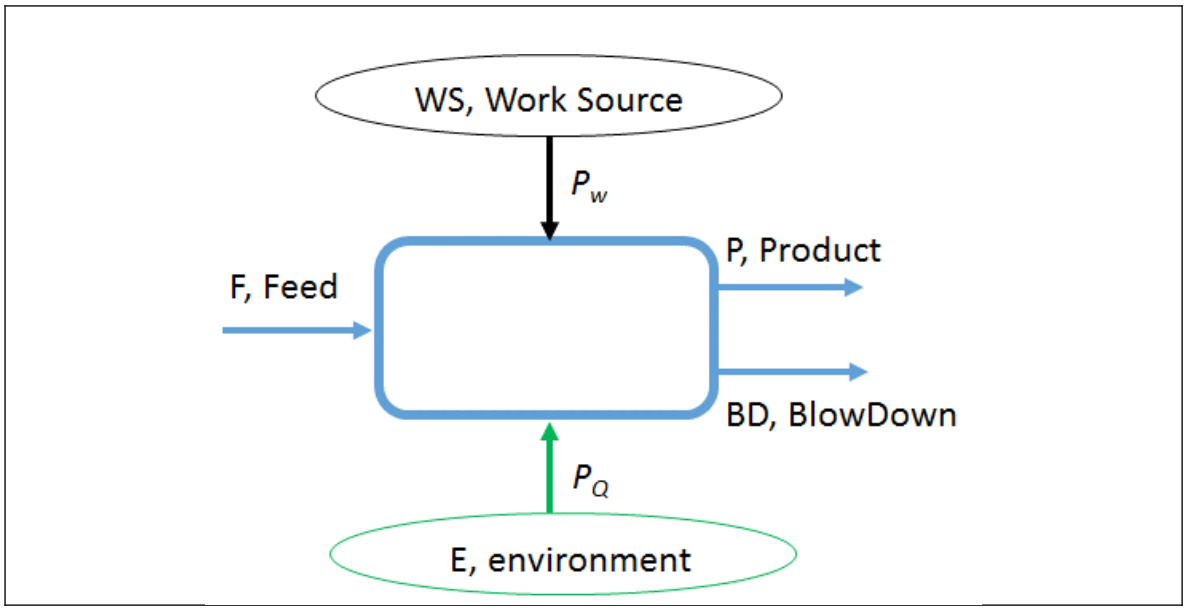


**Figure 3.1. Basic process of desalination.**

Equations related to mass balances and changes of extensive thermodynamic quantities are summarized in tables 3.3-3.5. Table 3.3 also includes definitions of quantities related to mass balances and salt concentration. Two points should be make clear concerning table 3.3:

- In table 3.3 two different definitions of recovery rate are provided to express the flow ratio of product and feed. In the literature both of them are used, referred to as "r". In order to avoid misunderstandings in this text a subscript is added, either "V" or "m" depending on the ratio used, namely, volumetric or mass flow rate respectively. In any case, both values are approximately equal.

- Salinity, S, used in this text corresponds to the definition of "Reference Salinity" given by Millero *et al* (2008) - a referent author in the field of seawater properties -: "the mass fraction of dissolved material in seawater", therefore,

  $$S = 35\frac{g}{kg} = 35\frac{mg}{g} = 0.035\frac{kg}{kg} = 0.035 = 3.5\,\% = 35\,000\,ppm = 35\,000\,mg/kg$$

  Besides that, 0.062808 kg/mol is the molar mass of sea salts (considered as a whole).

**Table 3.3. Mass balances in a desalination process – see figure 3.1 – and related parameters under the assumption that no salt precipitation occurs.**

| | |
|---|---|
| Mass balances: | Solvent: $q_{w,P}+q_{w,BD}=q_{w,F}$<br>Solute: $q_{s,P}+q_{s,BD}=q_{s,F}$<br>Where $q$ is the mass flow rate, $q=\frac{dm}{dt}$, and subscripts $w$ and $s$ mean water and salts, respectively. Other subscripts are Feed, F; Product, P, and BlowDown, BD.<br>Global balance: $q_P+q_{BD}=q_F$ (solvent + solute balances) |
| Recovery rate, $r$ | $r_m=\frac{q_P}{q_F}$<br>$\frac{q_F}{q_P}=\frac{1}{r_m};\frac{q_{BD}}{q_P}=\frac{q_F-q_P}{q_P};\frac{q_{BD}}{q_P}=\frac{1}{r_m}-1$<br>In the desalination literature, $r_m$ is usually assumed to be:<br>$r_m\approx\frac{q_{V,P}}{q_{V,F}}$, where $q_V=\frac{dV}{dt}$ is the flow (or volumetric flow)<br>$r_V=\frac{q_{V,P}}{q_{V,F}};\quad r_V=\frac{q_P/\rho_P}{q_F/\rho_F};\quad r_V=r_m\cdot\frac{\rho_F}{\rho_P}$ |
| Salt concentration: | S, salinity – mass fraction of salts -, kg/kg: $S=\frac{m_s}{m_w+m_s}$<br>C, salt concentration – ratio between mass of salts and volume of solution -, kg/m$^3$ (normally expressed in mg/L): $C=\frac{m_s}{V}$<br>Related equations: $C=S\cdot\rho$<br>If the extraction of pure water is assumed: |

| | |
|---|---|
| | $S_{BD}=\frac{m_{s,BD}}{m_{s,BD}+m_{w.BD}}=\frac{m_{s,F}}{(m¿¿s,F+m_{w.F})-m_P=\frac{S_F}{1-r_m}¿}$ |

**Table 3.4. Change of extensive thermodynamic quantities in a desalination process: general equations - no salt precipitation is assumed -.**

| | |
|---|---|
| Change of an extensive quantity, Y: | Change of Y on a desalination process, $\Delta_{des} Y$:<br>$\Delta_{des} Y_{\square} = Y_P + Y_{BD} - Y_F$<br>Mass quantities:<br>$y = \frac{Y}{m}$ ; $\Delta_{des} y_{\square} = \frac{\Delta_{des} Y_{\square}}{m_P}$<br>Temporal change of Y to analyse an open system at steady state (fig.3.1): $\frac{dY}{dt} = \frac{dm}{dt} \cdot \frac{Y}{m} = q \cdot y$<br>$q_P \cdot \Delta_{des} y_{\square} = q_P \cdot y_P + q_{BD} \cdot y_{BD} - q_F \cdot y_F$<br>$\Delta_{des} y_{\square} = y_P + \frac{q_{BD}}{q_P} \cdot y_{BD} - \frac{q_F}{q_P} \cdot y_F$<br>Final expressions as a function of the recovery rate – see table 1 -:<br>$\Delta_{des} y_{\square} = y_P + \left( \frac{1}{r_m} - 1 \right) \cdot y_{BD} - \frac{1}{r_m} \cdot y_F$<br>$By\, adding \pm y_F, finally:_{\square}$<br>$\Delta_{des} y_{\square} = (y¿¿P - y_F) + \left( \frac{1}{r_m} - 1 \right) \cdot (y¿¿BD - y_F)¿¿$ |

**Table 3.5. Change of extensive thermodynamic quantities on a desalination process: particular equations - no salt precipitation is assumed -.**

| | |
|---|---|
| Enthalpy:<br>$\Delta H$ in J<br>$\Delta h$ in J/kg | $\Delta_{des} h = \frac{\Delta_{des} H}{m_P}$<br><br>$\Delta_{des} h = \Delta h_P + \left(\frac{1}{r_m} - 1\right) \cdot \Delta h_{BD} - \frac{1}{r_m} \cdot \Delta h_F$<br><br>$\Delta_{des} h = (\Delta h ¿¿ P - \Delta h_F) + \left(\frac{1}{r_m} - 1\right) \cdot (\Delta h ¿¿ BD - \Delta h_F) ¿¿$<br><br>Where $\Delta_{des}$ means change on a desalination process and $\Delta$ means difference from a reference state. |
| Entropy:<br>$\Delta S$ in J/K<br>$\Delta s$ in J/K/kg | $\Delta_{des} s = \frac{\Delta_{des} S}{m_P}$<br><br>$\Delta_{des} s = \Delta s_P + \left(\frac{1}{r_m} - 1\right) \cdot \Delta s_{BD} - \frac{1}{r_m} \cdot \Delta s_F$<br><br>$\Delta_{des} s = (\Delta s ¿¿ P - \Delta s_F) + \left(\frac{1}{r_m} - 1\right) \cdot (\Delta s ¿¿ BD - \Delta s_F) ¿¿$ |
| Flow exergy:<br>$Ex_f$ in J<br>$ex_f$ in J/kg | $\Delta_{des} ex_f = \frac{\Delta_{des} Ex_f}{m_P}$<br>$\Delta_{des} ex_f = ex_{f,P} + \left(\frac{1}{r_m} - 1\right) \cdot ex_{f,BD} - \frac{1}{r_m} \cdot ex_{f,F}$<br><br>Where: $ex_f = (\Delta h - \Delta h^E) - T^E \cdot (\Delta s - \Delta s^E)$<br>and superscript E means ambient conditions of temperature, pressure and seawater salt concentration.<br><br>If feed water is seawater at ambient conditions $ex_{f,F} = 0$<br><br>If $r_m = 0$; $S_{BD} \cong S_F$; $ex_{f,BD} \cong ex_{f,F} = 0$. Hence, $\Delta_{des} ex_f = ex_{f,P}$ |

Besides that, Thermodynamic Principles applied to this system result in equations given in table 3.6, as function of thermodynamic properties [Sharqawy *et al*, 2010] reported in tables 3.7-3.8. The mechanical power and the thermal power interchanged by the control volume are related to the change of entropy of the universe and exergy destruction per time unit, $dS_{\square}^{U}/dt$ and $P_x^D$, respectively.

**Table 3.6. Thermodynamic Principles applied to the desalination process depicted in figure 3.1.**

| | |
|---|---|
| First Principle: | $0 = P_Q + P_W - q_P \cdot \Delta h_P - q_{BD} \cdot \Delta h_{BD} + q_F \cdot \Delta h_F$<br><br>$0 = P_Q + P_W - \left(q_P \cdot \Delta_{des} h\right)$ |
| Second Principle: | $\frac{dS^U}{dt} = \frac{-P_Q}{T^E} + q_P \cdot \Delta s_P + q_{BD} \cdot \Delta s_{BD} - q_F \cdot \Delta s_F \geq 0$<br><br>$\frac{dS^U}{dt} = \frac{-P_Q}{T^E} + \left(q_P \cdot \Delta_{des} s\right) \geq 0$ |
| Exergy Balance: (Lineal combination: 1st Principle + $T^E$· 2nd Principle) | $0 = P_W - q_P \cdot ex_{fP} - q_{BD} \cdot ex_{fP} + q_F \cdot ex_{fF} - T^E \cdot \frac{dS^U}{dt}$<br><br>$0 = P_W - \left(q_P \cdot \Delta_{des} ex_f\right) - P_x^D$<br><br>where $P_x^D = T^E \cdot \frac{dS^U}{dt} \geq 0$<br><br>The exergetic performance of the process is defined as:<br>$\eta_{x,des} = \frac{q_P \cdot \Delta_{des} ex_f}{P_W^{\square}} \leq 1$<br><br>, being 1 if the process is reversible $\left(\frac{dS^U}{dt} = 0\right)$ |

Sharqawy *et al* (2010) obtained accurate correlations to calculate thermodynamic properties of seawater and in general of sea salt solutions. The reference state is saturated liquid water at triple point. Data of liquid water at 0.1 MPa were used to fit equations up to the normal boiling point. Upper temperatures were fit by means of properties at saturation pressure. Other authors proposed functions based on combining theoretical procedures and experimental data validation [Slesarenko and Shtim, 1989][Leyendekkers, 1976][García-Rodríguez, 1999][Safarov, 2012][Safarov, 2013].

**Table 3.7. Correlations of thermodynamic properties of pure water used in this work to calculate the thermodynamic analysis [Sharqawy *et al*, 2010].**

| |
|---|
| **Pure water density:** |
| Density:<br>$\rho_w = a_1 + a_2 t + a_3 t^2 + a_4 t^3 + a_5 t^4$<br>where<br>$a_1 = 9.999 \times 10^2, a_2 = 2.034 \times 10^{-2}, a_3 = -6.162 \times 10^{-3}, a_4 = 2.261 \times 10^{-5}, a_5 = -4.657 \times 10^{-8}$<br>Validity: $\rho_w$ in (kg/m$^3$); $0 \le t \le 180$ °C<br>Accuracy: ±0.01 % (best fit to IAPWS 1995 [24] data) |
| **Mass enthalpy of saturated pure water:** |
| **Specific saturated water enthalpy:**<br>$h_w = 141.355 + 4202.07 \times t - 0.535 \times t^2 + 0.004 \times t^3$<br>Validity: $h_w$ in (J/kg); $5 \le t \le 200$ °C<br>Accuracy: ±0.02% (best fit to IAPWS 1995 [24] data) |
| **Mass entropy of saturated pure water:** |
| **Specific saturated water entropy:**<br>$s_w = 0.1543 + 15.383 \times t - 2.996 \times 10^{-2} \times t^2 + 8.193 \times 10^{-5} \times t^3 - 1.370 \times 10^{-7} \times t^4$<br>Validity: $s_w$ in (J/kg K); $5 \le t \le 200$°C<br>Accuracy: ±0.1 % (best fit to IAPWS 1995 [24] data) |
| IAPWS 1995: International Association for the Properties of Water and Steam, Release on the IAPWS Formulation 1995 for the Thermodynamic Properties of Ordinary Water Substance for General and Scientific Use, 1996. |

**Table 3.8. Correlations of thermodynamic properties of seawater used in this work to calculate the thermodynamic analysis [Sharqawy *et al*, 2010].**

**Seawater density:**

$$\rho_{sw} = \left(a_1 + a_2 t + a_3 t^2 + a_4 t^3 + a_5 t^4\right) + \left(b_1 S + b_2 S\, t + b_3 S\, t^2 + b_4 S\, t^3 + b_5 S^2 t^2\right)$$

where

$a_1 = 9.999 \times 10^2$, $a_2 = 2.034 \times 10^{-2}$, $a_3 = -6.162 \times 10^{-3}$, $a_4 = 2.261 \times 10^{-5}$, $a_5 = -4.657 \times 10^{-8}$,
$b_1 = 8.020 \times 10^2$, $b_2 = -2.001$, $b_3 = 1.677 \times 10^{-2}$, $b_4 = -3.060 \times 10^{-5}$, $b_5 = -1.613 \times 10^{-5}$

Validity: $\rho_{sw}$ in (kg/m$^3$); $0 < t < 180$ °C; $0 < S < 0.16$ kg/kg
Accuracy: ±0.1 %

**Mass enthalpy of saturated seawater:**

$$h_{sw} = h_w - S\left(a_1 + a_2 S + a_3 S^2 + a_4 S^3 + a_5 t + a_6 t^2 + a_7 t^3 + a_8 S\, t + a_9 S^2\, t + a_{10} S\, t^2\right)$$

$a_1 = -2.348 \times 10^4$, $a_2 = 3.152 \times 10^5$, $a_3 = 2.803 \times 10^6$, $a_4 = -1.446 \times 10^7$, $a_5 = 7.826 \times 10^3$
$a_6 = -4.417 \times 10^1$, $a_7 = 2.139 \times 10^{-1}$, $a_8 = -1.991 \times 10^4$, $a_9 = 2.778 \times 10^4$, $a_{10} = 9.728 \times 10^1$

Validity: $h_{sw}$ and $h_w$ in (J/kg K); $10 \le t \le 120$ °C; $0 \le S \le 0.12$ kg/kg;
Accuracy: ±0.5 % from IAPWS 2008 [27]

**Mass entropy of saturated seawater:**

$$s_{sw} = s_w - S\left(a_1 + a_2 S + a_3 S^2 + a_4 S^3 + a_5 t + a_6 t^2 + a_7 t^3 + a_8 S\, t + a_9 S^2\, t + a_{10} S\, t^2\right)$$

$a_1 = -4.231 \times 10^2$, $a_2 = 1.463 \times 10^4$, $a_3 = -9.880 \times 10^4$, $a_4 = 3.095 \times 10^5$, $a_5 = 2.562 \times 10^1$
$a_6 = -1.443 \times 10^{-1}$, $a_7 = 5.879 \times 10^{-4}$, $a_8 = -6.111 \times 10^1$, $a_9 = 8.041 \times 10^1$, $a_{10} = 3.035 \times 10^{-1}$

Validity: $s_{sw}$ and $s_w$ in (J/kg K); $10 \le t \le 120$ °C; $0 \le S \le 0.12$ kg/kg
Accuracy: ±0.5 % from IAPWS 2008 [27]

IAPWS 2008: International Association for the Properties of Water and Steam, Release on the IAPWS formulation for the thermodynamic properties of seawater, available at www.iapws.org (2008).

Equations from table 3.6 are applicable in general to any desalination process represented by figure 3.1 if the blowdown concentration is lower than that of saturation. This is the usual case of any desalination technology normally used. The corresponding recovery rate to achieve the saturation of the blowdown, $r^{sat}$, is around 91% [García-Rodríguez, 1999, p.165]. In addition, in the case of extracting a very small part of the solvent the recovery rate is 0% from seawater with

ambient conditions of temperature, $T^E$, pressure, $p^E$, and salinity, $S^E$. Equation applicable to calculate the change of flow exergy is the following, adapted from García-Rodríguez (1999), as function of the solvent osmotic coefficient – Table 3.9 -:

$$\Delta_{0\%} ex_f\left(T^E, p^E, S^E\right) = R \cdot T^E \cdot \left(\frac{mol/kg}{31.4038218 \cdot 10^{-3}}\right) \cdot \left(\frac{S^E}{1-S^E}\right) \cdot \phi\left(T^E, p^E, S^E\right)$$

**Table 3.9. Correlations of solvent osmotic coefficient of seawater used in this work within the ranges of high and low salinities, respectively [Sharqawy *et al*, 2010].**

| |
|---|
| $\phi = a_1 + a_2 t + a_3 t^2 + a_4 t^4 + a_5 S + a_6 S t + a_7 S t^3 + a_8 S^2 + a_9 S^2 t + a_{10} S^2 t^2$ (49)<br>Present work based on Bromley's et al. [79] data<br>where<br>$a_1 = 8.9453 \times 10^{-1}, a_2 = 4.1561 \times 10^{-4}, a_3 = -4.6262 \times 10^{-6}, a_4 = 2.2211 \times 10^{-11}$<br>$a_5 = -1.1445 \times 10^{-1}, a_6 = -1.4783 \times 10^{-3}, a_7 = -1.3526 \times 10^{-8}, a_8 = 7.0132$<br>$a_9 = 5.696 \times 10^{-2}, a_{10} = -2.8624 \times 10^{-4}$<br>Validity: $0 \le t \le 200$ °C; $10 \le S \le 120$ g/kg<br>Accuracy: ±1.4 % |
| $\phi = 1 - \left[A \times B \times I^{1/2} + C \times I + D \times I^{3/2} + E \times I^2\right]$ (48)<br>where<br>$A = 20.661 - 432.579 / t_{68} - 3.712 \ln(t_{68}) + 8.638 \times 10^{-3} t_{68}$<br>$B = \frac{2.303}{I^{3/2}}\left[\left(1 + I^{1/2}\right) - 1/\left(1 + I^{1/2}\right) - 2\ln\left(1 + I^{1/2}\right)\right]$<br>$C = -831.659 + 17022.399 / t_{68} + 157.653 \ln(t_{68}) - 0.493\, t_{68} + 2.595 \times 10^{-4} t_{68}^2$<br>$D = 553.906 - 11200.445 / t_{68} - 105.239 \ln(t_{68}) + 0.333\, t_{68} - 1.774 \times 10^{-4} t_{68}^2$<br>$E = -0.15112$, $I = 19.915\, S_P / \left(1 - 1.00487\, S_P\right)$<br>Validity: $0 \le t_{68} \le 40$ °C; $0 \le S_p \le 0.04$ kg/kg<br>Accuracy: ±0.3 % |

# 3. THEORETICAL MINIMUM WORK OF SOLVENT EXTRACTION

In order to calculate the theoretical minimum work needed to a partial solvent separation from a seawater solution, the following hypothesis are required to apply the Thermodynamic principles – see table 3.10 -:

- First, work consumption is only that required to obtain the useful change of thermodynamic state, which is the change of salt concentration. Then, ambient temperature and pressure are assumed for feed, product and blowdown.

- Second, the desalination process is reversible. Then, nil exergy destruction is assumed.

Figures 3.2-3.3 are obtained from the calculation procedure described in table 3.9 to obtain the minimum net work required for partial solvent extraction at ambient temperature, $T^E$, and pressure, $p^E$, from seawater at ambient salinity, $S^E$, in J/kg:

$$P_{W,rev}/q_P = \Delta_{des} ex_f(T^E, p^E, S^E, r<r^{sat})$$

Alternatively, the SEC is usually expressed in terms of kWh/m$^3$:

$$P_{W,rev}/q_{V,P} = \rho_P \cdot \Delta_{des} ex_f(T^E, p^E, S^E, r<r^{sat})$$

The graphs depicted allow the analysis of the effects of temperature and salt concentration on the SEC of a reversible process of solvent extraction. In figure 3.2, the salinity of standard seawater (0.03516504 kg/kg [Millero, 2008]) is assumed. The effect of salt concentration is shown in figure 3.3.

**Table 3.10. Thermodynamic analysis of a reversible desalination process at ambient conditions.**

| | |
|---|---|
| First Principle: | General equation:<br>$0 = P_Q + P_W - q_P \cdot \Delta h_P - q_{BD} \cdot \Delta h_{BD} + q_F \cdot \Delta h_F$<br>Reversible process at ambient temperature and pressure:<br>$0 = P_{Q,rev} + P_{W,rev} - \left( q_P \cdot \Delta_{des} h \right)$ |
| Second Principle: | General equation:<br>$\frac{dS^U}{dt} = \frac{-P_Q}{T^E} + q_P \cdot \Delta s_P + q_{BD} \cdot \Delta s_{BD} - q_F \cdot \Delta s_F$<br>Reversible process at ambient temperature ($T^E$) and pressure:<br>$0 = \frac{-P_{Q,rev}}{T^E} + \left( q_P \cdot \Delta_{des} s \right)$ |
| Exergy Balance: | General equation:<br>$0 = P_W - q_P \cdot ex_{fP} - q_{BD} \cdot ex_{fBD} + q_F \cdot ex_{fF} - T^E \cdot \frac{dS^U}{dt}$<br>Reversible process at ambient temperature and pressure:<br>$0 = P_{W,rev} - \left( q_P \cdot \Delta_{des} ex_f \right)$ |

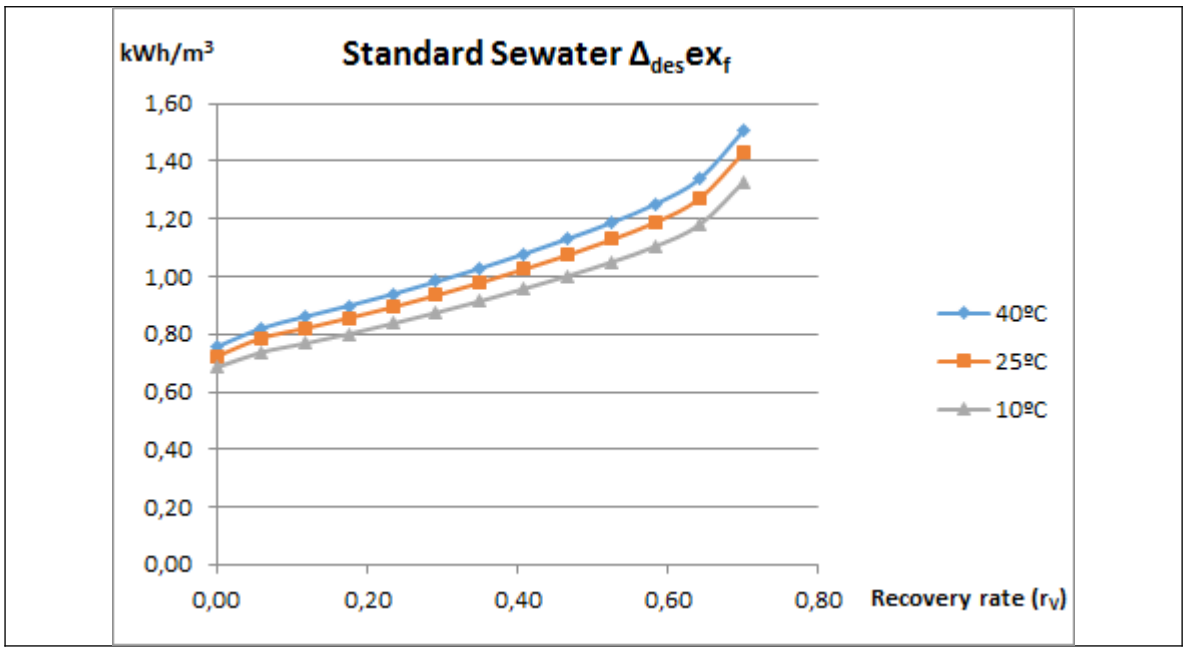


**Figure 3.2. Specific work required to obtain pure water from seawater (0.03510504 kg/kg) by means of a reversible desalination process at ambient temperature and pressure.**

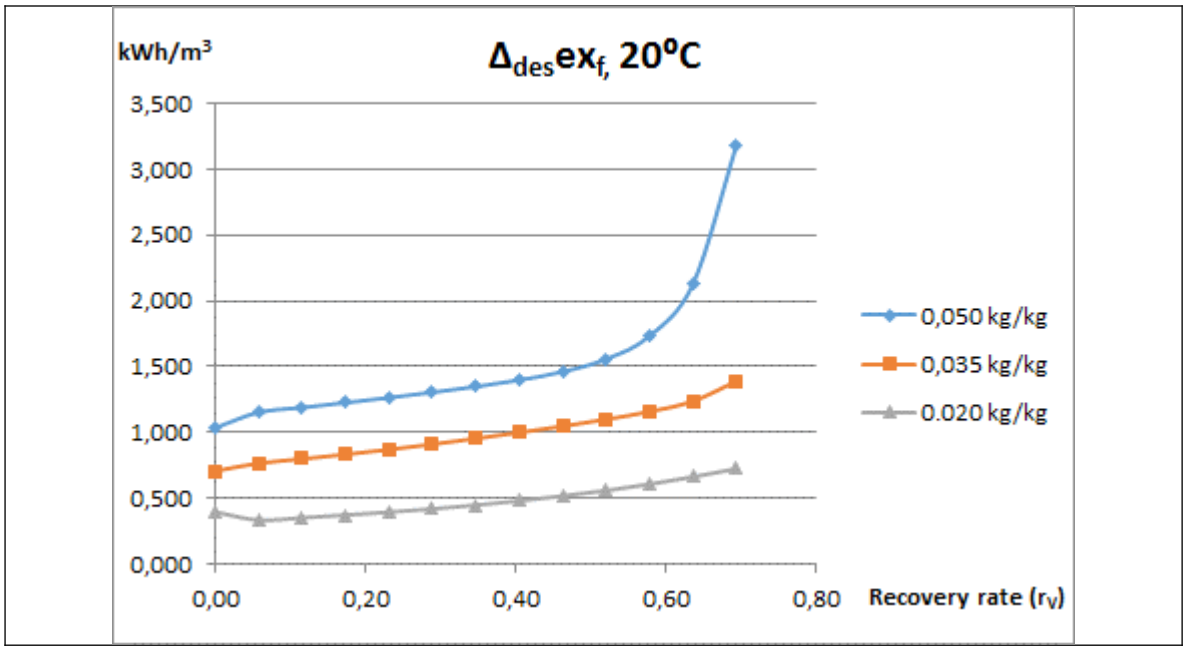


**Figure 3.3. Specific work required to obtain pure water from seawater (20ºC) by means of a reversible desalination process at ambient temperature and pressure.**

# 4. ACTUAL MINIMUM WORK REQUIRED FOR A DESALINATION PROCESS BASED ON REVERSE OSMOSIS

The spontaneous water flow through a Reverse Osmosis (RO) membrane goes from the less concentrated solution to the high concentrated solution, unless the feed pressure is higher than a given value.

Osmotic pressure, Π, is the value at which a saline solution reach the equilibrium with respect to the pure solvent when there is a semipermeable interface between the pure solvent and the solution. Osmotic pressure is defined as the pressure of the solution minus the pressure of the pure solvent when they reach the equilibrium state separated by a limit that is semipermeable to the solvent. If a pressure higher than Π is applied to the solution, the solvent passes through the semipermeable interface, flows from the solution to the pure solvent, just the opposite to the spontaneous solvent flow. This phenomena is referred as reverse osmosis.

The osmotic pressure is related to the osmotic coefficient of the solvent, $\phi$, given in table 3.9 by means of – adapted from Romero Ternero (2005) -:

$$\Pi = \phi \cdot \rho_w \cdot R \cdot T \cdot \frac{2 \cdot S/(1-S)}{62.808 \cdot 10^{-3}\, kg/mol}$$

Where $R$ is the universal gas constant, $S$ is the salinity and $\rho_w$ is the pure water density.

The osmotic pressure is positive and increases with salt concentration – see figure 3.4 -. Then, if two saline solutions are separated by a membrane, the difference of pressures required to invert the spontaneous water flow is the difference of their osmotic pressures. If salt concentrations are $S_1 > S_2$, water passes spontaneously from solution 2 to solution 1 unless the following equation is satisfied:

$$p_1 - p_2 > \Pi_1 - \Pi_2$$

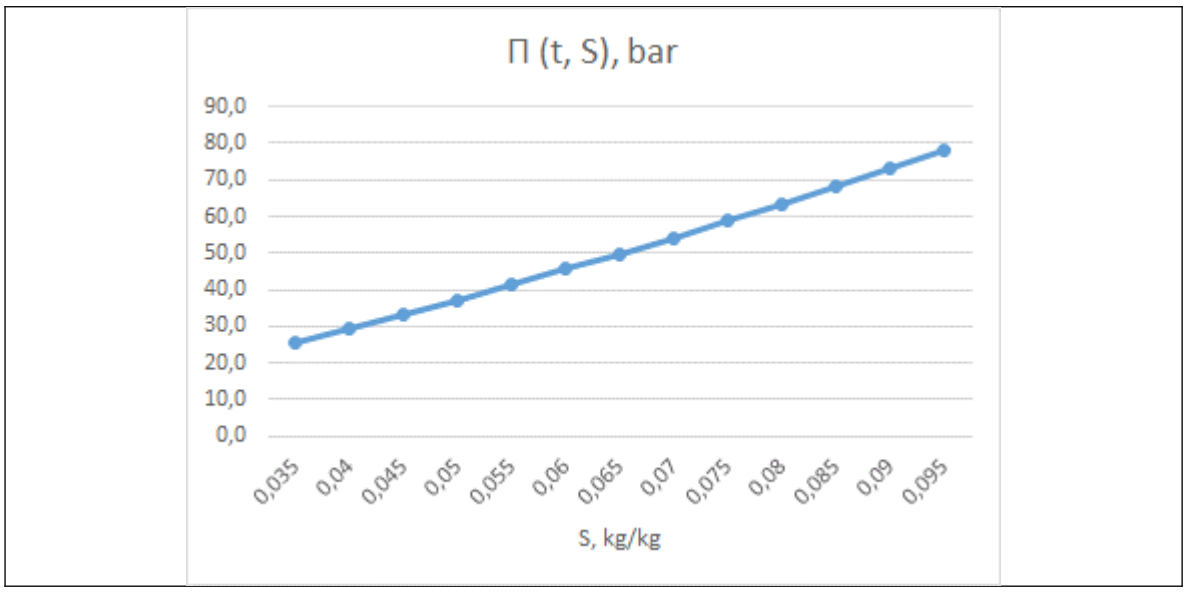


**Figure 3.4. Osmotic pressure of sea salts solutions.**

In reverse osmosis technology, a pressurised feed flow circulates parallel to the membrane surface while some water and a small portion of salts pass through the membrane to the Permeate (or Product) channel, P. Therefore, the condition required to desalinate the feed solution by means of a reverse osmosis process is:

$$p_F - p_P > \Pi_F - \Pi_P$$

Feed channel is referred to as Feed-BlowDown channel (F-BD) since the saline solution progressively increases its salt concentration. For a given feed flow, the recovery rate of the desalination process depends on the membrane area, among other parameters. At the opposite sides of the membrane there are:

- A Feed-BlowDown channel (F-BD), which exhibits a significant change of salt concentration due to the current status of commercial membranes. The output is usually called concentrate. This would be brine if feed is seawater. Besides, the relatively high solvent flow through the membrane results in the effect known as concentration polarization. This consists in an increased salt concentration near the membrane surface, attributable to the fact that salt passage is quite small in comparison to the water transmembrane flow. Note that values of osmotic pressure in the aforementioned equations correspond to those of the membrane surface. Finally, another effect to be considered is the pressure losses through the channel, $\Delta P_{Loss,F-BD}$. These issues are thoroughly analysed in chapter 4.

- A Permeate or product channel (P), which receives both water and salt flows coming through the membrane. These flows per unitary area are not constant, thus resulting in variable permeate quality alongside the axis of feed flow. However, salt flow in commercial membranes is quite small, so the value of permeate osmotic pressure is normally assumed to be nil. Due to the configuration of commercial membrane elements, pressure losses in the permeate channel are normally neglected.

Therefore, the conditions required for RO desalination are:

- Operating condition required at any point x of the OX-axis of the F-BD channel is:

$$p_{F-BD}(x) - p_P(x) > \Pi_{F-BD}(x) - \Pi_P(x)$$

The driving force of the RO process is known as Net Driving Pressure (NDP), which is defined as:

$$NDP(x) = \left[ p_{F-BD}(x) - p_P(x) \right] - \left[ \Pi_{F-BD}(x) - \Pi_P(x) \right]$$

- Operating condition required in the RO system as a whole is:

$$(p¿¿F - \Delta p_{Loss,F-BD}) - p_P > \Pi_{BD} - \Pi_P ¿$$

Figure 3.5 shows a conceptual diagram of the core of the reverse osmosis technology, consisting in the three basic processes described in table 3.11.

**Table 3.11. Unitary processes that normally comprises a reverse osmosis desalination process.**

| | |
|---|---|
| First process: | Compression of the seawater flow from ambient pressure up to any pressure with the compliance of: $(p¿¿F - \Delta p_{Loss,F-BD}) - p_P > \Pi_{BD} - \Pi_P ¿$ |
| Second process: | Separation process through the reverse osmosis membrane. |
| Third process: | Energy recovery from the pressurized blowdown stream by means of blowdown expansion. |
| | |

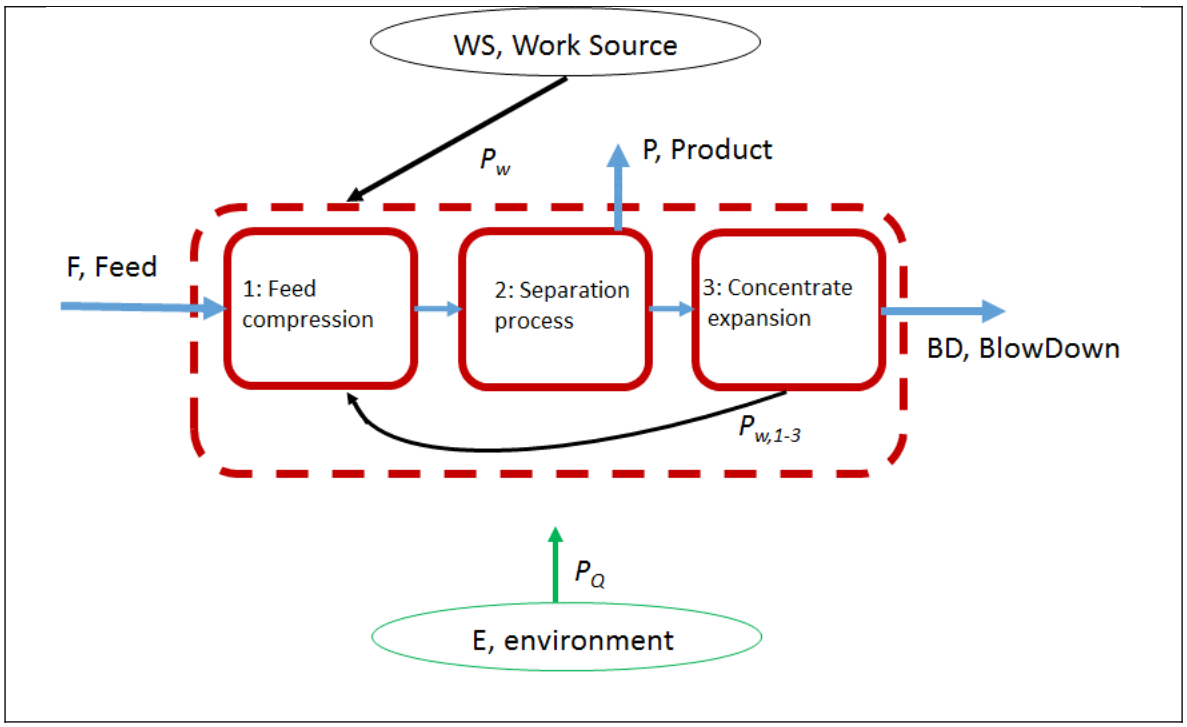


**Figure 3.5. Conceptual diagram of a desalination process based on reverse osmosis.**

There are diverse options of implementing the conceptual diagram shown in figure 3.5, as figure 3.6 describes. In these days, two different Energy Recovery Devices (ERD) could be used:

- TurboChargers (TC), which normally act as booster pumps after the High Pressure Pump (HPP). Both, TC and HPP pressurise the total feed flow – see fig.3.6.a -, except if Danfoss iSave is used – see fig. 3.6.b -. The latter is the only TC that requires a power consumption and exhibits 90% of energy efficiency.
- Isobaric Chambers (ICH) are the most efficient option. They pressurise part of the feed flow, around $100 \cdot (1-r_V)$ %, up to a pressure slightly below that of the blowdown at the membrane module outlet. Thus requiring a Booster Pump (BP) after the ICH. The rest of the feed flow, around $100 \cdot r_V$%, is pressurised by the HPP – see fig.3.6.c -.

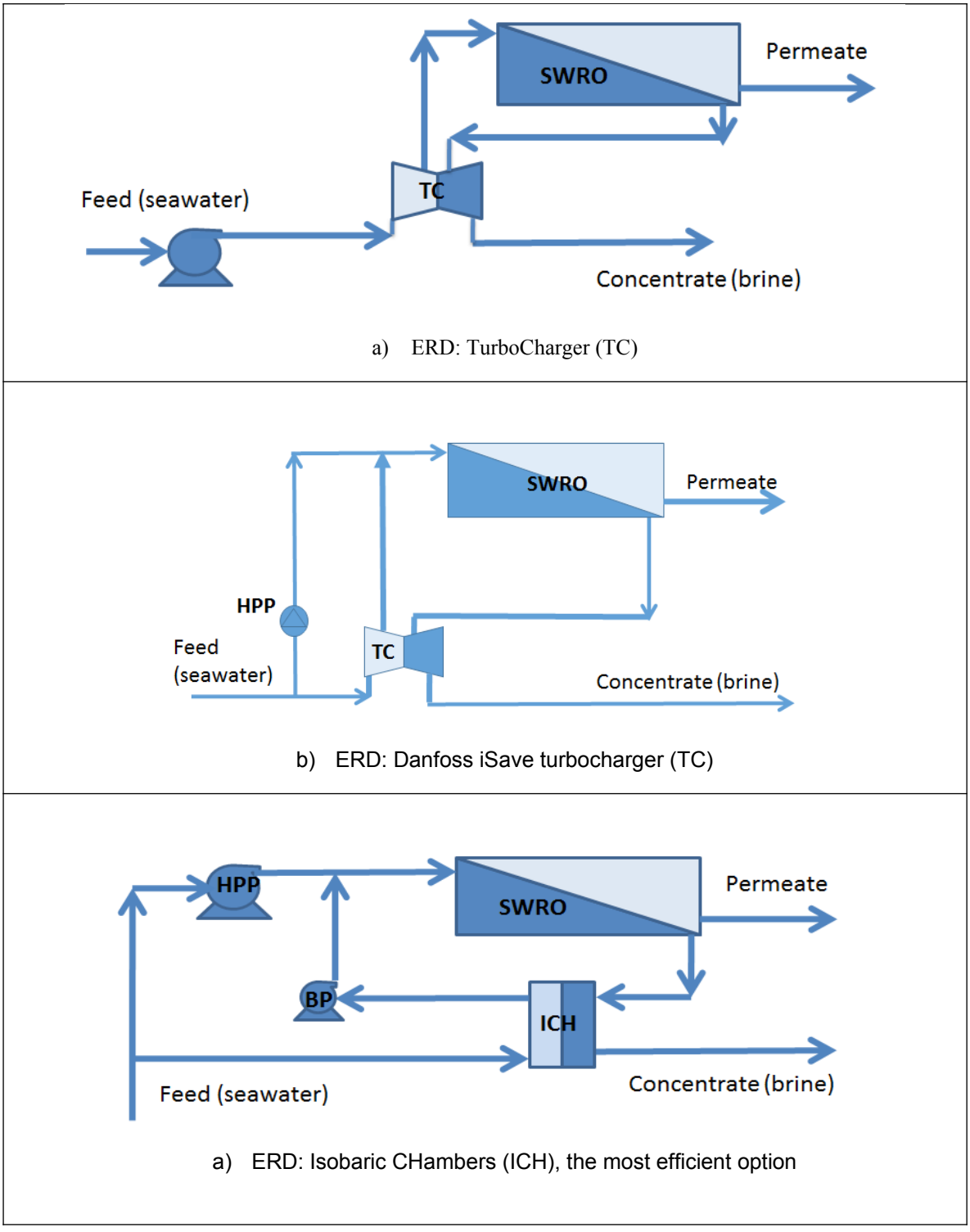


**Figure 3.6. Configurations to implement the three basic processes of reverse osmosis desalination, depending on the Energy Recovery Device (ERD) selected [García-Rodríguez, 2012].**

Besides that, the separation process could be implemented with a single pump, the High Pressure Pump (HPP), which drives a serial connection of seawater membrane elements (First pass). Permeate quality decreases alongside the membrane series. Therefore, permeate flow could be extracted from both ends of the serial connection. This configuration is referred to as split partial – see figure 3.7.a -. Sometimes, the permeate production of the first pass requires further treatment by means of a second serial connection of brackish water membrane elements (Second pass). The second pass may treat all the permeate flow or only part of this.

The second pass requires a feed pressure significantly lower than that of the first pass since permeate from the first pass exhibits relatively low salt concentration. There are two options to pressurize the permeate flow of the first pass (feed of the second pass):

- To install a valve to generate the required pressure at the permeate outlet of the first pass.
- To install a Low Pressure Pump (LPP), as figure 3.7.b shows.

In configurations with second pass, the concentrate outlet of the second pass is brackish water. Then, this is blended with the seawater feed before entering the HPP in order to decrease the salt concentration of first pass feed – see figure 3.7.b -.

Also the concentrate of the first pass could be further treated by a second serial connection of membrane elements (second stage). To install an additional pump (Interstage Booster Pump, BP) may be optional since the concentrate exits the first pass at a pressure slightly lower than that of the HPP outlet. Decision on installing this BP depends on blowdown pressure in comparison to osmotic pressure at the tail of the membrane series. In this days the second stage is only normally used in Brackish Water Reverse Osmosis (BWRO) desalination. However in the past, SWRO plants with second stage were common in The Canary Islands [Sadwani and Veza, 2008]. Figure 3.7.c depicts a diagram of this configuration.

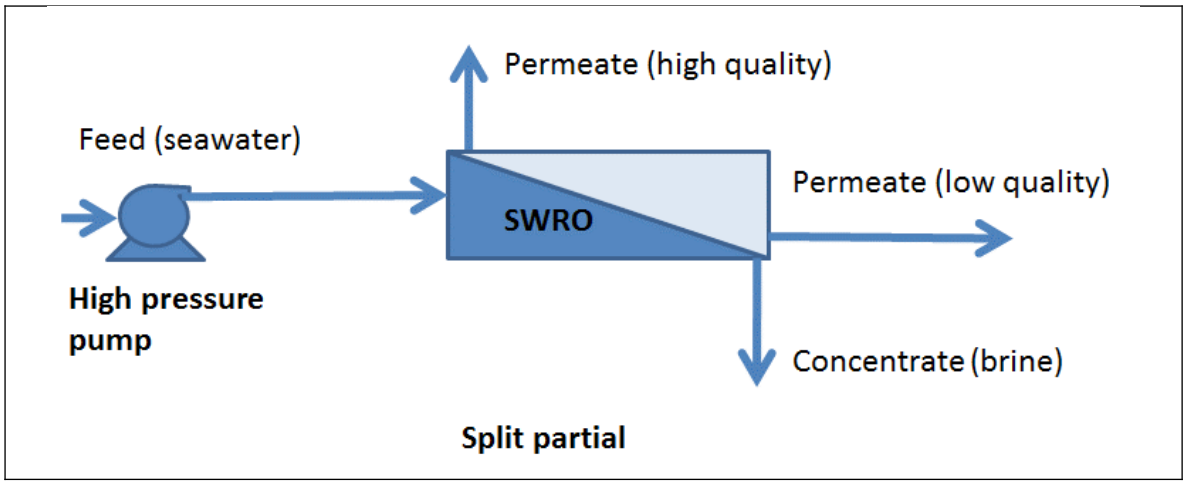

a) Single pass (with split partial). Only the rear permeate outlet is normally installed.

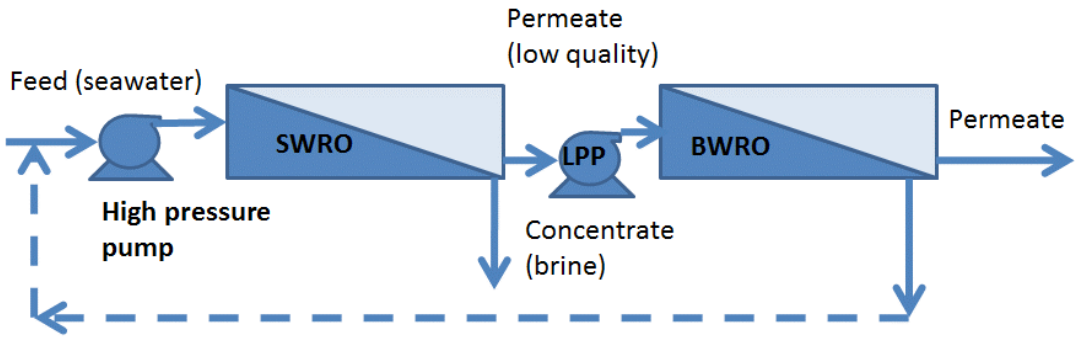


b) Two pass. The second pass may treat only part of the permeate flow.

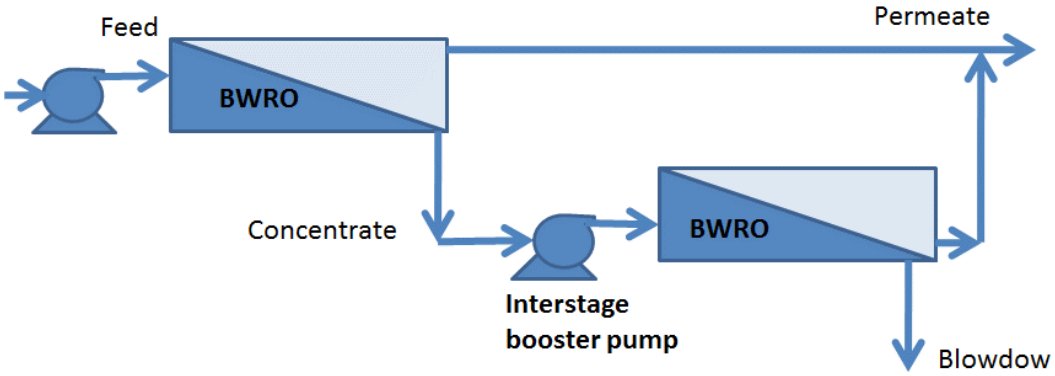


c) Two stages, normally used only in Brackish Water Reverse Osmosis (BWRO).

**Figure 3.7. Configurations in SWRO desalination plants [García-Rodríguez, 2012].**

Finally, more complex configurations could also be used, specifically in plant locations with very restrictive normative on permeate quality – figure 3.8 -.

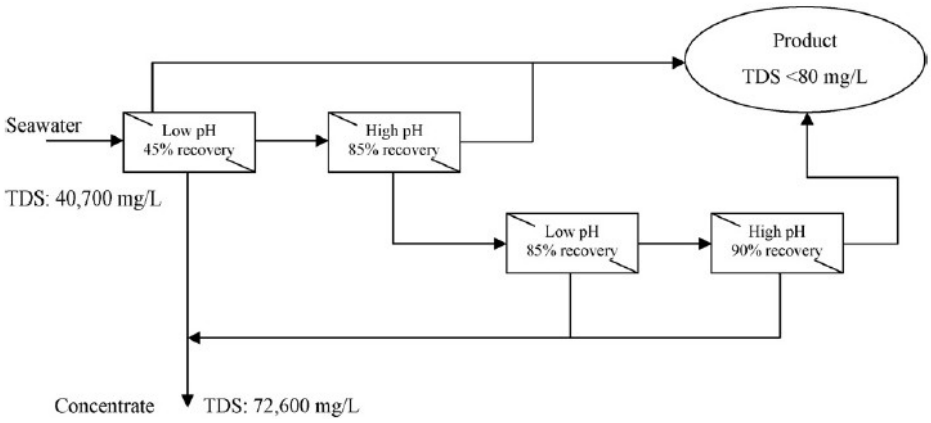


a) Flow diagram of the Aschelon plant, Israel

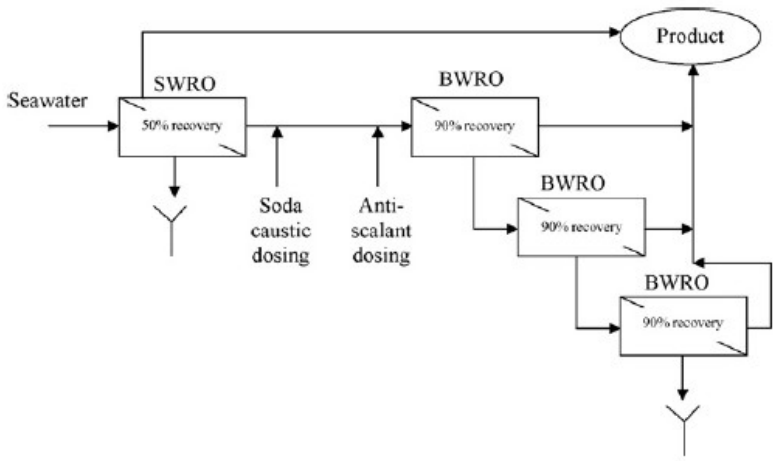


b) Flow diagram of the Eilat plant, Israel

**Figure 3.8. Examples of complex configuration due to high restrictive normative regarding boron content in permeate [Tu *et al*, 2010].**

With the aim of calculating the minimum energy consumption with the present status of the SWRO desalination technology, modelling of the three basic process – see figure 3.9 - are presented in table 3.12 and 3.13. They also give values of main design and operation parameters used in this work.

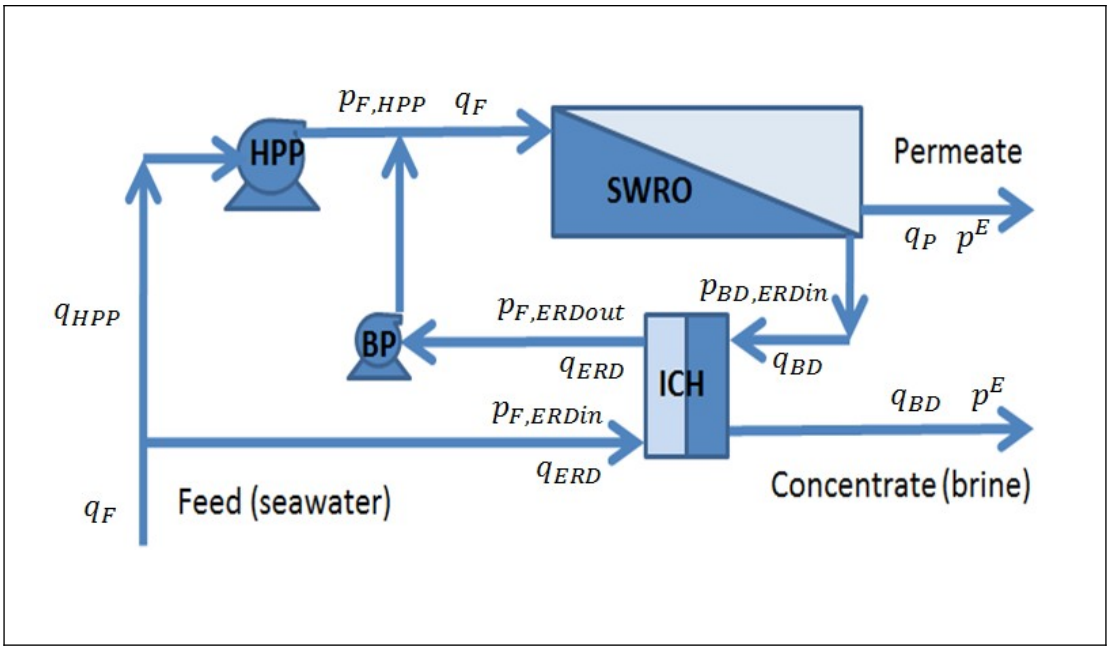


**Figure 3.9. Diagram considered to SWRO modelling based on ERI-PX Energy Recovery Device (ERD).**

General equations from tables 3.12-3.13 are particularized – table 3.14-3.16 - by assuming the most favorable hypothesis in order to assess the actual limits of the SWRO desalination process.

**Table 3.12. Feed compression and separation processes within a SWRO desalination process at ambient conditions with Energy Recovery Device (ERD) based on isobaric chamber.**

| | |
|---|---|
| Seawater pressurisation (single pass, single stage): | Power consumption of the High Pressure Pump (HPP) – flow rate, $q_{V,HPP}$; pressure increase from $p^E$ to $p_{F,HPP}$ - :<br>$P^{\square}_{W,HPP} = \frac{\left(\frac{q_{V,HPP}}{m^3 \cdot h^{-1} \cdot 3600}\right) \cdot \left(\frac{p_{F,HPP} - p^E}{bar \cdot 100^{-1}}\right)}{\eta_{HPP} \cdot \eta_{eng}} \cdot kW$<br>where: $q_F = q_{ERD} + q_{HPP}$; $q_{V,F} \cdot \rho_F = q_{V,ERD} \cdot \rho_F + q_{V,HPP} \cdot \rho_F$<br>$\eta_{eng} = 0.95$<br>Power needed by the Booster Pump (BP) – flow rate of the seawater side of ERD, $q_{V,ERD}$; pressure increase from this side outlet, $p_{F,ERDout}$, to $p_{F,HPP}$ - :<br>$P^{\square}_{W,BP} = \frac{\left(\frac{q_{V,ERD}}{m^3 \cdot h^{-1} \cdot 3600}\right) \cdot \left(\frac{p_{F,HPP} - p_{F,ERDout}}{bar \cdot 100^{-1}}\right)}{\eta_{BP} \cdot \eta_{eng}} \cdot kW$<br>$\eta_{BP} = 0.75 ; \eta_{eng} = 0.93$ |
| Separation process: | $0 = P_{W,HPP} + \sum P_{W,LPP} + \sum P_{W,BP} - \left[q_P \cdot \Delta_{des} ex_a(r)\right] - P^D_x$<br>Where: $\frac{q_F}{q_P} = \frac{1}{r_m} ; \frac{q_{DB}}{q_P} = \frac{q_F - q_P}{q_P} = \frac{1}{r_m} - 1$<br>$\Delta_{des} ex_a\left(r_m < r^{sat}\right) = \frac{q_P}{q_P} \cdot ex_{aP} + \frac{q_{BD}}{q_P} \cdot ex_{aBD} - \frac{q_F}{q_P} \cdot ex_{aF}$<br>$\Delta_{des} ex_a\left(r_m < r^{sat}\right) = ex_{aP} + \left(\frac{1}{r_m} - 1\right) \cdot ex_{aBD} - \frac{1}{r_m} \cdot ex_{aF}$<br>Specific Energy Consumption: |

| | |
|---|---|
| | $SEC_{net}=\frac{P_{W,HPP}+\sum P_{W,LPP}+\sum P_{W,BP}}{q_{V,P}}$ where: $q_{V,P}=q_P/\rho_P$ |

**Table 3.13. Analysis of an Energy Recovery Device (ERD) based on isobaric chamber, type ERI-PX, in a SWRO desalination process at ambient conditions.**

| | |
|---|---|
| Energy recovery: | Experimental parameters [ERI, 2006] assumed by hypothesis:<br>- Efficiency, $Eff$, 0.95:<br>$Eff=\frac{q_{V,ERD}\cdot\left(p_{F,ERDout}-p^E\right)+q_{V,BD}\cdot\left(p_{BD,ERDout}-p^E\right)}{q_{V,ERD}\cdot\left(p_{F,ERDin}-p^E\right)+q_{V,BD}\cdot\left(p_{BD,ERDin}-p^E\right)}$<br>- High Pressure flow Differential Pressure (HP_DP), 0.7 bar:<br>$HP_{DP}=p_{BD,ERDin}-p_{F,ERDout}$<br>- Low Pressure flow Differential Pressure (LP_DP), 0.6 bar:<br>$LP\,DP=p_{F,ERDin}-p_{BD,ERDout}$<br>$p_{BD,ERDout}\geq p^E$; $p_{F,ERDin}\geq LP_{DP}$ (prior feed compression)<br>Flow pressurized by the ERD, $q_{V,ERD}$:<br>$q_{V,ERD}\cdot\left[p_{F,ERDin}\cdot Eff-p_{F,ERDout}\right]=$¿<br>¿$q_{V,BD}\cdot\left[p_{BD,ERDout}-p_{BD,ERDin}\cdot Eff\right]$<br>$q_{V,ERD}=q_{V,BD}\cdot\frac{\left[\left(p_{F,ERDin}-LP_{DP}\right)-p_{BD,ERDin}\cdot Eff\right]}{\left[p_{F,ERDin}\cdot Eff-\left(p_{BD,ERDin}-HP_{DP}\right)\right]}$<br>Where $q_{V,BD}(r_m)=\left(\frac{1}{r_m}-1\right)\cdot\frac{q_{V,P}\cdot\rho_P}{\rho_{BD}}$<br>Flow compression by the HPP, $q_{V,HPP}$:<br>$q_F=q_{ERD}+q_{HPP}$; $q_{V,F}\cdot\rho_F=q_{V,ERD}\cdot\rho_F+q_{V,HPP}\cdot\rho_F$<br>$q_{V,HPP}=q_{V,F}-q_{V,ERD}$ |

| | |
|---|---|
| | Where $q_{V,F}(r_m)=\left(\frac{1}{r_m}\right)\cdot\frac{q_{V,P}\cdot\rho_P}{\rho_F}$<br><br>Pressure increasing required at the BP:<br><br>$p_{F,HPP}-p_{F,ERDout}=p_{F,HPP}-\left(p_{BD,ERDin}-HP_{DP}\right)=¿\,\Delta p_{Loss,F-BD}+HP_{DP}$ |

**Table 3.14. Energy recovery process under the most favourable hypothesis.**

| | |
|---|---|
| Energy recovery: | ERI-PX parameters:<br><br>$HP_{DP}=0\Rightarrow \quad p_{F,ERDout}=p_{BD,ERDin}$<br><br>$p_{F,ERDin}=p^E$<br><br>$LP_{DP}=0\Rightarrow \quad p_{BD,ERDout}=p^E$<br><br>$Eff=1$<br><br>Therefore, equations from table 3.12:<br><br>$q_{V,ERD}=q_{V,BD}\cdot\frac{\left[\left(p_{F,ERDin}-LP_{DP}\right)-p_{BD,ERDin}\cdot Eff\right]}{\left[p_{F,ERDin}\cdot Eff-\left(p_{BD,ERDin}-HP_{DP}\right)\right]}$<br><br>$q_{V,HPP}=q_{V,F}-q_{V,ERD}$<br><br>become: $q_{V,ERD}=q_{V,BD}$<br><br>$q_{V,HPP}=q_{V,F}-q_{V,BD}$<br><br>Where:<br><br>$q_{V,F}(r)=\left(\frac{1}{r_m}\right)\cdot\frac{q_{V,P}\cdot\rho_P}{\rho_F}$<br><br>$q_{V,BD}(r)=\left(\frac{1}{r_m}-1\right)\cdot\frac{q_{V,P}\cdot\rho_P}{\rho_{BD}}$ |

**Table 3.15. Pressurisation process in a single-pass RO desalination with the most favourable hypothesis.**

| | |
|---|---|
| Seawater compression (single pass, single stage): | HPP and BP parameters: $\eta_{HPP}=1;\eta_{BP}=1;\eta_{eng}=1$<br>Operating pressure: $(p¿¿F-\Delta p_{Loss,F-BD})-p_P \geq \Pi_{BD}-\Pi_P ¿$<br>With $\Delta p_{Loss,F-BD}=0;\quad \Pi_P=0;\quad p_P=p^E$<br>$\Rightarrow p_{F,HPP}=\Pi_{BD}+p^E$ and negligible polarization effect, thus $S_{BD}$ is used to calculate $\Pi_{BD}$<br>Equations from table 3.11:<br>$P_{W,HPP}^{\square}=\frac{\left(\frac{q_{V,HPP}}{m^3\cdot h^{-1}\cdot 3600}\right)\cdot\left(\frac{p_{F,HPP}-p^E}{bar\cdot 100^{-1}}\right)}{\eta_{HPP}\cdot\eta_{eng}}\cdot kW$<br>$P_{W,BP}^{\square}=\frac{\left(\frac{q_{V,ERD}}{m^3\cdot h^{-1}\cdot 3600}\right)\cdot\left(\frac{p_F-p_{F,ERDout}}{bar\cdot 100^{-1}}\right)}{\eta_{BP}\cdot\eta_{eng}}\cdot kW$<br>where $p_F-p_{F,ERDout}=\Delta p_{Loss,F-BD}+HP\,DP$<br>Hence: $P_{W,BP}^{\square}=0\cdot kW$<br>$P_{W,HPP}^{\square}=\frac{\left(\frac{q_{V,F}-q_{V,BD}}{m^3\cdot h^{-1}\cdot 3600}\right)\cdot\left(\frac{\Pi_{BD}-p^E}{bar\cdot 100^{-1}}\right)}{1\cdot 1}\cdot kW$<br>Where: $q_{V,F}(r_m)=\left(\frac{1}{r_m}\right)\cdot\frac{q_{V,P}\cdot\rho_P}{\rho_F}$ ; $q_{V,BD}(r)=\left(\frac{1}{r_m}-1\right)\cdot\frac{q_{V,P}\cdot\rho_P}{\rho_{BD}}$ |

**Table 3.16. Separation process with the most favourable hypothesis.**

| | |
|---|---|
| Separation process: | Hypothesis:<br>- Input and output temperature and pressure are the same (ambient values), and feed concentration is that of seawater ( $ex_{aF}=0$¿<br>- Feed compression and energy recovery processes as described in table 3.14-3.15.<br>- Permeate obtained in the first pass is approximately pure water.<br>Final equations: $0=P_{W,HPP}-\left[q_P\cdot\Delta_{des}ex_a(r_m)\right]-P_x^D$<br>$\Delta_{des}ex_a(r_m)=ex_{aP}+\left(\frac{1}{r_m}-1\right)\cdot ex_{aBD};$<br>$SEC_{net}=\frac{P_{W,HPP}}{q_{V,P}}$ |

Results obtained for different seawater conditions and 80% of HPP efficiency are depicted in figures 3.10-3.12 as function of the Tail Differential Pressure (TDP), defined as the NDP at the tail of the membrane series if concentration polarization is neglected. At 49% of recovery rate, the SEC decreases 0.038 kWh/m$^3$ per bar of TDP decreasing.

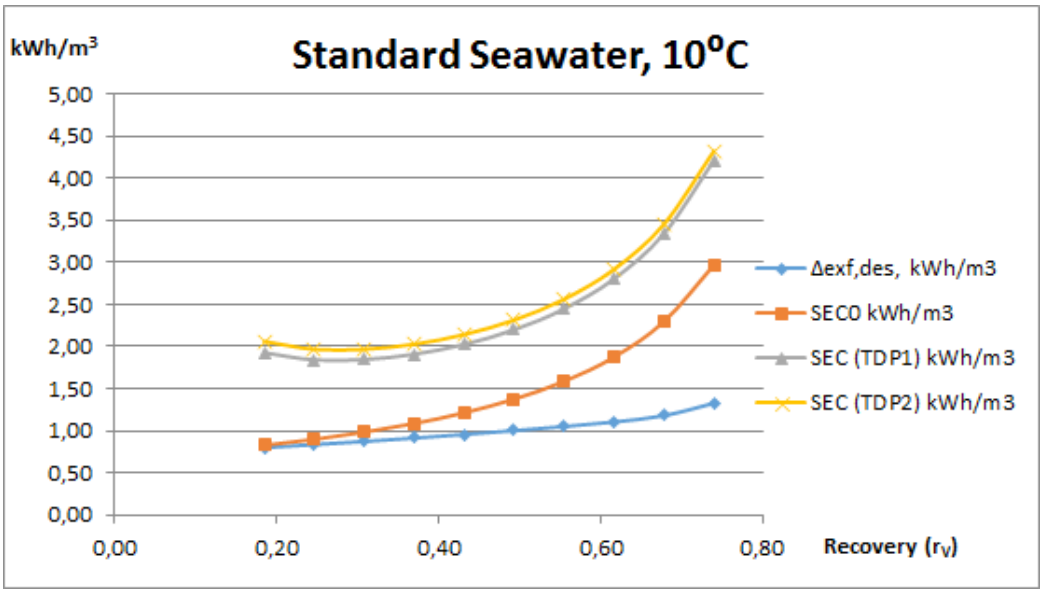

**Figure 3.10.a. Specific Energy Consumption (SEC) with $\eta_{HPP}$= 80%, $TDP_1$= 5 bar and $TDP_2$= 8 bar; SEC0 - SEC of ideal SWRO process -, and thermodynamic limit of seawater desalination, $\Delta ex_{f,des}$.**

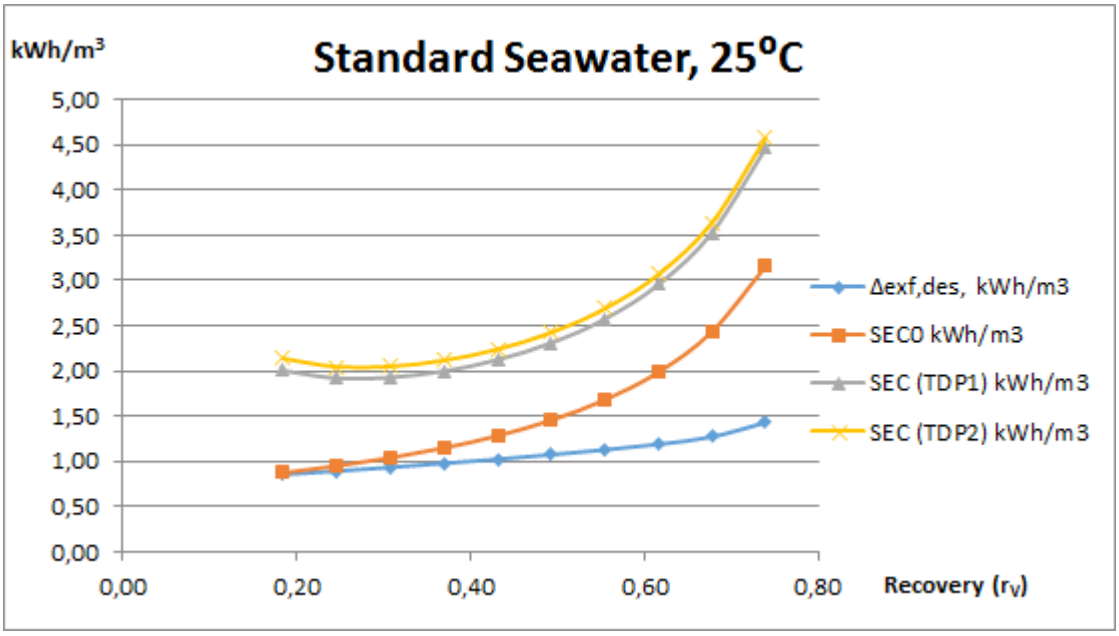


b)

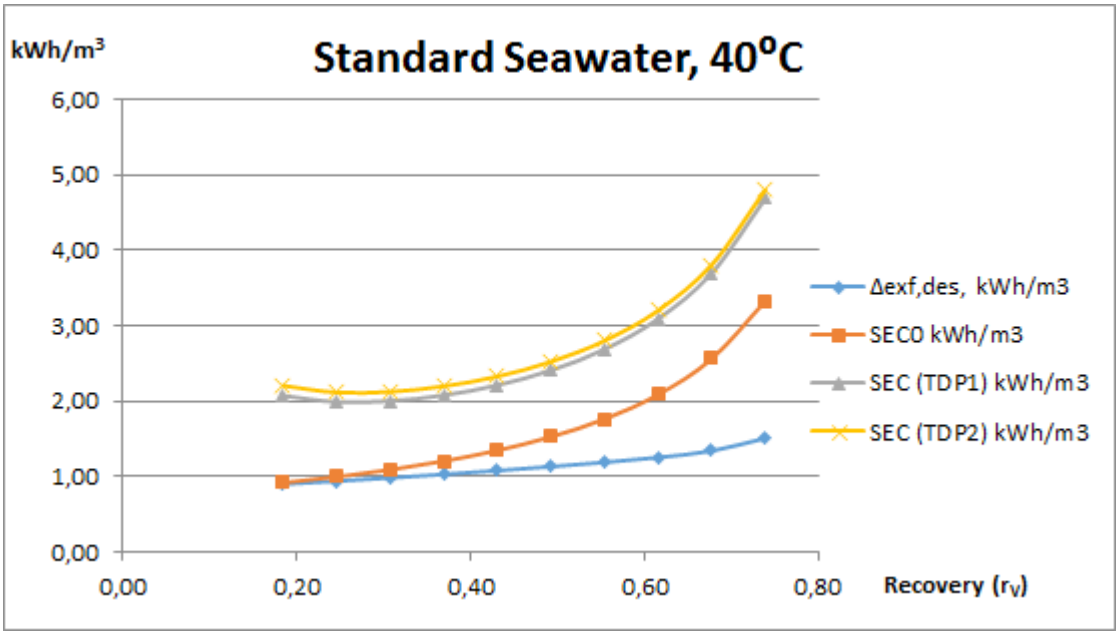


c)

**Figure 3.10. Specific Energy Consumption (SEC) with $\eta_{HPP}$= 80%, $TDP_1$= 5 bar and $TDP_2$= 8 bar; SEC0 - SEC of ideal SWRO process -, and thermodynamic limit of seawater desalination, $\Delta ex_{f,des}$.**

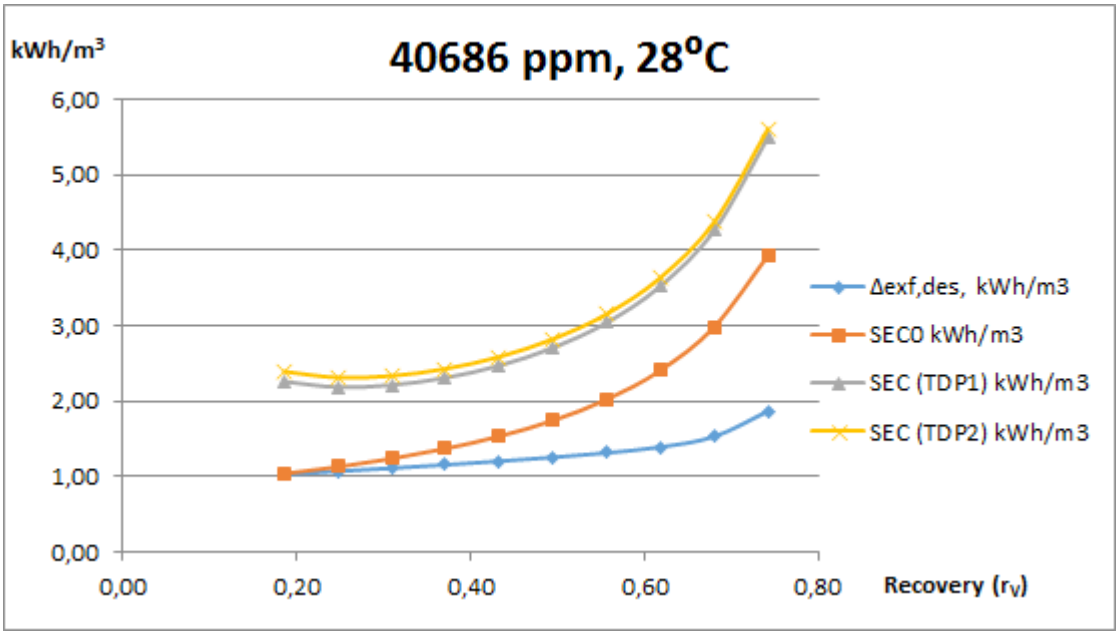


**Figure 3.11. Specific Energy Consumption (SEC) with $\eta_{HPP}$= 80%, $TDP_1$= 5 bar and $TDP_2$= 8 bar; SEC0 - SEC of ideal SWRO process -, and thermodynamic limit of seawater desalination, $\Delta ex_{f,des}$. Mediterranean conditions [Wilf, 2007].**

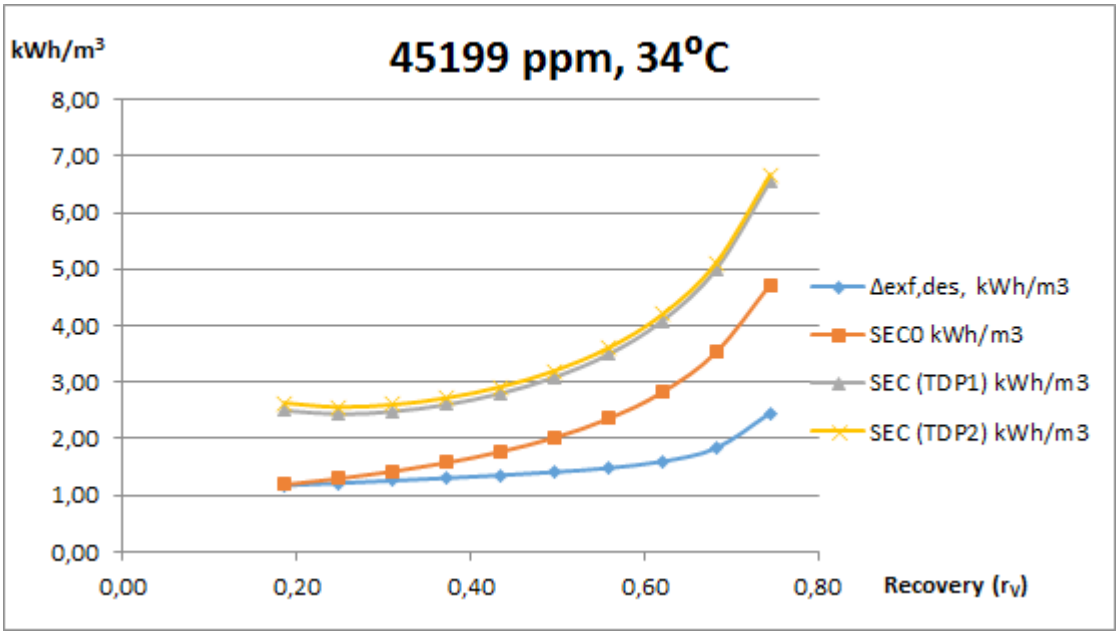


**Figure 3.12. Specific Energy Consumption (SEC) with $\eta_{HPP}$= 80%, $TDP_1$= 5 bar and $TDP_2$= 8 bar; SEC0 - SEC of ideal SWRO process -, and thermodynamic limit of seawater desalination, $\Delta ex_{f,des}$. Persian Gulf conditions [Wilf, 2007].**

In addition, figs.3.13-3.17 show the effect of pumping efficiency at different seawater conditions with TDP of 5 bar.

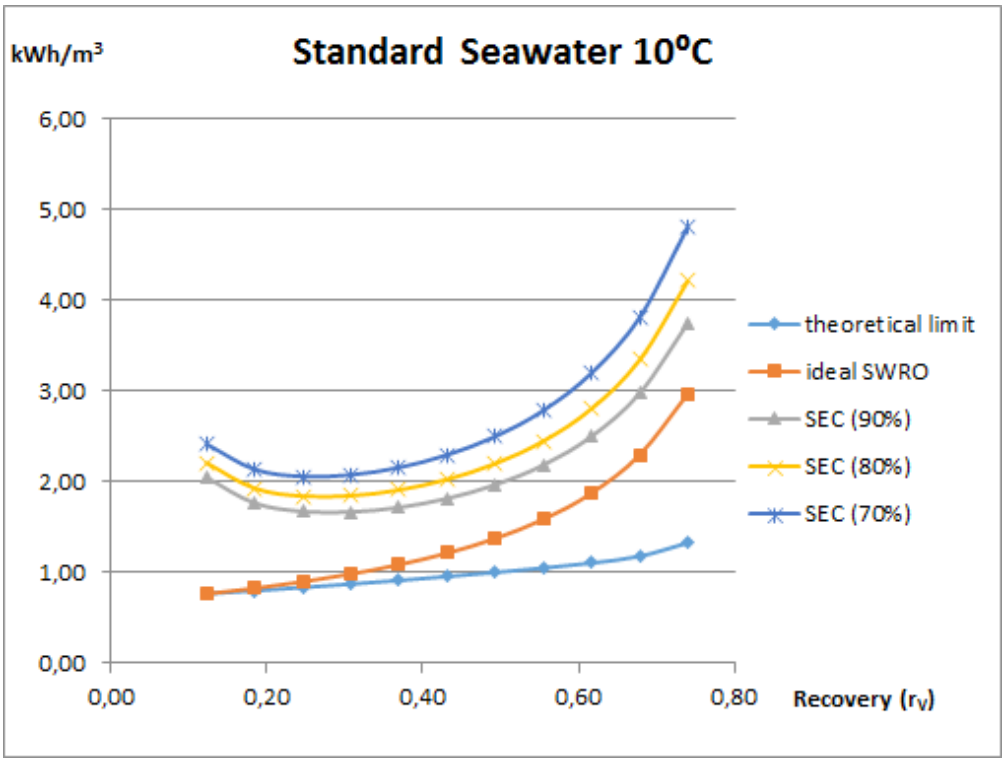


a) 10ºC

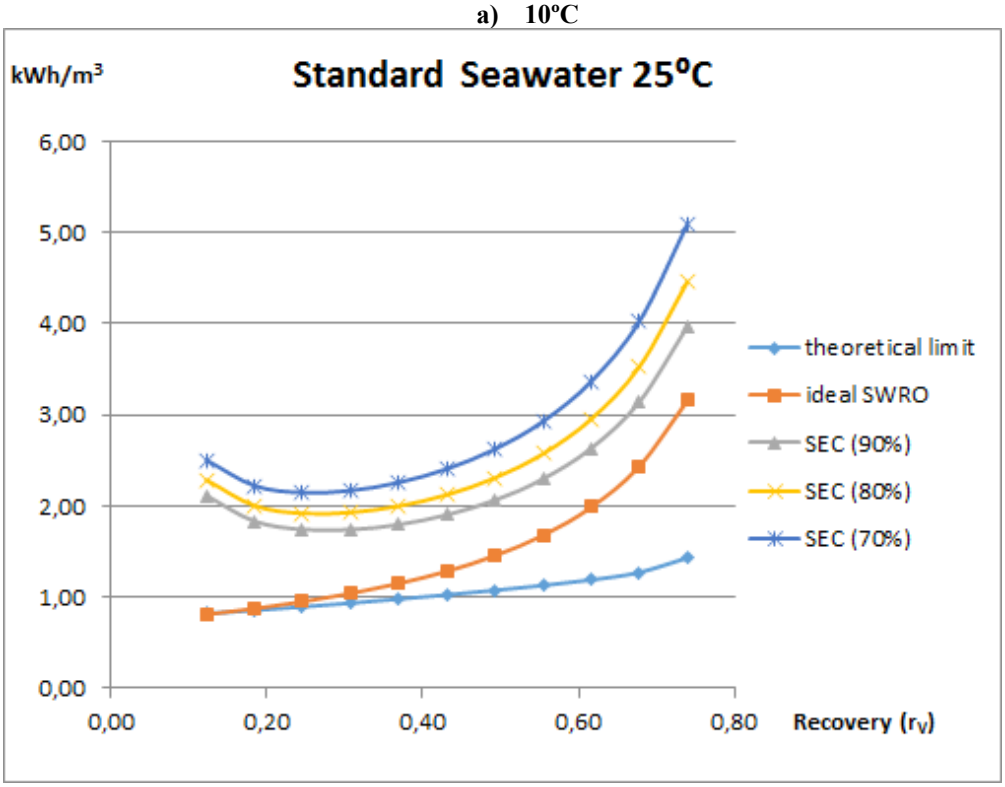


b) 25ºC

**Figure 3.13.a-b. Specific Energy Consumption (SEC) of SWRO desalination (TDP= 5 bar) of Standard Seawater [Millero, 2008] for $\eta_{HPP}$= 70%, 80% and 90% in comparison to ideal processes.**

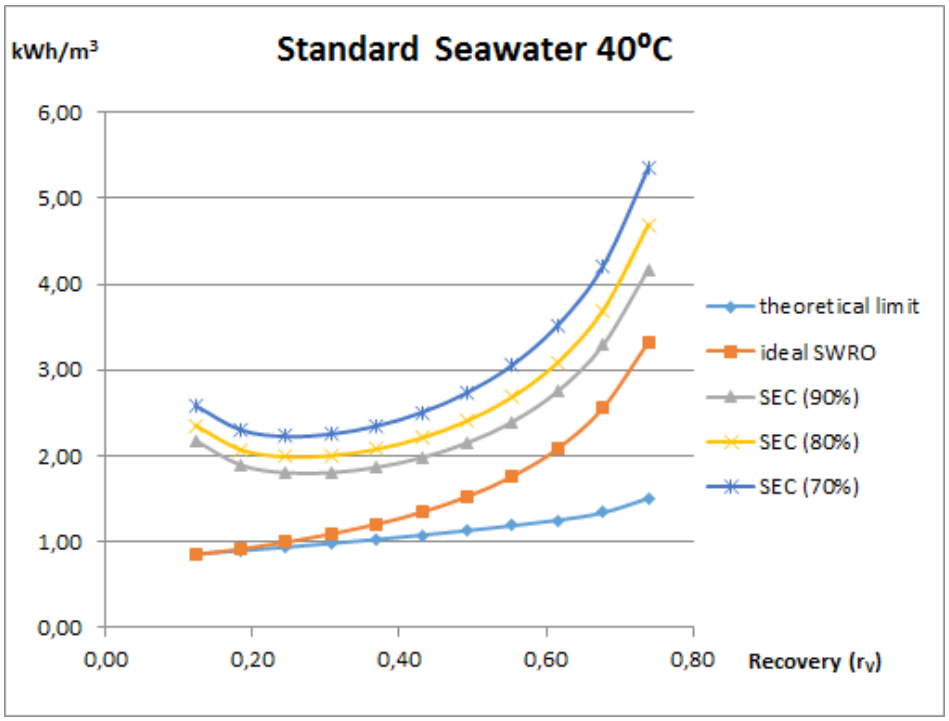


**c) 40°C**

**Figure 3.13.c. Specific energy consumption of SWRO desalination (TDP= 5 bar) of Standard Seawater [Millero, 2008] for $\eta_{HPP}$= 70%, 80% and 90% in comparison to ideal processes.**

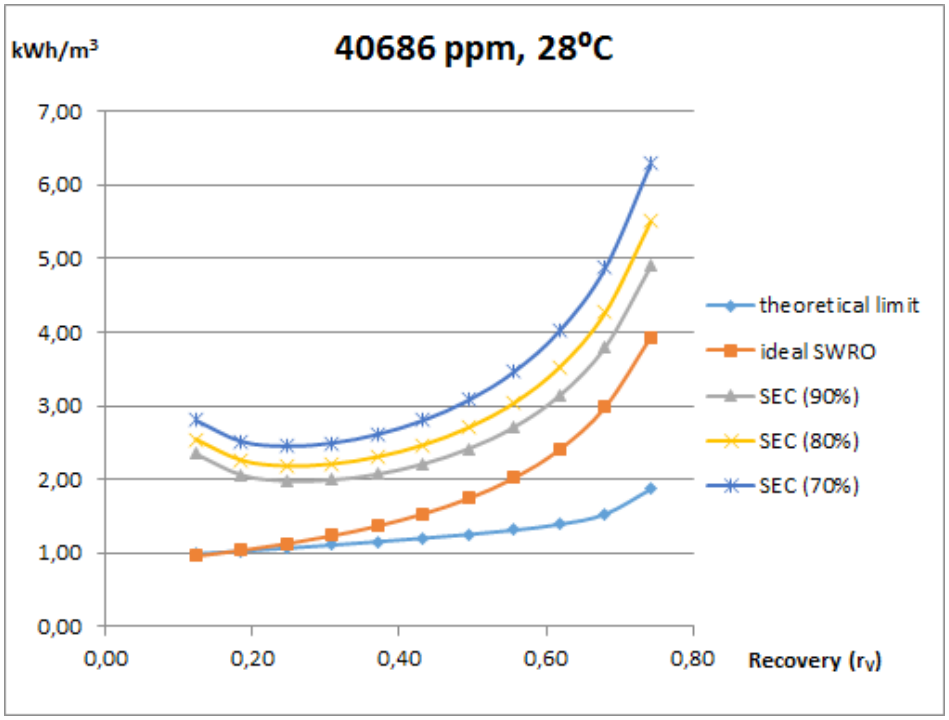


**Figure 3.14. Specific energy consumption of SWRO desalination (TDP= 5 bar) of Mediterranean Seawater [Wilf, 2007] for $\eta_{HPP}$= 70%, 80% and 90% in comparison to ideal processes.**

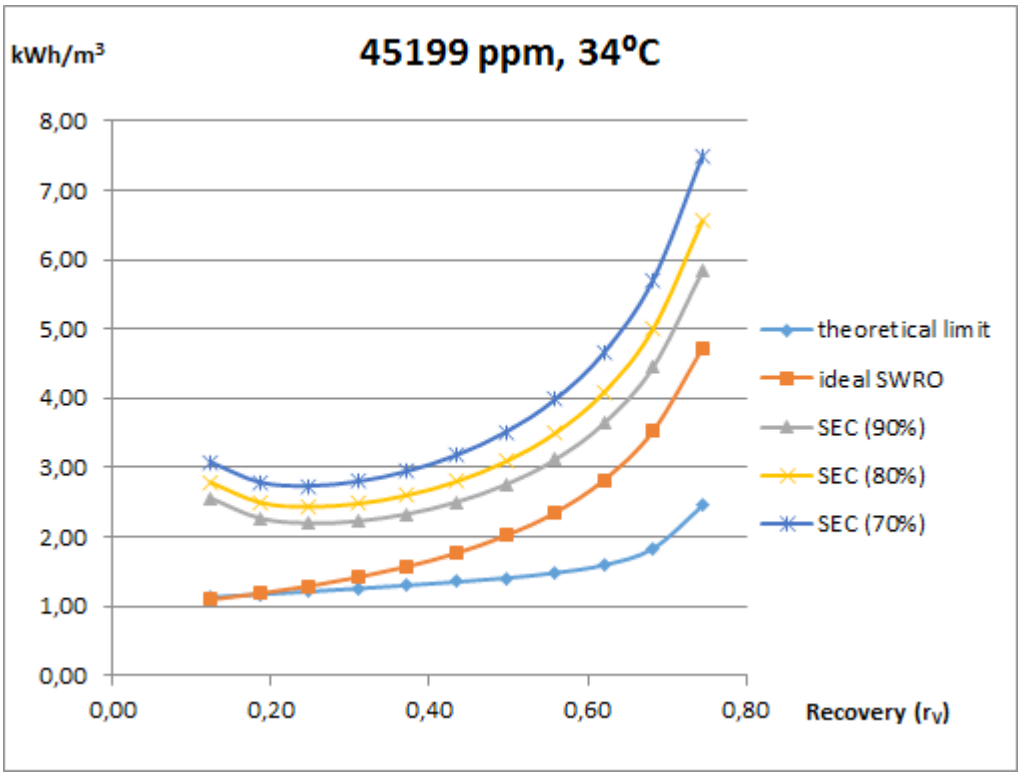


**Figure 3.15. Specific energy consumption of SWRO desalination (TDP= 5 bar) of Persian Gulf Seawater [Wilf, 2007] for $\eta_{HPP}$= 70%, 80% and 90% in comparison to ideal processes.**

# 5. FUTURE PROSPECTS OF REDUCING ENERGY CONSUMPTION IN SWRO DESALINATION

## 5.1. Conceptual diagrams of the state-of-the-art

Figure 3.16 depicts the conceptual diagram of feed pressure and osmotic pressure versus salt concentration in conventional configurations with single pass. A wide range of salinities is shown in order to make easy to understand the effect of operating with high recovery rates. If permeate collection from both ends (split partial) is used - see Fig. 3.7.a – the conceptual diagram remains unchanged.

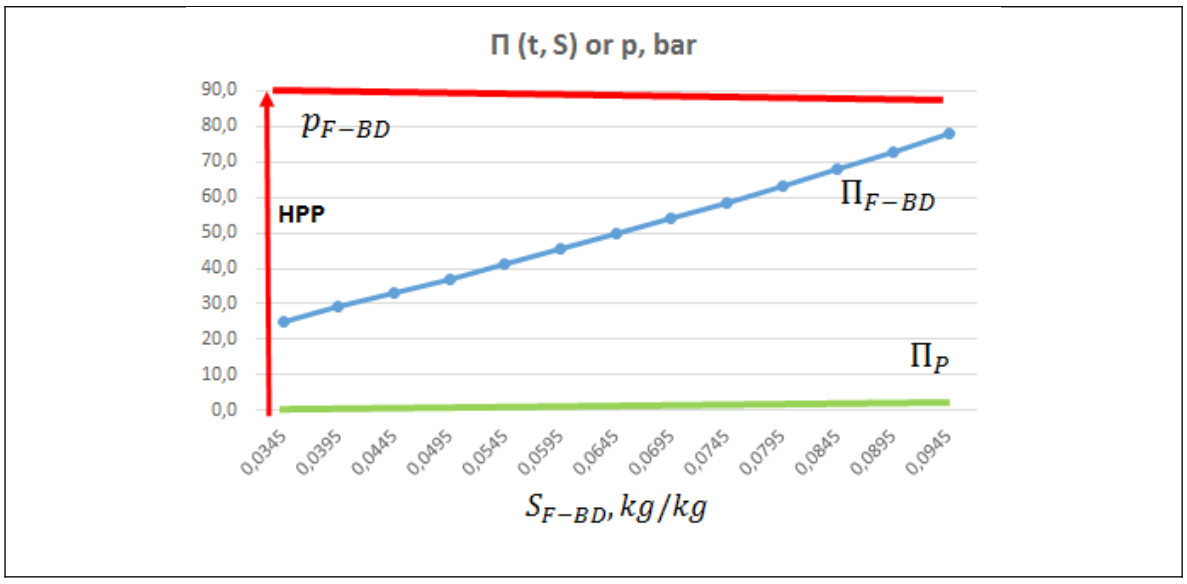


**Figure 3.16. Feed pressure and osmotic pressure in a SWRO desalination process with conventional single-pass configuration. A representative value of blowdown salinity could be around 0.070 and maximum operating pressure of commercial membrane modules is 80 bar.**

If two passes are installed – see Fig. 3.7.b -, the concentrate of the second pass (BWRO) is recycled in order to reduce feed concentration, thus resulting in lower osmotic pressure than that of the feed at the membrane module inlet. This results in higher NDP at the front membrane elements as figure 3.17 shows. However, the NDP at the tail element would be the same for a given blowdown concentration.

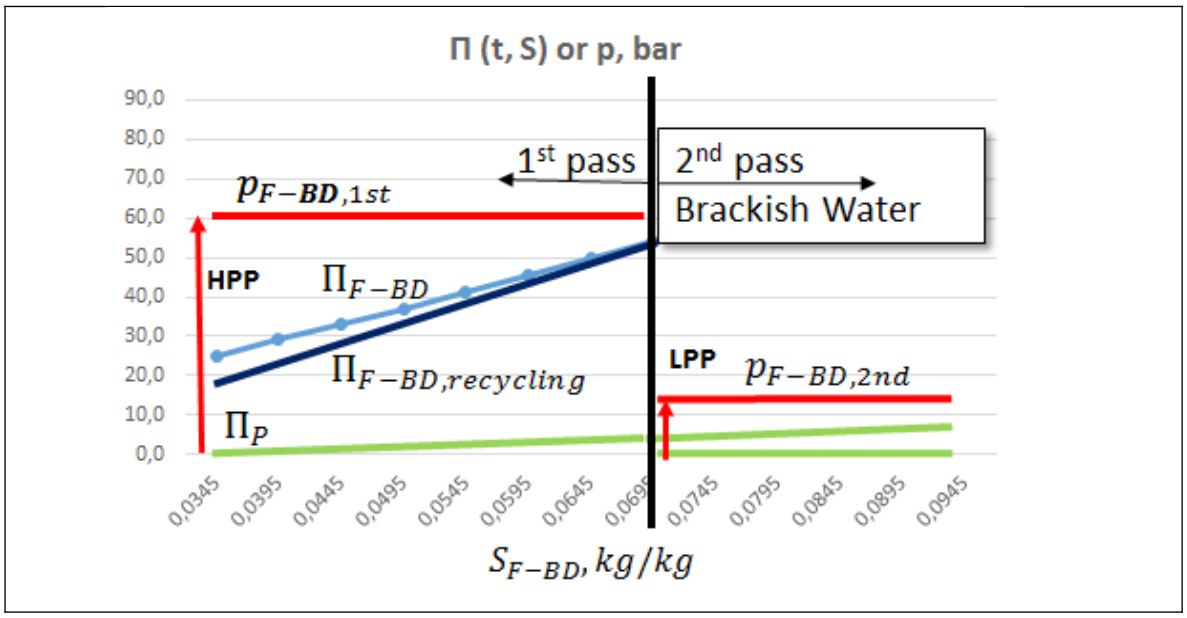


**Figure 3.17. Feed pressure and osmotic pressure in a SWRO desalination process with conventional two-pass configuration.**

## 5.2. Towards minimising exergy destruction

Even though ideal pressurisation and energy recovery are technically possible, the single-pass concept result in compressing all the feed flow up to a pressure higher than osmotic pressure of the blowdown. Nevertheless, the thermodynamic ideal limit (reversible process) means to reduce the NDP as much as possible. Therefore, an advance towards the thermodynamic limit should be to carry out the compression process in multiple stages – see Fig. 3.18 -. Thus, the inter-stage Low Pressure Pump (LPP) only pressurises the blowdown of the previous stage – see fig. 3.7 and 3.9 -. Regardless capital costs, multistage configurations would result in a significant reduction of energy consumption. Up to recovery rates normally used in current SWRO technology, only two stages could be a reliable and cost-effective option. Energy consumption and exergy destruction can be calculated from equations given in tables 3.17-3.18. Results are depicted in figure 3.15-3.17. There are a number of recent patents related to the two-stage concept Kurihara *et al* (2008), Viera-Curbelo (2013), Wittmann *et al* (2013) and Zhou (2012), among others.

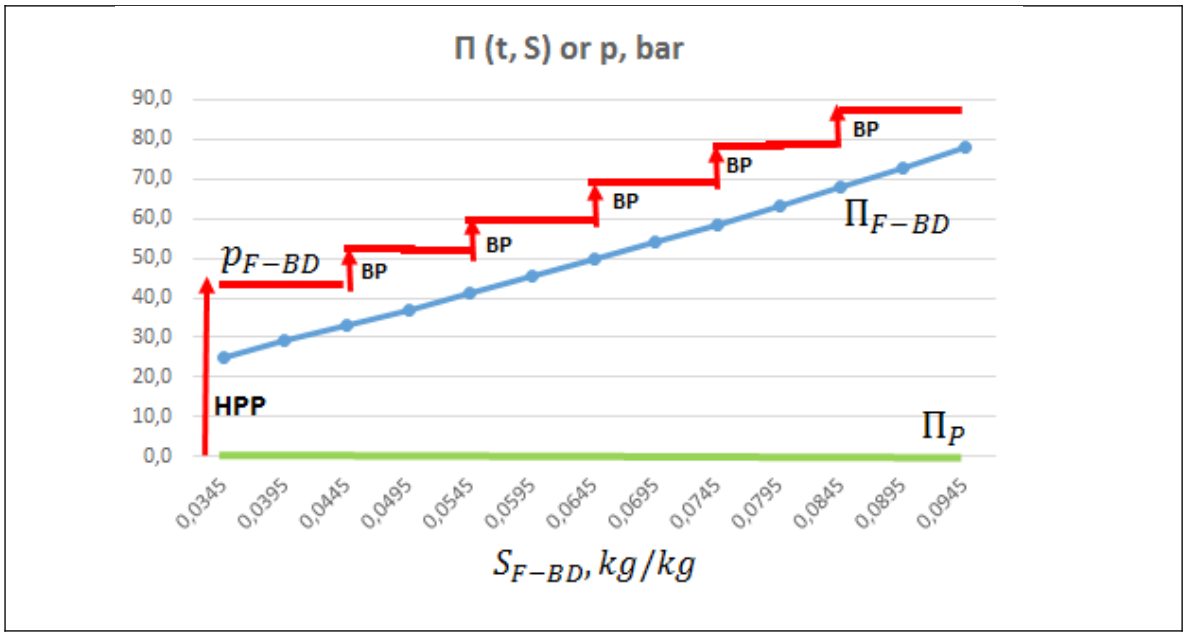


**Figure 3.18. Feed pressure and osmotic pressure in a theoretical SWRO desalination process with multiple stages with inter-stage Booster Pumps (BP´s).**

**Table 3.17. Thermodynamic analysis of the most favourable but reliable desalination process based on SWRO with two-stages.**

| | |
|---|---|
| Seawater pressurisation and energy recovery: | Particular equations under the most favorable hypothesis:<br>- ERD feed flow: $q_{V,ERD}=q_{V,BD,stg2}$<br>- HPP feed flow: $q_{Fstg1}=q_{ERD}+q_{HPP}$<br>$q_{V,Fstg1}\cdot\rho_F=q_{V,ERD}\cdot\rho_F+q_{V,HPP}\cdot\rho_F$<br>$q_{V,HPP}=q_{V,Fstg1}-q_{V,ERD}$<br>- Feed flow of the inter-stage pump, LPP:<br>$q_{Fstg2}=q_{ERD}+q_{LPP}$<br>$q_{V,Fstg2}\cdot\rho_{Fstg2}=q_{V,ERD}\cdot\rho_{Fstg2}+q_{V,LPP}\cdot\rho_{Fstg2}$<br>$q_{V,LPP}=q_{V,Fstg2}-q_{V,ERD}$<br>- Pump consumption: $P^{\square}_{W,BP}=0\cdot kW$<br>$P^{\square}_{W,HPP}=\frac{\left(\frac{q_{V,Fstg1}-q_{V,BD,stg2}}{m^3\cdot h^{-1}\cdot 3600}\right)\cdot\left(\frac{\Pi_{BD,stg1}-p^E}{bar\cdot 100^{-1}}\right)}{1\cdot 1}kW$<br>$P^{\square}_{W,LPPstg2}=\frac{\left(\frac{q_{V,Fstg2}-q_{V,BD,stg2}}{m^3\cdot h^{-1}\cdot 3600}\right)\cdot\left(\frac{\Pi_{BD,stg2}-\Pi_{BD,stg1}}{bar\cdot 100^{-1}}\right)}{1\cdot 1}\cdot kW$<br>Where:<br>$q_{V,F,stg1}=q_{V,F};\quad q_{V,BD,stg2}=q_{V,BD};\quad q_P=q_{P,stg1}+q_{P,stg2}$<br>$q_{V,F2}=\frac{q_F-q_{P,stg1}}{\rho_{F,stg2}};\qquad S_{BD}=\frac{S_F}{1-r_m}$<br>$\frac{q_F}{q_P}=\frac{1}{r_m};\ q_{V,F}(r_m)=\frac{q_{V,P}}{r_m}\cdot\frac{\rho_P}{\rho_F};\qquad q_{V,BD}(r_m)=\left(\frac{1}{r_m}-1\right)\cdot\frac{q_{V,P}\cdot\rho_P}{\rho_{BD}(r_m)}$ |

| | |
|---|---|

**Table 3.18. Power consumption of a desalination process based on SWRO with two-stages.**

| | |
|---|---|
| Seawater pressurisation and energy recovery: | $P^{\square}_{W,HPP} = \frac{\left(\frac{q_{V,Fstg1} - q_{V,ERD}}{m^3 \cdot h^{-1} \cdot 3600}\right) \cdot \left(\frac{p_{F,stg1} - p^E}{bar \cdot 100^{-1}}\right)}{\eta_{HPP} \cdot \eta_{eng,HPP}} kW$<br><br>$P^{\square}_{W,LPPstg2} = \frac{\left(\frac{q_{V,Fstg2} - q_{V,ERD}}{m^3 \cdot h^{-1} \cdot 3600}\right) \cdot \left(\frac{p_{F,stg2} - p_{BD,stg1}}{bar \cdot 100^{-1}}\right)}{\eta_{LPPstg2} \cdot \eta_{eng,LPPstg2}} \cdot kW$<br><br>$P^{\square}_{W,BP} = \frac{\frac{q_{V,ERD}}{m^3 \cdot h^{-1} \cdot 3600} \cdot \left(\frac{LP\,DP + HP\,DP + \sum \Delta p_{Loss,F-BD}}{bar \cdot 100^{-1}}\right)}{\eta_{BPstg2} \cdot \eta_{eng,stg2}} \cdot kW$<br><br>Where:<br>$q_{V,ERD} = q_{V,BDstg2} \cdot \frac{\left[\left(p_{F,ERDin} - LP\,DP\right) - p_{BD,ERDin} \cdot Eff\right]}{\left[p_{F,ERDin} \cdot Eff - \left(p_{BD,ERDin} - HP\,DP\right)\right]}$<br>$q_{V,F,stg1} = q_{V,F}; \quad q_{V,BD,stg2} = q_{V,BD}; \quad q_P = q_{P,stg1} + q_{P,stg2}$<br><br>$q_{V,F2} = \frac{q_F - q_{P,stg1}}{\rho_{F,stg2}}$<br><br>$\frac{q_F}{q_P} = \frac{1}{r_m}; q_{V,F}(r_m) = \frac{q_{V,P}}{r_m} \cdot \frac{\rho_P}{\rho_F}; \quad q_{V,BD}(r_m) = \left(\frac{1}{r_m} - 1\right) \cdot \frac{q_{V,P} \cdot \rho_P}{\rho_{BD}(r_m)}$<br><br>$S_{BD} = \frac{S_F}{1 - r_m}$ |

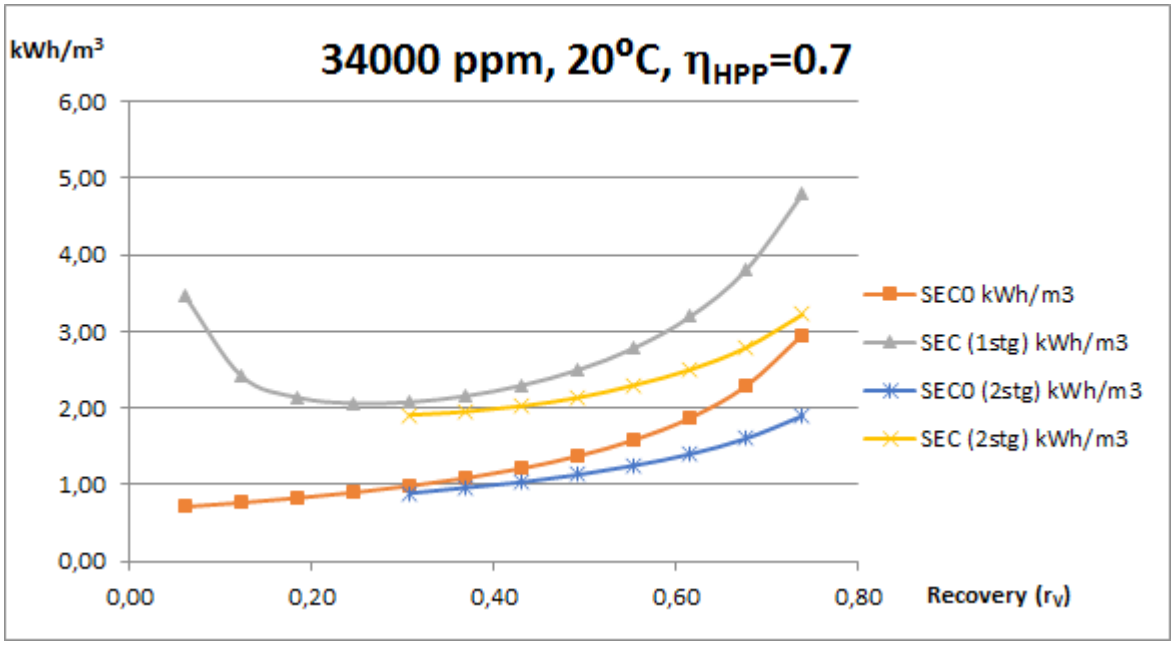


a) $\eta_{HPP}$= 0.70

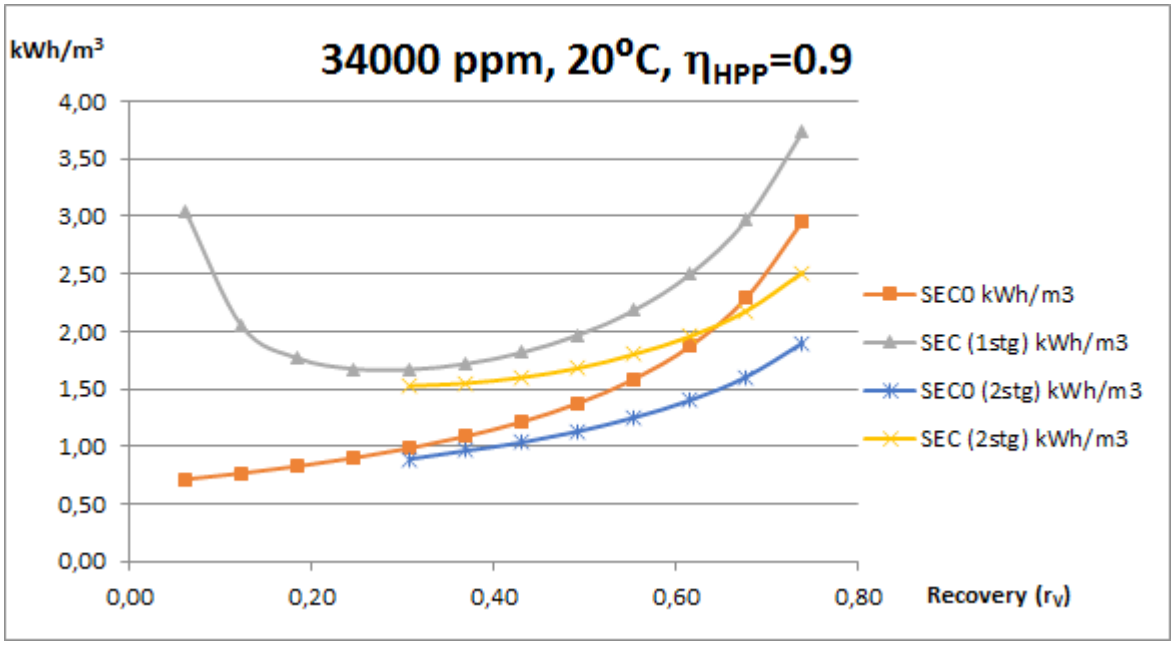


b) $\eta_{HPP}$= 0.90

**Figure 3.19. Specific Energy Consumption (SEC) with two stages in comparison conventional single-stage configuration, SEC (1stg), and to the ideal SWRO process with single stage, SEC0 (1stg) and double stage, SEC0 (2stg). Pacific conditions [Wilf, 2007].**

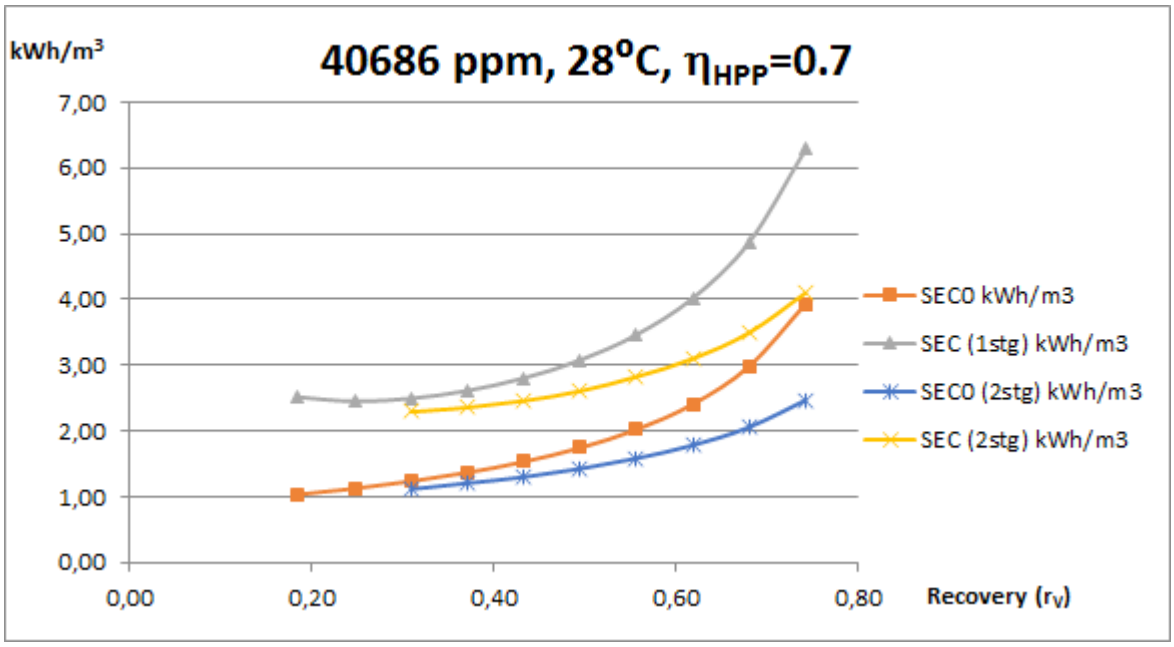


**a)** $\eta_{HPP}$**= 0.70**

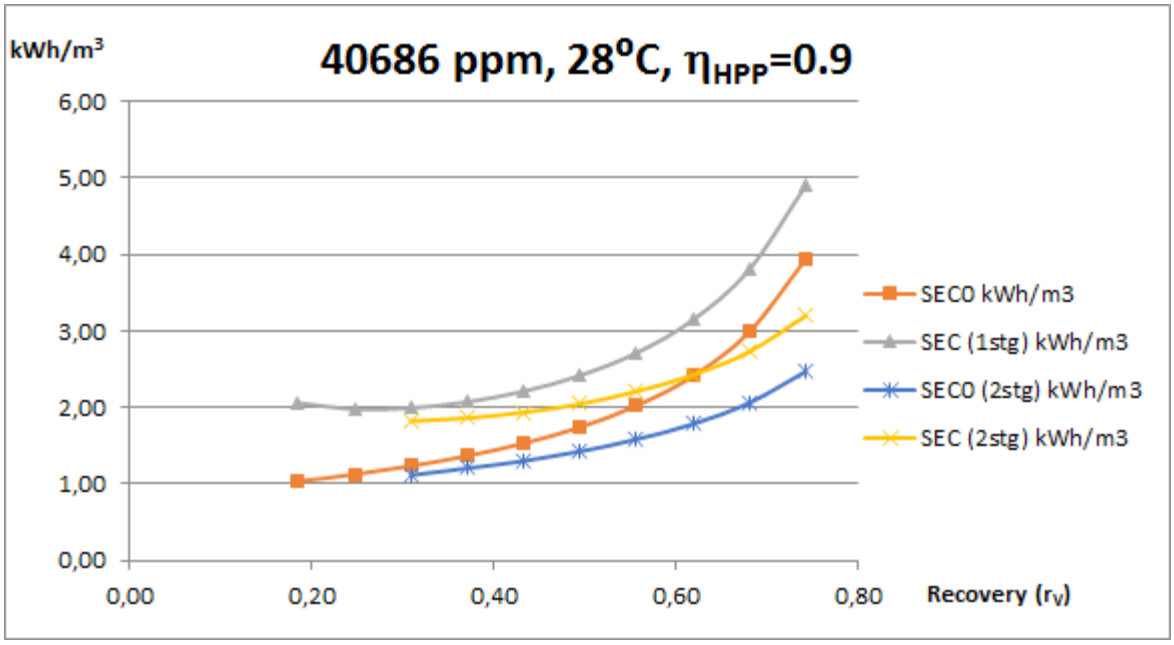


**b)** $\eta_{HPP}$**= 0.90**

**Figure 3.20. Specific Energy Consumption (SEC) with two stages in comparison conventional single-stage configuration, SEC (1stg), and to the ideal SWRO process with single stage, SEC0 (1stg) and double stage, SEC0 (2stg). Mediterranean conditions [Wilf, 2007].**

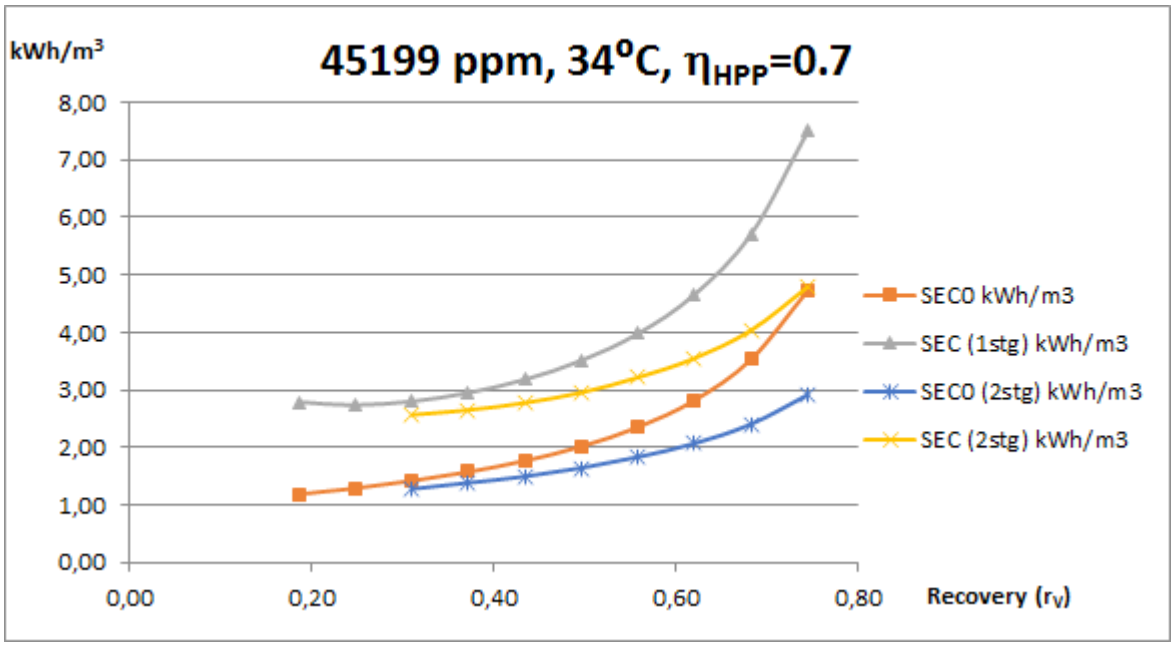


**a) $\eta_{HPP}$= 0.70**

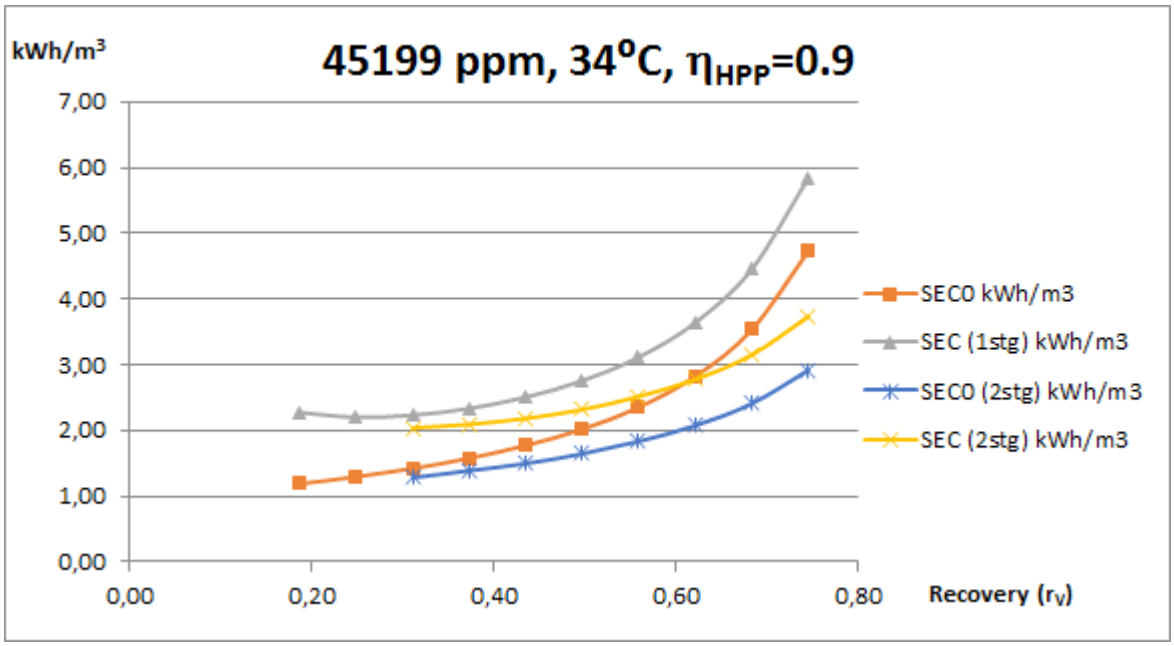


**a) $\eta_{HPP}$= 0.90**

**Figure 3.21. Specific Energy Consumption (SEC) with two stages in comparison conventional single-stage configuration, SEC (1stg), and to the ideal SWRO process with single stage, SEC0 (1stg) and double stage, SEC0 (2stg). Pacific conditions [Wilf, 2007].**

### 5.3. Innovative configurations proposed in the literature

A few candidate configuration were identified with some prospects of achieving significant advances on energy efficiency. They are thoroughly analysed in chapter 5.

- Veolia configuration [Wittmann *et al*, 2013] – see Figure 3.22-: This is conceptually similar to a two-stage configuration with no BP – see Figure 3.23 -. The advantages could be to achieve a more balanced permeate flow by means of adjusting the feed flow and membrane area from a specific intermediate positions of the membrane serial. The possible advantages of this configuration is thoroughly assessed in chapter 5. However, if no BP is used, no significant advantages on energy needs would be achieved. Since the HPP should pressurize the feed above osmotic pressure of the blowdown, only slight improvements in SEC are expected. Therefore, design and operating issues with influence in CAPital EXpenses (CAPEX) and OPeration EXpenses (OPEX) should be important to adopt this innovative configuration.

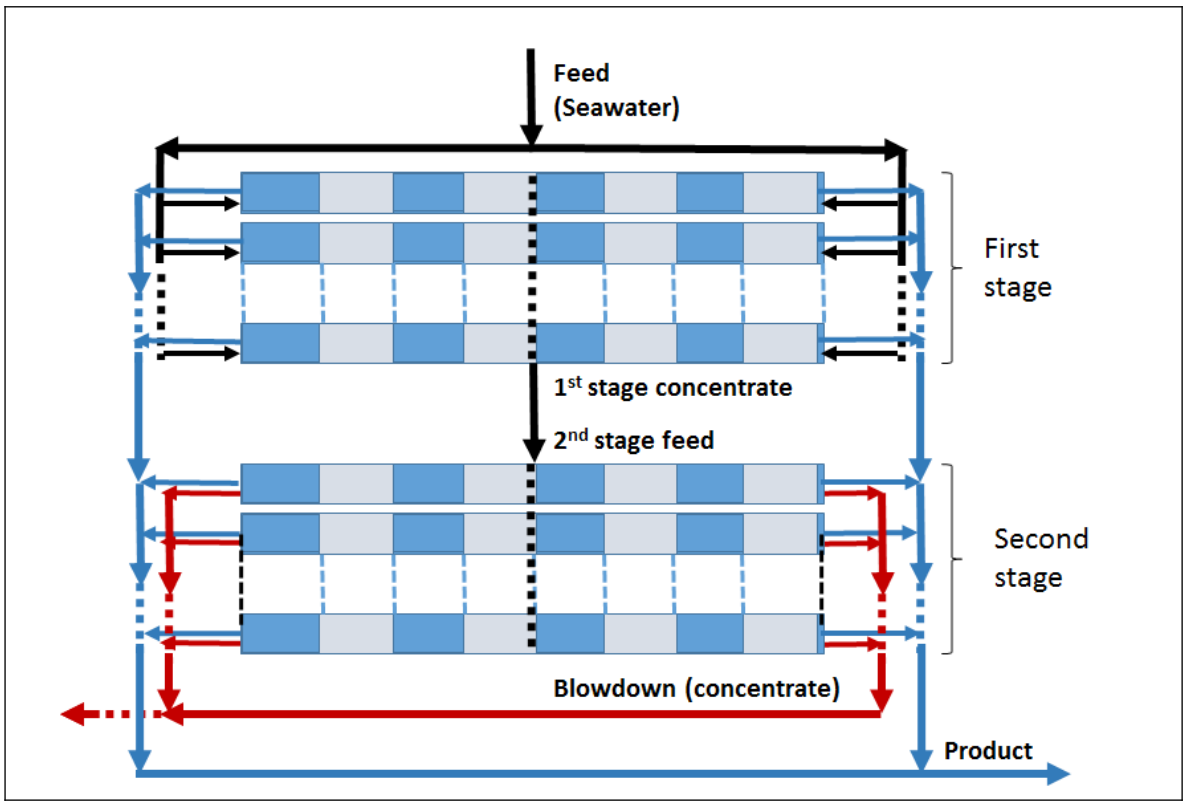


**Figure 3.22. Veolia configuration adapted from Wittmann *et al*, (2013).**

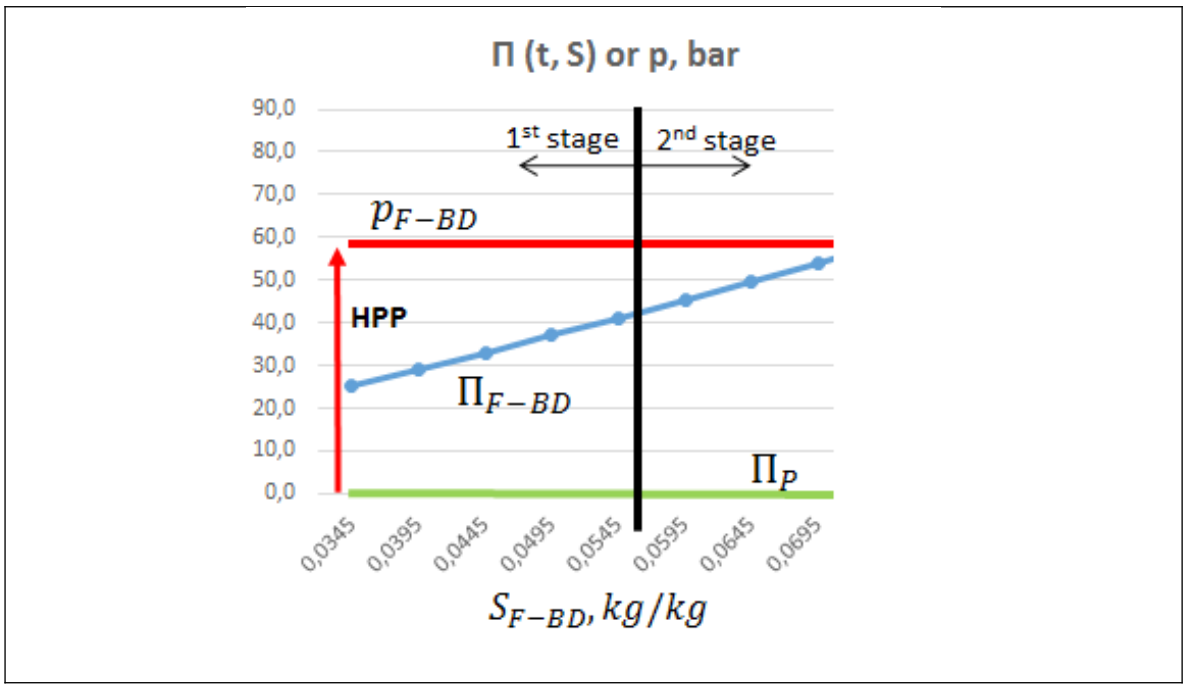


**Figure 3.23. Conceptual diagram of Veolia configuration.**

- General Electric (GE) configuration [Viera-Curbelo, 2013] – see Figures 3.24-3.25 -: This is conceptually similar to a two-stage configuration with no BP in which part of the feed flow bypasses the first stage – see Figure 3.26 -. Therefore, second stage can reach the same blowdown concentration with less requirement of membrane area since the average NDP is higher than that in conventional configurations. This configuration may result in CAPEX decreasing but no significant SEC decrease is expected since the HPP pressurised all the feed flow up to the required pressure at the tail of the second stage.

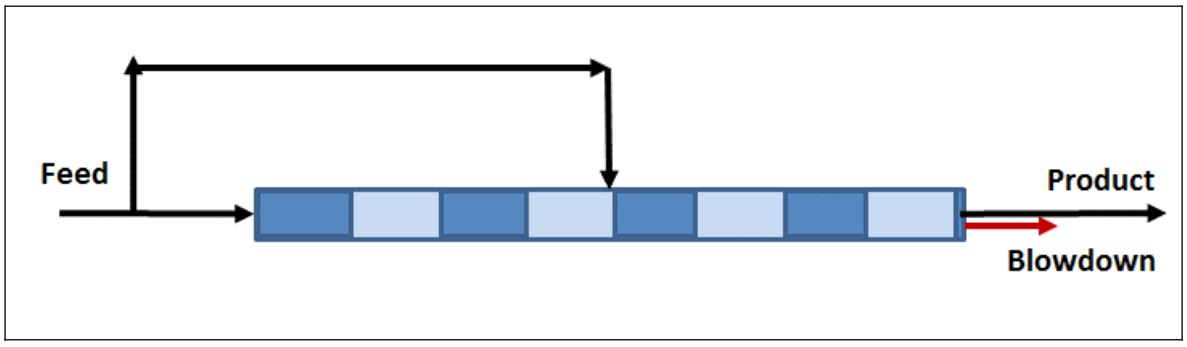


**Figure 3.24. GE configuration adapted from [Viera-Curbelo, 2013].**

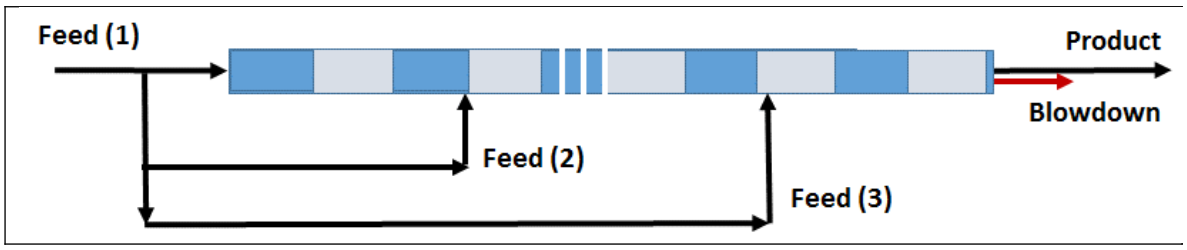


**Figure 3.25. Second configuration compatible with description reported by [Viera-Curbelo, 2013].**

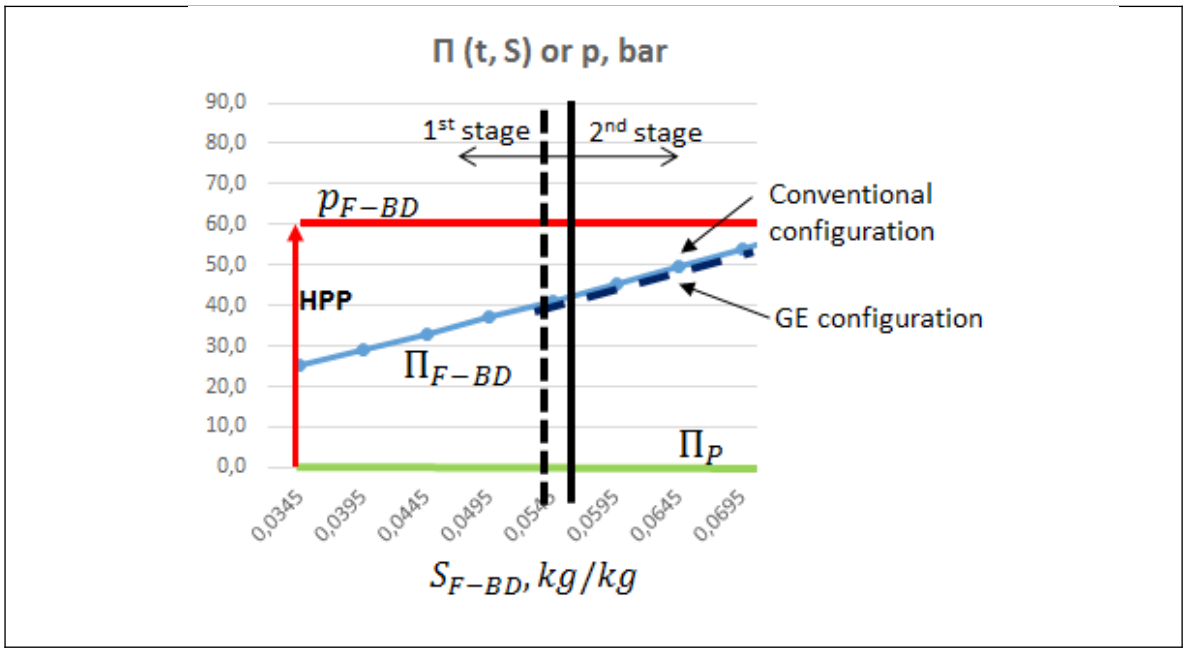


**Figure 3.26. Conceptual effect of GE configuration (dashed lines).**

- Desalitech- CCD (Closed Circuit Desalination): Figure 3.27 depicts the configuration referred to as Desalitech-CCD. This concept takes advantage of the multi-stage configuration along with the decreasing of the NDP (Fig. 3.28). Regardless CAPEX, this is a candidate configuration to dramatically reduce the SEC. The expected SEC should be ranged between two-stage and three-stage configurations. Nevertheless, it should be noted that the number of membrane elements, HPP´s and BP´s is similar than those of conventional two-stage configuration. A thorough analyses is reported in chapter 5.

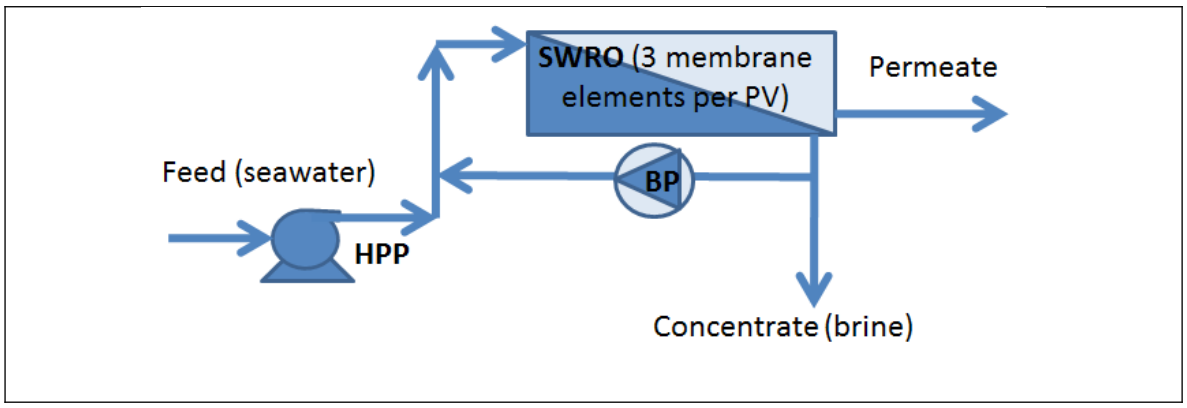


**Figure 3.27. Desalitech-CCD (Closed Circuit Desalination) concept. Energy recovery from the brine is not shown in the figure.**

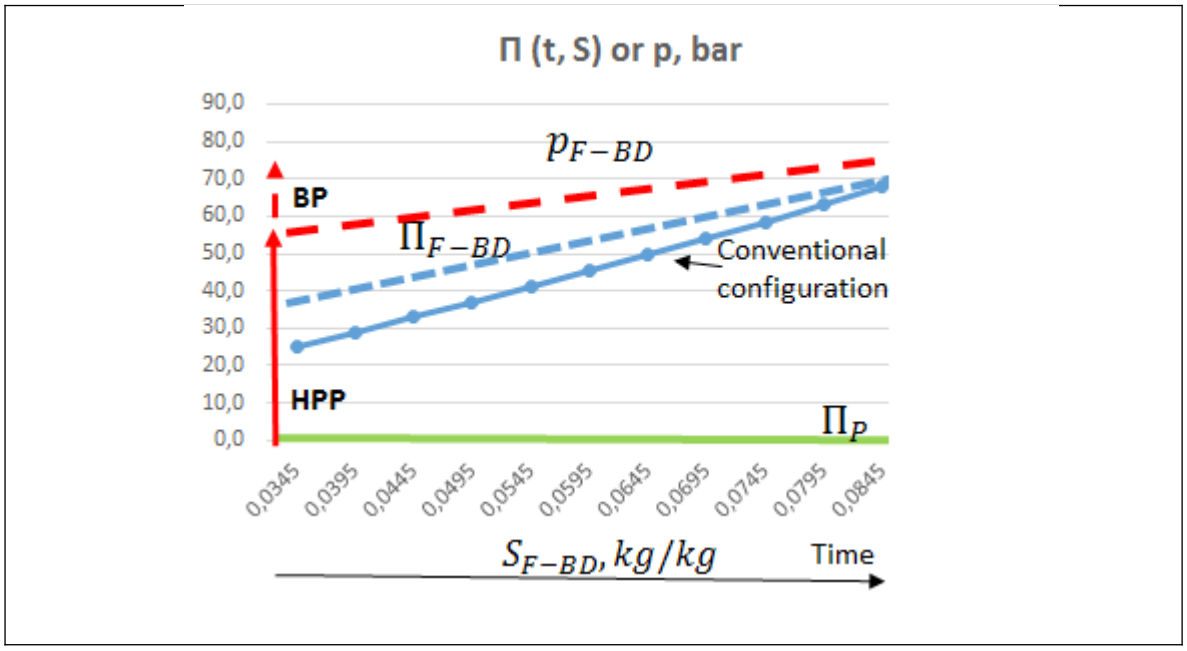


**Figure 3.28. Conceptual comparison of Desalitech-CCD (Closed Circuit Desalination) to conventional configuration.**

- Pressure Retarded Osmosis (PRO) concept as an additional energy recovery device – see Figure 3.29 -. In order to simplify the conceptual analysis carried out, a configuration based on conventional turbocharger is considered in order to avoid power consumption or booster pumps required if iSave or ERI-PX isobaric chambers are selected, respectively. Very high energy efficiency is assumed, 0.95, thus, resulting in optimistic hypothesis considering current technology. It is assumed that an external aqueous flow with low osmotic pressure is available. Any aqueous effluent that could be rejected to the sea could be used, as partially treated wastewater or treated industrial effluents. No reuse of this flow as part of the SWRO permeate is considered in this work. Solvent of the aqueous effluent passes spontaneously thorough a membrane that separates this from the brine outlet of an energy recovery device of the SWRO desalination process, thus increasing the mass flow rate of the pressurised brine flow (PRO).

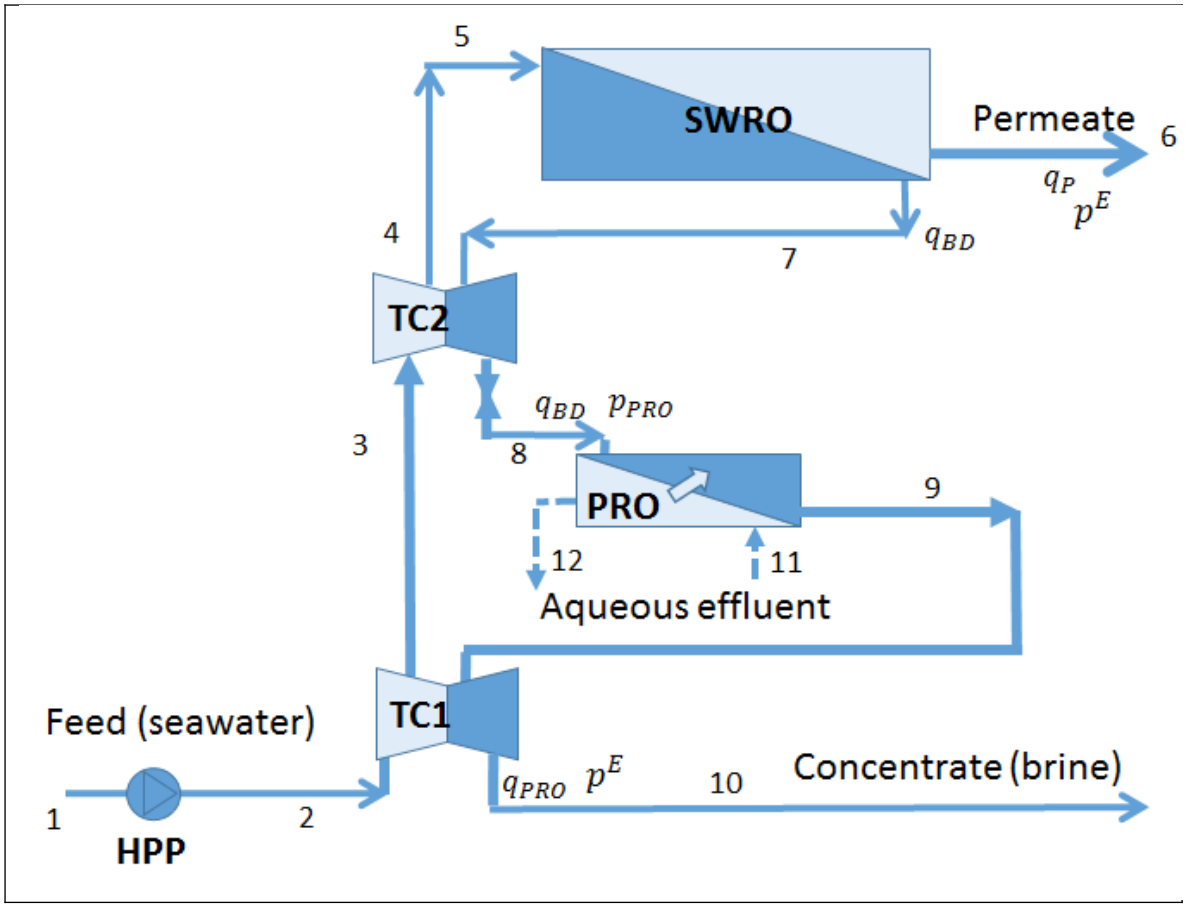


**Figure 3.29. Configuration of SWRO desalination and PRO with an external aqueous effluent in order to decrease the SEC of the SWRO desalination process.**

Table 3.19 summarises mass and exergy balances for a PRO process in which the inputs are blowdown (BD) of a desalination process and partially treated wastewater or other aqueous effluent. Part of the external aqueous effluent passes through the membrane, transferred water (tw). Therefore, their respective mass flow rates, $q_{BD}$ and $q_{tw}$, generates the outlet saline stream, $q_{PRO}$. The remaining aqueous effluent could be recycled or discharged from the system. In this work, the recovery rate of the PRO process is given by the ratio of either mass flow rate or volumetric flow:

$$r_{m,PRO} = \frac{q_{tw}}{q_{PRO}}$$

$$r_{V,PRO} = \frac{q_{V,tw}}{q_{V,PRO}}$$

Note that $q_{tw}$ is the water that passes the PRO membrane and that the maximum pressure achievable by the PRO steam in an ideal process is the osmotic pressure of the brine at the PRO system outlet.

Table 3.20 provides the calculation procedure of power saving attributable to a PRO process coupled to the SWRO desalination as follows. The energy transfer from PRO to SWRO desalination is carry out by means of a turbocharger as energy recovery device with efficiency, $\eta_{TC}$. Theoretically, the PRO system would be able to provide a mass flow rate $q_{PRO}$ at pressure $p_{PRO}$ lower than osmotic pressure of the PRO stream. This energy recovered from the hydraulic power of the PRO stream results in higher power saving in comparison to a conventional SWRO with energy recovery devices based on turbochargers. Input parameters to solve equations are recovery rate of both PRO and RO processes, ambient temperature $T^E$ and seawater salinity $S_{sw}$, and recovery rate of both SWRO and PRO processes. Theoretical results obtained for different input parameters are provided by tables 3.21-3.24, under the assumption of energy recovery of 95% in the turbocharger, which is better than those of current status of the technology.

**Table 3.19. Exergy analysis of a Pressure Retarded Osmosis (PRO) process.**

| | |
|---|---|
| Input parameters: | $r_{m,PRO}=\frac{q_{tww}}{q_{PRO}}$; $S_{BD}$; $q_{BD}$; $p_{PRO}<\Pi_{PRO}$ |
| Mass balances: | Solvent (water, w): $q_{tww}+q_{BD}=q_{PRO}$<br>Solute (s): $q_{s,BD}=q_{s,PRO}$<br>Hence, $\frac{q_{BD}}{q_{PRO}}=\frac{q_{PRO}-q_{tww}}{q_{PRO}}=1-r_{m,PRO}$<br>$S_{BD}=\frac{q_{s,BD}}{q_{BD}}$; $S_{PRO}=\frac{q_{s,PRO}}{q_{PRO}}=\frac{q_{s,BD}}{q_{PRO}}=\frac{q_{BD}\cdot S_{DB}}{q_{PRO}}$<br>$S_{PRO}=\left(1-r_{m,PRO}\right)\cdot S_{BD}$<br>Regarding RO process, feed is seawater: $S_{BD}=\frac{S_{sw}}{1-r_{m,RO}}$;<br>Then, by combining PRO and RO processes $S_{PRO}=\frac{\left(1-r_{m,PRO}\right)}{\left(1-r_{m,RO}\right)}S_{sw}$ |
| Energy recovered: | Energy transfer within the TurboCharger 1 (TC1):<br>$q_{V,F}\cdot\Delta p_{TC1}=\eta_{TC1}\cdot q_{V,PRO}\cdot\left(p_{PRO}-\Delta p_{Loss}-p^{E}\right)$<br>Energy transfer within the TurboCharger 2 (TC2):<br>$q_{V,F}\cdot\Delta p_{TC2}=\eta_{TC2}\cdot q_{V,BD}\cdot\left(p_{BD}-p_{PRO}\right)$ |

**Table 3.20. Energy analysis of a Pressure Retarded Osmosis (PRO) process.**

| | |
|---|---|
| Input parameters: | $r_{m,PRO}=\frac{q_{tww}}{q_{PRO}};\qquad p_{PRO}<\Pi_{PRO}=\Pi\left(T^{E},S_{PRO}\right)$ |
| Results of mass balances: | $S_{PRO}=\frac{\left(1-r_{m,PRO}\right)}{\left(1-r_{m,RO}\right)}S_{sw}$<br>$\frac{q_{BD}}{q_{PRO}}=1-r_{m,PRO};\qquad \frac{q_{BD}}{q_{P}}=\left(\frac{1}{r_{m,RO}}-1\right);$<br>$q_{V,PRO}=\frac{q_{PRO}}{\rho_{PRO}}=\left(\frac{1}{r_{m,RO}}-1\right)\frac{q_{P}}{\rho_{PRO}\cdot\left(1-r_{m,PRO}\right)}$ |
| Specific Energy Consumption: | - Energy consumption of the HPP:<br>$P_{W,HPP}=¿\frac{\left(\frac{q_{V,F}}{m^{3}\cdot h^{-1}\cdot 3600}\right)\cdot\left(\frac{\left(\Pi_{BD}+TDP-p^{E}\right)-\Delta p_{TC1}-\Delta p_{TC1}}{bar\cdot 100^{-1}}\right)}{\eta_{BP}\cdot\eta_{motor}}\cdot kW$<br>Where<br>$\Delta p_{TC1}=\eta_{TC1}\cdot\frac{q_{V,PRO}}{q_{V,F}}\cdot\left(p_{PRO}-\Delta p_{Loss}-p^{E}\right)$<br>$\Delta p_{TC2}=\eta_{TC2}\cdot\frac{q_{V,BD}}{q_{V,F}}\cdot\left(p_{BD}-p_{PRO}\right)$<br>- SEC of the SWRO/PRO desalination plant:<br>$SEC=\frac{P_{W,HPP}}{q_{V,P}}$ |

**Table 3.21.**
**Analysis of**

$$\Delta p_{TC2} = \eta_{TC2} \cdot \frac{q_{V,BD}}{q_{V,F}} \cdot (p_{BD} - p_{PRO})$$

$$\Delta p_{TC1} = \eta_{TC1} \cdot \frac{q_{V,PRO}}{q_{V,F}} \cdot (p_{PRO} - \Delta p_{Loss} - p^E)$$

$$P_{W,HPP} == \frac{\left(\frac{q_{V,F}}{m^3 \cdot h^{-1} \cdot 3600}\right) \cdot \left(\frac{\{\Pi_{BD} + TDP - p^E\} - \Delta p_{TC1} - \Delta p_{TC1}}{bar \cdot 100^{-1}}\right)}{\eta_{BP} \cdot \eta_{motor}} \cdot kW$$

$$S_{PRO} = \frac{(1 - r_{m,PRO})}{(1 - r_{m,RO})} S_{sw}$$

$$q_{V,PRO} = \frac{q_{PRO}}{\rho_{PRO}} = \left(\frac{1}{r_{m,RO}} - 1\right) \frac{q_p}{\rho_{PRO} \cdot (1 - r_{m,PRO})}$$

$$\frac{q_{BD}}{q_p} = \frac{1}{r_m} - 1$$

$$p_{PRO} < \Pi_{PRO} = \Pi(T^E, S_{PRO})$$

| $r_{m,PRO}$= | 0,5 | $p_{PRO,max}$, bar= | 20 | T, ºC= | 25 | $S_{sw}$, kg/kg= | 0,035165 | $q_p$, kg/h= | 996,9 | $r_{m,RO}$= | 0,48 |
|---|---|---|---|---|---|---|---|---|---|---|---|

| PRO process | | | | Energy recovery ($\eta_{TC}$= 0,95) | | | PRO + SWRO: Specific energy consumption (kWh/m³) | | | | |
|---|---|---|---|---|---|---|---|---|---|---|---|
| $S_{PRO}$, kg/kg | $\Pi_{PRO}$, kg/kg | $\rho_{PRO}$, kg/kg | $q_{V,wwt}$, m³/h | $p_{PRO}$, bar | $\Delta p_{,TC1}$ bar | $\Delta p_{,TC2}$ bar | $\Delta_{des}ex_f$ | $SEC_0$ | SEC (90%) | SEC (80%) | SEC (70%) |
| 0,033813 | 25,0 | 1022,7 | 1,0560 | 5 | 2,97 | 24,60 | 1,08 | 1,46 | 1,94 | 2,19 | 2,50 |
| PRO + SWRO: | | $q_{V,PRO}$, m³/h | 2,1121 | 6 | 3,96 | 24,11 | 1,08 | 1,46 | 1,91 | 2,15 | 2,46 |
| | | | | 7 | 4,94 | 23,63 | 1,08 | 1,46 | 1,88 | 2,11 | 2,41 |
| | | | | 8 | 5,93 | 23,15 | 1,08 | 1,46 | 1,84 | 2,07 | 2,37 |
| | | | | 9 | 6,92 | 22,67 | 1,08 | 1,46 | 1,81 | 2,04 | 2,33 |
| | | | | 10 | 7,91 | 22,19 | 1,08 | 1,46 | 1,78 | 2,00 | 2,28 |
| | | | | 11 | 8,90 | 21,70 | 1,08 | 1,46 | 1,74 | 1,96 | 2,24 |
| | | | | 12 | 9,89 | 21,22 | 1,08 | 1,46 | 1,71 | 1,92 | 2,20 |
| | | | | 13 | 10,88 | 20,74 | 1,08 | 1,46 | 1,68 | 1,89 | 2,16 |
| | | | | 14 | 11,87 | 20,26 | 1,08 | 1,46 | 1,64 | 1,85 | 2,11 |
| | | | | 15 | 12,86 | 19,78 | 1,08 | 1,46 | 1,61 | 1,81 | 2,07 |
| | | | | 16 | 13,85 | 19,30 | 1,08 | 1,46 | 1,58 | 1,77 | 2,03 |
| | | | | 17 | 14,83 | 18,81 | 1,08 | 1,46 | 1,54 | 1,74 | 1,98 |
| | | | | 18 | 15,82 | 18,33 | 1,08 | 1,46 | 1,51 | 1,70 | 1,94 |
| | | | | 19 | 16,81 | 17,85 | 1,08 | 1,46 | 1,48 | 1,66 | 1,90 |
| | | | | 20 | 17,80 | 17,37 | 1,08 | 1,46 | 1,44 | 1,62 | 1,85 |

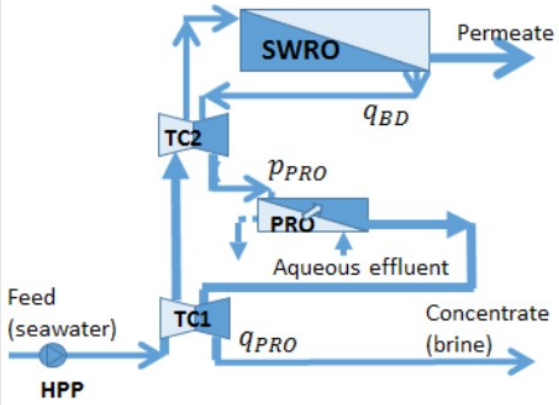

**Table 3.22. Analysis of PRO coupled to SWRO desalination, case 2.**

$$\Delta p_{TC2} = \eta_{TC2} \cdot \frac{q_{V,BD}}{q_{V,F}} \cdot (p_{BD} - p_{PRO})$$

$$\Delta p_{TC1} = \eta_{TC1} \cdot \frac{q_{V,PRO}}{q_{V,F}} \cdot (p_{PRO} - \Delta p_{Loss} - p^{E})$$

$$P_{W,HPP} == \frac{\left(\frac{q_{V,F}}{m^3 \cdot h^{-1} \cdot 3600}\right) \cdot \left(\frac{\{\Pi_{BD} + TDP - p^{E}\} - \Delta p_{TC1} - \Delta p_{TC1}}{bar \cdot 100^{-1}}\right)}{\eta_{BP} \cdot \eta_{motor}} \cdot kW$$

$$S_{PRO} = \frac{(1 - r_{m,PRO})}{(1 - r_{m,RO})} S_{sw}$$

$$q_{V,PRO} = \frac{q_{PRO}}{\rho_{PRO}} = \left(\frac{1}{r_{m,RO}} - 1\right) \frac{q_P}{\rho_{PRO} \cdot (1 - r_{m,PRO})}$$

$$\frac{q_{BD}}{q_P} = \frac{1}{r_m} - 1$$

$$p_{PRO} < \Pi_{PRO} = \Pi(T^{E}, S_{PRO})$$

| $r_{m,PRO}$= | 0,35 | $p_{PRO,max}$, bar= | 27,5 | T, ºC= | 25 | $S_{sw}$, kg/kg= | 0,035165 | $q_P$, kg/h= | 996,9 | $r_{m,RO}$= | 0,48 |
|---|---|---|---|---|---|---|---|---|---|---|---|

| PRO process | | | | Energy recovery ($\eta_{TC}$= 0,95) | | | PRO + SWRO: Specific energy consumption (kWh/m³) | | | | |
|---|---|---|---|---|---|---|---|---|---|---|---|
| $S_{PRO}$, kg/kg | $\Pi_{PRO}$, kg/kg | $\rho_{PRO}$, kg/kg | $q_{V,wwt}$, m³/h | $p_{PRO}$, bar | $\Delta p_{,TC1}$ bar | $\Delta p_{,TC2}$ bar | $\Delta_{des}ex_f$ | $SEC_0$ | SEC (90%) | SEC (80%) | SEC (70%) |
| 0,043956 | 33,0 | 1030,4 | 0,5644 | 5,0 | 2,27 | 24,60 | 1,08 | 1,46 | 1,99 | 2,24 | 2,56 |
| PRO + SWRO: | | $q_{V,PRO}$, m³/h | 1,6125 | 6,5 | 3,40 | 23,87 | 1,08 | 1,46 | 1,96 | 2,21 | 2,52 |
| | | | | 8,0 | 4,53 | 23,15 | 1,08 | 1,46 | 1,94 | 2,18 | 2,49 |
| | | | | 9,5 | 5,66 | 22,43 | 1,08 | 1,46 | 1,91 | 2,15 | 2,45 |
| | | | | 11,0 | 6,80 | 21,70 | 1,08 | 1,46 | 1,88 | 2,12 | 2,42 |
| | | | | 12,5 | 7,93 | 20,98 | 1,08 | 1,46 | 1,86 | 2,09 | 2,39 |
| | | | | 14,0 | 9,06 | 20,26 | 1,08 | 1,46 | 1,83 | 2,06 | 2,35 |
| | | | | 15,5 | 10,19 | 19,54 | 1,08 | 1,46 | 1,80 | 2,03 | 2,32 |
| | | | | 17,0 | 11,33 | 18,81 | 1,08 | 1,46 | 1,77 | 2,00 | 2,28 |
| | | | | 18,5 | 12,46 | 18,09 | 1,08 | 1,46 | 1,75 | 1,97 | 2,25 |
| | | | | 20,0 | 13,59 | 17,37 | 1,08 | 1,46 | 1,72 | 1,93 | 2,21 |
| | | | | 21,5 | 14,72 | 16,65 | 1,08 | 1,46 | 1,69 | 1,90 | 2,18 |
| | | | | 23,0 | 15,86 | 15,92 | 1,08 | 1,46 | 1,67 | 1,87 | 2,14 |
| | | | | 24,5 | 16,99 | 15,20 | 1,08 | 1,46 | 1,64 | 1,84 | 2,11 |
| | | | | 26,0 | 18,12 | 14,48 | 1,08 | 1,46 | 1,61 | 1,81 | 2,07 |
| | | | | 27,5 | 19,25 | 13,76 | 1,08 | 1,46 | 1,58 | 1,78 | 2,04 |

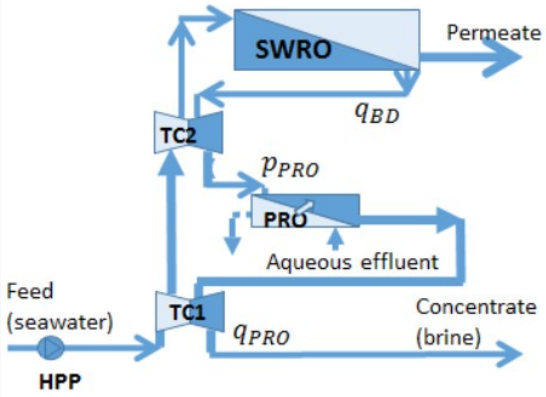

**Table 3.23. Analysis of PRO coupled to SWRO desalination, case 3.**

$$\Delta p_{TC2} = \eta_{TC2} \cdot \frac{q_{V,BD}}{q_{V,F}} \cdot (p_{BD} - p_{PRO})$$

$$\Delta p_{TC1} = \eta_{TC1} \cdot \frac{q_{V,PRO}}{q_{V,F}} \cdot (p_{PRO} - \Delta p_{Loss} - p^E)$$

$$P_{W,HPP} == \frac{\left(\frac{q_{V,F}}{m^3 \cdot h^{-1} \cdot 3600}\right) \cdot \left(\frac{\{\Pi_{BD} + TDP - p^E\} - \Delta p_{TC1} - \Delta p_{TC1}}{bar \cdot 100^{-1}}\right)}{\eta_{BP} \cdot \eta_{motor}} \cdot kW$$

$$S_{PRO} = \frac{(1 - r_{m,PRO})}{(1 - r_{m,RO})} S_{sw}$$

$$q_{V,PRO} = \frac{q_{PRO}}{\rho_{PRO}} = \left(\frac{1}{r_{m,RO}} - 1\right) \frac{q_P}{\rho_{PRO} \cdot (1 - r_{m,PRO})}$$

$$\frac{q_{BD}}{q_P} = \frac{1}{r_m} - 1$$

$$p_{PRO} < \Pi_{PRO} = \Pi(T^E, S_{PRO})$$

| $r_{m,PRO}$= | 0,2 | $p_{PRO,max}$, bar= | 35 | T, ºC= | 25 | $S_{sw}$, kg/kg= | 0,035165 | $q_P$, kg/h= | 996,9 | $r_{m,RO}$= | 0,48 |
|---|---|---|---|---|---|---|---|---|---|---|---|

| PRO process | | | | Energy recovery ($\eta_{TC}$= 0,95) | | | PRO + SWRO: Specific energy consumption (kWh/m³) | | | | |
|---|---|---|---|---|---|---|---|---|---|---|---|
| $S_{PRO}$, kg/kg | $\Pi_{PRO}$, kg/kg | $\rho_{PRO}$, kg/kg | $q_{V,wwt}$, m³/h | $p_{PRO}$, bar | $\Delta p_{,TC1}$ bar | $\Delta p_{,TC2}$ bar | $\Delta_{des}ex_f$ | $SEC_0$ | SEC (90%) | SEC (80%) | SEC (70%) |
| 0,054100 | 41,3 | 1038,1 | 0,2601 | 5,0 | 1,83 | 24,60 | 1,08 | 1,46 | 2,02 | 2,27 | 2,60 |
| PRO + SWRO: | | $q_{V,PRO}$, m³/h | 1,3004 | 7,0 | 3,04 | 23,63 | 1,08 | 1,46 | 2,00 | 2,25 | 2,57 |
| | | | | 9,0 | 4,26 | 22,67 | 1,08 | 1,46 | 1,99 | 2,23 | 2,55 |
| | | | | 11,0 | 5,48 | 21,70 | 1,08 | 1,46 | 1,97 | 2,21 | 2,53 |
| | | | | 13,0 | 6,70 | 20,74 | 1,08 | 1,46 | 1,95 | 2,20 | 2,51 |
| | | | | 15,0 | 7,92 | 19,78 | 1,08 | 1,46 | 1,94 | 2,18 | 2,49 |
| | | | | 17,0 | 9,13 | 18,81 | 1,08 | 1,46 | 1,92 | 2,16 | 2,47 |
| | | | | 19,0 | 10,35 | 17,85 | 1,08 | 1,46 | 1,90 | 2,14 | 2,45 |
| | | | | 21,0 | 11,57 | 16,89 | 1,08 | 1,46 | 1,88 | 2,12 | 2,42 |
| | | | | 23,0 | 12,79 | 15,92 | 1,08 | 1,46 | 1,87 | 2,10 | 2,40 |
| | | | | 25,0 | 14,01 | 14,96 | 1,08 | 1,46 | 1,85 | 2,08 | 2,38 |
| | | | | 27,0 | 15,22 | 14,00 | 1,08 | 1,46 | 1,83 | 2,06 | 2,36 |
| | | | | 29,0 | 16,44 | 13,03 | 1,08 | 1,46 | 1,82 | 2,05 | 2,34 |
| | | | | 31,0 | 17,66 | 12,07 | 1,08 | 1,46 | 1,80 | 2,03 | 2,32 |
| | | | | 33,0 | 18,88 | 11,11 | 1,08 | 1,46 | 1,78 | 2,01 | 2,29 |
| | | | | 35,0 | 20,09 | 10,14 | 1,08 | 1,46 | 1,77 | 1,99 | 2,27 |

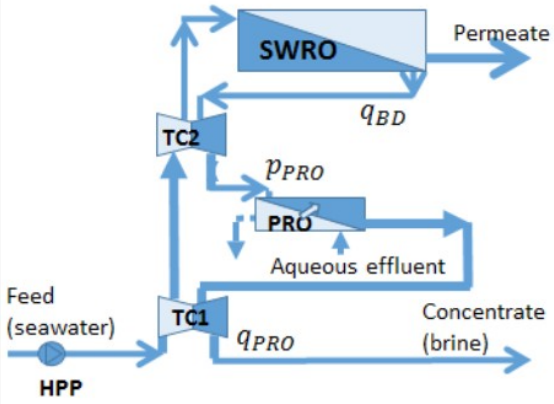

**Table 3.24. Analysis of PRO coupled to SWRO desalination, case 4.**

$$\Delta p_{TC2} = \eta_{TC2} \cdot \frac{q_{V,BD}}{q_{V,F}} \cdot (p_{BD} - p_{PRO})$$

$$\Delta p_{TC1} = \eta_{TC1} \cdot \frac{q_{V,PRO}}{q_{V,F}} \cdot (p_{PRO} - \Delta p_{Loss} - p^E)$$

$$P_{W,HPP} == \frac{\left(\frac{q_{V,F}}{m^3 \cdot h^{-1} \cdot 3600}\right) \cdot \left(\frac{\{\Pi_{BD} + TDP - p^E\} - \Delta p_{TC1} - \Delta p_{TC1}}{bar \cdot 100^{-1}}\right)}{\eta_{BP} \cdot \eta_{motor}} \cdot kW$$

$$S_{PRO} = \frac{(1 - r_{m,PRO})}{(1 - r_{m,RO})} S_{sw}$$

$$q_{V,PRO} = \frac{q_{PRO}}{\rho_{PRO}} = \left(\frac{1}{r_{m,RO}} - 1\right) \frac{q_P}{\rho_{PRO} \cdot (1 - r_{m,PRO})}$$

$$\frac{q_{BD}}{q_P} = \frac{1}{r_m} - 1$$

$$p_{PRO} < \Pi_{PRO} = \Pi(T^E, S_{PRO})$$

| $r_{m,PRO}$= | 0,05 | $p_{PRO,max}$, bar= | 50 | T, ºC= | 25 | $S_{sw}$, kg/kg= | 0,035165 | $q_P$, kg/h= | 996,9 | $r_{m,RO}$= | 0,48 |
|---|---|---|---|---|---|---|---|---|---|---|---|

| PRO process | | | | Energy recovery ($\eta_{TC}$= 0,95) | | | PRO + SWRO: Specific energy consumption (kWh/m$^3$) | | | | |
|---|---|---|---|---|---|---|---|---|---|---|---|
| $S_{PRO}$, kg/kg | $\Pi_{PRO}$, kg/kg | $\rho_{PRO}$, kg/kg | $q_{V,wwt}$, m$^3$/h | $p_{PRO}$, bar | $\Delta p_{,TC1}$ bar | $\Delta p_{,TC2}$ bar | $\Delta_{des}ex_f$ | $SEC_0$ | SEC (90%) | SEC (80%) | SEC (70%) |
| 0,064244 | 50,0 | 1045,8 | 0,0543 | 5,0 | 1,53 | 24,60 | 1,08 | 1,46 | 2,04 | 2,29 | 2,62 |
| PRO + SWRO: | | $q_{V,PRO}$, m$^3$/h | 1,0870 | 7,5 | 2,80 | 23,39 | 1,08 | 1,46 | 2,03 | 2,29 | 2,62 |
| | | | | 10,0 | 4,07 | 22,19 | 1,08 | 1,46 | 2,03 | 2,28 | 2,61 |
| | | | | 12,5 | 5,34 | 20,98 | 1,08 | 1,46 | 2,03 | 2,28 | 2,60 |
| | | | | 15,0 | 6,62 | 19,78 | 1,08 | 1,46 | 2,02 | 2,27 | 2,60 |
| | | | | 17,5 | 7,89 | 18,57 | 1,08 | 1,46 | 2,02 | 2,27 | 2,59 |
| | | | | 20,0 | 9,16 | 17,37 | 1,08 | 1,46 | 2,01 | 2,26 | 2,59 |
| | | | | 22,5 | 10,43 | 16,16 | 1,08 | 1,46 | 2,01 | 2,26 | 2,58 |
| | | | | 25,0 | 11,71 | 14,96 | 1,08 | 1,46 | 2,00 | 2,25 | 2,58 |
| | | | | 27,5 | 12,98 | 13,76 | 1,08 | 1,46 | 2,00 | 2,25 | 2,57 |
| | | | | 30,0 | 14,25 | 12,55 | 1,08 | 1,46 | 1,99 | 2,24 | 2,56 |
| | | | | 32,5 | 15,52 | 11,35 | 1,08 | 1,46 | 1,99 | 2,24 | 2,56 |
| | | | | 35,0 | 16,80 | 10,14 | 1,08 | 1,46 | 1,98 | 2,23 | 2,55 |
| | | | | 37,5 | 18,07 | 8,94 | 1,08 | 1,46 | 1,98 | 2,23 | 2,55 |
| | | | | 40,0 | 19,34 | 7,73 | 1,08 | 1,46 | 1,98 | 2,22 | 2,54 |
| | | | | 42,5 | 20,61 | 6,53 | 1,08 | 1,46 | 1,97 | 2,22 | 2,53 |

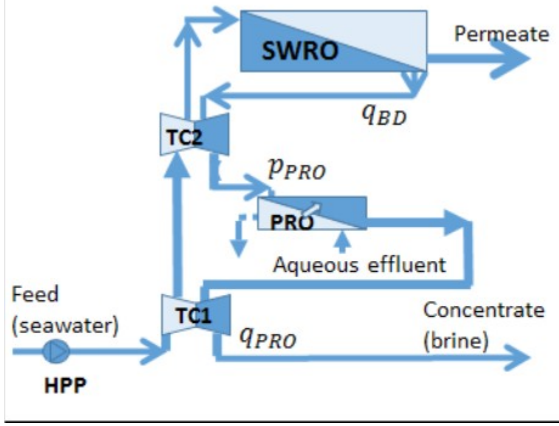

**Table 3.25. Power saving in case 1 ($r_{PRO}$= 0.50) with 0.95 of energy efficiency of the ERD.**

| CASE 1: Energy saving | | | |
|---|---|---|---|
| $\eta_{HPP}$= 0,90 kWh/m$^3$ | $\eta_{HPP}$= 0,80 kWh/m$^3$ | $\eta_{HPP}$= 0,70 kWh/m$^3$ | PRO system $p_{PRO}$, bar |
| 0,08 | 0,08 | 0,07 | **5,0** |
| 0,11 | 0,11 | 0,12 | **6,0** |
| 0,15 | 0,15 | 0,16 | **7,0** |
| 0,18 | 0,19 | 0,20 | **8,0** |
| 0,21 | 0,23 | 0,24 | **9,0** |
| 0,25 | 0,27 | 0,29 | **10,0** |
| 0,28 | 0,30 | 0,33 | **11,0** |
| 0,31 | 0,34 | 0,37 | **12,0** |
| 0,35 | 0,38 | 0,42 | **13,0** |
| 0,38 | 0,42 | 0,46 | **14,0** |
| 0,41 | 0,45 | 0,50 | **15,0** |
| 0,45 | 0,49 | 0,55 | **16,0** |
| 0,48 | 0,53 | 0,59 | **17,0** |
| 0,51 | 0,57 | 0,63 | **18,0** |
| 0,55 | 0,60 | 0,67 | **19,0** |
| 0,58 | 0,64 | 0,72 | **20,0** |

**Table 3.26. Power saving in case 2 ($r_{PRO}$= 0.35) with 0.95 of energy efficiency of the ERD.**

| CASE 2 | | | |
|---|---|---|---|
| $\eta_{HPP}$= 0,90 kWh/m$^3$ | $\eta_{HPP}$= 0,80 kWh/m$^3$ | $\eta_{HPP}$= 0,70 kWh/m$^3$ | PRO system $p_{PRO}$, bar |
| 0,03 | 0,03 | 0,01 | **5,0** |
| 0,06 | 0,06 | 0,05 | **6,5** |
| 0,09 | 0,09 | 0,08 | **8,0** |
| 0,11 | 0,12 | 0,12 | **9,5** |
| 0,14 | 0,15 | 0,15 | **11,0** |
| 0,17 | 0,18 | 0,19 | **12,5** |
| 0,20 | 0,21 | 0,22 | **14,0** |
| 0,22 | 0,24 | 0,26 | **15,5** |
| 0,25 | 0,27 | 0,29 | **17,0** |
| 0,28 | 0,30 | 0,33 | **18,5** |
| 0,30 | 0,33 | 0,36 | **20,0** |
| 0,33 | 0,36 | 0,40 | **21,5** |
| 0,36 | 0,39 | 0,43 | **23,0** |
| 0,39 | 0,42 | 0,46 | **24,5** |
| 0,41 | 0,45 | 0,50 | **26,0** |
| 0,44 | 0,48 | 0,53 | **27,5** |

**Table 3.27. Power saving in case 3 ($r_{PRO}$= 0.20) with 0.95 of energy efficiency of the ERD.**

| CASE 3 | | | |
|---|---|---|---|
| $\eta_{HPP}$= 0,90 kWh/m$^3$ | $\eta_{HPP}$= 0,80 kWh/m$^3$ | $\eta_{HPP}$= 0,70 kWh/m$^3$ | PRO system $p_{PRO}$, bar |
| 0,00 | -0,01 | -0,02 | **5,0** |
| 0,02 | 0,01 | 0,00 | **7,0** |
| 0,04 | 0,03 | 0,02 | **9,0** |
| 0,06 | 0,05 | 0,04 | **11,0** |
| 0,07 | 0,07 | 0,06 | **13,0** |
| 0,09 | 0,09 | 0,08 | **15,0** |
| 0,11 | 0,11 | 0,11 | **17,0** |
| 0,12 | 0,12 | 0,13 | **19,0** |
| 0,14 | 0,14 | 0,15 | **21,0** |
| 0,16 | 0,16 | 0,17 | **23,0** |
| 0,17 | 0,18 | 0,19 | **25,0** |
| 0,19 | 0,20 | 0,21 | **27,0** |
| 0,21 | 0,22 | 0,23 | **29,0** |
| 0,22 | 0,24 | 0,26 | **31,0** |
| 0,24 | 0,26 | 0,28 | **33,0** |
| 0,26 | 0,28 | 0,30 | **35,0** |

**Table 3.28. Power saving in case 4 ($r_{PRO}$= 0.05) with 0.95 of energy efficiency of the ERD.**

| CASE 4 | | | |
|---|---|---|---|
| $\eta_{HPP}$= 0,90 kWh/m$^3$ | $\eta_{HPP}$= 0,80 kWh/m$^3$ | $\eta_{HPP}$= 0,70 kWh/m$^3$ | PRO system $p_{PRO}$, bar |
| -0,01 | -0,03 | -0,05 | **5,0** |
| -0,01 | -0,02 | -0,04 | **7,5** |
| -0,01 | -0,02 | -0,04 | **10,0** |
| 0,00 | -0,01 | -0,03 | **12,5** |
| 0,00 | -0,01 | -0,03 | **15,0** |
| 0,01 | 0,00 | -0,02 | **17,5** |
| 0,01 | 0,00 | -0,01 | **20,0** |
| 0,02 | 0,01 | -0,01 | **22,5** |
| 0,02 | 0,01 | 0,00 | **25,0** |
| 0,03 | 0,02 | 0,00 | **27,5** |
| 0,03 | 0,02 | 0,01 | **30,0** |
| 0,03 | 0,03 | 0,01 | **32,5** |
| 0,04 | 0,03 | 0,02 | **35,0** |
| 0,04 | 0,04 | 0,03 | **37,5** |
| 0,05 | 0,04 | 0,03 | **40,0** |
| 0,05 | 0,05 | 0,04 | **42,5** |

Finally, future evolution of commercial products is assessed considering configuration shown in fig.3.29. To this end, working pressure of the PRO system will be only limited by creating positive driving force for the solvent pass and energy efficiency of turbochargers of 0.90 and 0.98 will be assumed. Next figures give results obtained.

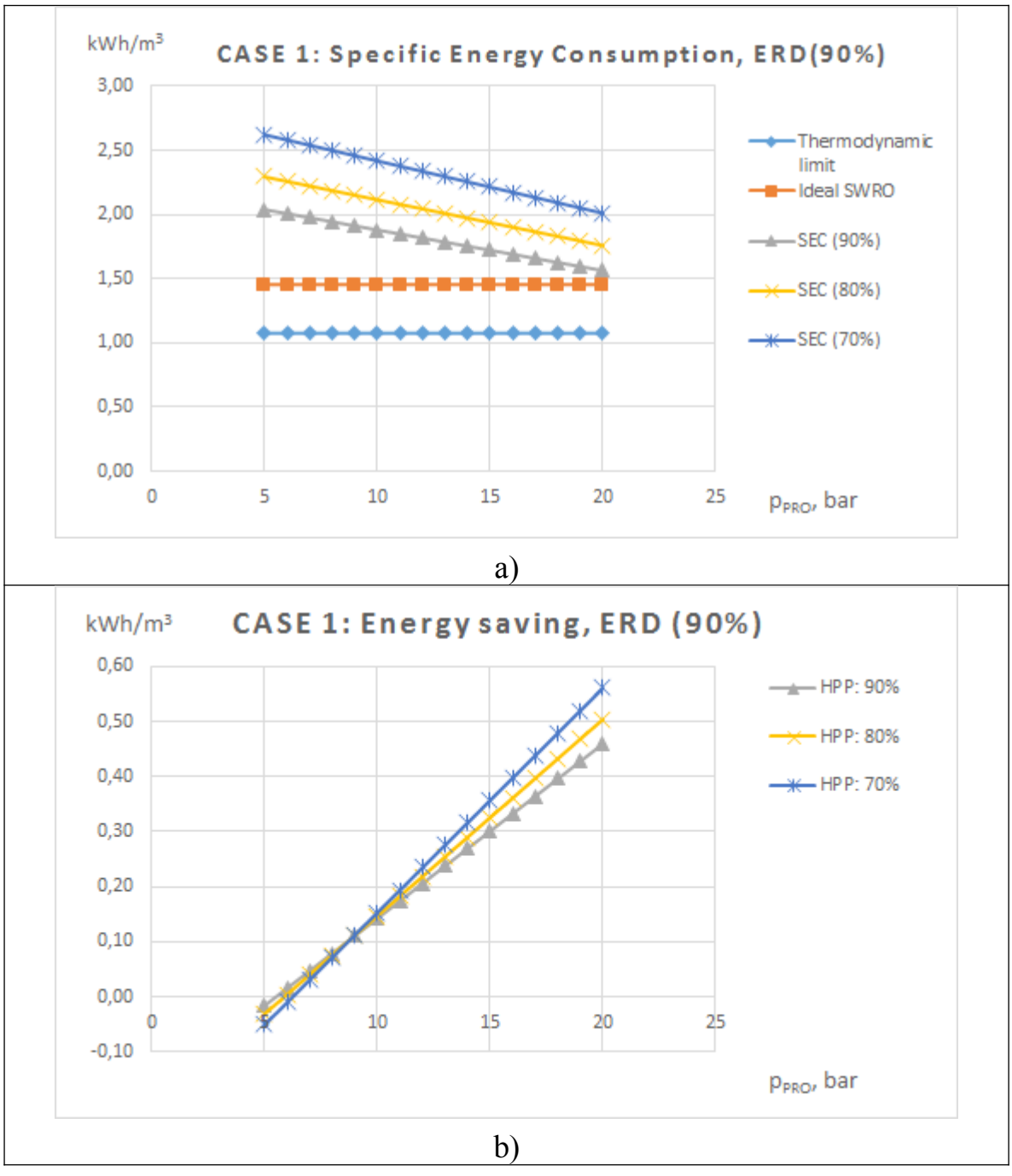


**Figure 3.30. Results of case 1 ($r_{PRO}$= 0.5) considering 0.90 of energy efficiency of the Energy Recovery Device (ERD).**


**Figure 3.31. Results of case 1 ($r_{PRO}$= 0.5) considering 0.98 of energy efficiency of the Energy Recovery Device (ERD).**

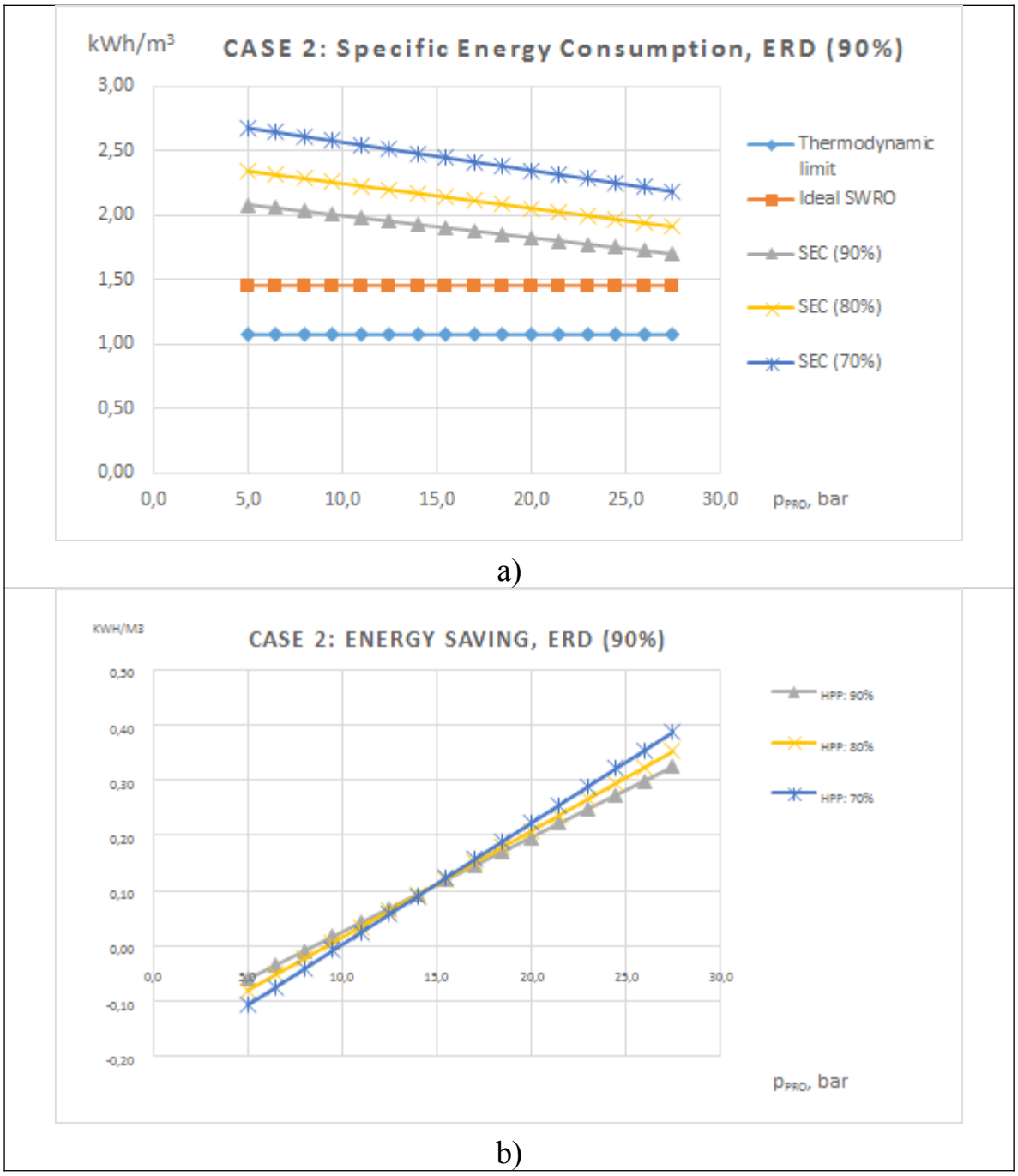


**Figure 3.32. Results of case 2 ($r_{PRO}$= 0.35) considering 0.90 of energy efficiency of the Energy Recovery Device (ERD).**

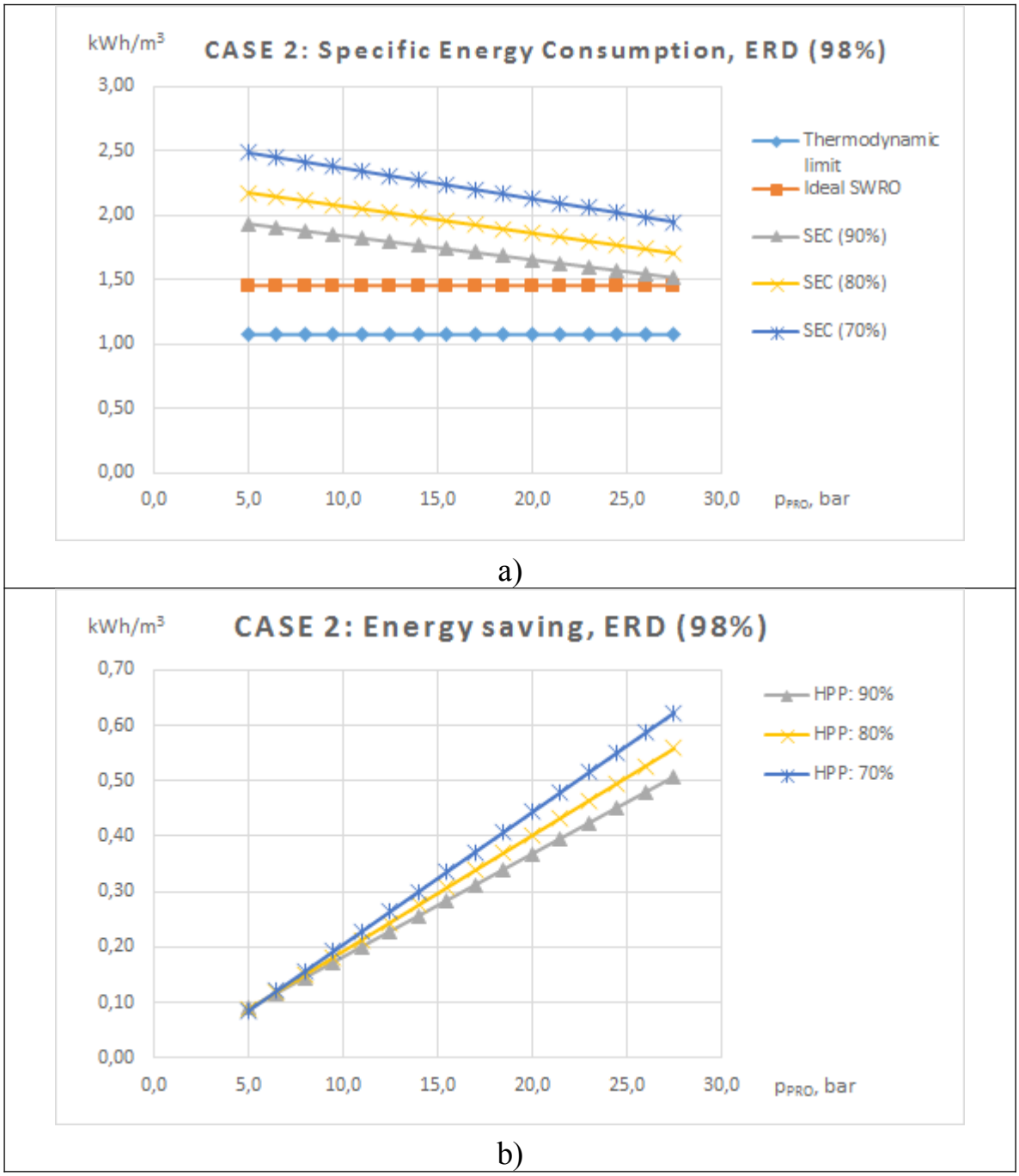


**Figure 3.33. Results of case 2 ($r_{PRO}$= 0.35) considering 0.98 of energy efficiency of the Energy Recovery Device (ERD).**

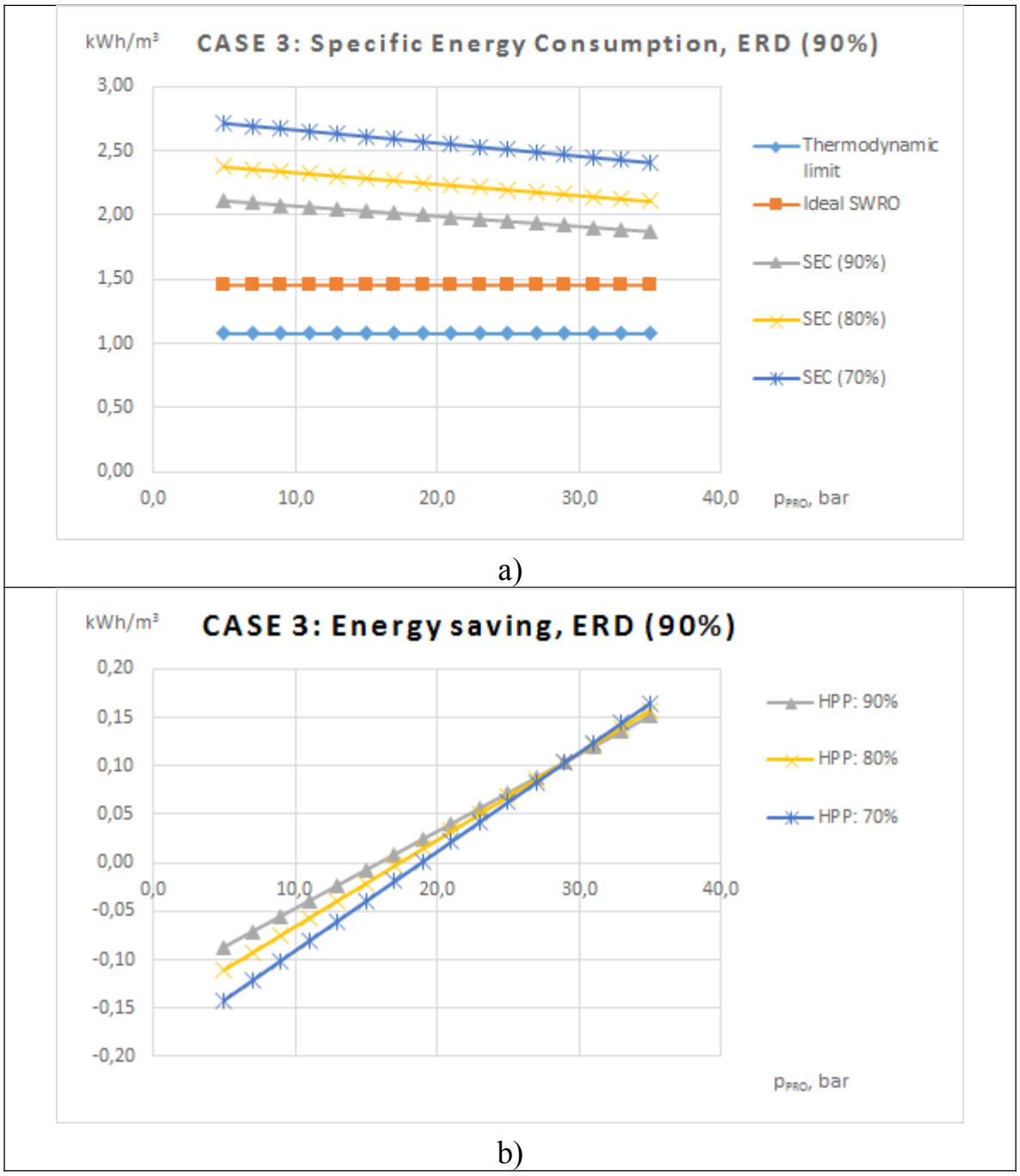


**Figure 3.34. Results of case 2 ($r_{PRO}$= 0.20) considering 0.90 of energy efficiency of the Energy Recovery Device (ERD).**

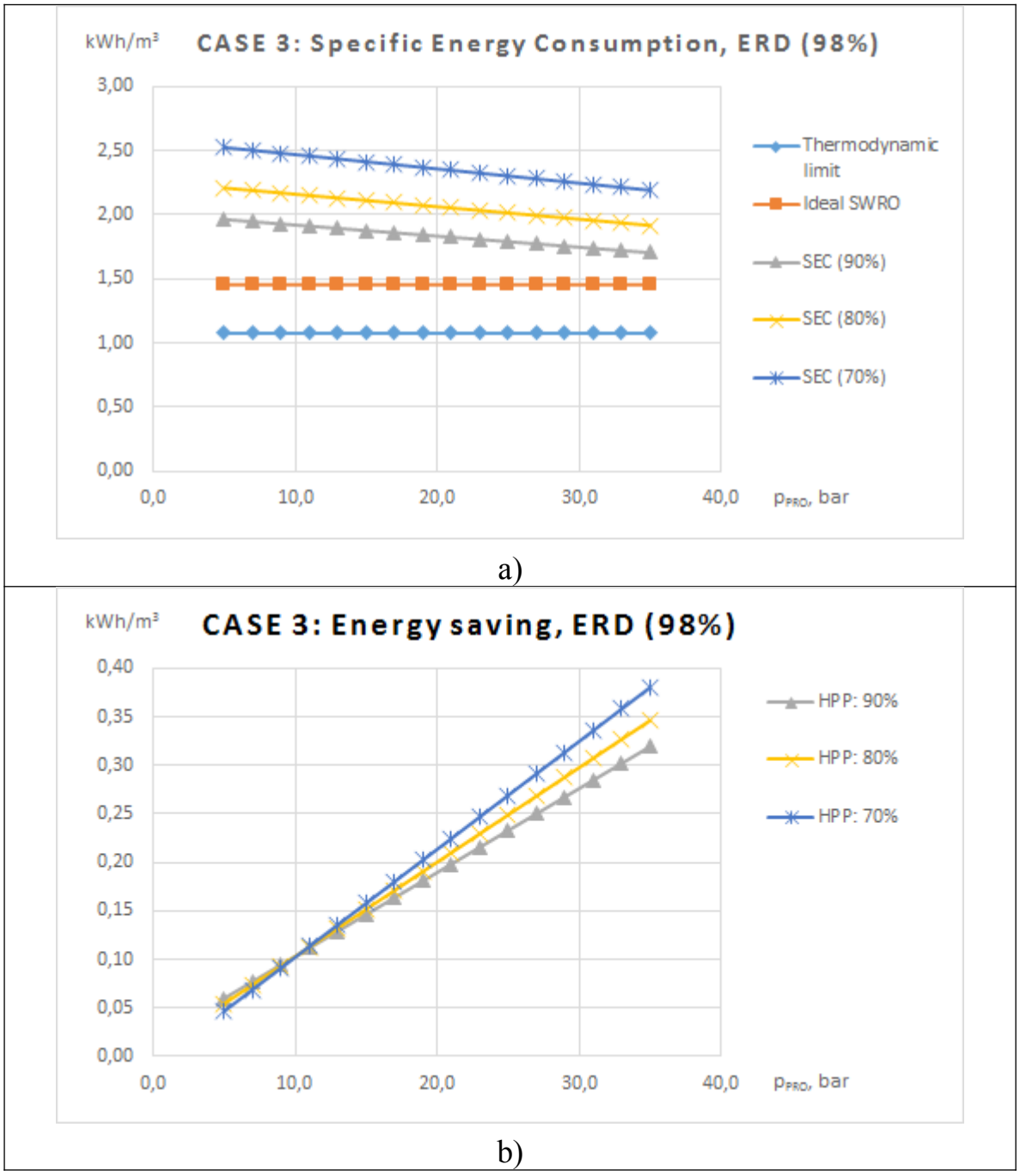


**Figure 3.35. Results of case 2 ($r_{PRO}$= 0.20) considering 0.98 of energy efficiency of the Energy Recovery Device (ERD).**

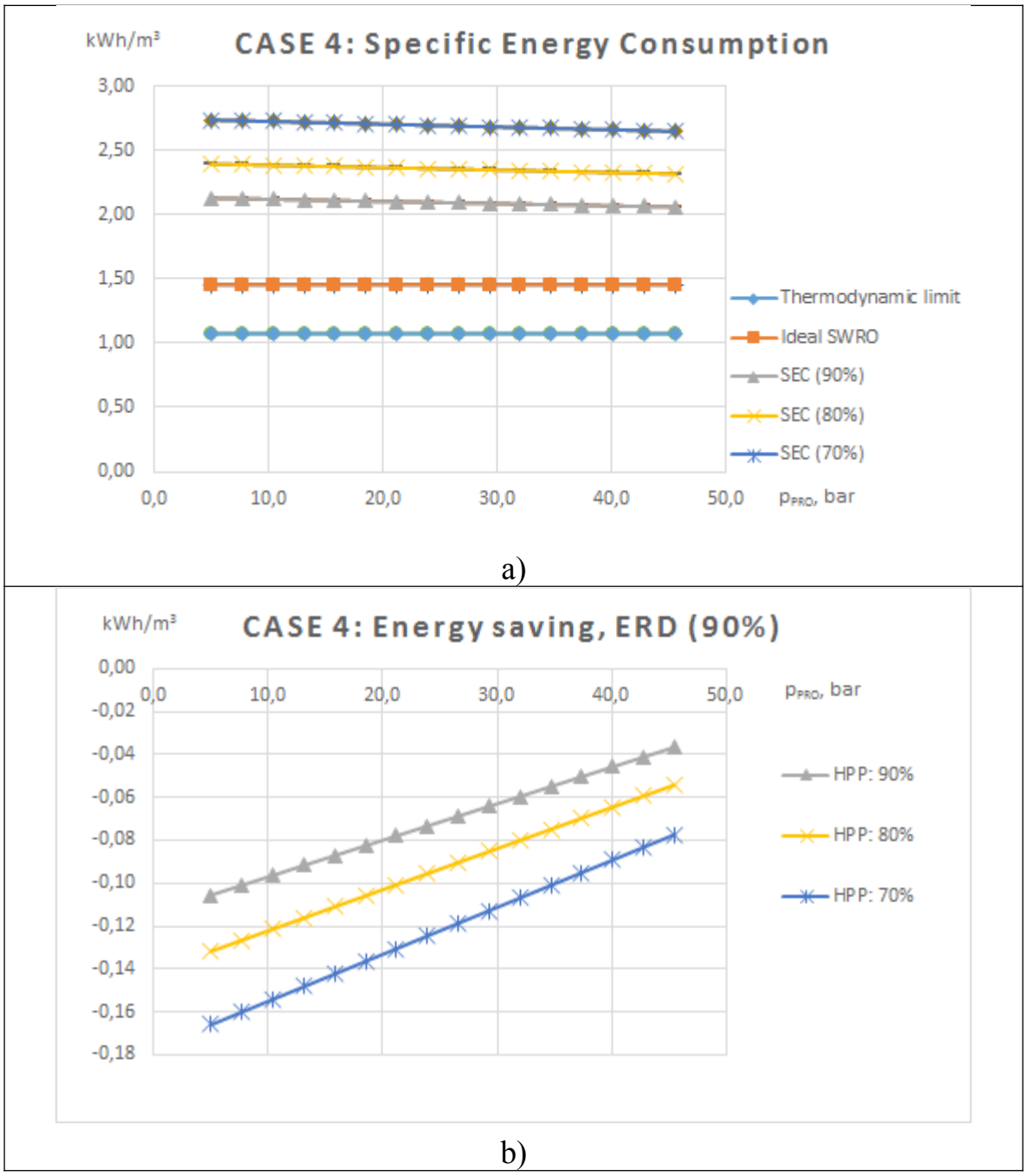


**Figure 3.36. Results of case 4 ($r_{PRO}$= 0.05) considering 0.90 of energy efficiency of the Energy Recovery Device (ERD).**

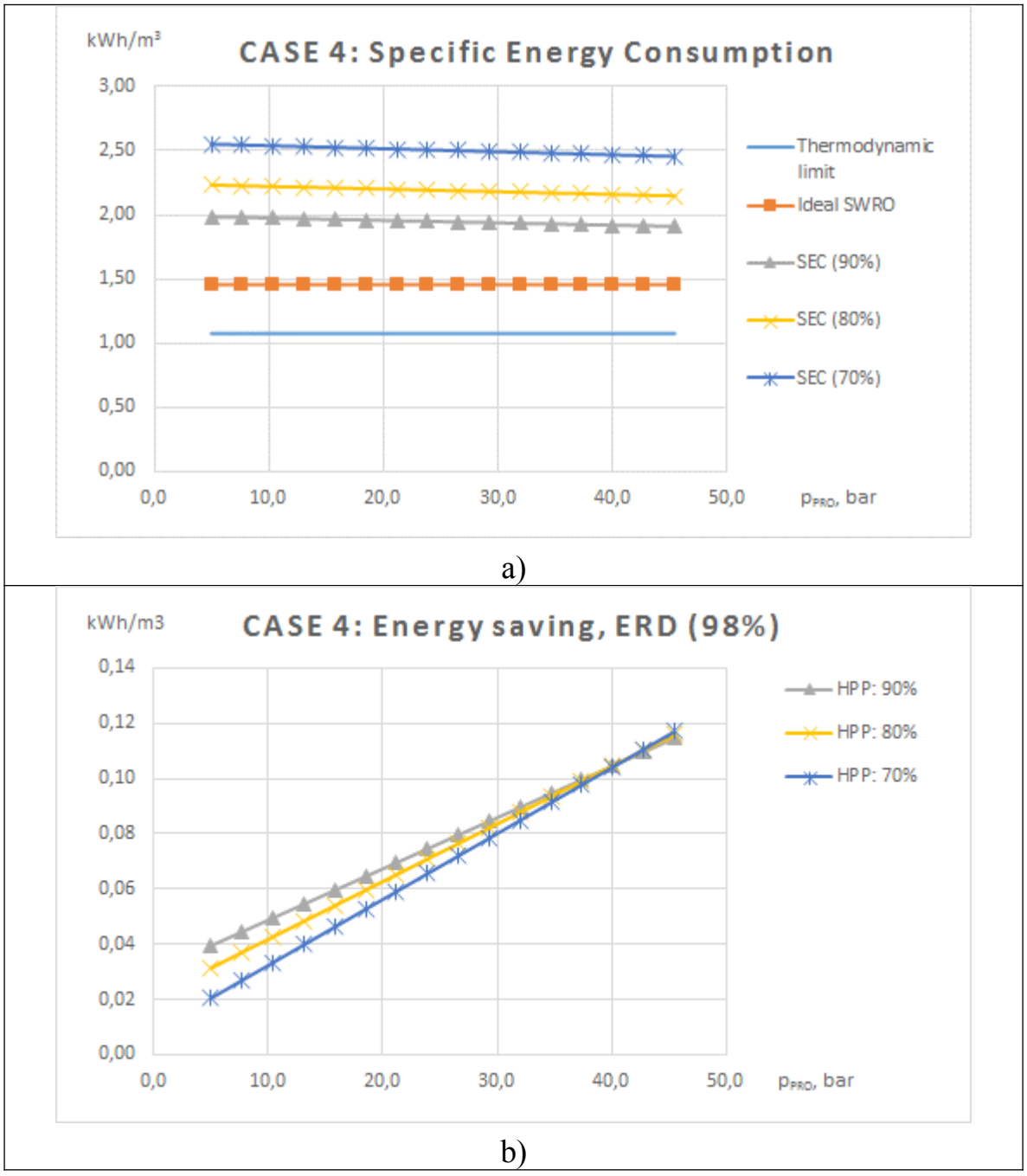


**Figure 3.37. Results of case 4 ($r_{PRO}$= 0.05) considering 0.98 of energy efficiency of the Energy Recovery Device (ERD).**

To sum up table 3.29 shows design parameters of four cases selected in order to study the use of PRO as an additional energy recovery. The last two columns give results of energy saving

attributable to the PRO/SWRO system corresponding to two different working pressure of the PRO, 8 bar and 16 bar, respectively. Energy recovery devices with energy efficiency of 0.98 are assumed.

**Table 3.29. Main parameters of RO/PRO cases analysed. Salinity, standard seawater; temperature, 25ºC; recovery rate, $r_{RO}$= 0.49.**

| | $r_{m,PRO}$ kg/kg | Ratio $q_{V,PRO}/q_{V,P}$ | $S_{PRO}$ kg/kg | $\Pi_{PRO}$ bar | $p_{PRO,max}$ bar | Ratio $q_{V,wtt}/q_{V,P}$ | Energy saving(*) kWh/m³ | Energy saving(**) kWh/m³ |
|---|---|---|---|---|---|---|---|---|
| **Case 1** | 0.50 | 2.112 | 0.0338 | 25.0 | 20.0 | 1.056 | 0.26 | 0.57 |
| **Case 2** | 0.35 | 1.613 | 0.0440 | 33.0 | 28.0 | 0.564 | 0.15 | 0.32 |
| **Case 3** | 0.20 | 1.300 | 0.0541 | 41.3 | 36.0 | 0.260 | 0.08 | 0.16 |
| **Case 4** | 0.05 | 1.087 | 0.0642 | 50.0 | 50.0 | 0.054 | 0.04 | 0.06 |
| (*)$p_{PRO}$= 8 bar; $\eta_{HPP}$=80%; $\eta_{ERD}$= 98% | | | | | | | | |
| (**)$p_{PRO}$= 16 bar; $\eta_{HPP}$= 80%; $\eta_{ERD}$= 98% | | | | | | | | |

Finally, as a preliminary comparison between configurations based on two stages and on PRO energy recovery, figure 3.31 shows the analysis of using two stage configuration at seawater conditions given in table 3.29. This figure shows that energy saving achieved by using PRO/SWRO might be similar to those attributable to two stages even if the most optimistic hypothesis are assumed. Therefore, considering the complexity due to including a PRO system in a SWRO plant, two staged configurations should be a better selection instead of adopting PRO energy recovery.

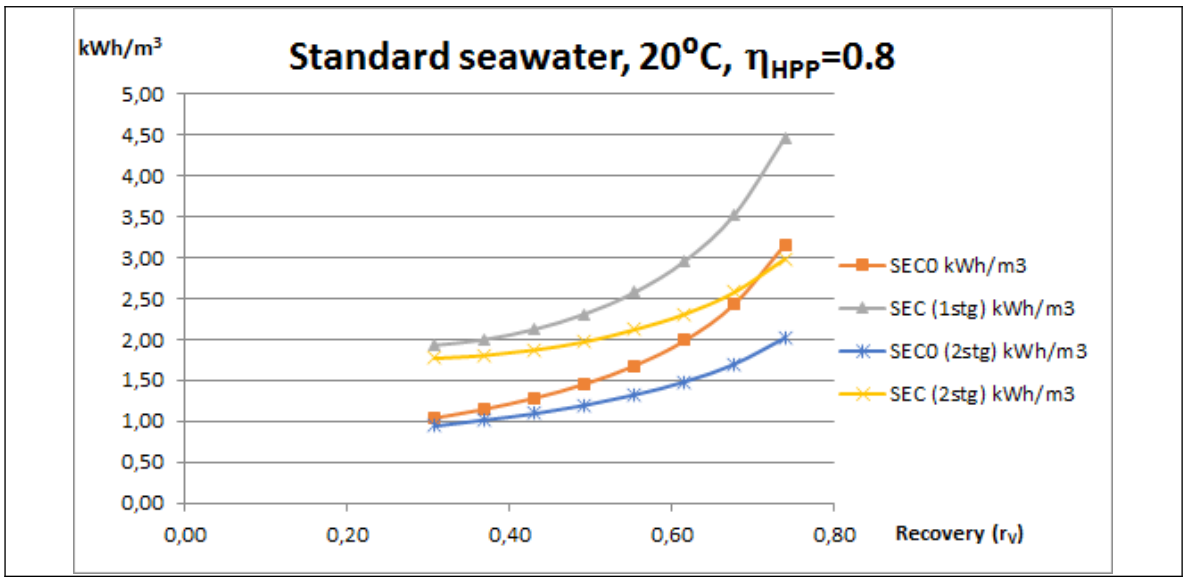


**Figure 3.38. Effect of two stage configuration on SEC – standard seawater salinity and 25ºC -.**

# 6. SUMMARY OF RESULTS

Main conclusions of the theoretical analysis performed of seawater desalination based on seawater reverse osmosis desalination could be summarised by means of the following points:

- If the recovery rate is 50%, the minimum theoretical energy required for solvent extraction is within 1.03-1.16 kWh/m$^3$ range for temperatures of 10ºC-40ºC and standard composition of seawater – see fig. 3.2 -. This range decreases up to 0.7-0.8 kWh/m$^3$ for recovery rate of 0%, which is the absolute minimum.

- If a conventional SWRO configuration is used, the Specific Energy Consumption (SEC) increases up to 2.2-2.5 kWh/m$^3$ (efficiency of high pressure pump, 80% and efficiency of the engine, 95%) – see figs. 3.10.a-3.10.c -. Therefore, around a 50% of the SEC in this case is attributable to the thermodynamic limit of a solvent extraction process at this specific conditions of salt concentration and temperatures.

- The minimum theoretical energy for solvent extraction strongly depends on the seawater salt concentration, 0.5-1.5 kWh/m$^3$ is required for salinities of 0.020-0.050 kg/kg and 50% of recovery rate – see fig. 3.3 -.

- If ideal feed pressurisation and ideal energy recovery is assumed, the SEC and theoretical minimum are approximately equal up to 30% of recovery rate and go down as recovery rate decreases – see figs. 3.13.a-3.15 -. On the contrary, when inefficiencies of pumping and energy recovery are considered, the SEC dramatically increases for values of recovery rate below 20%. Therefore, the use of SWRO technology at low recovery rates makes no sense not only from the point of view of auxiliary energy consumption but also concerning main energy consumption.

- The Net Diving Pressure (NDP) at the tail of the membrane serial is assessed in this work by means of the Tail Differential Pressure (TDP), which is this operational parameter when the effect of concentration polarization is neglected. Depending on membrane features, the TDP should be higher than a given value in order to obtain permeate with appropriate low salinity. Results show that the effect of TDP in the SEC is negligible according to figs. 3.10.a to 3.12, around 0.038 kWh/m$^3$ for each bar of TDP decreasing. Therefore, further improvements on membrane permeability would be important only on other OPEX parameters and on CAPEX.

- The influence on the SEC of HPP efficiency from 70% to 90% ($\eta_{eng}$= 95%) is around 0.5-1.0 kWh/m$^3$ for conventional SWRO configuration (one stage), depending of recovery rate, temperature and feed salinity – see Figs. 13.a – 3.15 -.

- In all cases analysed, even with 90% of $\eta_{HPP}$, a range of 0.6-0.7 kWh/m$^3$ of the SEC is attributable to the inefficiency of equipment for 43-49% of recovery rate. Besides that, 0.3-0.6 is due to plant configuration within the same range of recovery rate, being possible energy saving of 0.2-0.3 by adopting configurations with two stages.

- Regarding SWRO desalination with two stages, the benefits on the SEC have been analysed in this work for a wide range of temperatures, seawater salinities, recovery rates and pumping efficiencies – see figs. 3.19.a-3.21 -. The influence of the second stage increases with recovery rate and feed salinity. If operating with 60% of recovery rate is reliable, around 0.6-0.8 kWh/m$^3$ could be the energy saving due to including a second stage.

- Theoretically, PRO concept could be coupled to a conventional SWRO plant as an additional energy recovery device if an aqueous solution to be rejected is available. By means of a conventional turbocharger configuration, hydraulic power of 0.5-0.8 kWh/m$^3$ could be recovered if 17 bar is achievable – see tables 3.20-3.22 -. This power recovery would lead to energy saving of about 0.64-1.0 kWh/m$^3$ if $\eta_{HPP}$= 80% and $\eta_{eng}$= 95% are considered.

- The integration of a PRO system in a SWRO plant may represent energy savings up to few tenths of kWh/$m^3$. This could represent for the SWRO plant to get SEC values of below 2 kwh/$m^3$ with $\eta_{HPP}$= 80% and $\eta_{eng}$= 95%.

# 7. CONCLUSIONS

Based on aforementioned results, innovative configurations based on the second stage concept have the most interesting prospects of achieving low values of SEC. Besides, further improvements on reliability of high efficiency HPP also would have high impact on SEC of large capacity desalination plants. On the contrary, low impact on SEC is expected for further developments in SWRO membranes.

Among the innovative configurations analysed, the concept Desalitech-CCD seems to be the most suitable to achieve significant energy saving on SWRO process. However, the advantages in comparison to a conventional two stages configuration with inter-stage pump is not significant.

Concerning the use of energy from salinity gradient by means of Pressure Retarded Osmosis (PRO). The use of a PRO system integrated in a SWRO plant has been analysed in order to assess the potential energy consumption savings to produce desalinated water. Different operating conditions for the PRO system have been considered, with PRO operating pressure ranging from 5 to more than 20 bar as a theoretical analysis, thus regardless the mechanical stability or feasibility of the PRO system. The energy saved thanks to the PRO system is directly proportional to the transferred water and the operating pressure of the PRO system. Therefore, the larger is the PRO System (in terms of PRO membrane surface under the assumption of enough mechanical stability) the better in terms of energy savings for the SWRO plant. However, integrating a large PRO System means duplicating the membrane systems of the plant, that is, on the one hand the RO system and on the other the PRO system. This represents an important increase in terms of CAPEX and, without any doubt, more complexity in terms of the operation of the plant during transients but also under steady state conditions. Besides, proposals of the literature that involve the use of treated wastewater as part of the fresh water production after passing through PRO membranes and SWRO membranes is not useful in SWRO plants. To reuse

treated wastewater by a conventional two-pass BWRO desalination plant would be the best option.

The benefits in terms of energy consumption reduction of integrating a PRO System in a SWRO plant turn to be similar to adding a second stage to a conventional RO Plant. The target energy consumption set by the EC at 1 kWh/$m^3$ with recovery rate around 50% is not realistic even though both, SWRO desalination with two stages and PRO are used.

## 8. REFERENCES


1. European Commission (EC): HORIZON 2020 WORK PROGRAMME 2014 – 2015: Leadership in enabling and industrial technologies ii. Nanotechnologies, Advanced Materials, Biotechnology and Advanced Manufacturing and Processing Revised. (https://ec.europa.eu/research/participants/data/ref/h2020/wp/2014_2015/main/h2020-wp1415-leit-nmp_en.pdf) Last visit: 22/09/2015.

2. ERI (Energy Recovery, Inc) (2006). Document Number 80074-01-00: ERI Technical Bulletin Flow in PX Arrays, 10/03/2006. http://www.energyrecovery.com/ (last visit 15/09/2011).

3. ERI (Energy Recovery, Inc) (2007). Document Number 80074-01-00: ERI Technical Bulletin Isobaric Device Mixing, 20/06/2007. http://www.energyrecovery.com/ (last visit 15/09/2011).

4. García Rodríguez, L. Chapter 2: Procesos de desalación mediante energía solar térmica. *In:* Estudio termoeconómico de los procesos de desalación de agua de mar mediante colectores solares cilindroparabólicos. Tesis Doctoral. Universidad de La Laguna, Junio, 1999. Sobresaliente cum laude.

5. Greenlee, F. L.; Desmond, F. L; Freeman, B. D.; Marrot, B., and Mouling, P. *Reverse osmosis desalination: Water sources, technology, and today´s challenges.* Water Research, 43, 2009, pp. 2317-2348.

6. Kurihara M.; Maeda, K., and Yamamura, H.; *Method for multi-stage separation.* PT1161981 (E) – 2008-04-01. Applicants: TORAY INDUSTRIES

7. Leyendekkers, J. V. *Thermodynamics of Seawater.1st Part.* Marcel Dekker Inc. 1976.

8. Millero,F.J.; Feistel, R.; Wright, D. G., McDougall, T. J., *The composition of Standard Seawater and the definition of the Reference-Composition Salinity Scale.* Deep Sea Research Part I: Oceanographic Research Papers, 55(1), 2008, pp. 50-72.

9. Safarov, J.; Berndt, S.; Millero, F. J.; Feistel, R.; Heintz, A., and Hassel, E. P., *(p,ρ,T) Properties of seawater at brackish salinities: Extensions to high temperatures and pressures.* Deep Sea Research Part I: Oceanographic Research Papers, 78, 2013, pp. 95-101.

10. Safarov, J.; Berndt, S.; Millero, F. J.; Feistel, R.; Heintz, A., and Hassel, E. P., *(p,ρ,T) properties of seawater: Extensions to high salinities.* Deep Sea Research Part I: Oceanographic Research Papers, 65, 2012, pp. 146-156.

11. Sadwani, J. J., and Veza, J. M., *Desalination and energy consumption in Canary Islands.* Desalination, 221, 2008, pp. 143-150.

12. Sharqawy, M. H.; Lienhard, J. H., and Zubair, S. M. *Thermophysycal properties of seawater: a review of existing correlation and data.* Desalination and Water Treatment, 16, 2010, pp. 354-380.

13. Slesarenko, V., and Shtim, A., *Determination of seawater enthalpy and entropy during the calculation of thermal desalination plants.* Desalination, 71, 1989, pp. 203-210.

14. Tu, K. I.; Nghiem, L. D., and Chivas, A. R. *Boron removal by reverse osmosis membranes in seawater desalination applications.* Separation and Purification Technology, 75, 2010, p. 87-101.

15. Viera Curbelo, O., *Pressure Vessel for sea water reverse osmosis and process that avoids scaling problems.* EP2576448(A1) – 2013-04-10. Applicant: GEN ELECTRIC (US).

16. Voros, N. G; Maroulis, Z. B., and Marinos-Kouris, D., *Short-cut structural design of reverse osmosis desalination plants.* Journal of Membrane Science, 127, 1997, pp. 47-68.

17. Wilf, M., *The Guidebook to Membrane Desalination Technology. Reverse Osmosis, Nanofiltration and Hybrid Systems Process, Design, Applications and Economics.* Balaban Desalination Publications, 2007. ISBN 0-86689-065-3.

18. Wittmann, E.; Ventresque, C.; Lacaze-Eslous, F.; *Reverse osmosis water treatment plant including a first pass having multiple stages.* WO2013017628 (A1) – 2013-02-07. Applicants: VOELIA WATER SOLUTIONS & TECH.

19. Zhao, D.; Chen, S.; Guo, C. X.; Zhao, Q., and Lu, X., *Multi-functional forward osmosis draw solutes for seawater desalination.* Chinese Journal of Chemical Engineering, 24, 2016, pp. 23-30.

20. Zhou, Y.; *Reverse osmosis membrane pile system.* CN202237803 (U) – 2012-05-30. Applicants: CHANGZHOU CONNECT MACHINERY EQUIPMENT CO LTD.

# Chapter 4. ANALYSIS OF MEMBRANE ELEMENTS IN SERIAL CONNECTION

A summary of this chapter will be submitted for publication to the international journal *Desalination* with the following authors, title and abstract:

**Authors:** Arturo Buenaventura Pouyfaucon[(1)] and Lourdes García-Rodríguez[(2)]

[(1)]Abengoa– Spain. C/ Energía Solar, nº1. 41014- Sevilla. abuenaventura@abengoa.com

[(2)]Dpto. Ingeniería Energética. Universidad de Sevilla. ETSI, Camino de Los Descubrimientos, s/n. 41092-Sevilla. mgarcia17@us.es

Title: *SWRO membrane elements: simple modelling and assessment of cost evolution*

# 1. INTRODUCTION

This chapter deals with a performance assessment of Reverse Osmosis (RO) membrane elements. Firstly, the individual behaviour is analysed at similar working conditions. Secondly, serial connections of membrane elements of the same model are compared. Finally, the most suitable selection of membrane model depending on their position within the serial connection is studied.

As has been described, feed water needs to be pressurized against a semi-permeable membrane so that the dissolvent will flow through the membrane as product and the salts will remain in the feed side, thus separating the feed water into a desalinated product and a concentrate where most of the salts remain (brine).

The design of Sea Water Reverse Osmosis (SWRO) membrane elements have been improved during the last decades coming to a standard design consisting in a module of typically 8 inches diameter and 1 meter long with spiral wounded flat sheets RO membranes. Besides, higher diameter modules are also commercially developed in order to decrease capital expenses [García-Molina and Casañas, 2010].

These flat sheets of RO membranes are build up in envelopes, each by sealing together in three of their boundaries two rectangular flat sheets (with a spacer in between them ensuring a channel for the permeate), connecting the forth one to a central conduit where the permeate coming from all of this kind of envelopes is collected.

The pressurized feed water enters the module in one end and flows axially in that direction towards the other end through channels build up with the help of spacers between the different wounded envelopes (see figure 4.1).

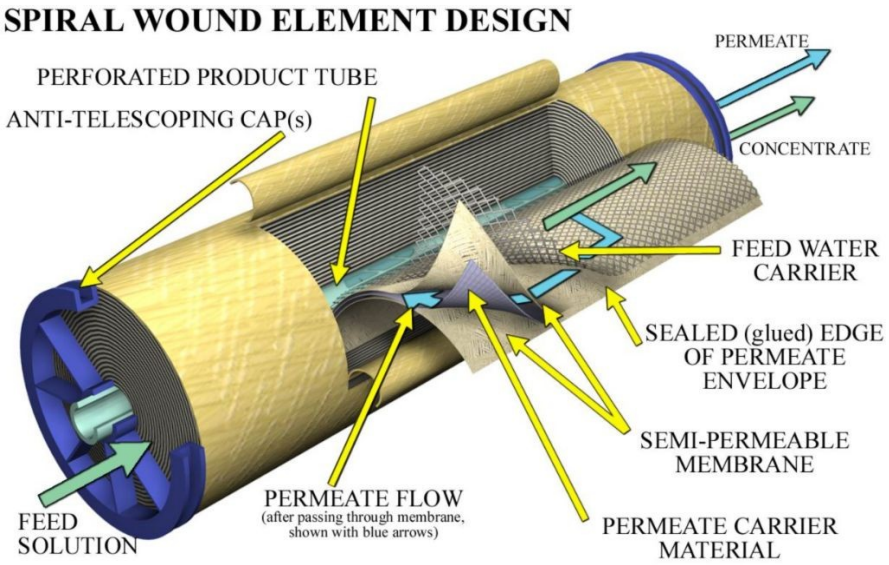


**Figure 4.1. RO membrane module.**

These RO membrane modules are placed inside a Pressure Vessel (PV) where a number of these modules can be installed in series. The PV´s have typically a feed in nozzle, a permeate exit nozzle and a brine exit nozzle.

The core of the RO technology is the RO membrane, therefore the RO membrane modules are the key components. This standard design allows having an important surface of RO membrane in a rather small volume, approximately 40 $m^2$/module, with dimensions and weigh that are also easy to handle.

Table 4.1 show representative membrane elements manufactured by some of the most recognized companies.

Previous analysis reported in Peñate (2010), Delgado Torres (2006) and García-Rodríguez (2007) proved that the behaviour of models of different manufacturers sorted in the same group of table 4.1 exhibit quite similar behaviour. Therefore, in this work this is assumed as initial hypothesis. Based on this, only Filmtec membranes, manufactured by DoW, are thoroughly studied. They are comparatively analysed by means of several sets of simulations carried out by using the design software ROSA [Filmtec, 2015]. Results are reported in sections 2, 3 and 4.

**Table 4.1. Representative commercial products sorted by main features as an updated of Peñate and García-Rodríguez (2011).**

| MANUFACTURERS /CRITERIA | Type of membranes | Permeate Flow rate (Flux) gpd ($m^3$/d) | Nominal Active Surface Area $ft^2$ ($m^2$) | Max. pressure MPa | Salt Rejection % |
|---|---|---|---|---|---|
| **FILMTEC[(1)]** | | | | | |
| High salt rejection | SW30HRLE -400i | 7,500 (28.4) | 400 (37.2) | 8.27 | 99.80 |
| | SW30HRLE -440i | 8,200 (31.0) | 440 (40.9) | 8.3 | 99.80 |
| Low energy, high flux | SW30XLE-400i | 9,000 (34.1) | 400 (37.2) | 8.27 | 99.80 |
| | SW30XLE-440i | 9,900 (37.5) | 440 (40.9) | 8.3 | 99.80 |
| | SW30ULE-400i | 11,000 (41.6) | 400 (37.2) | 8.27 | 99.7 |
| | SW30ULE-440i | 12,000 (45.4) | 440 (40.9) | 8.3 | 99.70 |
| | SEAMAXX$^{T}_{M}$ | 17,000 (64.4) | 440 (40.9) | 6.9 (at T<35ºC) 6.2 (at 35-45ºC) | 99.70 |
| **HYDRANAUTICS[(2)]** | | | | | |
| High salt rejection | SWC4+Max | 7,200 (28.5) | 400 (37.2) | 8.27 | 99.80 (99.70) |
| Extra high salt rejection, Low energy, high flux | SWC5+Max | 9,900 (37.6) | 440 (40.9) | n.a. | 99.8 |
| High salt rejection, extra low energy, extra high flux | SWC6 MAX | 13,200 (50.0) | 440 (40.8) | 8.27 | 99.80 |
| | SWC6 | 12,000 (45.6) | 400 (37.2) | n.a. | 99.80 |
| **TORAY[(3)]** | | | | | |
| High salt rejection | TM820K-440 | 6,400 (24.2) | 440 (40.9) | 8.3 | 99.86 |
| High flux | TM820E-400 | 7,500 (28.4) | 400 (37.2) | 8.27 | 99.75 (99.50) |
| | TM820R-400 | 8,500 (32.2) | 400 (37.2) | 8.3 | 99.80 |
| | TM820R-440 | 9,400 (35.6) | 440 (40.9) | 8.3 | 99.80 |
| Low energy, High flux | TM820F-400 | 9,000 (34.1) | 400 (37.2) | 6.89 | 99.70 (99.50) |
| | TM820V-440 | 9,900 (37.5) | 440 (40.9) | 8.3 | 99.80 |

[(1)]Dow (2017)
[(2)]Hydranautics (2017)
[(3)]Toray (2017)

Data from table 4.1 correspond to the following test conditions:

- Filmtec, 32,000 ppm NaCl, 800 psi (5.5 MPa), 77°F (25°C), pH 8 and 8% recovery.
- Hydranautics, 32,000 ppm NaCl; applied pressure, 800 psi (5.4 MPa); Operating temperature, 25ºC; recovery, 10%; pH range, 6.5-7.0.
- Toray, 32,000 mg/L NaCl; applied pressure, 800 psi (5.52 MPa); Operating temperature, 25ºC; recovery, 8%; pH range, 7.0.

## 2. PERFORMANCE OF A SINGLE MEMBRANE ELEMENT

As described in the previous section, there are a number of phenomena that are inherent to the RO technology and to the fact that is based on the flow of the dissolvent through a membrane. Therefore these phenomena take place in the RO membrane modules and thus are affected by the design and configuration of these modules.

The flux, $J_v$, is defined as the permeate volumetric flow per unitary area, normally expressed in L/(h·m$^2$):

$$J_V = \frac{q_{V,P}}{A} \qquad \text{eq. 4.1}$$

, where $q_{V,P}$ means volumetric flow of permeate and A is the membrane area.

Typical average flux is around 14 L/(h·m$^2$) within a PV [Wilf, 2007], besides Peñate and García-Rodríguez (2011) mentioned pilot tests by DoW reported by Bush *et al* (2009) with recoveries of 50-60% and average flux rates of 18-27 L/(h·m$^2$) per PV.

### 2.1. Solvent transport

The pass of the dissolvent from the feed channels into the permeate channel through the RO membrane (the permeate flux) is governed by the transport equation and depends mainly on the Net Driving Pressure (NDP). This NDP varies along the module since the feed pressure decays due to hydraulic pressure losses and the concentration of the feed increases due to the pass

of dissolvent through the membrane. Therefore the product flux in the module in not constant but typically referred as the average flux in the module.

Another phenomenon that may occur in the RO membrane surface is the precipitation of salts in the feed side due to the high concentration of ions, referred as scaling. As the dissolvent passes through the membrane, the concentration of salts increases and it may reach the point where the concentration of different ions is higher enough to have precipitation. At that moment small crystals of salts start to build up in the membrane surface limiting the pass of dissolvent, thus reducing the permeate flux.

The RO membrane modules are designed in a way that the turbulence of the feed water is increased in the feed channels with the help of the spacers. This turbulence is beneficial to prevent precipitation since the velocity of the feed flux avoids up to some extent the deposition of salt crystals on the membrane surface.

Finally, desalinating sea or brackish waters, when the dissolvent passes through the pores of the membrane some of these pores start to clog with the organic matter present in the feed water. This phenomenon is known as bio-fouling and limits the pass of dissolvent, thus reduces the permeate flux. Vrouwenvelder et al (2009) conclude that in full-scale installations, the major effect of biofouling is an increase in feed channel pressure drop. Feed pretreatment is specifically designed case by case in order to minimise these effects. Moreover, a periodical cleaning procedure in situ is also carried out. Fouling and scaling are thoroughly described in Roya (2007) and Edzwald (2011). Research objectives and findings are reported by Malaeb and Ayoub (2011). Useful references on pretreatment procedures are Wilf (2007), Cui et al (2011), Prihasto et al (2009), among others.

After cleaning, membranes should nearly recover the initial flux. The flow factor (*f*) describes the actual performance of a membrane element, *f* is equal to one when starting its lifetime (t= 0). Normally this parameters is set by 0.85 in performance calculations [Peñate and Gracía-Rodríguez, 2011]. For specific working conditions, the initial solvent flux through the membrane should be multiplied by the factor *f* to obtain the actual flow.

$$q_{V,P} = f \cdot q_{V,P}(t=0) \qquad \text{eq. 4.2}$$

The solvent pass expressed in volumetric flow units, $q_{V,w}$, is characterised by the following expression:

$$q_{V,w} = L_w \cdot A \cdot (\Delta p - \Delta \Pi) \quad \text{eq. 4.3}$$

where $(\Delta p - \Delta \Pi)$ is the NDP across the membrane,

$$NDP = (\Delta p - \Delta \Pi) \quad \text{eq. 4.4}$$

which is the driving force of the solvent pass. Symbols in eq.4.3 are as follows:

- $L_w$, hydraulic permeability of water, m/(s·kPa): volumetric flow of water per unit of area and of net differential pressure. Hydraulic permeability is normally ranged between 1 L/(m$^2$·h·bar) to 2.5 L/(m$^2$·h·bar) [Kim and Jeong, 2015] – see fig. 4.3. -. As exemplary cases, in Fujairah SWRO plant $L_w$ is given by Kim et al (2009), 1.056·10$^{-3}$ m/(h·bar) for SWROHRLE-400i [Altaee, 2012]. Hydraulic permeability is related to the membrane thickness, $e$, by means of the following equation:

  $$L_w = k_w / e \quad \text{eq. 4.5}$$

  , where $k_w$ is a coefficient associated to the water permeability. The water transport coefficient across the membrane is

  $$K_w = L_w \cdot A \quad \text{eq. 4.6}$$

  Therefore:

  $$q_{V,w} = K_w \cdot NDP \quad \text{eq. 4.7}$$

  Where $K_w$ is expressed in m$^3$/(s·kPa).
- $A$, membrane area, m$^2$.
- $\Delta \Pi$, differential osmotic pressure between both sides of the membrane, feed-concentrate (F-BD) side and permeate (P) side, kPa.
- $\Delta p$, differential pressure between the channels separated by the membrane, namely, feed-concentrate and permeate channels, kPa.

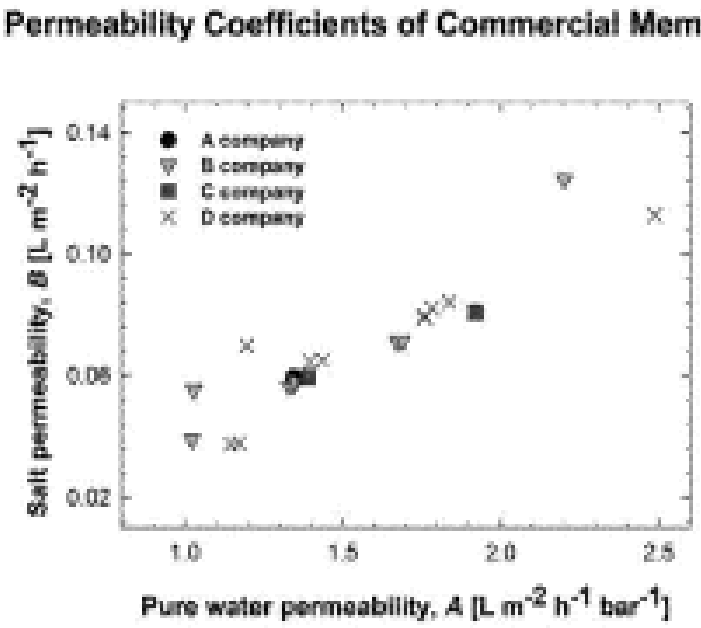


**Figure 4.3. Permeability of water and salts of some commercial membrane elements by [Kim and Jeong, 2015].**

Water permeability, $L_w$, depends on the membrane materials and internal structure, on membrane thickness, time in operation of the membrane and on withstanding operating conditions of temperature and pressure. Pressure increases membrane compaction, which makes decrease the water permeability. Also membrane fouling and scaling reduce water permeability. Periodic membrane cleaning recovers, partially or totally, the initial water permeability. After operating a membrane element, the actual water permeability is normally obtained by including a factor, $f$, referred to as flow factor or fouling factor.

A detailed expression of eq.4.3 is

$$q_{V,w} = f \cdot L_{w,0} \cdot A \cdot \left[ \left( p_{F-BD} - p_P \right) - \left( \Pi_{F-BD} - \Pi_P \right) \right] \qquad \text{eq. 4.8}$$

, where $L_{w,0}$ is the initial value of water hydraulic permeability, $p_P$ is the permeate outlet pressure; $p_{F-BD}$ is normally calculated by the arithmetic mean between feed pressure, $p_F$, and brine pressure, $p_F - \Delta p_{Loss}$,

$$p_{F-BD} = \frac{p_F + \left( p_F - \Delta p_{Loss} \right)}{2} \qquad \text{eq. 4.9}$$

, where $\Delta p_{Loss}$ corresponds to pressure losses attributable to the PV (or membrane element). Hence,

$$p_{F-BD} = p_F - \frac{\Delta p_{Loss}}{2} \qquad \text{eq. 4.10}$$

Concerning$\Delta p_{Loss}$, Wilf (2007) reports on an empirical correlation to obtain this:

$$\Delta p_{Loss} = A_1 \cdot \left(q_{V,F-BD}\right)^{B_1} \qquad \text{eq. 4.11}$$

Coefficients $A_1$ and $B_1$ in eq. 4.11 are specific constants depending on the membrane element, and $q_{V,F-BD}$ is the average flow circulating within the F-BD channel.

Besides that, $\Pi_P$ is the osmotic pressure of the permeate channel. Finally, $\Pi_{F-BD}$ is the average osmotic pressure of the F-BD channel, which is calculated based on the following procedure.

The average salt concentration in the feed-concentrate channel given in terms of the ratio of salt mass and total volume, $C_{F-BD}$, is expressed by eq. 4.12 [Wilf, 2007]:

$$C_{F-BD} = C_F \cdot \frac{\ln \frac{1}{1-r_V}}{r_V} \qquad \text{eq. 4.12}$$

, where $r_V$ is the ration between permeate and feed volumetric flows. This is known as AFS (Average Feed Salinity) if salt concentration is given in terms of salinity, defined as mass fraction of salts. Salt concentrations of the Feed (F) and the concentrate or BlowDown (BD) in kg/m$^3$ are $C_F$, and $C_{BD}$, respectively, and recovery rate, $r_V$, is related to aforementioned concentrations:

$$C_{BD} = \frac{C_F}{1-r_V} \qquad \text{eq. 4.13}$$

In the F-BD cannel, salt concentration on the membrane surface is greater than that in bulk feed solution. This effect is known as “concentration polarization” that results in higher $\Pi_{F-BD}$, thus decreasing the NDP. Moreover, this increases the probability of exceeding the solubility product of given salts and subsequent precipitation. The Concentration Polarization

Factor (*CPF*) is defined as the ratio of salt concentration at the membrane surface to bulk concentration:

$$CPF = \frac{C_{surf}}{C_{bulk}} \qquad \text{eq. 4.14}$$

For a membrane element, Wilf (2007) provides a relationship of CPF and recovery rate of the element ($r_{V,i}$) as follows:

$$CPF = K_{Pol} \cdot \exp\left(\frac{2 \cdot r_{V,i}}{2 - r_{V,i}}\right) \qquad \text{eq. 4.15}$$

, where $K_{Pol}$ is a constant depending on the features of the membrane element i, and $r_{V,i}$ is related to $C_{BD,i}$ and $C_{F,i}$ by means of:

$$C_{BD,i} = \frac{C_{F,i}}{1 - r_{V,i}} \qquad \text{eq. 4.16}$$

Alternatively, Wilf (2007) offers a nearly linear relationship between CPF and $r_{V,i}$ . Values of 1.1 and 1.2 CPF corresponds to 10% and 18%, respectively. The latter is fixed by some manufacturers as the design limit in conventional membrane elements. Then

$$CPF \cong a_{CPF,1} \cdot r_V + a_{CPF,2} \qquad \text{eq. 4.17}$$

Once the CPF is obtained, the average osmotic pressure at the membrane surface is calculated by using eqs. 4.18-4.19:

$$\frac{\Pi_{surf}}{c_{surf}} \simeq \frac{\Pi_{bulk}}{c_{bulk}} \qquad \text{eq. 4.18}$$

$$\Pi_{surf} = CPF \cdot \Pi_{bulk} \qquad \text{eq. 4.19}$$

Hence, by combining equations given in this subsections, the volumetric flow rate of product is given by eq.18:

$$q_{V,P} = f \cdot L_{w,0} \cdot \left[ \left( p_F - \frac{\Delta p_{Loss}}{2} - p_P \right) - \left( CPF \cdot \Pi_{F-BD} - \Pi_{P,surf} \right) \right] \quad \text{eq. 4.20}$$

Finally, eq. 4.20 becomes eq.4.21, considering eq.10 and negligible concentration polarisation in the permeate channel. Eq. 4.21 can be solved by using eqs. 4.12 and 4.17.

$$q_{V,P} = f \cdot L_{w,0} \cdot ¿ \quad \text{eq. 4.21}$$

**2.2. Salt transport**

The mass flow rate of salts through the membrane, $q_s$, is expressed as follows,

$$q_s = L_s \cdot A \cdot \Delta C \quad \text{eq. 4.22}$$

, as a function of the salt permeability, $L_s$, membrane area, $A$, and the difference of concentration between both surfaces of the membrane, $\Delta C$. This is the main term, which does not depend on the applied pressure. Alternatively, this can be rewritten in term of a coefficient associated to the salt permeability, $K_s$:

$$q_s = K_s \cdot \Delta C \quad \text{eq. 4.23}$$

Note that concentration polarisation not only affects water flux, but also the salt passage. The latter increases with CPF. Normally, $L_s$ is expressed in L/(m$^2$·h), usually ranged from 0.036 to 0.132 L/(m$^2$·h) [Kim and Jeong, 2015].

Eq. 4.22 indicates that the driving force is the difference of salt concentration at the both sides of the membrane, expressed for a given point (x) on the flow axis by means of:

$$\Delta C(x) = C_{F,surf}(x) - C_{P,surf}(x) \quad \text{eq. 4.24}$$

Besides, in the analysis of a membrane module if the effect of concentration polarisation in the permeate channel is neglected:

$$\Delta C = CPF \cdot C_{F-BD} - C_P \quad \text{eq. 4.25}$$

Where permeate salt concentration, $C_P$, is:

$$C_P = \frac{q_s}{q_{V,P}} \qquad \text{eq. 4.26}$$

and $C_{F-BD}$ is the salt concentration of the F-BD channel, given by eq. 4.12.

Two factor related to the performance of a membrane element concerning salts flow are normally used:

- The factor of salt passage, $f_{SP}$,

$$f_{SP} = \frac{C_P}{C_F} \qquad \text{eq. 4.27}$$

or *SP* (Salt Passage)

$$SP = 100 \cdot \frac{C_P}{C_F} \qquad \text{eq. 4.28}$$

- The factor of salt rejection, $f_{SR}$,

$$f_{SR} = 1 - f_{SP} \qquad \text{eq. 4.29}$$

or Salt Rejection (SR):

$$SR = 100 - SP \qquad \text{eq. 4.30}$$

Although every ion has its own value of salt passage, normally, aforementioned parameters express the average. The pass of monovalent ions is greater than that of divalent ions in RO membranes. The salt passage increases due to fouling and chemical damage of membrane cleaning. Nevertheless, phenomena of membrane compaction results in reducing salt passage [Veza, 2002].

### 2.3. Modelling of the performance of a membrane element

The permeate flow expressed either in kg/s or $m^3/s$, $q_P$ and $q_{V,P}$, respectively are given by:

$$q_P = q_s + q_{V,w} \cdot \rho_w \qquad \text{eq. 4.31}$$

$$q_{V,P}=\frac{q_s+q_{V,w}\cdot\rho_w}{\rho_P} \qquad \text{eq. 4.32}$$

Finally, eq. 4.33 summarises transport mechanisms and effects described in sections 2.1 and 2.2 – eqs. 4.21- 4.22, 4.25 and 4.32 -, under the assumption of no effect of:

- concentration polarization in the permeate channel.
- fouling factor in the salt transport.

$$q_{V,P}=\frac{A}{\rho_P}\cdot ¿ \qquad \text{eq. 4.33}$$

To sum up, permeate concentration can be calculated by combining eqs. 4.22, 4.25-4.26 and 4.33:

$$C_P=\frac{L_s\cdot A\cdot\left(CPF\cdot C_{F-BD}-C_P\right)}{\frac{A}{\rho_P}\cdot ¿¿} \qquad \text{eq. 4.34}$$

Permeate salinity is obtaining by multiplying eq. 4.34 by permeate density:

$$S_P=\frac{L_s\cdot A\cdot\left(CPF\cdot C_{F-BD}-C_P\right)}{L_s\cdot A\cdot\left(CPF\cdot C_{F-BD}-C_P\right)+f\cdot L_{w,0}\cdot A\cdot ¿¿} \qquad \text{eq. 4.35}$$

Concerning operation temperature, given the product flow measured at test conditions, $q_{P,0}$, the product flow under any other operating conditions,$q_P$, is:

$$q_P=f_P\cdot f_T\cdot f_t\cdot q_{P,0} \qquad \text{eq. 4.36}$$

Where the following factors are:

- $f_P$: correction factor of membrane productivity depending on operation pressure.
- $f_T$: correction factor attributable to feed temperature.
- $f_f$: flow factor, factor of productivity diminishing due to time of operation.

Therefore, the factor $f_T$ should be applied to eq. 4.33-4.35 in order to obtain the corresponding value at different operation temperature. Membrane manufacturers normally give this factor based on test condition at 25ºC – see table 4.2 [DoW, 2014] and Safar et al (1998) -.

**Table 4.2. Example of temperature correction factor, $f_T$ , of the SW30HRLE-440i membrane element – courtesy of DoW -.**

| Temperature/ºC | $f_T$ | Temperature/ºC | $f_T$ |
|---|---|---|---|
| 19.0 | 1.232 | 21.5 | 1.128 |
| 19.5 | 1.210 | 22.0 | 1.109 |
| 20.0 | 1.189 | 22.5 | 1.090 |
| 20.5 | 1.168 | 23.0 | 1.071 |
| 21.0 | 1.148 | 23.5 | 1.053 |

Finally, to predict the permeate parameters $q_{V,P}$ and $C_P$ of a membrane element at a given working requires the iterative evaluation of the system equations consisting in eqs. 4.11, 4.17, 4.33 and 4.34 along with equations of seawater properties and definitions given in chapter 3: density of pure water and permeate, osmotic pressure for average salt concentration in F-BD channel. Besides that, equation 4.11 is modified in order to make easier the iterative calculation carried out by replacing $q_{V,F-BD}$ by $q_{V,F}$.

$$\Delta p_{Loss} = A_1 \cdot \left(q_{V,F}\right)^{B_1} \qquad \text{eq. 4.37}$$

Figure 4.2 depicts results obtained from simulation of Filmtec membranes by applying logarithm to eq. 4.37 – see eq. 4.38 - in order to obtain values of $A_1$ and $B_1$ for three commercial membrane elements, namely, SW30HRLE-440i, SW30XLE-440i and SW30ULE-440i.

$$\ln\left(\Delta p_{Loss}\right) = B_1 \cdot \ln\left(A_1\right) + B_1 \cdot \ln\left(q_{V,F}\right) \qquad \text{eq. 4.38}$$

If permeability of water and salt is not known, permeate concentration and permeate flow, $C_P$ and $q_{V,P}$, can be used to calculate both by solving eqs. 34.33 and 4.34. Permeate values can be obtained by direct experimental data or by using software provided by membrane manufacturers. Values of membrane permeability representative of current technology are given by Kim and Jeong (2015). Recent advances on membrane materials and manufacture procedures could result in the near future in significant improved values. Current trends on membrane research are reported by Peñate and García-Rodríguez (2012), Lee et al (2011) and Macedonio et al (2012), among others.

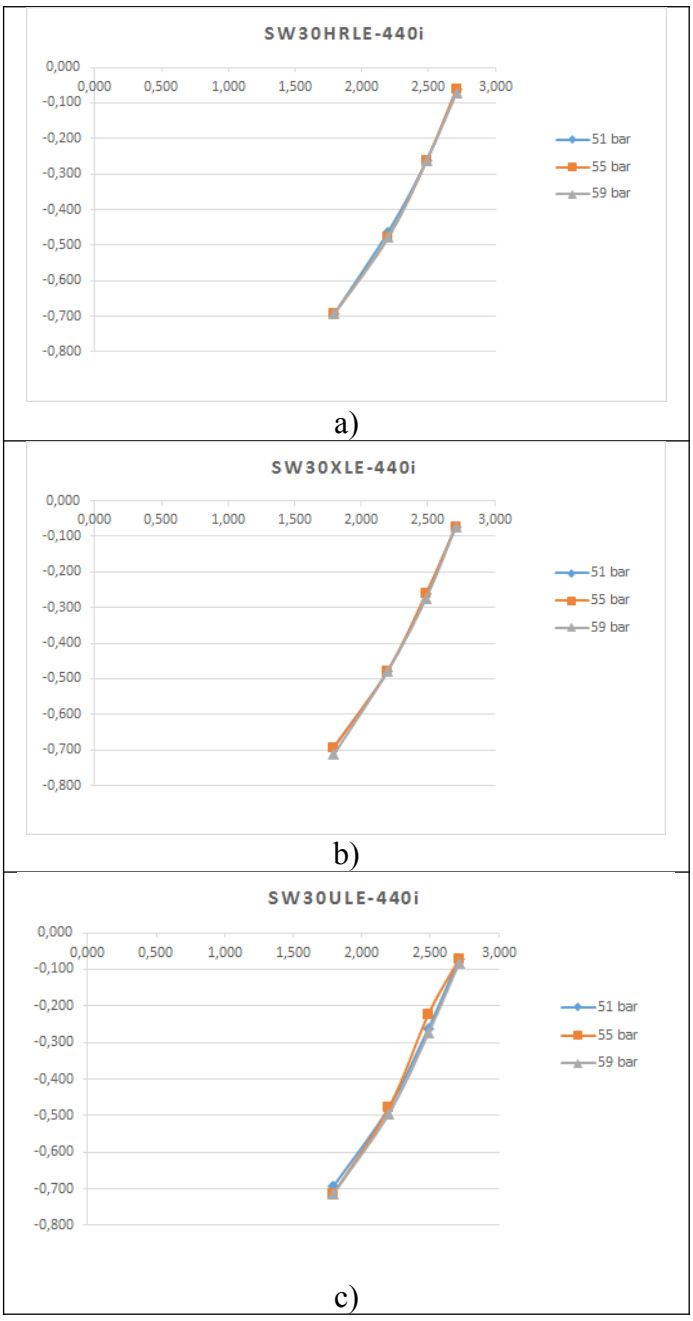


**Figure 4.2. Results of simulation of Filmtec membranes by applying logarithm to eq. 4.37.**

Validation of the model proposed in this section is discussed in sections 3 and 4.

# 3. ASSESSMENT OF A SINGLE MEMBRANE ELEMENT

In this section, an assessment of the performance of Filmtec membranes is conducted along with validation of the model presented in section 2. First, a single membrane element is analysed. Columns of next tables shows the following parameters:

- Feed pressure, $p_F$ (bar)
- Feed flow, $q_{V,F}$ ($m^3/h$)
- Specific Energy Consumption, SEC ($kWh/m^3$)
- Power consumption, Pw (kW)
- Average flux ($L/m^2/h$)
- Maximum permeate flow, Max. $q_{V,P}$ ($m^3/h$)
- Permeate Total Dissolved Solids, $TDS_P$ (mg/L)
- Boron concentration in permeate, Boron (mg/L)
- Recovery rate, r (%)
- Permeate flow, $q_{V,P}$ ($m^3/h$), equal to maximum permeate flow if a single element is analysed.
- BlowDown flow, $q_{V,BD}$ ($m^3/h$)
- BlowDown pressure, $p_{BD}$ (bar)
- Power saving attributable to an energy recovery device similar to ERI-PX, expressed by a negative quantity to be added to the power consumption, ERI-PX (kW)
- Net power consumption, $PW_{net}$ (kW)
- Net Specific Energy Consumption, $SEC_{net}$ ($kWh/m^3$)
- Maximum flux ($L/m^2/h$) – equal to average flux if a single element is analysed -

The latest four parameters are calculated by using some of the previous ones provided by design software ROSA.

Tables 4.3-4.5 show results obtained by setting as input parameters feed pressure and feed flow for membrane models SW30HRLE-440i, SW30XLE-440i and SW30ULE-440i, respectively. The last four columns are calculated from the main outputs of the ROSA software, namely:

- PW (ERI-PX). Power saving due to the energy recovery device based on ERI-PX, expressed by means of a negative magnitude.
- $PW_{net}$, net power consumption calculated by means of the power consumption calculated by the ROSA software minus the power saving of the ERI-PX.
- $SEC_{net}$, net Specific Energy Consumption, $PW_{net}/q_{V,P}$.

- Maximum flux, which occurs at the first membrane element. This is the ratio between product flow and the area of the first membrane element.

**Table 4.3. Results obtained for the membrane model SW30HRLE- 440i.**

| SW30HRLE-440i | | | | | | | | | Area= 40,88 $m^2$ | | | | | | |
|---|---|---|---|---|---|---|---|---|---|---|---|---|---|---|---|
| $p_F$ | $q_{V,F}$ | SEC | Pw | Avg. flux | $q_{V,P}$ | $TDS_P$ | Boron | r | $q_{V,BD}$ | $p_{BD}$ | $q_{V,ERD}$ | Pw (ERD) | $PW_{net}$ | $SEC_{net}$ | Max. flux |
| bar | $m^3/h$ | $kWh/m^3$ | kW | $L/(m^2 \cdot h)$ | $m^3/h$ | mg/L | mg/L | % | $m^3/h$ | bar | $m^3/h$ | kW | kW | $kWh/m^3$ | $L/(m^2 \cdot h)$ |
| **51** | **6** | 14,6 | 10,6 | 17,8 | 0,73 | 90 | 0,61 | 12,1 | 5,3 | 50,5 | 5,1 | **-8,8** | **1,9** | **2,6** | **17,9** |
| **51** | **9** | 20,6 | 15,9 | 19,0 | 0,78 | 81 | 0,55 | 8,6 | 8,2 | 50,4 | 8,0 | **-13,6** | **2,4** | **3,0** | **19,1** |
| **51** | **12** | 26,5 | 21,3 | 19,7 | 0,8 | 76 | 0,53 | 6,7 | 11,2 | 50,2 | 10,9 | **-18,4** | **2,9** | **3,6** | **19,6** |
| **51** | **15** | 32,4 | 26,6 | 20,1 | 0,82 | 73 | 0,51 | 5,5 | 14,2 | 50,1 | 13,8 | **-23,1** | **3,5** | **4,2** | **20,1** |
| **55** | **6** | 13,9 | 11,5 | 20,2 | 0,83 | 81 | 0,56 | 13,8 | 5,2 | 54,5 | 5,0 | **-9,3** | **2,2** | **2,6** | **20,3** |
| **55** | **9** | 19,5 | 17,2 | 21,6 | 0,88 | 73 | 0,51 | 9,8 | 8,1 | 54,4 | 7,9 | **-14,5** | **2,7** | **3,0** | **21,5** |
| **55** | **12** | 25,1 | 22,9 | 22,4 | 0,91 | 69 | 0,48 | 7,6 | 11,1 | 54,2 | 10,8 | **-19,7** | **3,2** | **3,5** | **22,3** |
| **55** | **15** | 30,7 | 28,7 | 22,8 | 0,93 | 66 | 0,46 | 6,2 | 14,1 | 54,1 | 13,7 | **-24,8** | **3,8** | **4,1** | **22,7** |
| **59** | **6** | 13,4 | 12,3 | 22,5 | 0,92 | 75 | 0,52 | 15,3 | 5,1 | 58,5 | 4,9 | **-9,8** | **2,5** | **2,7** | **22,5** |
| **59** | **9** | 18,8 | 18,4 | 24,0 | 0,98 | 67 | 0,47 | 10,9 | 8,0 | 58,4 | 7,8 | **-15,4** | **3,0** | **3,1** | **24,0** |
| **59** | **12** | 24,2 | 24,6 | 24,9 | 1,02 | 63 | 0,44 | 8,5 | 11,0 | 58,2 | 10,7 | **-21,0** | **3,6** | **3,5** | **25,0** |
| **59** | **15** | 29,5 | 30,7 | 25,5 | 1,04 | 60 | 0,42 | 6,9 | 14,0 | 58,1 | 13,6 | **-26,5** | **4,2** | **4,0** | **25,4** |

**Table 4.4. Results for SW30XLE-440i element.**

| SW30XLE-440i | | | | | | | | | Area= 40,88 $m^2$ | | | | | | |
|---|---|---|---|---|---|---|---|---|---|---|---|---|---|---|---|
| $p_F$ | $q_{V,F}$ | SEC | Pw | verage flu | $q_{V,P}$ | $TDS_P$ | Boron | r | $q_{V,BD}$ | $p_{BD}$ | $q_{V,ERD}$ | PW (ERI-PX) | $PW_{net}$ | $SEC_{net}$ | Max. flux |
| bar | $m^3/h$ | $kWh/m^3$ | kW | $L/(m^2 \cdot h)$ | $m^3/h$ | mg/L | mg/L | % | $m^3/h$ | bar | $m^3/h$ | kW | kW | $kWh/m^3$ | $L/(m^2 \cdot h)$ |
| **51** | **6** | 12,6 | 10,6 | 20,7 | 0,84 | 95 | 0,67 | 14,1 | 5,2 | 50,5 | 5,0 | **-8,6** | **2,1** | **2,4** | **20,5** |
| **51** | **9** | 17,4 | 15,9 | 22,4 | 0,91 | 84 | 0,60 | 10,2 | 8,1 | 50,4 | 7,9 | **-13,4** | **2,6** | **2,8** | **22,3** |
| **51** | **12** | 22,3 | 21,3 | 23,3 | 0,95 | 78 | 0,56 | 8,0 | 11,1 | 50,2 | 10,8 | **-18,1** | **3,1** | **3,3** | **23,2** |
| **51** | **15** | 27,1 | 26,6 | 24,0 | 0,98 | 75 | 0,54 | 6,5 | 14,0 | 50,1 | 13,7 | **-22,9** | **3,7** | **3,8** | **24,0** |
| **55** | **6** | 12,0 | 11,5 | 23,4 | 0,96 | 87 | 0,62 | 15,9 | 5,0 | 54,5 | 4,9 | **-9,1** | **2,4** | **2,5** | **23,5** |
| **55** | **9** | 16,6 | 17,2 | 25,3 | 1,04 | 76 | 0,55 | 11,5 | 8,0 | 54,4 | 7,7 | **-14,2** | **3,0** | **2,8** | **25,4** |
| **55** | **12** | 21,2 | 22,9 | 26,5 | 1,08 | 71 | 0,51 | 9,0 | 10,9 | 54,2 | 10,6 | **-19,4** | **3,5** | **3,3** | **26,4** |
| **55** | **15** | 25,7 | 28,7 | 27,2 | 1,11 | 67 | 0,49 | 7,4 | 13,9 | 54,1 | 13,5 | **-24,5** | **4,1** | **3,7** | **27,2** |
| **59** | **6** | 11,6 | 12,3 | 25,9 | 1,06 | 81 | 0,58 | 17,7 | 4,9 | 58,5 | 4,8 | **-9,5** | **2,7** | **2,6** | **25,9** |
| **59** | **9** | 16,0 | 18,4 | 28,2 | 1,15 | 70 | 0,51 | 12,8 | 7,9 | 58,4 | 7,6 | **-15,1** | **3,4** | **2,9** | **28,1** |
| **59** | **12** | 20,4 | 24,6 | 29,5 | 1,2 | 65 | 0,48 | 10,0 | 10,8 | 58,2 | 10,5 | **-20,7** | **3,9** | **3,3** | **29,4** |
| **59** | **15** | 24,8 | 30,7 | 30,3 | 1,24 | 62 | 0,45 | 8,3 | 13,8 | 58,1 | 13,4 | **-26,1** | **4,6** | **3,7** | **30,3** |

**Table 4.5. Results of SW30ULE-440i element simulation.**

| SW30ULE-440i | | | | | Area= 40,88 $m^2$ | | | | | | | | | | |
|---|---|---|---|---|---|---|---|---|---|---|---|---|---|---|---|
| $p_F$ | $q_{v,F}$ | SEC | Pw | Average flu | $q_{v,P}$ | $TDS_P$ | Boron | r | $q_{v,BD}$ | $p_{BD}$ | $q_{v,ERD}$ | PW (ERI-PX) | $PW_{net}$ | $SEC_{net}$ | Max. flux |
| bar | $m^3/h$ | $kWh/m^3$ | kW | $L/(m^2 \cdot h)$ | $m^3/h$ | mg/L | mg/L | % | $m^3/h$ | bar | $m^3/h$ | kW | kW | $kWh/m^3$ | $L/(m^2 \cdot h)$ |
| 51 | 6 | 10,9 | 10,6 | 23,8 | 0,97 | 153 | 0,92 | 16,2 | 5,0 | 50,5 | 4,9 | -8,4 | 2,3 | 2,7 | 23,7 |
| 51 | 9 | 14,9 | 15,9 | 26,2 | 1,07 | 133 | 0,82 | 11,9 | 7,9 | 50,4 | 7,7 | -13,1 | 2,8 | 3,1 | 26,2 |
| 51 | 12 | 18,8 | 21,3 | 27,6 | 1,13 | 122 | 0,76 | 9,4 | 10,9 | 50,2 | 10,6 | -17,8 | 3,4 | 3,6 | 27,6 |
| 51 | 15 | 22,8 | 26,6 | 28,6 | 1,17 | 116 | 0,73 | 7,8 | 13,8 | 50,1 | 13,5 | -22,5 | 4,0 | 4,1 | 28,6 |
| 55 | 6 | 10,4 | 11,5 | 26,9 | 1,1 | 140 | 0,86 | 18,3 | 4,9 | 54,5 | 4,8 | -8,8 | 2,7 | 2,8 | 26,9 |
| 55 | 9 | 14,2 | 17,2 | 29,6 | 1,21 | 121 | 0,76 | 13,5 | 7,8 | 54,4 | 7,6 | -13,9 | 3,3 | 3,1 | 29,6 |
| 55 | 12 | 17,9 | 22,9 | 31,3 | 1,28 | 111 | 0,70 | 10,7 | 10,7 | 54,2 | 10,4 | -19,0 | 3,9 | 3,6 | 31,3 |
| 55 | 15 | 21,7 | 28,7 | 32,4 | 1,32 | 105 | 0,67 | 8,8 | 13,7 | 54,1 | 13,3 | -24,1 | 4,5 | 4,1 | 32,3 |
| 59 | 6 | 10,1 | 12,3 | 29,7 | 1,21 | 132 | 0,82 | 20,3 | 4,8 | 58,5 | 4,7 | -9,3 | 3,0 | 2,9 | 29,6 |
| 59 | 9 | 13,7 | 18,4 | 32,8 | 1,34 | 113 | 0,71 | 14,9 | 7,7 | 58,4 | 7,4 | -14,7 | 3,7 | 3,2 | 32,8 |
| 59 | 12 | 17,3 | 24,6 | 34,7 | 1,42 | 103 | 0,66 | 11,8 | 10,6 | 58,2 | 10,3 | -20,2 | 4,4 | 3,6 | 34,7 |
| 59 | 15 | 20,9 | 30,7 | 36,0 | 1,47 | 97 | 0,62 | 9,8 | 13,5 | 58,1 | 13,1 | -25,7 | 5,0 | 4,0 | 36,0 |

Next table 4.6 shows results of modelling the membrane elements SW30HRLE-440i.

**Table 4.6. Modeling of the SW30HRLE-440i element - Lw= 1.080 $L/(m^2 \cdot h \cdot bar)$; Ls= 0.0360 $L/(m^2 \cdot h)$ -: Error from table 4.4 results.**

| # Elements | $q_{VF}$, $m^3/h$ | $p_F$, bar | Error $q_{VP}$, % | Error $C_P$, % | Error $p_{BD}$, % | Error r, % |
|---|---|---|---|---|---|---|
| 1 | 6,0 | 51 | 5,0 | 3,6 | 0,5 | -4,5 |
| 1 | 9,0 | 51 | -3,1 | 0,3 | 0,5 | 2,4 |
| 1 | 12,0 | 51 | -1,2 | -0,8 | 0,7 | -1,6 |
| 1 | 15,0 | 51 | -0,9 | -1,5 | 0,7 | -1,5 |
| 1 | 6,0 | 55 | -3,2 | 2,3 | 0,5 | -2,9 |
| 1 | 9,0 | 55 | -0,3 | -1,9 | 0,5 | -0,5 |
| 1 | 12,0 | 55 | 1,0 | -4,3 | 0,6 | 0,8 |
| 1 | 15,0 | 55 | 1,6 | -4,9 | 0,7 | 1,6 |
| 1 | 6,0 | 59 | -0,7 | 0,0 | 0,4 | -0,4 |
| 1 | 9,0 | 59 | 1,9 | -4,0 | 0,4 | 1,8 |
| 1 | 12,0 | 59 | 2,7 | -6,3 | 0,6 | 2,7 |
| 1 | 15,0 | 59 | 3,6 | -6,8 | 0,6 | 4,1 |

Besides, table 4.7 shows the comparative behaviour of those membranes operated at the same recovery rate, 10%, and product flow – i.e. same feed flow -. This is a theoretical analysis, then some working conditions are not feasible since working pressure is above the maximum allowed.

**Table 4.7. Comparative analysis of Filmtec membrane elements - SW30HR-440i, SWHRLE30-440i, SW30XLE-440i and SW30ULE-440i - at recovery rate 10% and different product flow.**

| $p_F$ | $q_{v,F}$ | SEC | Pw | ıverage flu | $q_{v,P}$ | $TDS_P$ | Boron | r | $q_{v,BD}$ | $p_{BD}$ | $q_{v,ERD}$ | PW (ERI-PX) | $PW_{net}$ | $SEC_{net}$ | Max. flux | Membrane |
|---|---|---|---|---|---|---|---|---|---|---|---|---|---|---|---|---|
| bar | $m^3/h$ | $kWh/m^3$ | kW | $L/(m^2 \cdot h)$ | $m^3/h$ | mg/L | mg/L | % | $m^3/h$ | bar | $m^3/h$ | kW | kW | $kWh/m^3$ | $L/(m^2 \cdot h)$ | model |
| | | | | | | | | | | | | | | | | SW30HR-440i |
| **115** | **20** | 39,9 | 79,8 | 48,9 | 2 | 34,9 | 0,25 | 10,0 | 18,0 | 113,6 | 17,3 | **-67,7** | **12,1** | **6,0** | **48,9** | SW30HRLE-440i |
| **88,7** | **20** | 30,8 | 61,6 | 48,9 | 2 | 41,3 | 0,31 | 10,0 | 18,0 | 87,5 | 17,4 | **-51,9** | **9,8** | **4,9** | **48,9** | SW30XLE-440i |
| **73,6** | **20** | 25,6 | 51,1 | 48,9 | 2 | 73,8 | 0,49 | 10,0 | 18,0 | 72,4 | 17,4 | **-42,7** | **8,4** | **4,2** | **48,9** | SW30ULE-440i |
| **95,7** | **15** | 33,3 | 49,9 | 36,7 | 1,5 | 33,0 | 0,23 | 10,0 | 13,5 | 94,8 | 13,0 | **-42,4** | **7,5** | **5,0** | **36,7** | SW30HR-440i |
| **79,3** | **15** | 27,5 | 41,3 | 36,7 | 1,5 | 0,5 | 0,32 | 10,0 | 13,5 | 78,3 | 13,0 | **-34,9** | **6,4** | **4,3** | **36,7** | SW30HRLE-440i |
| **68,3** | **15** | 23,7 | 35,6 | 36,7 | 1,5 | 53,4 | 0,40 | 10,0 | 13,5 | 67,3 | 13,1 | **-29,9** | **5,7** | **3,8** | **36,7** | SW30XLE-440i |
| **59,9** | **15** | 20,8 | 31,2 | 36,7 | 1,5 | 95,4 | 0,61 | 10,0 | 13,5 | 59,0 | 13,1 | **-26,1** | **5,1** | **3,4** | **36,7** | SW30ULE-440i |
| **68** | **10** | 23,6 | 23,6 | 24,5 | 1 | 47,7 | 0,33 | 10,0 | 9,0 | 67,3 | 8,7 | **-20,0** | **3,6** | **3,6** | **24,5** | SW30HR-440i |
| **59,2** | **10** | 20,5 | 20,5 | 24,5 | 1 | 65,2 | 0,46 | 10,0 | 9,0 | 58,5 | 8,7 | **-17,3** | **3,2** | **3,2** | **24,5** | SW30HRLE-440i |
| **53,2** | **10** | 18,5 | 18,5 | 24,5 | 1 | 77,1 | 0,56 | 10,0 | 9,0 | 52,6 | 8,8 | **-15,5** | **3,0** | **3,0** | **24,5** | SW30XLE-440i |
| **48,5** | **10** | 16,9 | 16,9 | 24,5 | 1 | 137,7 | 0,84 | 10,0 | 9,0 | 47,9 | 8,8 | **-14,1** | **2,8** | **2,8** | **24,5** | SW30ULE-440i |
| **46,9** | **5** | 16,3 | 8,1 | 12,2 | 0,5 | 90,7 | 0,59 | 10,0 | 4,5 | 46,4 | 4,4 | **-6,9** | **1,3** | **2,5** | **12,2** | SW30HR-440i |
| **43** | **5** | 15,0 | 7,5 | 12,2 | 0,5 | 123,8 | 0,81 | 10,0 | 4,5 | 42,5 | 4,4 | **-6,2** | **1,2** | **2,4** | **12,2** | SW30HRLE-440i |
| **40,5** | **5** | 14,1 | 7,0 | 12,2 | 0,5 | 146,4 | 0,97 | 10,0 | 4,5 | 40,0 | 4,4 | **-5,9** | **1,1** | **2,3** | **12,2** | SW30XLE-440i |
| **38,3** | **5** | 13,3 | 6,7 | 12,2 | 0,5 | 261,1 | 1,40 | 10,0 | 4,5 | 37,8 | 4,4 | **-5,6** | **1,1** | **2,2** | **12,2** | SW30ULE-440i |

$SEC_{net}$ shown in table 4.7 for given values of recovery rate, are consistent to the ratio of 0.04 $kWh/m^3/bar$ obtained in chapter 3. Based on table 4.7, figures 4.3-4.8 show main operating parameters. The behaviour of all membrane elements are qualitatively similar. Water permeability is related to salt permeability according to fig.4.3. Consequently, same working conditions lead to lower quality as water permeability is greater. Besides that, the lower the $SEC_{net}$, the lower water quality. Low $SEC_{net}$ is achieved for low values of feed flow at constant feed pressure since the increasing of feed flow has no significant effect in permeate production. Feed flow reduces the concentration polarization but pressure losses go up. Therefore, power increases with feed flow more than the permeate flow does, thus resulting in $SEC_{net}$ increase.

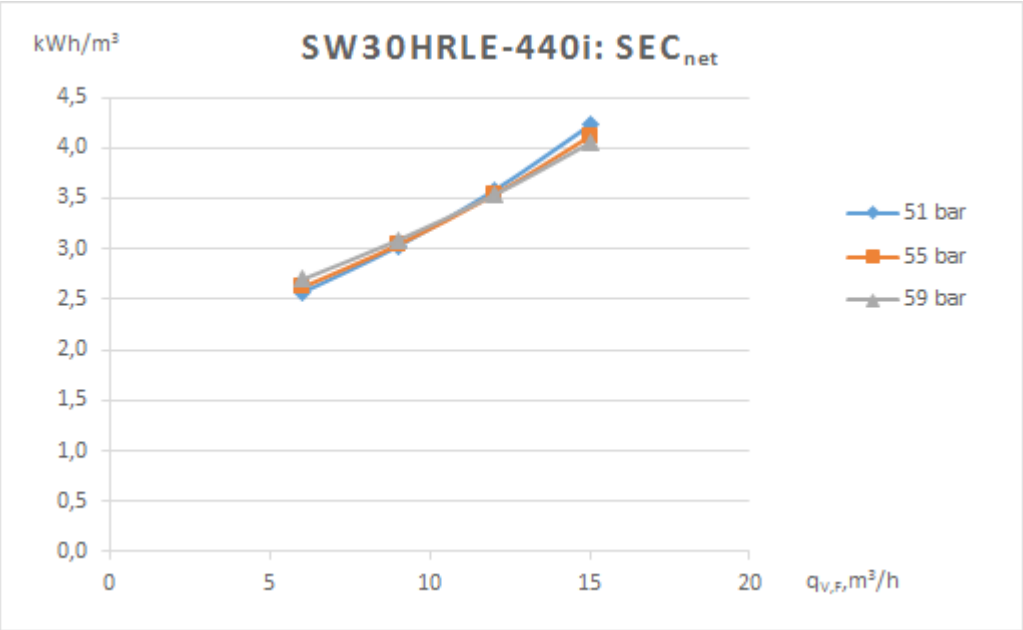


**Figure 4.3. Net Specific Energy Consumption, $SEC_{net}$, as function of feed flow for SW30HRLE-440i.**

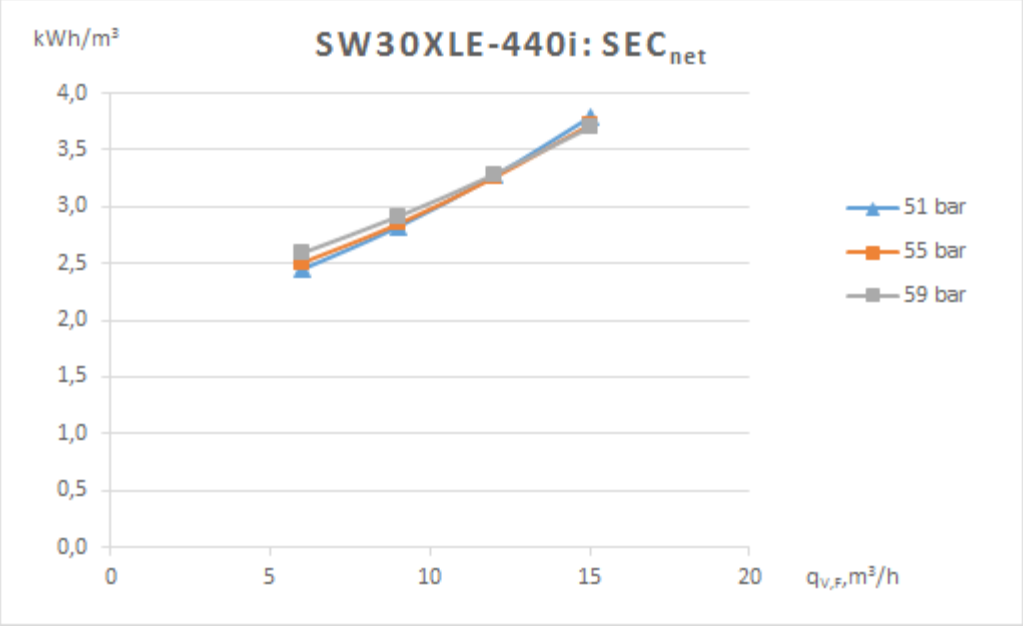


**Figure 4.4. Net Specific Energy Consumption, $SEC_{net}$, as function of feed flow for SW30XLE-440i.**

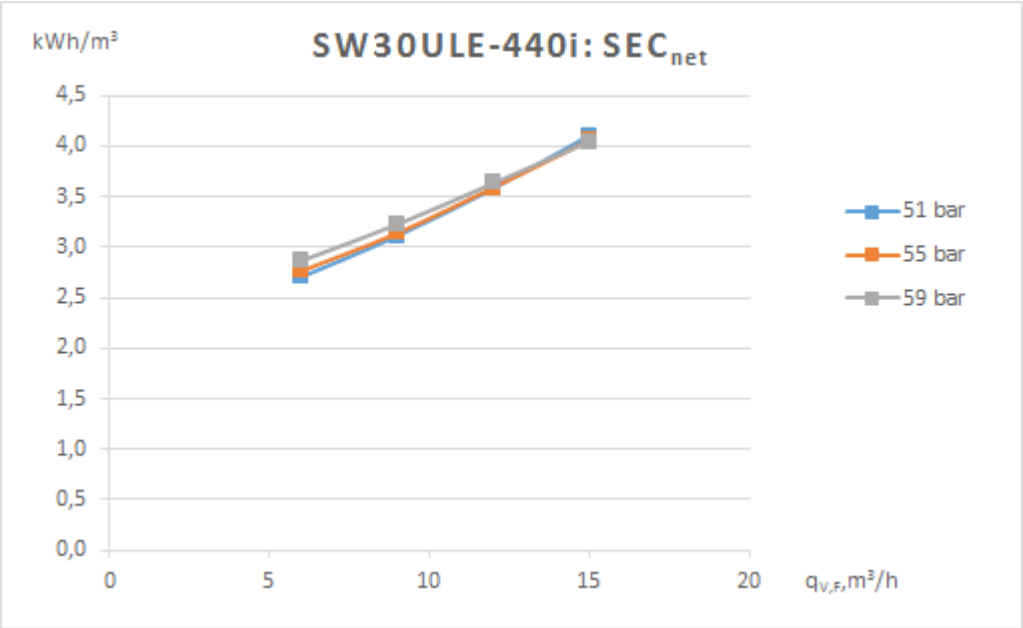


**Figure 4.5. Net Specific Energy Consumption, $SEC_{net}$, as function of feed flow for SW30ULE-440i.**

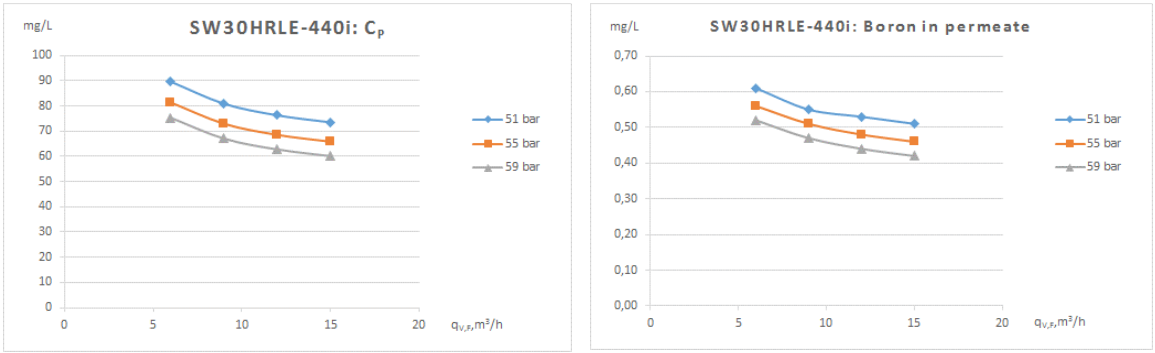


**Figure 4.6. Results obtained for permeate quality of membrane model SW30HRLE-440i.**

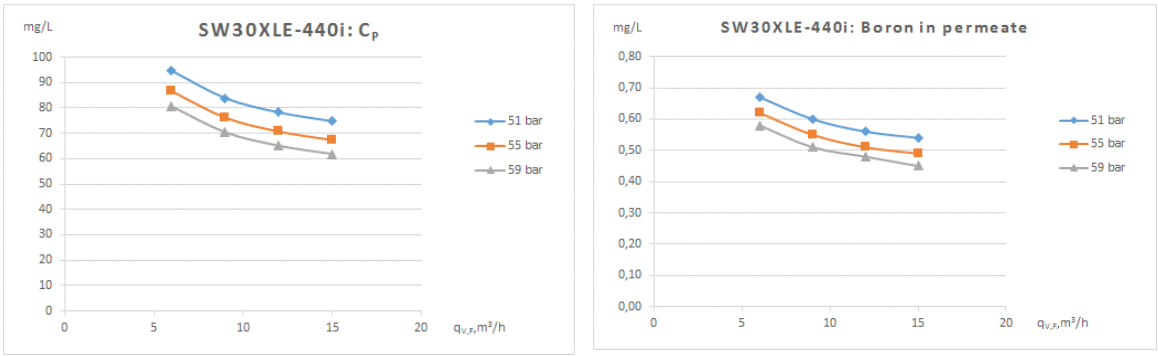


**Figure 4.7. Results obtained for permeate quality of SW30XLE-440i model.**

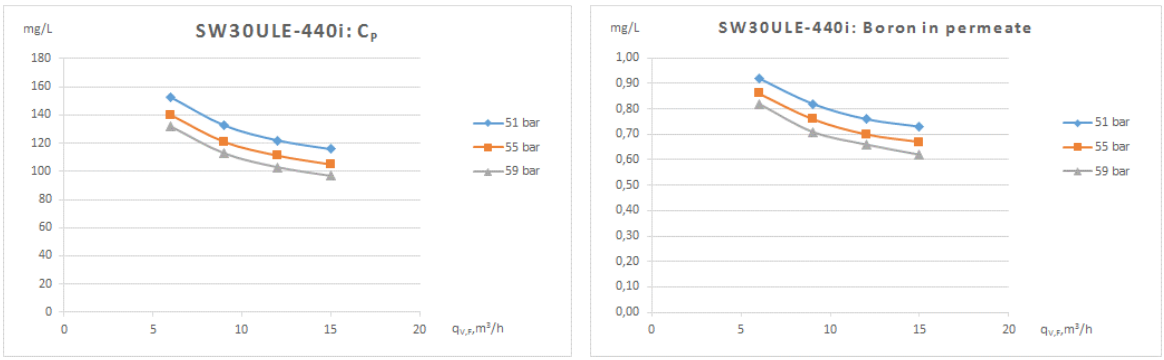


**Figure 4.8. Results obtained for permeate quality of SW30ULE-440i model.**

Besides that, water permeability is calculated by using the calculation procedure described in section 2.3 for the three membrane elements studied. They are consistent to data provided by the manufacturer. Based on these values obtained, permeate flow and quality are obtained for a 7 membrane elements in serial connection by using both, ROSA 9.1 software and the model described in section 2.3. Modelling validation is shown in tables 4.8-4.10 and parameters of each membrane elements are given in table 4.11. Values of water and salt permeability are consistent with figure 4.3 – see fig 4.9 -.

**Table 4.8. Validation of the model developed: SW30HRLE-440i element - Lw= 1.080 L/(m²·h·bar); Ls= 0.0360 L/(m²·h) -.**

| Element | $q_{VP}$, $m^3/h$ | $q_{VP}$, $m^3/h$ (ROSA) | Error $q_{VP}$, % | $C_P$, mg/L | $C_P$, mg/L (ROSA) | Error $C_P$, % | $p_{BD}$, bar | $p_{BD}$, bar (ROSA) | Error $p_{BD}$, % | r, % | r, % (ROSA) | Error r, % |
|---|---|---|---|---|---|---|---|---|---|---|---|---|
| 1 | 1,00 | 0,98 | 2,1 | 62,9 | 65,9 | -4,5 | 58,0 | 57,7 | 0,5 | 9,8 | 9,7 | 1,5 |
| 2 | 1,87 | 1,84 | 1,6 | 70,7 | 73,6 | -4,0 | 57,6 | 57,4 | 0,4 | 18,4 | 18,1 | 1,5 |
| 3 | 2,61 | 2,56 | 1,9 | 79,5 | 82,5 | -3,6 | 57,3 | 57,1 | 0,3 | 25,6 | 25,2 | 1,8 |
| 4 | 3,21 | 3,17 | 1,3 | 89,9 | 92,6 | -2,9 | 57,0 | 56,9 | 0,1 | 31,6 | 31,1 | 1,5 |
| 5 | 3,69 | 3,66 | 0,8 | 101,8 | 103,8 | -1,9 | 56,7 | 56,7 | -0,1 | 36,3 | 36,0 | 0,8 |
| 6 | 4,06 | 4,05 | 0,2 | 115,1 | 116,3 | -1,0 | 56,4 | 56,5 | -0,2 | 39,9 | 39,8 | 0,3 |
| 7 | 4,34 | 4,35 | -0,3 | 129,7 | 129,9 | -0,1 | 56,1 | 56,4 | -0,5 | 42,6 | 42,8 | -0,4 |

**Table 4.9. Validation of the model developed: SW30XLE-440i element - Lw= 1.370 L/(m²·h·bar); Ls= 0.0425 L/(m²·h) -.**

| Element | $q_{VP}$, $m^3/h$ | $q_{VP}$, $m^3/h$ (ROSA) | Error $q_{VP}$, % | $C_P$, mg/L | $C_P$, mg/L (ROSA) | Error $C_P$, % | $p_{BD}$, bar | $p_{BD}$, bar (ROSA) | Error $p_{BD}$, % | r, % | r, % (ROSA) | Error r, % |
|---|---|---|---|---|---|---|---|---|---|---|---|---|
| 1 | 0,99 | 0,98 | 1,4 | 74,7 | 78,2 | -4,5 | 52,1 | 51,8 | 0,6 | 9,8 | 9,6 | 2,1 |
| 2 | 1,83 | 1,81 | 1,1 | 84,9 | 88,3 | -3,9 | 51,8 | 51,5 | 0,6 | 18,0 | 17,8 | 1,1 |
| 3 | 2,52 | 2,49 | 1,0 | 96,6 | 99,8 | -3,2 | 51,5 | 51,3 | 0,3 | 24,7 | 24,5 | 0,8 |
| 4 | 3,05 | 3,04 | 0,4 | 110,3 | 112,7 | -2,1 | 51,2 | 51,1 | 0,2 | 30,0 | 29,9 | 0,3 |
| 5 | 3,46 | 3,47 | -0,2 | 125,8 | 127,1 | -1,0 | 50,9 | 50,8 | 0,2 | 34,1 | 34,1 | 0,0 |
| 6 | 3,77 | 3,81 | -1,0 | 142,9 | 142,9 | 0,0 | 50,6 | 50,6 | 0,0 | 37,1 | 37,4 | -0,8 |
| 7 | 4,00 | 4,06 | -1,5 | 161,3 | 159,8 | 1,0 | 50,4 | 50,5 | -0,3 | 39,3 | 39,9 | -1,5 |

**Table 4.10. Validation of the model developed: SW30ULE-440i element - Lw= 1.760 L/(m²·h·bar); Ls= 0.0762 L/(m²·h) -.**

| Element | $q_{VP}$, $m^3/h$ | $q_{VP}$, $m^3/h$ (ROSA) | Error $q_{VP}$, % | $C_P$, mg/L | $C_P$, mg/L (ROSA) | Error $C_P$, % | $p_{BD}$, bar | $p_{BD}$, bar (ROSA) | Error $p_{BD}$, % | r, % | r, % (ROSA) | Error r, % |
|---|---|---|---|---|---|---|---|---|---|---|---|---|
| 1 | 1,00 | 0,98 | 2,2 | 133 | 139 | -4,6 | 47,6 | 47,3 | 0,7 | 9,9 | 9,7 | 1,6 |
| 2 | 1,81 | 1,79 | 1,3 | 153 | 159 | -3,8 | 47,3 | 47,0 | 0,6 | 17,8 | 17,6 | 1,3 |
| 3 | 2,45 | 2,42 | 1,0 | 177 | 182 | -2,6 | 47,0 | 46,8 | 0,4 | 24,0 | 23,8 | 0,9 |
| 4 | 2,92 | 2,92 | -0,1 | 205 | 207 | -1,0 | 46,7 | 46,5 | 0,4 | 28,7 | 28,7 | -0,2 |
| 5 | 3,26 | 3,3 | -1,1 | 236 | 235 | 0,5 | 46,4 | 46,3 | 0,2 | 32,1 | 32,5 | -1,2 |
| 6 | 3,51 | 3,59 | -2,1 | 269 | 265 | 1,8 | 46,1 | 46,1 | 0,0 | 34,5 | 35,3 | -2,1 |
| 7 | 3,70 | 3,81 | -2,9 | 304 | 296 | 2,9 | 45,8 | 45,8 | 0,1 | 36,4 | 37,5 | -3,0 |

**Table 4.11. Parameters obtained for Filmtec membrane elements.**

| Membrane element | Lw L/(m²·h·bar) | Ls L/(m²·h) | $\Delta p_{Loss} = A_1 \cdot (q_{V,F-BD})^{B_1}$ | | *CPF* |
|---|---|---|---|---|---|
| | | | $A_1$ | $B_2$ | |
| SW30HRLE-440i | 1.080 | 0.036 | 0.06179081 | 0.8146819 | $1.25 \cdot r_V + 0.975$ |
| SW30XLE-440i | 1.370 | 0.0425 | 0.06084179 | 0.7937447 | |
| SW30ULE-440i | 1.760 | 0.0760 | 0.06084179 | 0.7937447 | |

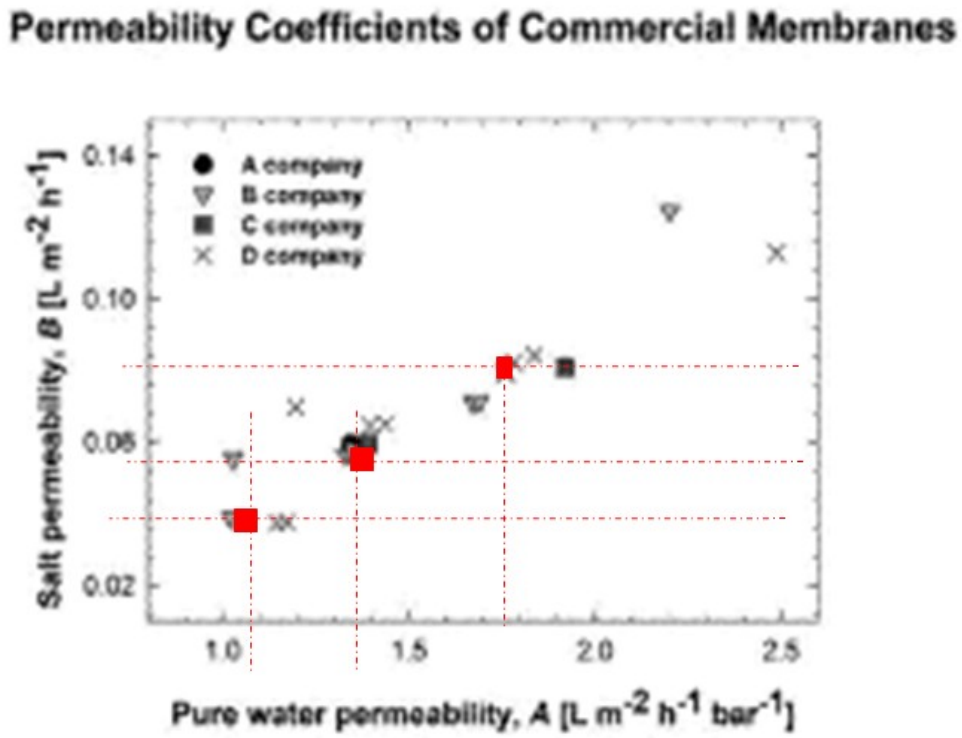


**Figure 4.9. Consistency of results obtained (marked in red) with those from the literature.**

# 4. PERFORMANCE ASSESSMENT OF A SERIE OF MEMBRANE ELEMENTS

In a conventional RO configuration there are a number of membrane elements in a row within a PV. Feed flow enters in the front, flows through the series of RO membranes producing desalinated water in each of the membranes and, after the last membrane, the remaining flow or blowdown comes out of the PV.

In Figure 4.10 a conventional Sea Water Reverse Osmosis (SWRO) system is represented. Feed water after being pressurised by the high pressure pump enters the pressure vessels (PV´s) where the RO membranes are. Raw water is separated in the membranes into a very low salinity product at ambient pressure and a pressurised brine. The energy of the brine in terms of pressure is recovered in the Energy Recovery Device (ERD), allowing pressurising part

of the feed water to a pressure slightly lower than the feed pressure, thus requiring a booster pump. The effluent is the brine once the pressure energy has been recovered.

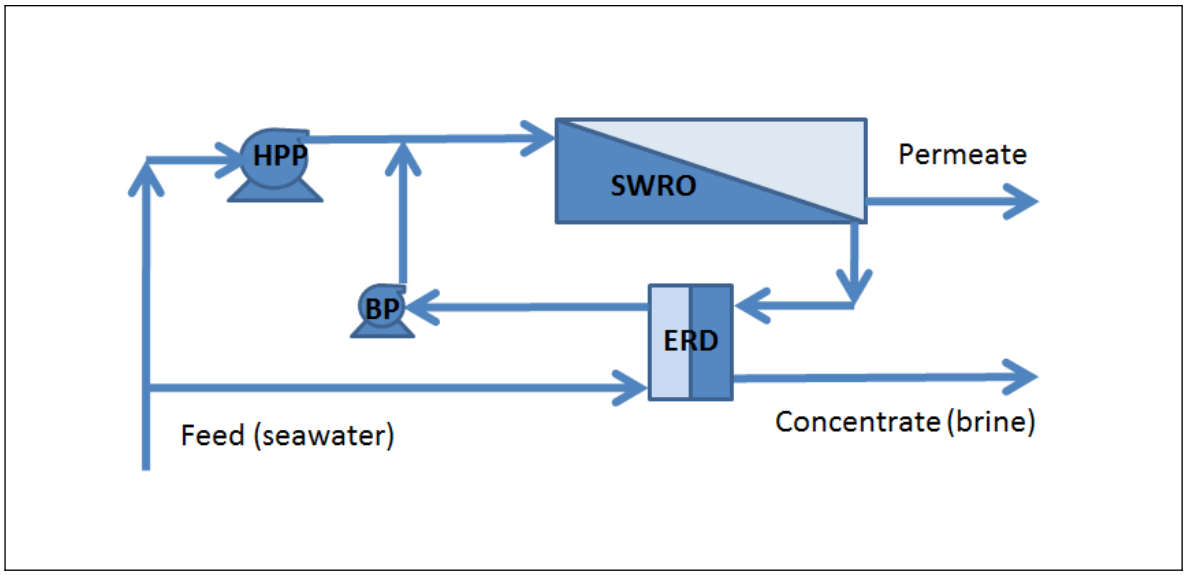


**Figure 4.10. Diagram of a conventional SWRO configuration.**

After the thermodynamic analysis of the RO technology and once understood the behaviour of a RO membrane, we analyse in this section the conventional configuration of RO systems, based on racks with pressure vessels in parallel, with series of RO membranes inside each PV. A SWRO system with a PV is analysed and calculations have been carried out for different number of RO membranes in series, ranging from 1 to 8 membranes. The objective is to find the optimum number of RO membranes inside a PV considering operating parameters such as the product flow and quality, the specific energy consumption and the CAPital EXpenses (CAPEX). Feed flow and pressure are set together with the number of membrane in the series in order to obtain the required product flow and quality, optimising for CAPEX and OPerational EXpenses (OPEX). That is, mainly optimising the cost of the equipment and the energy consumption.

As the number of RO membranes inside the PV increases, more product is obtained but reducing its quality, the recovery of the system increases and the specific energy consumption improves, as shown in figures 4.11-4.14 – see also Annex A -. Fouling factor of 0.85 and pumping efficiency of 80% was assumed. Therefore, the membrane serial improves its performance as much as it is enlarged, except with regard to product quality. The final decision

concerning the number of elements per PV should be mainly based on the product quality, having regard that a second pass could be installed in order to comply permeate quality requirements. Small number of membranes in the series leads to low total product water in comparison with the feed flow, that is, low recovery. It also leads to relatively high SEC since the energy required to pressurise the feed water has already been consumed but the total product water is low. Including more membranes in the series will help producing more water thus increasing recovery and reducing the SEC. However, the number of membranes in the series has also a limit. Going to recoveries higher than 45% will have as a consequence operational problems related to scaling in the last membrane of the series. On the other hand, from a given number of membranes the increase of recovery and decrease of SEC starts to be negligible representing an increase in CAPEX.

Therefore, for conventional RO configurations and membranes (such as SW30HRLE-440i with a seawater feed flow of 10.17 $m^3/h$, at a feed pressure of 58.36 bar and with series of 7 membranes will lead to a SWRO system with 42.8% recovery, producing 4.35 $m^3/h$ of product water with less than 130 mg/L of TDS, and requiring a SEC of 2.37 $kwh/m^3$. Besides that, by using 7 SW30ULE-440i elements, with similar fouling risk in the first element, SEC of 2.17 $kwh/m^3$ is obtained for feed pressure and flow, 52.5 bar and 10.17 $m^3/h$, respectively, with recovery rate of 39.9% and permeate TDS of 160 mg/L.

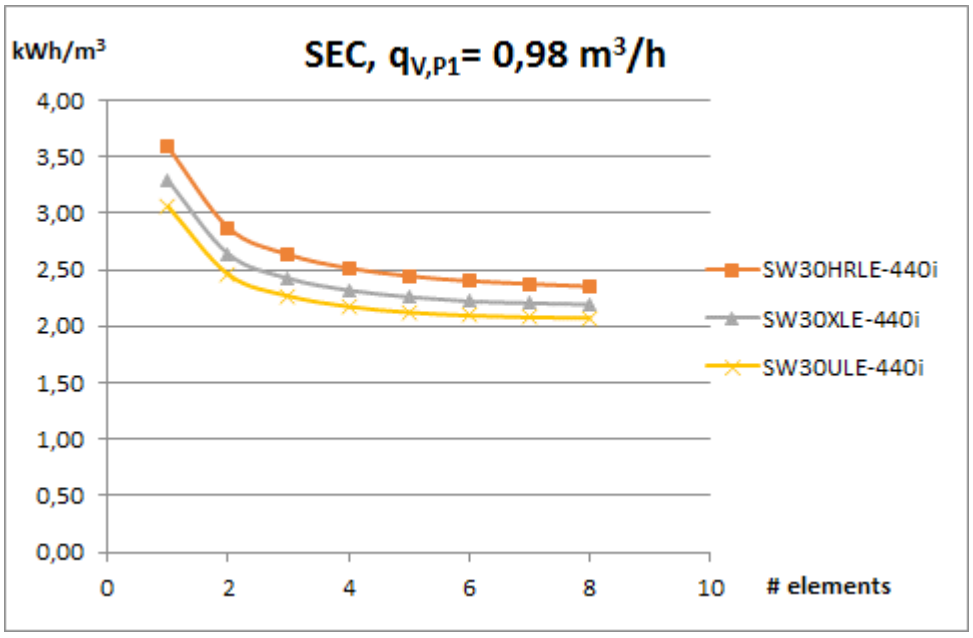


**Figure 4.11. Net Specific Energy Consumption in membrane series with constant flux in the first element in order to assumed similar fouling problems.**

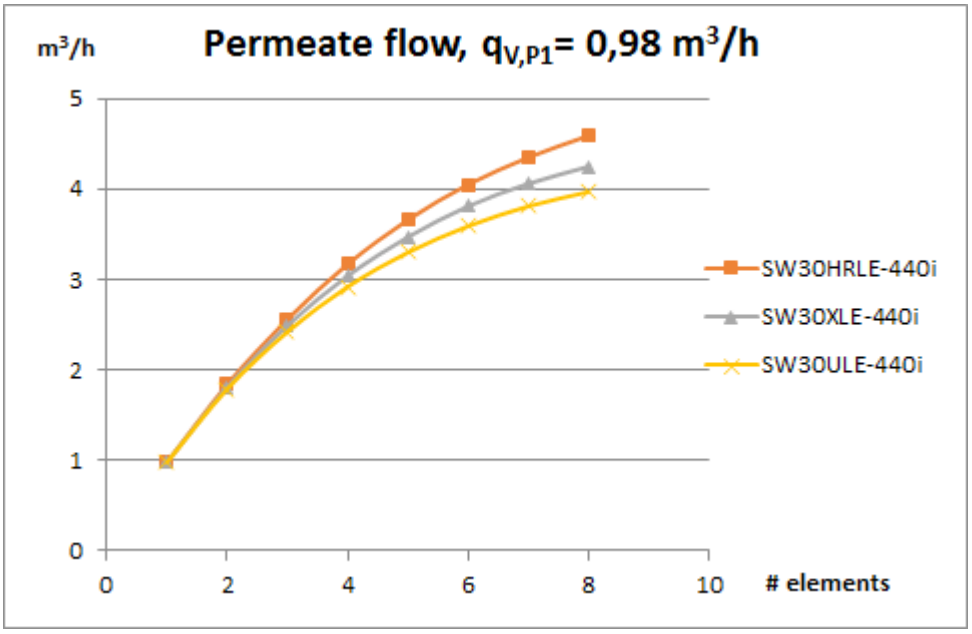


**Figure 4.12. Permeate flow of the pressure vessel at constant flux of the first membrane element.**

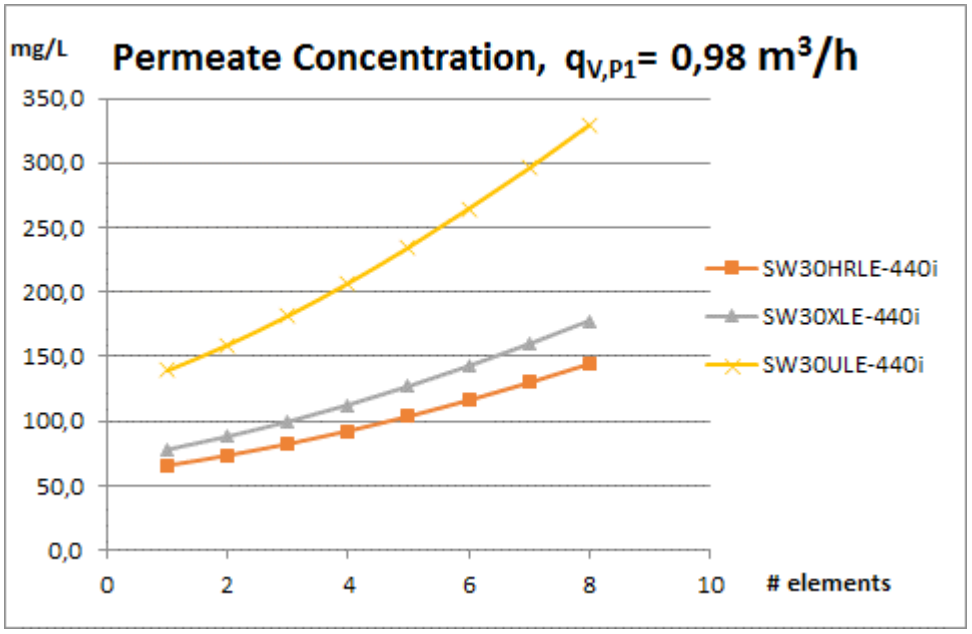


**Figure 4.13. Permeate concentration at constant flux of the first membrane element.**

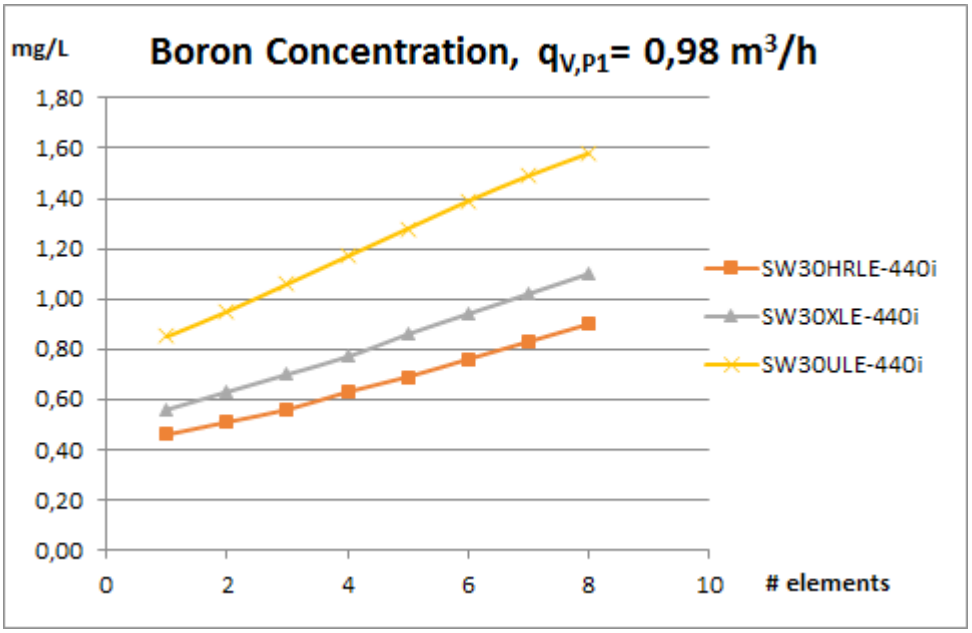


**Figure 4.14. Permeate concentration at constant flux of the first membrane element.**

Membrane manufactures have been looking for new RO membrane developments that would allow improving the performance of SWRO systems. The key objective was to reduce the energy required with the same CAPEX, that is, to allow same product flow but at a lower feed pressure. Extra-low (such as SW30XLE-440i) and Ultra-low (such as SW30ULE-440i) energy membranes have then been developed.

For the same given seawater feed flow of 10.17 $m^3/h$, utilising Extra-low and Ultra-low energy membranes allow to reduce the feed pressure to 52.5 bar and 48 bar respectively maintaining the maximum flow in the first membrane, leading to a SEC reduction of 7.2% and 12.2% in each case. However, the recovery will also be reduced (to 39.9% and 37.49% respectively), thus producing less product water and with lower quality (increasing TDS up to 261 mg/L and 295 mg/L in each case).

Finally, CAPEX and OPEX considerations have to be analysed. For the conventional RO system (configuration and membranes) that has been considered, assuming per each membrane element a cost of 500 € and 5 years average lifetime, the impact of the RO membranes in the total CAPEX would be of 0.022 €/$m^3$ of product water. And the required SEC for a system designed

like this, assuming a cost of electricity of 0.08 €/kWh, would have an impact in the total OPEX of 0.19 €/$m^3$ of product water.

For the capex analysis, all basic components of the installation are considered. The CAPEX for the high pressure pump and piping and valves is the same regardless the number of membranes. However, as the number of membranes in series is increased, the CAPEX of the pressure vessel and membranes is also increased, but the capex of the ERD and the booster pump is reduced. In figure 4.14 the CAPEX depending on the number of membranes is represented obtained for the following parameters: maximum flux 0.98 $m^3$/h (first membrane element) and feed flow, 10.17 $m^3$/h.

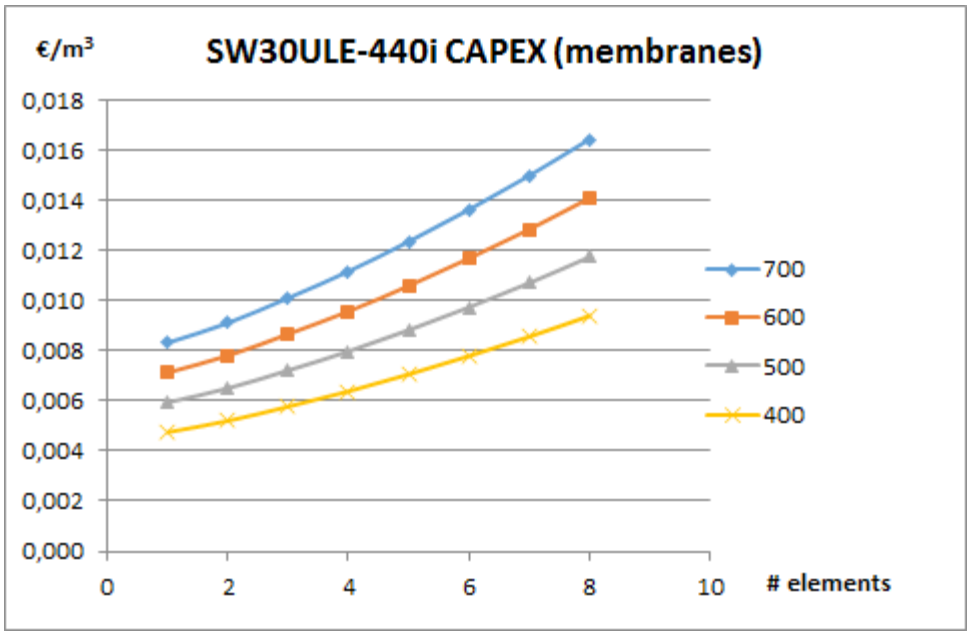


**Figure 4.15. Results obtained for the membrane model SW30ULE-440i - Unitary cost: 700, 600, 500 and 400 €/element -.**

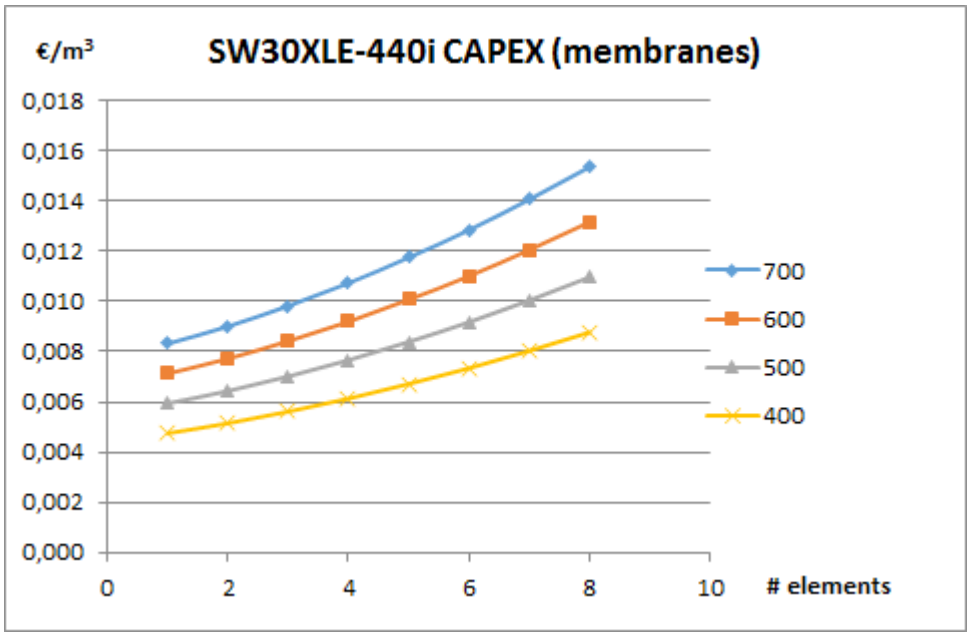


**Figure 4.16. Results obtained for the membrane model SW30XLE-440i - Unitary cost: 700, 600, 500 and 400 €/element -.**

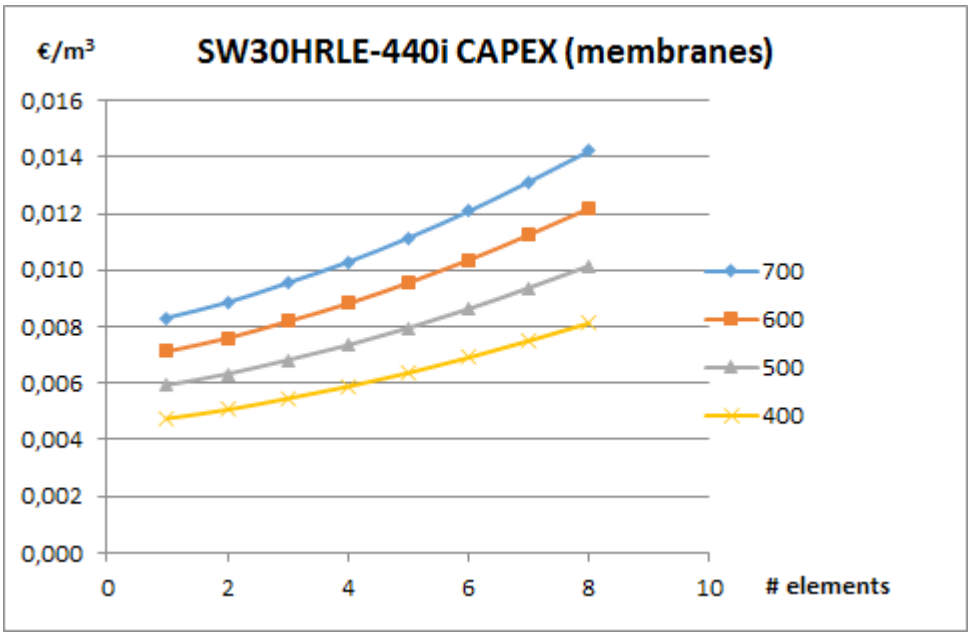


**Figure 4.17. Results obtained for the membrane model SW30HRLE-440i - Unitary cost: 700, 600, 500 and 400 €/element -.**

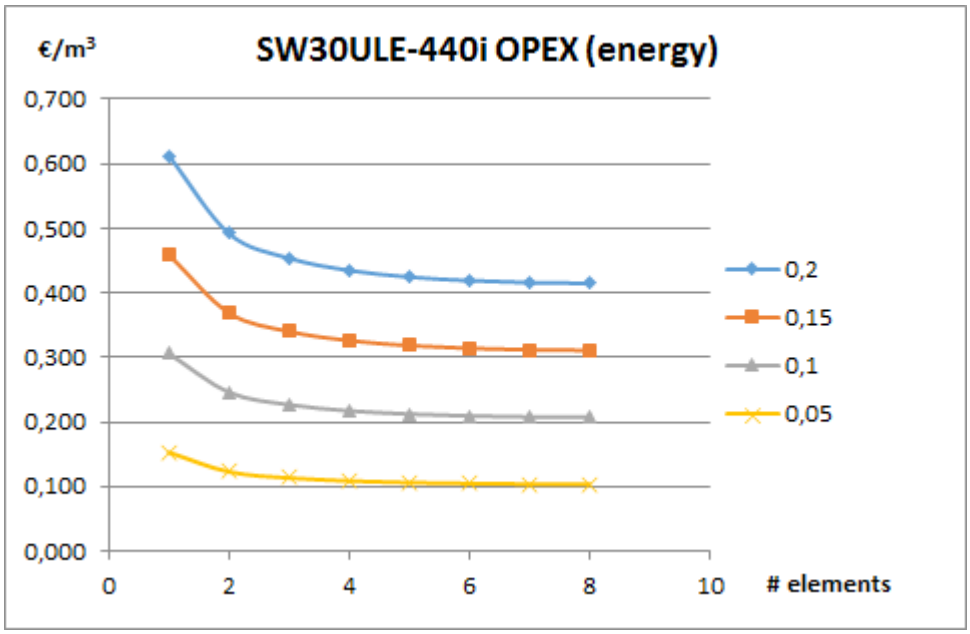


**Figure 4.18. Results obtained for the membrane model SW30ULE-440i - Unitary cost: 0.20, 0.15, 0.10, 0.05 €/kWh -.**

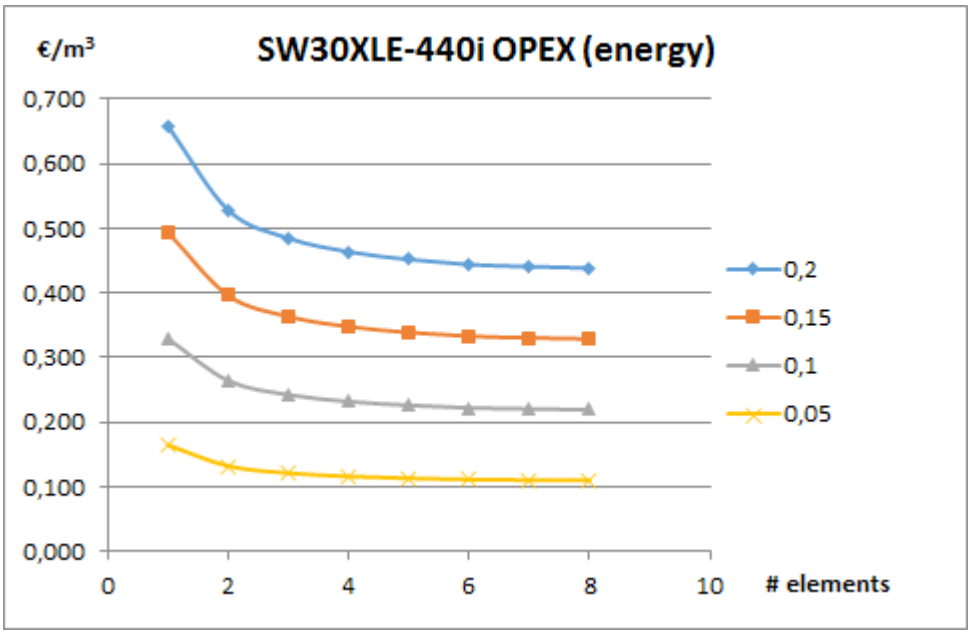


**Figure 4.19. Results obtained for the membrane model SW30XLE-440i - Unitary cost: 0.20, 0.15, 0.10, 0.05 €/kWh -.**

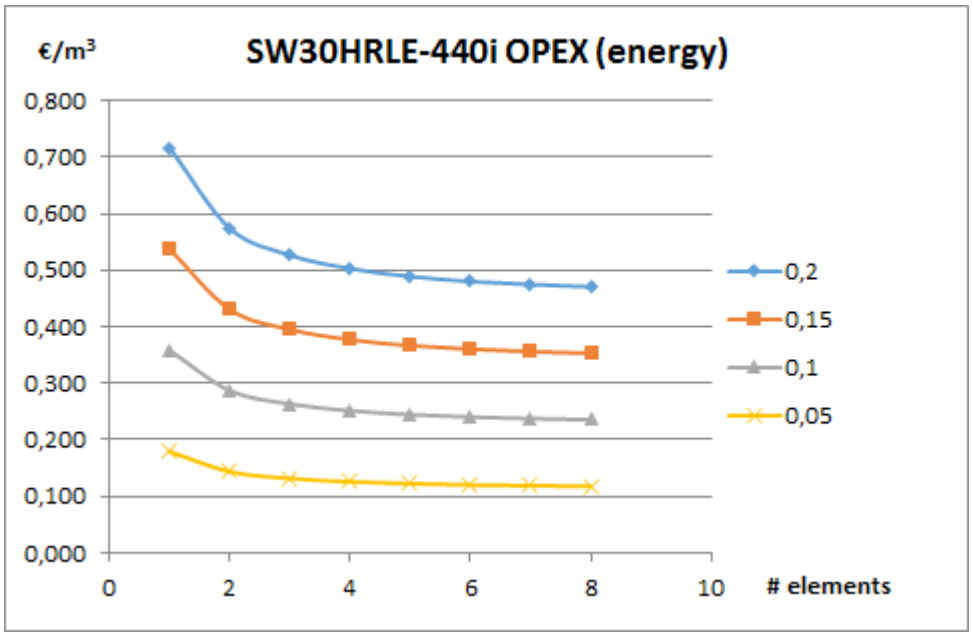


**Figure 4.20. Results obtained for the membrane model SW30HRLE-440i - Unitary cost: 0.20, 0.15, 0.10, 0.05 €/kWh -.**

# 5. ANALYSIS OF ELEMENT POSITION IN A PRESSURE VESSEL

In order to take advantage of the energy consumption reduction utilising Extra/Ultra-low membranes but without reducing significantly the total product quality, a combination of Low-Energy, Extra-low and Ultra-low membranes can be considered. Specialized literature report on SWRO plants based on this concept, called in this work Hybrid membrane Inter-Stage (HID) designs. Representative examples are [Peñate and García-Rodríguez, 2011]:

- Las Palmas III SWRO plant (Las Palmas de Gran Canaria, Spain).
- The Mazarrón SWRO plant (Murcia, Spain).
- El Coloso SWRO plant (El Coloso, Chile).

Design criteria were established by DoW concerning its own Filmtec membrane elements to apply HID concept, called by DoW Internally Stage Design [García-Molina and Casañas, 2010] -. Besides, similar assessment focused on Filmtec, Toray and Hydranautics commercial membranes were published by [Peñate and García-Rodríguez, 2011]. In conclusion, the PV should exhibit the most balanced flux as possible. Since the NDP is higher in the front than in the

tail, severe fouling could appear in the first element if excessive flux is not prevented. Besides that, NDP at the tail is quite low.

Therefore, membrane elements with the lowest flux and high salt rejections at the front positions ensures moderate fluxes in order to prevent of suffering from severe fouling and scaling. On the contrary, membrane elements with the highest flux are placed at the tail, or even in the first intermediate positions. For the rest of intermediate positions, either low, intermediate or high flux elements could be selected, depending on permeate quality and seawater composition and temperature.

The specific recommended design for Canary Islands consists in selecting the two first elements with high rejections, followed by five elements with ultralow energy consumption [Peñate and García-Rodríguez, 2011][Nagle, 2016].

# 6. CONCLUSIONS

The assessment of single membrane elements manufactured by DoW, Filmtec membranes, shows that:

- Water permeability is the main parameter on Specific Energy Consumption (SEC), gross values as much as net. In order to compare different membrane elements, simulations were carried out by setting the recovery rate and product flow.
- The corresponding recovery rate at the same operation conditions of feed flow and feed pressure increases as water permeability goes up, namely, SW30HRLE-440i, SW30XLE-440i and SW30ULE-440i. On the contrary, product quality improves as water permeability decreases.
- The feed flow has significant influence on the SEC. Within the range of 51-59 bar of feed pressure, the net SEC, $SEC_{net}$ ranges as follows:
    - SW30HRLE-440i: From 2.6-2.7 kWh/$m^3$ by setting a feed flow of 6 $m^3$/h to 4.0-4.2 kWh/$m^3$ for feed flow of 15 $m^3$/h.
    - SW30XLE-440i: Corresponding results are from 2.4-2.6 kWh/$m^3$ (feed flow, 6 $m^3$/h) to 43.7-3.8 kWh/$m^3$ (feed flow, 15 $m^3$/h).
    - SW30ULE-440i: From 2.7-2.9 kWh/$m^3$ to 4.0-4.1 kWh/$m^3$ for feed flow of 6 and 15 $m^3$/h, respectively.

This is attributable to its notable effect on pumping energy consumption but slight effect on permeate production.

A thorough membrane performance model has been implemented by including effects of pressure losses and concentration polarization at the feed-blowdown channel. A two-parameter function proposed in the literature was fitted from ROSA software. The concentration polarisation factor was calculated as a lineal function of a single parameter, the recovery rate of the membrane element, as proposed in the literature. Water and salt permeability are input data. On the contrary, this software allows to calculate said parameters from experimental data of an unknown membrane or from commercial software. Alternatively, this calculates salt concentration and flow of permeate from once given design parameters of a specific membrane module. The model has been validated by using Filmtec membrane elements.

Concerning a membrane serial:

- A quantitative assessment of CAPEX and OPEX has been performed in order to compare membrane elements with different water and salt permeability.
- Criteria of selecting the best membrane type for each position in the pressure vessel, depending on their permeability, have been reviewed. Membrane permeability should increase along the serial of membrane elements, having high rejection low energy elements in the first positions. In Canary Islands, two of those elements are enough to comply the required permeate quality. Besides that, the SEC reduces as the length of the series increases. The limiting factor is the product quality.

## 7. REFERENCES


1. Altaee, A., *Computational model for estimating reverse osmosis system design and performance: Part-one binary feed solution.* Desalination, 291, 2012, pp. 101-105.
2. Buonomenna, M. G., *Nano-enhanced reverse osmosis membranes.* Desalination, 314, 2013, pp. 73-88.
3. Cui, Z.; Xing, W.; Fan, Y., and Xu, N., *Pilot study on the ceramic membrane pre-treatment for seawater desalination with reverse osmosis in Tianjin Bohai Bay.* Desalination, 279, 2011, pp. 190-194.
4. DoW (2014) form 609-02129-804. Filmtec SW30HR LE-440i - courtesy of DoW -.
5. DoW: Filmtec membrane datasheets (https://www.dow.com/en-us/water-and-process-solutions/products/reverse-osmosis), Last visit 12/12/2017.

6. Edzwald, J. K., and Haarhoff, J., *Seawater pretreatment for reverse osmosis: Chemistry, contaminants, and coagulation.* Water Research, 45, 2011, pp. 5428-5440.
7. Fathizadeh, M.; Aroujalian, A., Raisi, A., *Effect of added NaX nano-zeolite into polyamide as a top thin layer of membrane on water flux and salt rejection in a reverse osmosis process.* Journal of membrane Science, 375, 2011, pp. 88-95.
8. García-Molina, V., and Casañas, A., *Reverse osmosis, a key technology in combating water scarcity in Spain.* Desalination, 250, 2010, pp. 950-955.
9. Hydranautics membrane datasheets (http://www.membranes.com/index.php?pagename=swc), Last visit 12/12/2017.
10. Kim, M.; Lin, N. H., and Lewis, G. T., and Cohen, Y., *Surface nano-structuring of reverse osmosis membranes via atmospheric pressure plasma-induced graft polymerization for reduction of mineral scaling propensity.* Journal of membrane Science, 354, 2010, pp. 142-149.
11. Kim, J.-H. and Jeong, K., *Seawater desalination method using arrangement optimizationof reverse osmosis membrane modules.* Applicant: Gwangju Institute of Science and Technology. United States Patent Application Publication. US2015/0251929 A1. Sep, 10, 2015.
12. Kim, Y. M.; Lee, Y. S.; Lee, Y. G.; Kim, S. J.; Yang, D. R.; Kim, I. S., and Kim, J. H., *Development of a package model for process simulation and cost estimation of seawater reverse osmosis desalination plant.* Desalination, 247, 2009, pp. 326-335.
13. Kimura, M.; Nakatsuji, K.; Sasaki, T., and Henmi, M., *The role of inorganic ions in the calcium carbonate scaling of seawater reverse osmosis systems.* Procedia Engineering, 44, 2012, pp. 598-599.
14. Kurihara, M., and Hanakawa. M., *Mega-ton Water System: Japanese national research and development project on seawater desalination and wastewater reclamation.* Desalination, 308, 2013, pp. 131-137.
15. Lee, K.P.; Arnot, T. C., and Mattia, D., *A review of reverse osmosis membrane materials for desalination – Development to date and future potential*, Journal of membrane science, 370, 2011, pp. 1-22.
16. Malaeb, L.; and Ayoub, G. M., *Reverse osmosis technology for water treatment: State of the art review.* Desalination, 267, 2011, pp. 1-8.
17. Macedonio, F.; Drioli, E.; Gusev, A. A.; Bardow, A.; Semiat, R., and Kurihara, M., *Efficient technologies for worldwide clean water supply.* Chemical Engineering and Processing: Process Intensification, 51, 2012, pp. 2-17.
18. Nagle, A. *Desalación de agua de mar por ósmosis inversa en Nueva Caledonia.* Master thesis. ETSI, University of Seville, 2016.

19. Pendergast, M. T. M.; Nygaard, J. N.; Ghosh, A. K., and Hoek, E. M. V., *Using nanocomposite materials technology to understand and control reverse osmosis membrane compaction.* Desalination, 314, 2013, pp. 73-88.
20. Peñate, B. and García-Rodríguez, L. *Reverse osmosis hybrid membrane inter-stage design: A comparative performance assessment*. Desalination, 281(1), 2011, pp. 354-363.
21. Peñate, B. and García-Rodríguez, L. *Current trends and future prospects in the design of seawater reverse osmosis desalination technology.* Desalination, 284, 2012, pp. 1-8.
22. Prihastro, N.; Liu, Q-F., and Kim, S-H., *Pre-treatment strategies for seawater desalination by reverse osmosis system.* Desalination, 249, 2009, pp. 308-316.
23. Safar, M.; Jafar, M.; Abdel-Jawad, M., and Bou-Hamad,S. *Standardization of RO membrane performance.* Desalination, 118 (1–3), 1998, pp. 13-21.
24. Sheikholeslami, Roya. *Fouling in membranes and termal units. Aunified approach – its principles, assessment, control and mitigation.* Balaban Desalination Publications, 2007. ISBN: 0-086689-066-1.
25. Toray membrane datasheets (http://www.toraywater.com/products/ro/ro_003_01.html), Last visit 12/12/2017.
26. Veza, J. M., *Introducción a la desalación de agua.* Consejo insular de aguas de Gran Canaria. Universidad de Las palmas de Gran Canaria. Servicio de Publicaciones, 2002. ISBN: 84-95792-98-2.
27. Vrouwenvelder, J. S.; van Paassen, J. A., M.; van Agtmaal, J.M. C., van Loosdrecht, M. C. M., and Kruithof, J. C., *A critical flux to avoid biofouling of spiral wound nanofiltration and reverse osmosis membranes: Fact or fiction.* Journal of membrane science, 326, 2009, pp.36-44.
28. Waly, T.; Kennedy, M. D.; Witkamp, G.-J.; Amy, G., and Schippers, J. C. *The role of inorganic ions in the calcium carbonate scaling of seawater reverse osmosis systems.* Desalination, 284, 2012, pp. 279-287.
29. Wilf, M., *The Guidebook to Membrane Desalination Technology. Reverse Osmosis, Nanofiltration and Hybrid Systems Process, Design, Applications and Economics.* Balaban Desalination Publications, 2007. ISBN 0-86689-065-3.

**ANNEX A**

| $p_F$ bar | $q_{V,F}$ $m^3/h$ | SEC $kWh/m^3$ | Pw kW | Avg. flux $L/(m^2 \cdot h)$ | Max. $q_{V,P}$ $m^3/h$ | $TDS_P$ mg/L | Boron mg/L | r % | $q_{V,P}$ $m^3/h$ | $q_{V,BD}$ $m^3/h$ | $p_{BD}$ bar | $q_{V,ERD}$ $m^3/h$ | Pw (ERD) kW | $PW_{net}$ kW | $SEC_{net}$ $kWh/m^3$ | Max. flux $L/(m^2 \cdot h)$ | # elements | Model |
|---|---|---|---|---|---|---|---|---|---|---|---|---|---|---|---|---|---|---|
| **58,36** | **10,17** | 20,98 | **20,6** | 24,03 | **0,98** | 65,9 | 0,46 | 9,7 | 0,98 | 9,19 | 57,7 | 8,9 | **-17,4** | **3,2** | **3,25** | **23,97** | **1** | SW30HRLE-440i |
| **58,36** | **10,17** | 11,20 | **20,6** | 22,47 | **0,98** | 73,6 | 0,51 | 18,1 | 1,84 | 8,33 | 57,4 | 8,1 | **-15,6** | **5,0** | **2,71** | **23,97** | **2** | SW30HRLE-440i |
| **58,36** | **10,17** | 8,04 | **20,6** | 20,91 | **0,98** | 82,5 | 0,56 | 25,2 | 2,56 | 7,61 | 57,1 | 7,4 | **-14,1** | **6,5** | **2,53** | **23,97** | **3** | SW30HRLE-440i |
| **58,36** | **10,17** | 6,51 | **20,6** | 19,37 | **0,98** | 92,6 | 0,63 | 31,1 | 3,17 | 7,00 | 56,9 | 6,8 | **-12,9** | **7,7** | **2,44** | **23,97** | **4** | SW30HRLE-440i |
| **58,36** | **10,17** | 5,64 | **20,6** | 17,89 | **0,98** | 103,8 | 0,69 | 36,0 | 3,66 | 6,51 | 56,7 | 6,3 | **-11,9** | **8,7** | **2,38** | **23,97** | **5** | SW30HRLE-440i |
| **58,36** | **10,17** | 5,09 | **20,6** | 16,50 | **0,98** | 116,3 | 0,76 | 39,8 | 4,05 | 6,12 | 56,5 | 5,9 | **-11,1** | **9,5** | **2,35** | **23,97** | **6** | SW30HRLE-440i |
| **58,36** | **10,17** | 4,74 | **20,6** | 15,21 | **0,98** | 129,9 | 0,83 | 42,8 | 4,35 | 5,82 | 56,4 | 5,7 | **-10,5** | **10,1** | **2,33** | **23,97** | **7** | SW30HRLE-440i |
| **58,36** | **10,17** | 4,50 | **20,6** | 14,02 | **0,98** | 144,4 | 0,90 | 45,1 | 4,59 | 5,59 | 56,2 | 5,4 | **-10,0** | **10,6** | **2,31** | **23,97** | **8** | SW30HRLE-440i |
| **52,5** | **10,17** | 18,93 | **18,5** | 23,97 | **0,98** | 78,2 | 0,56 | 9,6 | 0,98 | 9,19 | 51,8 | 9,0 | **-15,6** | **2,9** | **2,99** | **23,97** | **1** | SW30XLE-440i |
| **52,5** | **10,17** | 10,26 | **18,5** | 22,10 | **0,98** | 88,3 | 0,63 | 17,8 | 1,81 | 8,36 | 51,5 | 8,1 | **-14,0** | **4,5** | **2,49** | **23,97** | **2** | SW30XLE-440i |
| **52,5** | **10,17** | 7,45 | **18,5** | 20,30 | **0,98** | 99,8 | 0,70 | 24,5 | 2,49 | 7,68 | 51,3 | 7,5 | **-12,7** | **5,8** | **2,33** | **23,97** | **3** | SW30XLE-440i |
| **52,5** | **10,17** | 6,10 | **18,5** | 18,58 | **0,98** | 112,7 | 0,77 | 29,9 | 3,04 | 7,13 | 51,1 | 6,9 | **-11,7** | **6,8** | **2,24** | **23,97** | **4** | SW30XLE-440i |
| **52,5** | **10,17** | 5,34 | **18,5** | 16,98 | **0,98** | 127,1 | 0,86 | 34,1 | 3,47 | 6,70 | 50,8 | 6,5 | **-10,9** | **7,6** | **2,20** | **23,97** | **5** | SW30XLE-440i |
| **52,5** | **10,17** | 4,87 | **18,5** | 15,52 | **0,98** | 142,9 | 0,94 | 37,4 | 3,81 | 6,37 | 50,6 | 6,2 | **-10,3** | **8,3** | **2,17** | **23,97** | **6** | SW30XLE-440i |
| **52,5** | **10,17** | 4,57 | **18,5** | 14,19 | **0,98** | 159,8 | 1,02 | 39,9 | 4,06 | 6,11 | 50,5 | 6,0 | **-9,8** | **8,8** | **2,16** | **23,97** | **7** | SW30XLE-440i |
| **52,5** | **10,17** | 4,36 | **18,5** | 13,01 | **0,98** | 177,8 | 1,10 | 41,8 | 4,25 | 5,92 | 50,3 | 5,8 | **-9,4** | **9,1** | **2,15** | **23,97** | **8** | SW30XLE-440i |
| **48** | **10,17** | 17,24 | **17** | 24,05 | **0,98** | 139,2 | 0,85 | 9,7 | 0,98 | 9,19 | 47,3 | 9,0 | **-14,2** | **2,7** | **2,79** | **23,97** | **1** | SW30ULE-440i |
| **48** | **10,17** | 9,49 | **17** | 21,84 | **0,98** | 159,1 | 0,95 | 17,6 | 1,79 | 8,38 | 47,0 | 8,2 | **-12,8** | **4,2** | **2,32** | **23,97** | **2** | SW30ULE-440i |
| **48** | **10,17** | 6,99 | **17** | 19,77 | **0,98** | 181,63 | 1,06 | 23,84 | 2,42 | 7,75 | 46,8 | 7,6 | **-11,7** | **5,3** | **2,18** | **23,97** | **3** | SW30ULE-440i |
| **48** | **10,17** | 5,80 | **17** | 17,87 | **0,98** | 206,86 | 1,17 | 28,73 | 2,92 | 7,25 | 46,5 | 7,1 | **-10,8** | **6,1** | **2,10** | **23,97** | **4** | SW30ULE-440i |
| **48** | **10,17** | 5,13 | **17** | 16,16 | **0,98** | 234,6 | 1,28 | 32,47 | 3,30 | 6,87 | 46,3 | 6,7 | **-10,1** | **6,8** | **2,06** | **23,97** | **5** | SW30ULE-440i |
| **48** | **10,17** | 4,72 | **17** | 14,63 | **0,98** | 264,56 | 1,39 | 35,29 | 3,59 | 6,58 | 46,1 | 6,4 | **-9,6** | **7,3** | **2,04** | **23,97** | **6** | SW30ULE-440i |
| **48** | **10,17** | 4,45 | **17** | 13,33 | **0,98** | 295,85 | 1,49 | 37,49 | 3,81 | 6,36 | 45,9 | 6,2 | **-9,2** | **7,7** | **2,03** | **23,97** | **7** | SW30ULE-440i |
| **48** | **10,17** | 4,27 | **17** | 12,15 | **0,98** | 329,22 | 1,58 | 39,08 | 3,97 | 6,20 | 45,8 | 6,1 | **-8,9** | **8,1** | **2,03** | **23,97** | **8** | SW30ULE-440i |

# Chapter 5. ANALYSIS OF REVERSE OSMOSIS INNOVATIVE CONFIGURATIONS

A summary of this chapter will be submitted in May, 2018 for publication to the international journal *Desalination* with the following authors, title and abstract:

**Authors:** Arturo Buenaventura Pouyfaucon[(1)] and Lourdes García-Rodríguez[(2)]

[(1)]Abengoa – Spain. C/ Energía Solar, nº1. 41014- Sevilla. abuenaventura@abengoa.com

[(2)]Dpto. Ingeniería Energética. Universidad de Sevilla. ETSI, Camino de Los Descubrimientos, s/n. 41092-Sevilla. mgarcia17@us.es

Title: *Assessment of innovative configurations in Sea Water Reverse Osmosis Desalination*

# 1. INTRODUCTION

Desalination has become part of the solution to water pollution and scarcity across the globe. It allows generating new water resources from seawater and brackish water in areas where there is a lack of natural resources.

Within desalination technologies, membrane technologies have become more relevant than distillation. Nowadays, nearly all of seawater desalination plants are designed and constructed based on Reverse Osmosis (RO), about 1.5 million $m^3$/d vs.0.27 million $m^3$/d based on thermal processes [Virgili, 2016].

The development of RO technology has been driven mainly by the integration of energy recovery devices in the system to recover from the brine as much pressure energy as possible and by the reduction in cost of the RO membranes, to the extent that membranes have become a commodity.

Therefore, in the last years some efforts have been focused in improving the configuration of the RO systems, trying to go a bit further in their efficiency. These innovative configurations pretend to improve parameters of the design and operation of the RO systems, such as, the recovery rate, the energy requirements or the availability, taking into consideration membrane biofouling and scaling effects, cleaning procedures, etc.

In this chapter relevant RO innovative configurations are analysed – see table 5.1 -, deep diving in their conceptual rational and what they aim, quantifying pros and cons of each of them and analysing their potential impact in terms of CAPital EXpenses (CAPEX) and OPeration EXpenses (OPEX) in desalination plants.

**Table 5.1. Innovative configurations analysed in this chapter.**

| Inventor | Reference |
|---|---|
| Wittmann, E.; Ventresque, C.; Lacaze-Eslous, F.;<br>Patent applicant: VOELIA WATER SOLUTIONS & TECH. | Wittmann *et al* (2013) |
| Viera Curbelo, O.,<br>Patent applicant: GEN ELECTRIC (US). | Viera Curbelo (2013) |
| Desalitech, Inc. – USA | Stover (2015) |

## 2. ANALYSIS METHODOLOGY OF INNOVATIVE REVERSE OSMOSIS CONFIGURATIONS

There are a number of parameters that are interdependent and have direct impact in the efficiency of a RO system: energy consumption, product quality, recovery, fouling and scaling.

The combination of these parameters has a direct impact in the CAPEX and OPEX of the RO system. For CAPEX analysis high pressure and booster pumps, number of membranes, pressure vessels, piping and valves, rack structure, cleaning system, etc should be considered. For OPEX analysis electricity, number and time of cleaning procedures, required chemicals, etc are considered, being the main parameter the specific energy consumption. However, CAPEX analysis is conducted only if advantages in OPEX are pointed out.

Raw water characteristics and RO membrane performance have also a significant impact in the design and efficiency of the system. However for the purpose of this analysis, conventional seawater characteristics and standard RO membrane performance parameters are considered, since variations of these aspects will likely have the same impact in the different configurations.

The membranes in the first positions perform better than the membranes in the tail of the pressure vessel. As feed moves through the pressure vessel, the concentration increases as permeate is produced and the pressure decreases due to the pressure losses. As a consequence, both the flow and the net driving pressure are smaller in the tail than in the front of the pressure vessel, leading to lower permeate production and less permeate quality in terms of concentration.

Therefore, types of analysis-charts to be carried out are as follows. For a given feed flow and pressure, energy consumption, recovery rate and product quality with the idea of assessing if there is an optimum for the design. Also the analysis should include the estimation of how fouling could vary with respect to recovery by assessing the maximum flux reduction. These analyses include as a reference conventional RO configuration.

## 3. CONFIGURATION PATENTED BY VEOLIA WATER SOLUTIONS & TECH IN 2013

A configuration patented by Veolia Water Solutions & Tech (Veolia) [Wittmann *et al*, 2013] is thoroughly analysed in this section. Simulations of the performance of the PV is carried

out by using the ROSA 9.1 software.

### 3.1. Configuration Description

The concept patented by Veolia is described by the following figure 5.1. The membrane skid is composed by Pressure Vessels (PV´s) consisting in eight membrane elements. The PV´s are arranged in two stages. The feed (seawater) inlet of the first stage is split to both ends of the PV´s. Then, feed water circulates from the ends to the centre of the PV, and the concentrate outlet is located between the fourth and the fifth membrane position. Nevertheless, permeate generated within the pressure vessel of the first stage is collected from both ends of the PV´s. Therefore, this RO process is analogous to a first pass with only four membranes per PV. As described by Veolia in the patent, the permeability of the membrane elements of the first stage is not higher than that of the elements corresponding to the second stage. The number of membranes within a PV could be different from eight.

Operating conditions of the first-stage elements should be quite similar than those of the first four position of a standard PV. Concentrate collected from the first stage enters the PV´s of the second stage at the central position - between the fourth and fifth element of an 8-element PV -. This second process acts as a second stage.

Configuration of the second stage PV exhibits the following layout: Concentrate from the first stage is fed through the center of the second stage PV´s. Permeate and concentrate are extracted from both ends and have similar salt concentration, respectively. Permeate quality from this second stage is lower than that of the first stage since the feed processed in the second stage has higher salt concentration. Finally, concentrate from both ends are mixed in a common pipeline to the inlet of the energy recovery devices.

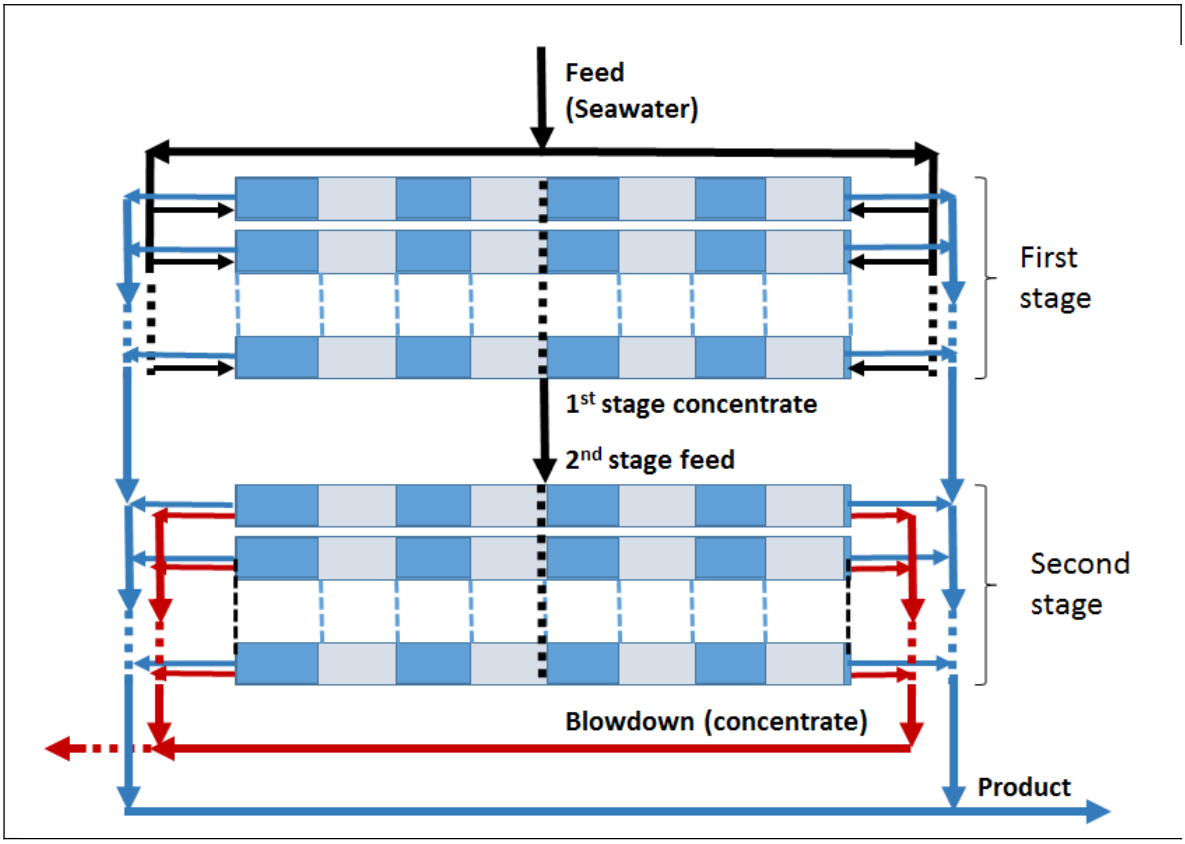


**Figure 5.1. Diagram of the SWRO train proposed by Veolia - adapted from Wittmann *et al*, (2013) -.**

### 3.2. Concept Assessment

Main advantages and drawbacks of Veolia´s configuration are summarised as follows:

***Main advantages:***

- The number of PV´s in the first and second stage may be different, allowing to adjust the feed flow per PV in the second stage, in order to optimise the productive process of the second stage. Nevertheless, the flow effect on the element productivity is only attributable to the concentration polarization, since feed flow is not directly related to the transport mechanisms through the membrane (refer to chapter 4).
- Inter-stage pH adjustment might be included if necessary.
- In order to ensure permeate quality under seawater temperature changes, concentrate at the first stage outlet could be blended with seawater to decrease salt concentration of the

second stage feed.

***Main drawbacks:***

- Reducing the number of PV´s in the second stage will also represent a reduction in the membrane surface of the second stage, thus very likely leading to a reduction in the permeate production of the second stage.
- Permeate collection requires four pipelines instead of one or two. The latter corresponds to the case of split partial configuration, which is the most suitable if a second pass is required to match the permeate quality requirements.
- Feed-concentrate pipeline length is increased in order to collect the concentrate from both sides of the PV´s in the second stage.

To sum up, the quantitative OPEX advantage of the proposed configuration with respect to the conventional design should compensate the increase in pressure losses and capital cost due to higher pipelines length and more complex layout.

Membrane operating conditions over the PV´s of the first stage remain the same of the first four membranes within the conventional design. Therefore, the advantages on operation and permeate quality should be achieved within the second stage, in comparison to the four tail positions of the PV in the standard design.

Once analysed the concept reported by Veolia in its patent, it should be highlighted that the concept could be understood as two stages with a serial of four membrane elements in each stage. This general concept of inter-stage adjustment of the flow by means of the second stage is described in the patent by Yi Zhou (2012). Neither Wittmann *et al* (2013), nor Yi Zhou (2012) mentioned the use of a booster pump between stages.

### 3.3. Assessment of proposed configuration

The quantitative assessment of Veolia´s configuration requires:

- The selection of the feed flow per PV (by adjusting the number of PV´s) of the second stage in order to optimise the use of the proposed configuration.
- The comparison with respect to the conventional configuration regarding the following operational and design parameters:
    - Specific Energy Consumption (SEC) and other operating conditions.

- Permeate quality, namely salinity and boron concentration.
- Analysis of CAPEX based on number of membrane element required.

Finally, also the possible use of a booster pump between stages could be analysed. Since this component is not considered in the patent description, this is out of the aim of this chapter.

Since the minimum energy consumption established by the Principles of the Thermodynamics strongly depends on recovery rate, this parameter is set to 45%. Besides, permeate flow is also a fixed input parameter in order to assess the SEC and CAPEX. The latter is assessed in terms of total number of membrane elements, piping and PV´s required. In addition, the comparison of the fluxes in the different membranes permits the assessment with regard to fouling and scaling tendency. Note that operating conditions of salt concentration on the tail elements remain unchanged since recovery rate is constant. The analysis should be complemented by the discussion of including other design and operational parameters.

Besides that, complementary information is obtained by means of an analogous analysis in which both, pressure and flow of the seawater stream are constant. These operating conditions results in similar flux of the first element position. As a consequence, similar behavior on fouling and scaling is expected. Results should be discussed focusing the assessment on SEC and recovery. The latter is important in OPEX since chemical dosing and auxiliary consumption mainly depend on it.

### 3.4. Results for Canary Islands

A standard configuration is set in order to assess the concept in which the configuration proposed by Veolia is based on. Seawater quality and temperatures suitable to produce adequate permeate quality with a single pass configuration is selected. The exemplary case use seawater quality representative of The Canary Islands – see table 5.2 -.

**Table 5.2 Seawater parameters for Canary Islands [Peñate and García-Rodríguez, 2011].**

Seawater composition (East Atlantic Ocean – Canary Islands).

| East Atlantic seawater – beach well water (SDI < 3) | | Cations (mg/l) | | Anions (mg/l) | |
|---|---|---|---|---|---|
| TDS | 37,125.92 mg/l | $NH_4^+$ | 0.08 | $CO_3^{2-}$ | 5.53 |
| pH | 7.50 | $K^+$ | 438.00 | $HCO_3^-$ | 158.60 |
| Temperature | 20 °C | $Na^+$ | 11,080.00 | $NO_3^-$ | 6.10 |
| $CO_2$ | 2.77 mg/l | $Mg^{2+}$ | 1486.00 | $Cl^-$ | 20,926.32 |
| $SiO_2$ | 34.00 mg/l | $Ca^{2+}$ | 558.00 | $F^-$ | 1.71 |
| $B_T$ | 5.50 mg/l | $Sr^{2+}$ | 0.12 | $SO_4^{2-}$ | 2400.00 |

Next figures present representative examples of a standard configuration – e.g. single pass - suitable for Canary Islands. Main components are depicted as follows: High Pressure Pump (HPP); Booster Pump (BP); Energy Recovery Device (ERD), and Sea Water Reverse Osmosis (SWRO) rack.

- Figure 5.2 depicts results obtained for a PV consisting in 8 membrane elements operated with an average flux of 14 L/(h·m$^2$). The element SW30HRLE-440i is selected for this example.
- Figure 5.3 shows results obtained for a PV composed of four elements of SW30HRLE-440i followed by four elements of the model SW30ULE-440i. This configuration is calculated for comparison with Veolia concept. Nevertheless, according to design recommendation by Peñate and García-Rodríguez (2011), it should be better to use two SW30HRLE-440i followed by six SW30ULE-440i.

Results given in figures 5.2-5.3 are used in this chapter as the base case for conventional configuration in order to assess the suitability of Veolia´s concept.

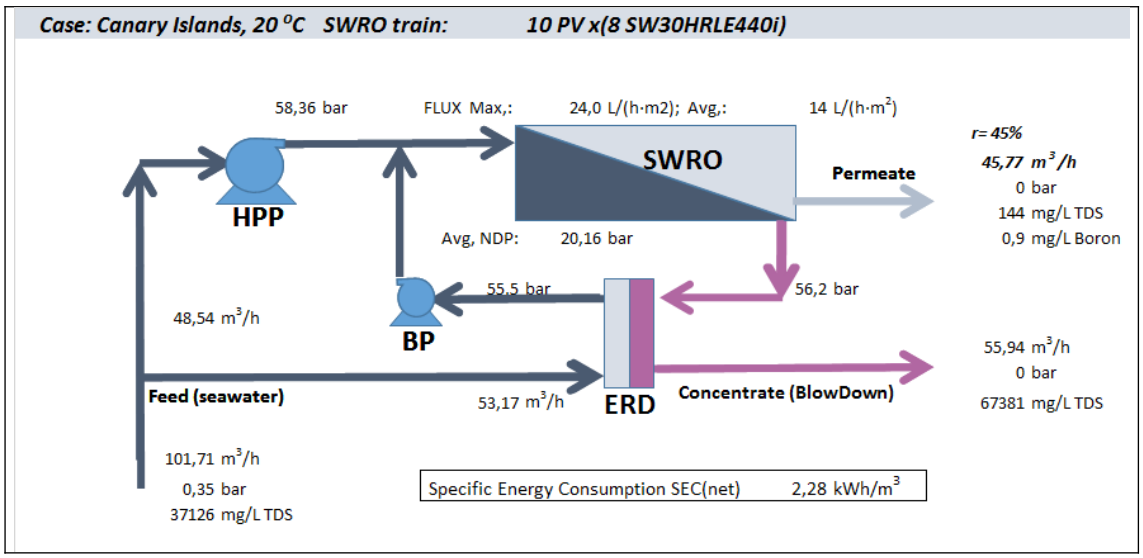


**Figure 5.2. Results of ten PV´s (8 elements model SW30HRLE-440i, each) with operating conditions corresponding to recovery, 45%, and permeate flow 45.77 m³/h, thus average flux is 14 L/(h·m²).**

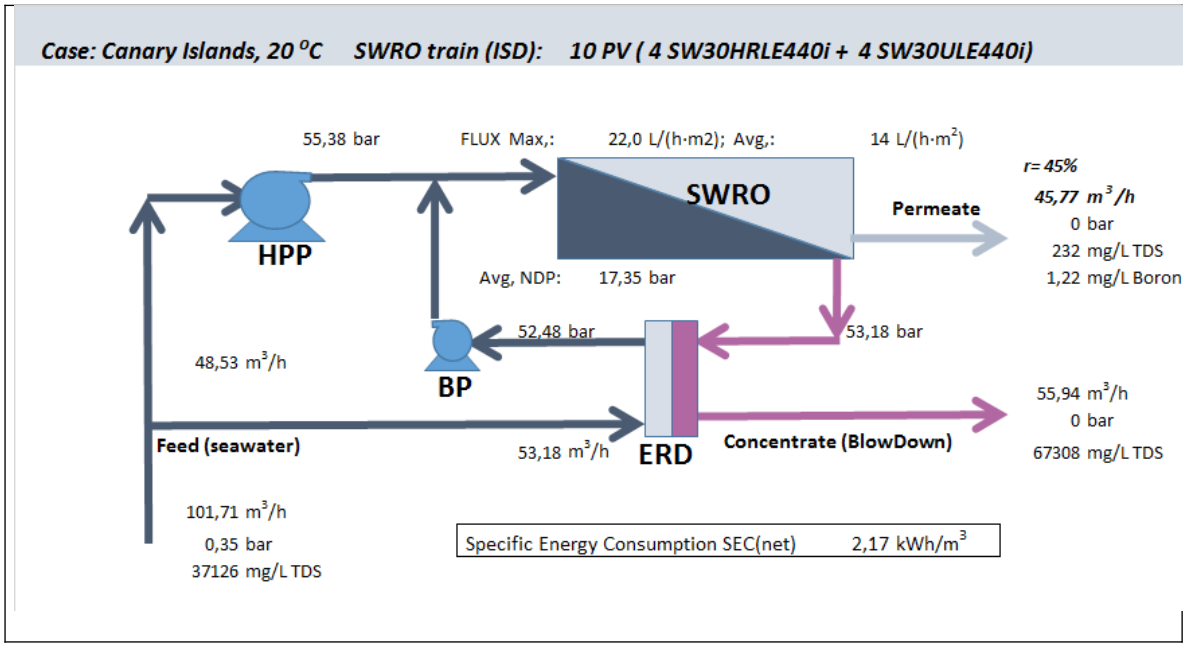


**Figure 5.3. Results of ten PV´s (HID: 4 elements model SW30HRLE-440i followed by 4 SW30ULE-440i, each) with operating conditions corresponding to recovery, 45%, and permeate flow 45.77 m³/h, thus average flux is 14 L/(h·m²).**

Firstly, the effect on the SEC of feed flow in the second stage is analysed under conditions of constant recovery rate and permeate flow. To this end, the effect of the number of

PV´s in the second stage is studied. To hold recovery constant may lead to unsuitable operating conditions due to high value of maximum flux. Therefore, the main goal of this analysis is limited to the assessment of a conceptual issue: the influence of feed flow in the second stage under similar conditions of osmotic pressure and salt concentration within the feed-concentrate channel. The comparative analysis discussed below is based on results depicted in figures 5.4-5.7. Figure 5.4 shows the main parameters of OPEX, the Specific Energy Consumption (SEC): $SEC_{gross}$ – with no energy recovery – and $SEC_{net}$ – SEC including energy recovery based on isobaric chambers –. Besides that, the main paremeter related to CAPEX is given, average flux. Figure 5.5 depicts maximum flux and other important parameters concerning permeate quality namely, salt concentration and boron concentration. The case of 10 PV´s in the second stage is conceptually equivalent to the standard configuration (Fig. 5.2).

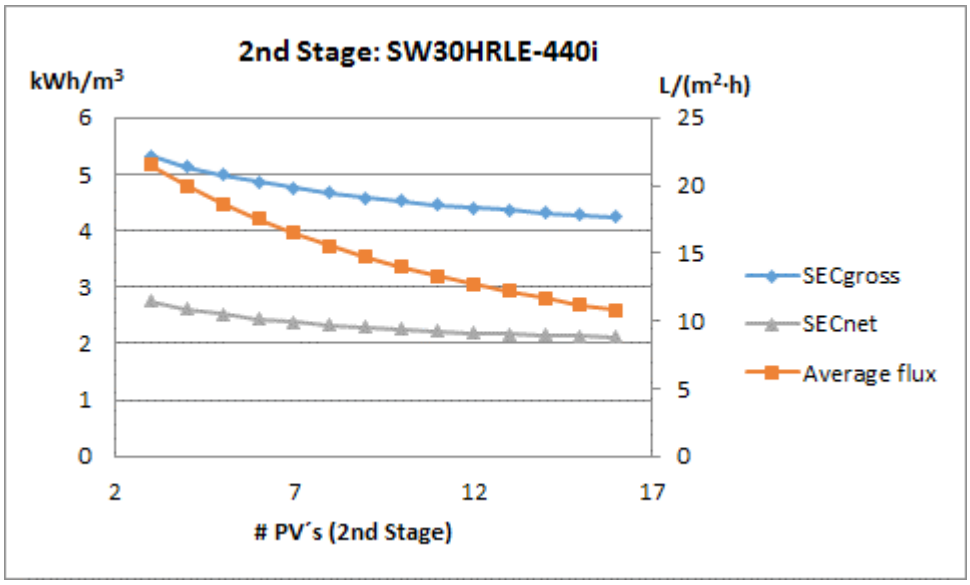


**Figure 5.4. Two-staged configuration with ten PV´s in the first stage and a variable number of PV´s in the second stage – recovery, 45%; permeate flow, 45.77 $m^3/h$; SW30HRLE-440i -: Main parameters of the economic assessment, namely, $SEC_{gross}$, $SEC_{net}$ and average flux.**

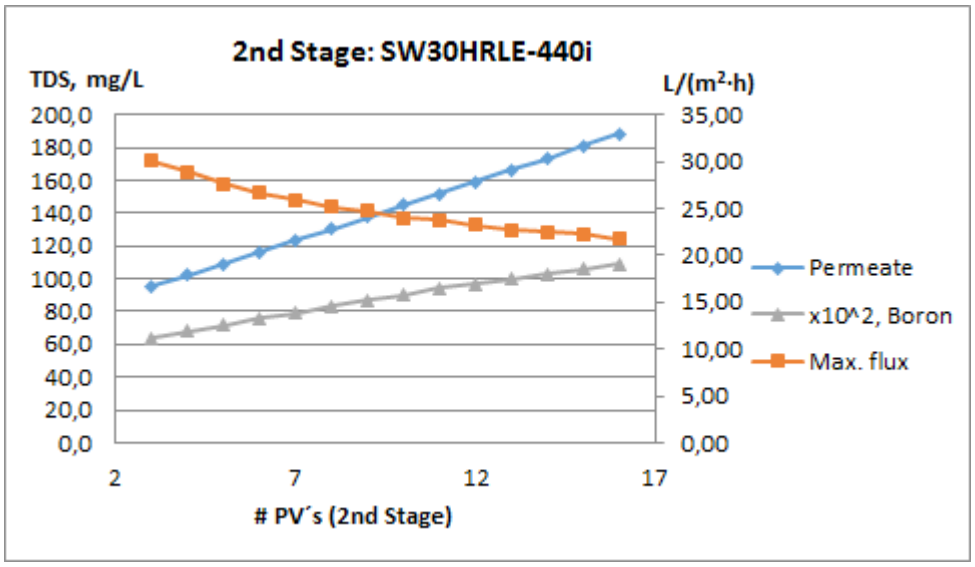


**Figure 5.5. Two-staged configuration with variable number of PV´s in the second stage – recovery, 45%; permeate flow, 45.77 $m^3$/h; SW30HRLE-440i -: Main parameters of the operating assessment: maximum flux, permeate TDS and boron TDS.**

Figure 5.6, shows the case of 10 PV´s in both, first and second stages, the evolution of flow rate, salt concentration and pressure have been obtained by using ROSA v9.1. Besides that, calculated flux, osmotic pressure and Net Driving Pressure are given.

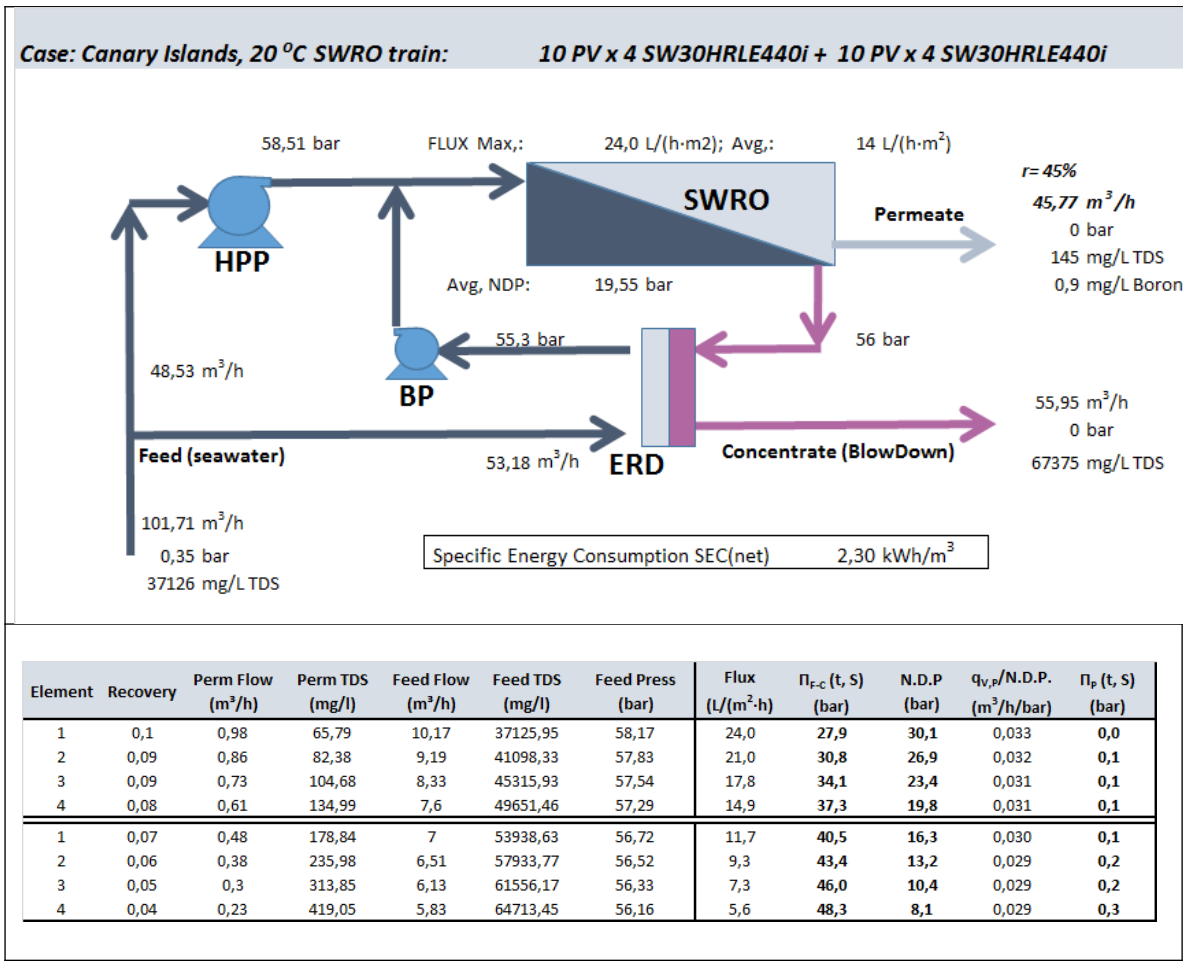


| Element | Recovery | Perm Flow ($m^3/h$) | Perm TDS (mg/l) | Feed Flow ($m^3/h$) | Feed TDS (mg/l) | Feed Press (bar) | Flux ($L/(m^2 \cdot h)$) | $\Pi_{F-C}$ (t, S) (bar) | N.D.P (bar) | $q_{v,P}$/N.D.P. ($m^3/h/bar$) | $\Pi_P$ (t, S) (bar) |
|---|---|---|---|---|---|---|---|---|---|---|---|
| 1 | 0,1 | 0,98 | 65,79 | 10,17 | 37125,95 | 58,17 | 24,0 | **27,9** | **30,1** | 0,033 | **0,0** |
| 2 | 0,09 | 0,86 | 82,38 | 9,19 | 41098,33 | 57,83 | 21,0 | **30,8** | **26,9** | 0,032 | **0,1** |
| 3 | 0,09 | 0,73 | 104,68 | 8,33 | 45315,93 | 57,54 | 17,8 | **34,1** | **23,4** | 0,031 | **0,1** |
| 4 | 0,08 | 0,61 | 134,99 | 7,6 | 49651,46 | 57,29 | 14,9 | **37,3** | **19,8** | 0,031 | **0,1** |
| 1 | 0,07 | 0,48 | 178,84 | 7 | 53938,63 | 56,72 | 11,7 | **40,5** | **16,3** | 0,030 | **0,1** |
| 2 | 0,06 | 0,38 | 235,98 | 6,51 | 57933,77 | 56,52 | 9,3 | **43,4** | **13,2** | 0,029 | **0,2** |
| 3 | 0,05 | 0,3 | 313,85 | 6,13 | 61556,17 | 56,33 | 7,3 | **46,0** | **10,4** | 0,029 | **0,2** |
| 4 | 0,04 | 0,23 | 419,05 | 5,83 | 64713,45 | 56,16 | 5,6 | **48,3** | **8,1** | 0,029 | **0,3** |

**Figure 5.6. Results of a two-staged configuration. Both stages: 10 PV´s with 4 SW30HRLE-440i elements each. Operating conditions: – recovery, 45%, permeate flow, 45.77 $m^3/h$ -).**

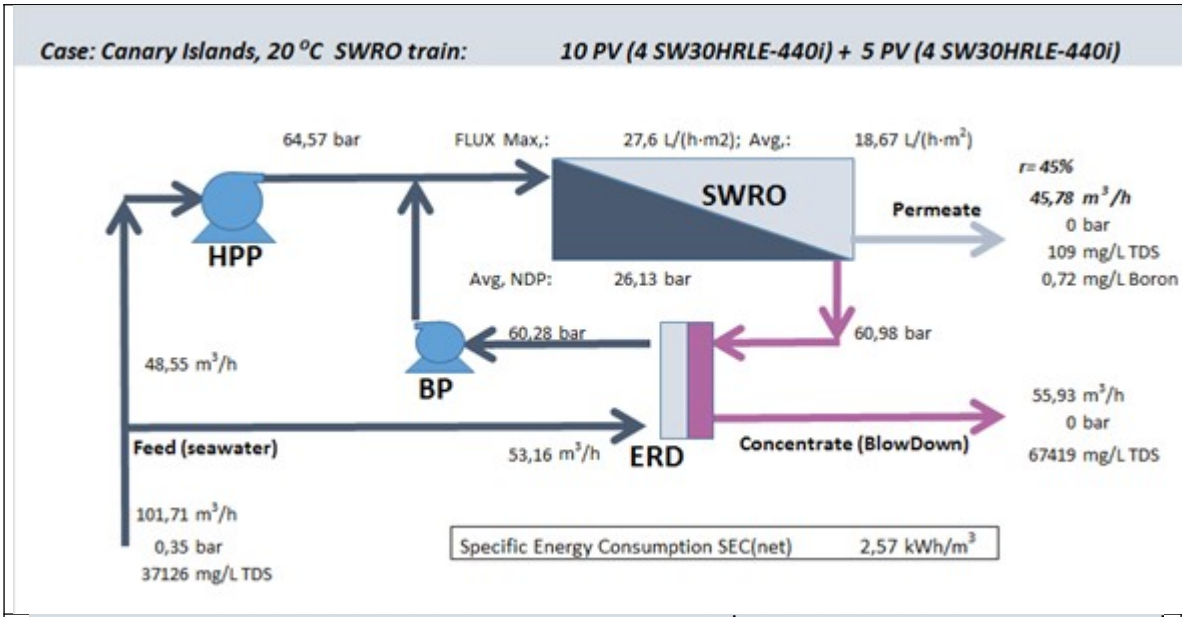


| Element | Recovery | Perm Flow ($m^3/h$) | Perm TDS (mg/l) | Feed Flow ($m^3/h$) | Feed TDS (mg/l) | Feed Press (bar) | Flux ($L/(m^2 \cdot h)$) | $\Pi_{f\text{-}c}$ (t, S) (bar) | N.D.P (bar) | $q_{v,p}$/N.D.P. ($m^3/h/bar$) | $\Pi_p$ (t, S) (bar) |
|---|---|---|---|---|---|---|---|---|---|---|---|
| 1 | 0,11 | 1,13 | 59 | 10,17 | 37126 | 64,2 | 27,6 | **26,5** | **37,7** | 0,030 | **0,0** |
| 2 | 0,11 | 0,98 | 75 | 9,04 | 41761 | 63,9 | 24,0 | **29,7** | **34,1** | 0,029 | **0,1** |
| 3 | 0,10 | 0,83 | 98 | 8,06 | 46832 | 63,6 | 20,3 | **33,3** | **30,3** | 0,027 | **0,1** |
| 4 | 0,09 | 0,68 | 130 | 7,23 | 52178 | 63,4 | 16,6 | **36,9** | **26,3** | 0,026 | **0,1** |
| 1 | 0,05 | 0,60 | 152 | 13,11 | 57558 | 62,8 | 14,7 | **40,5** | **22,2** | 0,027 | **0,1** |
| 2 | 0,04 | 0,51 | 182 | 12,51 | 60295 | 62,3 | 12,5 | **43,9** | **18,4** | 0,028 | **0,2** |
| 3 | 0,04 | 0,44 | 219 | 12,00 | 62874 | 61,9 | 10,8 | **46,8** | **15,1** | 0,029 | **0,3** |
| 4 | 0,03 | 0,37 | 265 | 11,56 | 65257 | 61,4 | 9,0 | **46,8** | **14,6** | 0,025 | **0,3** |

**Figure 5.7. Exemplary results of a two-staged configuration. First stage: 10 PV´s with 4 SW30HRLE-440i elements each. Second stage: 5 PV´s consisting in 4 30HRLE-440i. Operating conditions: – recovery, 45%, permeate flow, 45.77 $m^3/h$ -).**

Secondly, the possible advantages of using different membrane elements are assessed. Figures 5.8-5.11 show a representative set of results at constant recovery and permeate flow.

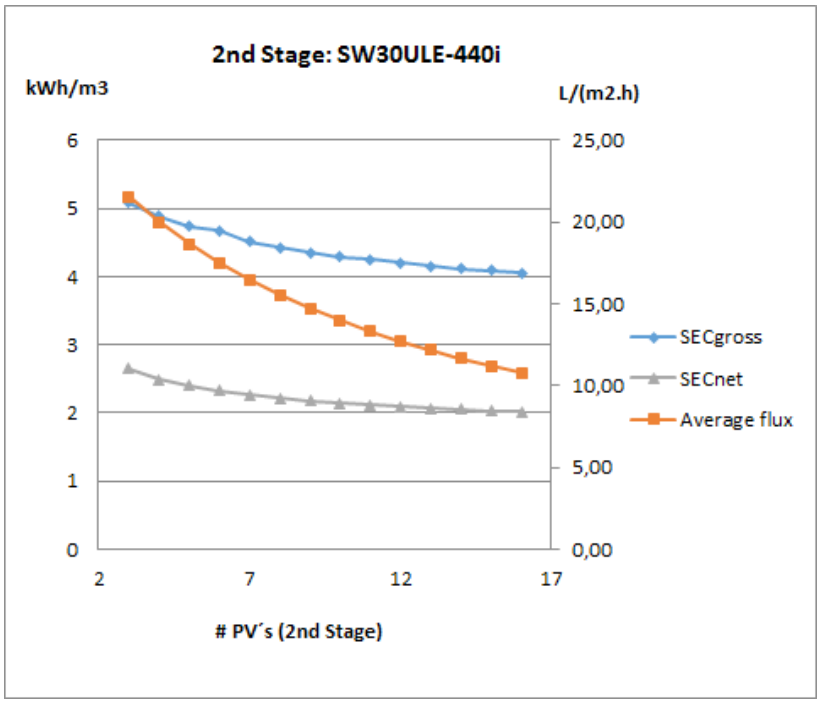


**Figure 5.8. Two-staged configuration (1st stage: 10 PV (4 HRLE-440i). 2nd stage: 4 ULE-440i) with variable number of PV´s in the second stage – recovery, 45%, permeate flow, 45.77 $m^3/h$ -: Main parameters of the economic assessment, namely, $SEC_{gross}$, $SEC_{net}$, average flux.**

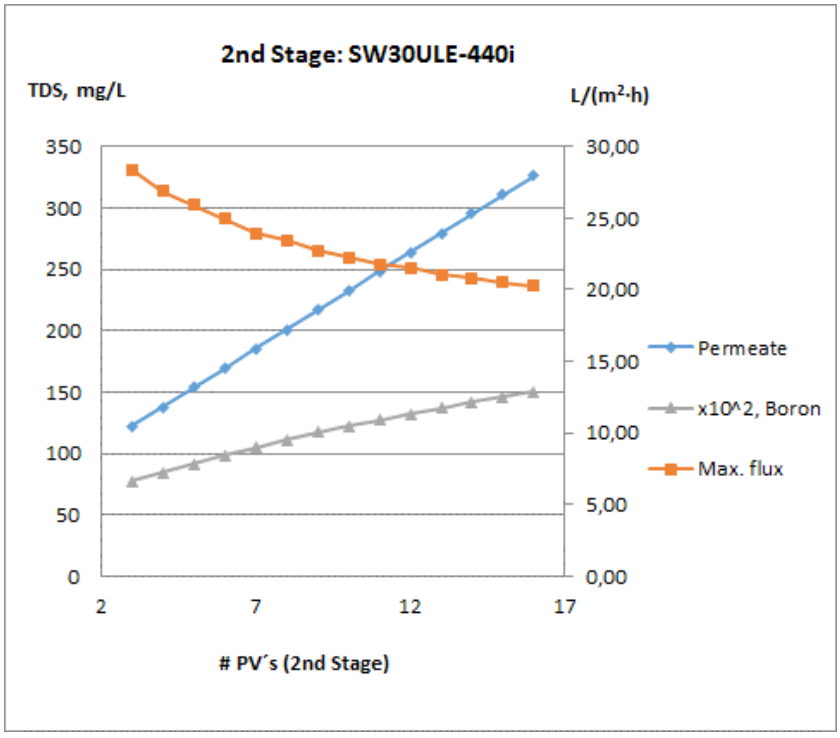


**Figure 5.9. Two-staged configuration (1st stage: 10 PV (4 HRLE-440i). 2nd stage: 4 ULE-440i) with variable number of PV´s in the second stage – recovery, 45%, permeate flow, 45.77 $m^3/h$ -: Main parameters of the operating assessment: maximum flux, permeate TDS, boron TDS.**

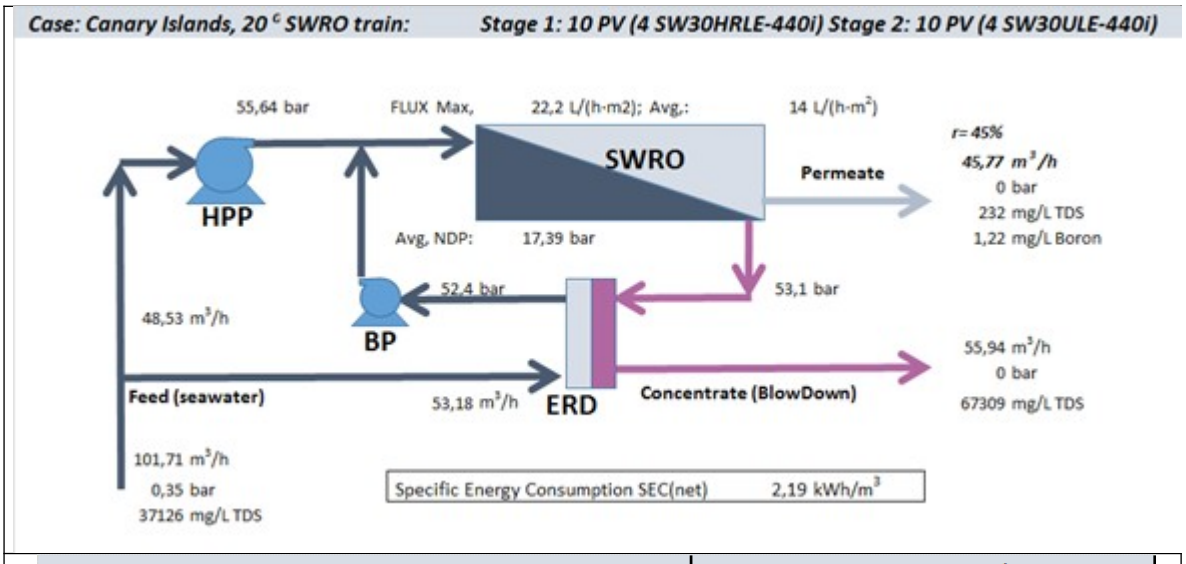


| Element | Recovery | Perm Flow ($m^3/h$) | Perm TDS (mg/l) | Feed Flow ($m^3/h$) | Feed TDS (mg/l) | Feed Press (bar) | Flux ($L/(m^2 \cdot h)$) | $\Pi_{F-C}$ (t, S) (bar) | N.D.P (bar) | $q_{V,P}$/N.D.P. ($m^3/h/bar$) | $\Pi_P$ (t, S) (bar) |
|---|---|---|---|---|---|---|---|---|---|---|---|
| 1 | 0,09 | 0,91 | 70 | 10,17 | 37126 | 55,3 | 22,2 | **27,8** | **27,4** | 0,033 | **0,0** |
| 2 | 0,09 | 0,79 | 87 | 9,26 | 40774 | 54,96 | 19,3 | **30,6** | **24,3** | 0,033 | **0,1** |
| 3 | 0,08 | 0,68 | 109 | 8,47 | 44590 | 54,67 | 16,6 | **33,4** | **21,3** | 0,032 | **0,1** |
| 4 | 0,07 | 0,57 | 139 | 7,79 | 48463 | 54,41 | 13,9 | **36,2** | **18,0** | 0,032 | **0,1** |
| 1 | 0,08 | 0,61 | 299 | 7,22 | 52259 | 53,83 | 14,9 | **39,4** | **14,6** | 0,042 | **0,2** |
| 2 | 0,07 | 0,45 | 426 | 6,61 | 57059 | 53,62 | 11,0 | **43,0** | **10,9** | 0,041 | **0,3** |
| 3 | 0,05 | 0,33 | 598 | 6,16 | 61201 | 53,43 | 8,1 | **45,8** | **8,0** | 0,041 | **0,4** |
| 4 | 0,04 | 0,23 | 878 | 5,83 | 64665 | 53,26 | 5,6 | **48,3** | **5,5** | 0,042 | **0,6** |

**Figure 5.10. Results of a two-staged configuration. First stage: 10 PV´s with 4 SW30HRLE-440i elements. Second stage: 10 PV´s with 4 SW30ULE-440i elements. Operating conditions: – recovery, 45%, permeate flow, 45.77 $m^3/h$ -).**

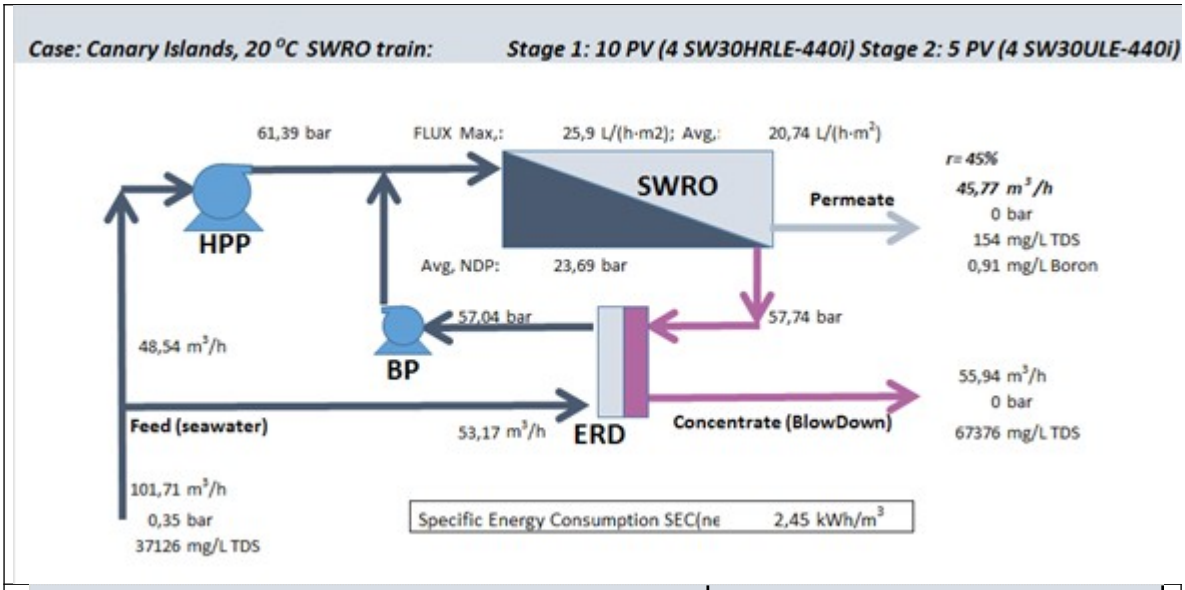


| Element | Recovery | Perm Flow ($m^3/h$) | Perm TDS (mg/l) | Feed Flow ($m^3/h$) | Feed TDS (mg/l) | Feed Press (bar) | Flux ($L/(m^2 \cdot h)$) | $\Pi_{F-C}$ (t, S) (bar) | N.D.P (bar) | $q_{V,P}$/N.D.P. ($m^3/h/bar$) | $\Pi_P$ (t, S) (bar) |
|---|---|---|---|---|---|---|---|---|---|---|---|
| 1 | 0,1 | 1,06 | 62 | 10,17 | 37126 | 61,05 | 25,9 | **27,9** | **33,0** | 0,032 | **0,0** |
| 2 | 0,1 | 0,92 | 79 | 9,12 | 41418 | 60,72 | 22,5 | **31,3** | **29,4** | 0,031 | **0,1** |
| 3 | 0,09 | 0,78 | 101 | 8,2 | 46041 | 60,43 | 19,1 | **34,7** | **25,7** | 0,030 | **0,1** |
| 4 | 0,09 | 0,64 | 132 | 7,42 | 50852 | 60,19 | 15,6 | **38,5** | **21,5** | 0,030 | **0,1** |
| 1 | 0,06 | 0,78 | 244 | 13,56 | 55651 | 59,62 | 19,1 | **41,6** | **17,9** | 0,044 | **0,2** |
| 2 | 0,05 | 0,64 | 308 | 12,77 | 59055 | 59,1 | 15,6 | **44,1** | **15,0** | 0,043 | **0,2** |
| 3 | 0,04 | 0,52 | 391 | 12,13 | 62177 | 58,62 | 12,7 | **46,3** | **12,4** | 0,042 | **0,3** |
| 4 | 0,04 | 0,42 | 499 | 11,61 | 64961 | 58,17 | 10,3 | **48,5** | **9,8** | 0,043 | **0,4** |

**Figure 5.11. Exemplary results of a two-staged configuration. First stage: 10 PV´s with 4 SW30HRLE-440i elements each. Second stage: 5 PV´s consisting in 4 30ULE-440i. Operating conditions: – recovery, 45%, permeate flow, 45.77 $m^3/h$ -).**

Finally, in order to compare a variety of different configurations at constant power consumption, pressure and flow of seawater input are hold constant. Results are depicted in figures 5.12-5.15.

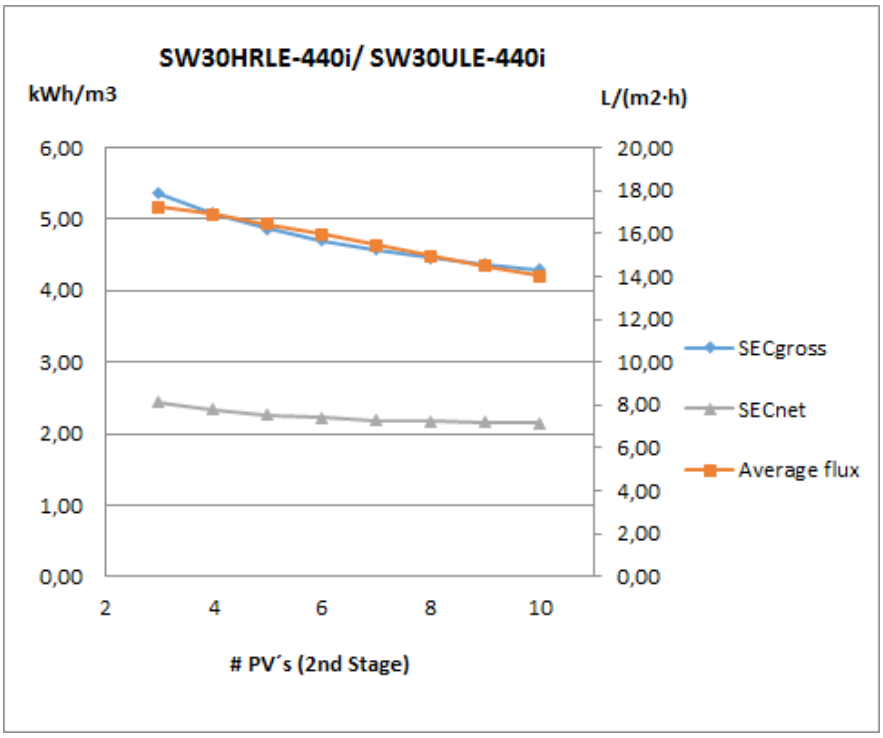


**Figure 5.12. Two-staged configuration (1st stage: 10 PV (4 HRLE-440i). 2nd stage: ULE-440i) with variable number of PV´s in the second stage – feed pressure, 55.64 bar, feed flow, 101.71 $m^3/h$ -: Main parameters of the economic assessment, namely, SECgross, SECnet, average flux.**

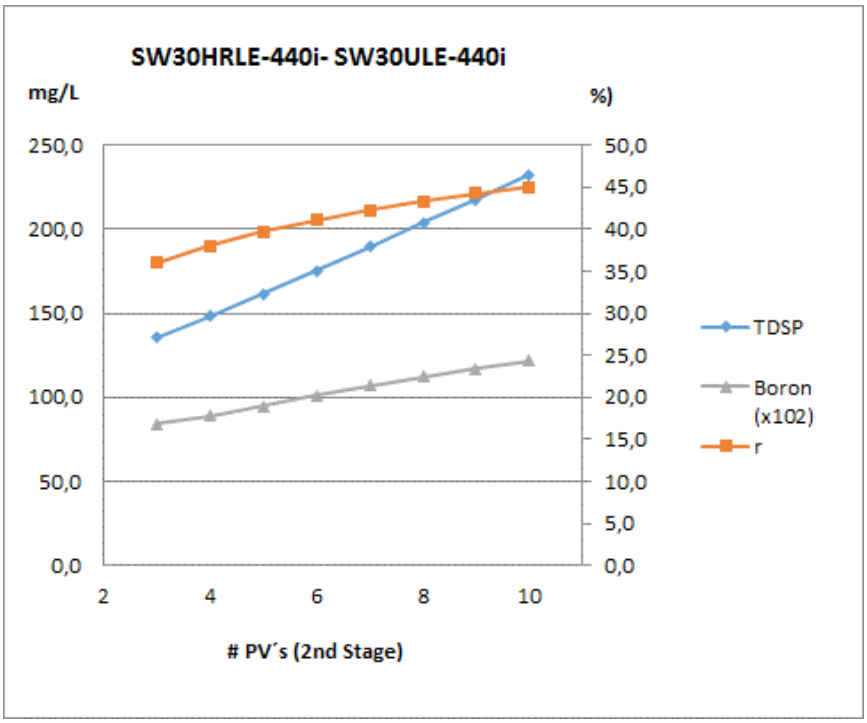


**Figure 5.13. Two-staged configuration (1st stage: 10 PV (4 HRLE-440i). 2nd stage: 4 ULE-440i) with variable number of PV´s in the second stage – feed pressure, 55.64 bar, feed flow, 101.71 $m^3/h$ -: Main parameters of the operating assessment: recovery, permeate TDS, boron TDS.**

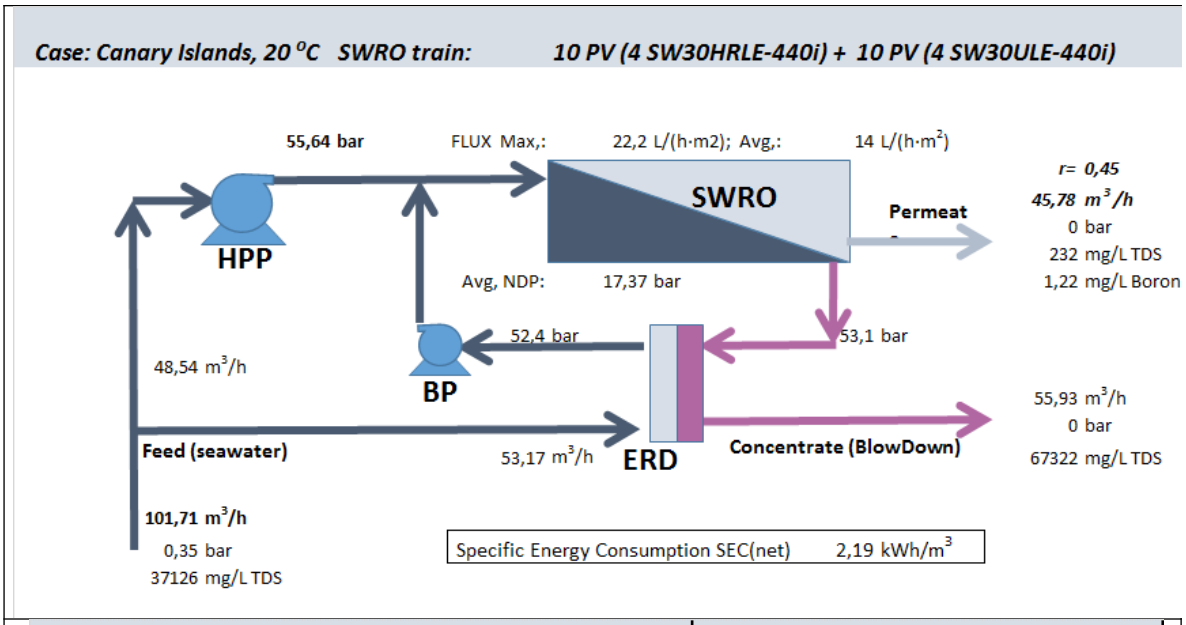


| Element | Recovery | Perm Flow ($m^3/h$) | Perm TDS (mg/l) | Feed Flow ($m^3/h$) | Feed TDS (mg/l) | Feed Press (bar) | Flux ($L/(m^2 \cdot h)$) | $\Pi_{f-c}$ (t, S) (bar) | N.D.P (bar) | $q_{v,p}$/N.D.P. ($m^3/h/bar$) | $\Pi_p$ (t, S) (bar) |
|---|---|---|---|---|---|---|---|---|---|---|---|
| 1 | 0,09 | 0,91 | 70 | 10,17 | 37126 | 55,3 | 22,2 | **27,8** | **27,4** | 0,033 | **0,0** |
| 2 | 0,09 | 0,79 | 87 | 9,26 | 40779 | 54,96 | 19,3 | **30,6** | **24,3** | 0,033 | **0,1** |
| 3 | 0,08 | 0,68 | 109 | 8,46 | 44601 | 54,67 | 16,6 | **33,4** | **21,2** | 0,032 | **0,1** |
| 4 | 0,07 | 0,57 | 139 | 7,78 | 48478 | 54,41 | 13,9 | **36,2** | **18,0** | 0,032 | **0,1** |
| 1 | 0,08 | 0,61 | 300 | 7,22 | 52276 | 53,83 | 14,9 | **39,4** | **14,5** | 0,042 | **0,2** |
| 2 | 0,07 | 0,45 | 427 | 6,61 | 57074 | 53,62 | 11,0 | **43,0** | **10,9** | 0,041 | **0,3** |
| 3 | 0,05 | 0,33 | 599 | 6,16 | 61214 | 53,43 | 8,1 | **45,8** | **8,0** | 0,041 | **0,4** |
| 4 | 0,04 | 0,23 | 878 | 5,82 | 64677 | 53,26 | 5,6 | **48,3** | **5,5** | 0,042 | **0,6** |

**Figure 5.14. Results of a two-staged configuration. First stage: 10 PV´s with 4 SW30HRLE-440i elements. Second stage: 10 PV´s with 4 SW30ULE-440i elements. Operating conditions: – feed flow, 101.71 $m^3/h$; feed pressure, 55.64 bar -).**

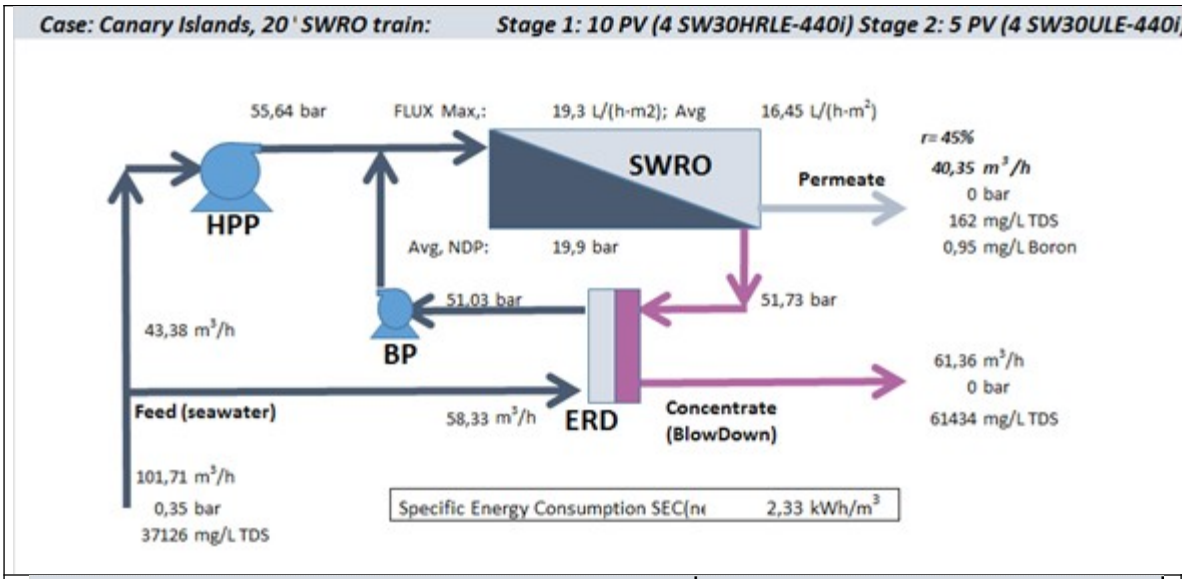


| Element | Recovery | Perm Flow ($m^3/h$) | Perm TDS (mg/l) | Feed Flow ($m^3/h$) | Feed TDS (mg/l) | Feed Press (bar) | Flux ($L/(m^2 \cdot h)$) | $\Pi_{F-C}$ (t, S) (bar) | N.D.P (bar) | $q_{v,P}$/N.D.P. ($m^3/h/bar$) | $\Pi_P$ (t, S) (bar) |
|---|---|---|---|---|---|---|---|---|---|---|---|
| 1 | 0,09 | 0,91 | 70 | 10,17 | 37126 | 55,3 | 22,2 | **27,8** | **27,4** | 0,033 | **0,0** |
| 2 | 0,09 | 0,79 | 87 | 9,26 | 40779 | 55,0 | 19,3 | **30,6** | **24,3** | 0,033 | **0,1** |
| 3 | 0,08 | 0,68 | 109 | 8,46 | 44601 | 54,7 | 16,6 | **33,4** | **21,2** | 0,032 | **0,1** |
| 4 | 0,07 | 0,57 | 139 | 7,78 | 48478 | 54,4 | 13,9 | **36,2** | **18,0** | 0,032 | **0,1** |
| 1 | 0,05 | 0,71 | 250 | 14,44 | 52276 | 53,8 | 17,4 | **38,7** | **15,0** | 0,047 | **0,2** |
| 2 | 0,04 | 0,59 | 310 | 13,73 | 54950 | 53,3 | 14,4 | **40,6** | **12,6** | 0,047 | **0,2** |
| 3 | 0,04 | 0,48 | 387 | 13,14 | 57386 | 52,7 | 11,7 | **42,5** | **10,2** | 0,047 | **0,3** |
| 4 | 0,03 | 0,39 | 486 | 12,66 | 59552 | 52,2 | 9,5 | **44,0** | **8,3** | 0,047 | **0,3** |

**Figure 5.15. Exemplary results of a two-staged configuration. First stage: 10 PV´s with 4 SW30HRLE-440i elements each. Second stage: 5 PV´s consisting in 4 SW30ULE-440i. Operating conditions: – feed flow, 101.71 $m^3/h$; feed pressure, 55.64 bar -).**

Besides, configurations with different number of membrane elements are compared by means of tables 5.3 and 5.4. They show the effect on $SEC_{net}$ of the number of PV´s installed in the second stage.

**Table 5.3. Comparison of several configurations with variable number of PV´s in the second stage and 10 PV ´s in the first stage. Membrane elements: SW30HRLE-440i in the first stage and SW30ULE-440i in the second stage. Results obtained at feed pressure of 55.64 bar with 101.7 $m^3/h$ of permeate flow.**

| $p_F$, bar= 55,64 | | $q_{V,F}$, $m^3/h$= | 101,71 | 10 PV´s in the 1st. stage | | | Area= | 40,9 $m^2$ | | | |
|---|---|---|---|---|---|---|---|---|---|---|---|
| # PV´s ($2^{nd}$ stage) | $SEC_{gross}$ kWh/$m^3$ | Pw kW | Average flux L/($m^2$·h) | Max. $q_{V,P}$ $m^3/h$ | $TDS_P$ mg/L | Boron (x$10^2$) mg/L | r % | $q_{V,P}$ $m^3/h$ | $q_{V,BD}$ $m^3/h$ | $p_{BD}$ bar | PW (ERI·PX) kW | P |
| **3** | 5,36 | 196 | 17,24 | 0,91 | 135,6 | 84 | 36,0 | 36,64 | 65,07 | 49,3 | **-106,4** | 8 |
| **4** | 5,08 | 197 | 16,89 | 0,91 | 148,4 | 89 | 38,0 | 38,67 | 63,04 | 50,9 | **-106,3** | 9 |
| **5** | 4,87 | 197 | 16,45 | 0,91 | 161,7 | 95 | 39,7 | 40,35 | 61,36 | 51,7 | **-105,2** | 9 |
| **6** | 4,70 | 197 | 15,97 | 0,91 | 175,4 | 101 | 41,1 | 41,78 | 59,93 | 52,2 | **-103,8** | 9 |
| **7** | 4,57 | 197 | 15,46 | 0,91 | 189,4 | 107 | 42,3 | 42,99 | 58,72 | 52,6 | **-102,3** | 9 |
| **8** | 4,46 | 197 | 14,96 | 0,91 | 203,6 | 112 | 43,3 | 44,03 | 57,68 | 52,8 | **-100,9** | 9 |
| **9** | 4,37 | 197 | 14,49 | 0,91 | 217,7 | 117 | 44,3 | 45,01 | 56,70 | 53,0 | **-99,5** | 9 |
| **10** | 4,29 | 197 | 14,00 | 0,91 | 232,3 | 122 | 45,0 | 45,78 | 55,93 | 53,1 | **-98,4** | 9 |

**Table 5.4. Comparison of several configurations with variable number of PV´s in the second stage and 10 PV ´s in the first stage. Membrane elements: SW30HRLE-440i in the first stage and SW30ULE-440i in the second stage. Results obtained at recovery rate of 45% and 45.77 $m^3/h$ of permeate flow.**

| 4 SW30HRLE-440i + 2nd stage: 4 SW30ULE-440i | | | | | | | | | | | |
|---|---|---|---|---|---|---|---|---|---|---|---|
| r, %= 45 | | $q_{V,P}$, $m^3/h$= | | 45,77 | 10 PV´s in the 1st. stage | | Area= | | 40,9 $m^2$ | | |
| # PV´s ($2^{nd}$ stage) | $SEC_{gross}$ kWh/$m^3$ | Pw kW | Average flux L/($m^2$·h) | Max. $q_{V,P}$ $m^3/h$ | $TDS_P$ mg/L | Boron (x$10^2$) mg/L | $q_{V,BD}$ $m^3/h$ | $p_{BD}$ bar | PW (ERI-PX) kW | $PW_{net}$ kW | S kW |
| **3** | 5,09 | 233 | 21,53 | 1,16 | 122,3 | 77 | 55,94 | 60,5 | **-112,1** | **121,1** | |
| **4** | 4,89 | 223 | 19,99 | 1,10 | 137,9 | 84 | 55,94 | 59,1 | **-109,5** | **113,9** | |
| **5** | 4,74 | 217 | 18,66 | 1,06 | 153,5 | 91 | 55,94 | 57,7 | **-107,0** | **109,9** | |
| **6** | 4,67 | 211 | 17,50 | 1,02 | 169,3 | 98 | 55,94 | 56,6 | **-104,8** | **106,4** | |
| **7** | 4,51 | 207 | 16,46 | 0,98 | 185,1 | 105 | 55,95 | 55,5 | **-102,9** | **103,7** | |
| **8** | 4,43 | 203 | 15,55 | 0,96 | 200,8 | 111 | 55,94 | 54,6 | **-101,2** | **101,5** | |
| **9** | 4,35 | 199 | 14,73 | 0,93 | 216,5 | 117 | 55,95 | 53,8 | **-99,7** | **99,6** | |
| **10** | 4,29 | 197 | 14,00 | 0,91 | 232,3 | 122 | 55,94 | 53,1 | **-98,4** | **98,1** | |
| **11** | 4,25 | 194 | 13,33 | 0,89 | 248,06 | 127 | 55,94 | 52,6 | **-97,4** | **96,9** | |
| **12** | 4,2 | 192 | 12,72 | 0,88 | 263,77 | 132 | 55,94 | 52,0 | **-96,4** | **95,7** | |
| **13** | 4,16 | 190 | 12,17 | 0,86 | 279,45 | 137 | 55,94 | 51,5 | **-95,5** | **94,7** | |
| **14** | 4,12 | 189 | 11,66 | 0,85 | 295,11 | 142 | 55,94 | 51,1 | **-94,7** | **93,8** | |
| **15** | 4,09 | 187 | 11,20 | 0,84 | 310,73 | 146 | 55,94 | 50,7 | **-94,0** | **93,0** | |
| **16** | 4,06 | 186 | 10,77 | 0,83 | 326,33 | 150 | 55,94 | 50,4 | **-93,4** | **92,3** | |

In order to compare Veolia´s configuration with the conventional one, the recovery is set to 45% for both configurations (table 5.4):

- Increasing the second stage flux per PV by reducing the number of the second stage PV´s does not improve production of the second stage, all the contrary, the membrane surface of the second stage is reduced and the permeate production is also reduced.
- Therefore, when reducing PV´s in the second stage of Veolia´s configuration the feed pressure needs to be increased in order to maintain the total permeate production and the recovery. This increase in feed pressure represents an increase in the energy consumption of the order of 20% (from 2,26 kWh/$m^3$ up to 2,7 kWh/$m^3$). It also represents an increase in the flux per membrane of the first stage (increasing the maximum flux, from 22 to 30 L/($m^2$·h) in the first membrane of the first stage and the average flux of the system from 14 to 22 L/($m^2$·h).

When operating Veolia´s configuration with variable number of PV´s in the second stage but with constant feed pressure and flow, the recovery ratio increases when increasing the number of PV´s in the second stage, from 40% recovery for 5 PVs to up to 45% for 10 PVs (Table 5.3). As a consequence, the effect on the energy consumption is the opposite, that is, reducing from 2,26 kwh/$m^3$ for 5 PVs to 2,14 kwh/$m^3$.

Besides that, permeate quality goes down as the SEC decreases as a result of increasing the number of PV´s in the second stage.

Qualitative results are consistent with the well-known behaviour of RO process, as chapter 3 reported for conventional configurations. To sum up, greater membrane area leads to lower SECnet along with lower permeate quality. Thus, selection of design parameters should balance CAPEX and OPEX, case by case. On the contrary, lower SECnet results in lower maximum flux. As a consequence, the adoption of Veolia configuration with greater number of PV´s in the second stage than in the first one avoids excesive flux in the first membrane element.

Based on results obtained, to study other plan locations is not required to draw general conclusions on Veolia´s configurations, so it is out of the aim of this study.

# 4. CONFIGURATION PATENTED BY GENERAL ELECTRICS IN 2013

General Electric (GE) configuration [Viera Curbelo, 2013] was conceptually described in chapter 3 as a two-stage configuration with no Booster Pump (BP) in which part of the feed flow bypasses the first stage. Figures 5.16 and 5.17 are compatible with patent application description.

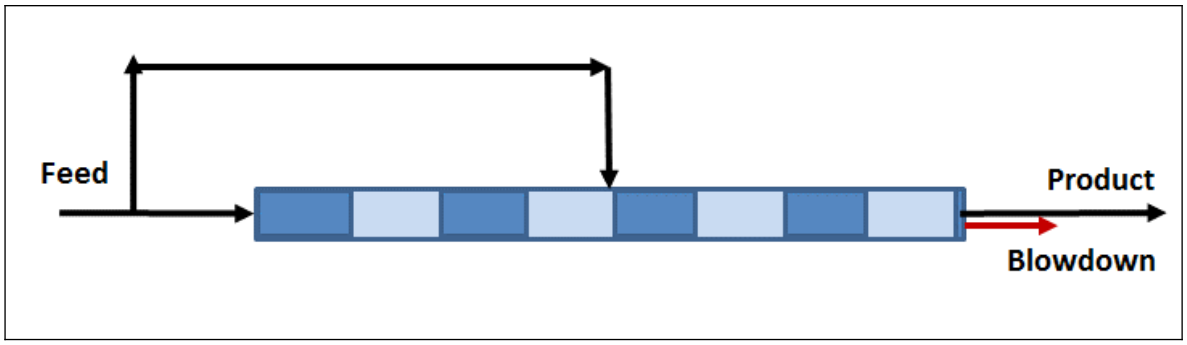


**Figure 5.16. GE configuration adapted from Viera-Curbelo (2013).**

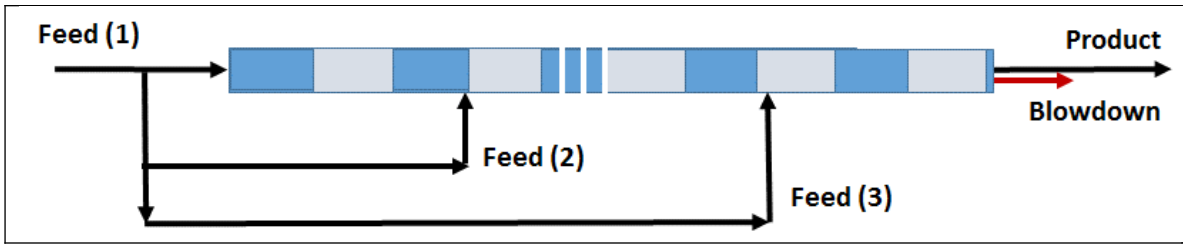


**Figure 5.17. Second configuration compatible with description reported by Viera-Curbelo (2013).**

In Figure 5.18 the feed and osmotic pressures through the PV are depicted. In the conventional configuration, as feed water goes through the PV producing permeate, the salinity of the feed flow increases thus the osmotic pressure increases proportionally. In GE´s configuration, adding seawater somewhere along the PV will reduce the salinity of the feed flow at that point. As a consequence, the osmotic pressure is also reduced at that point. As figure 5.18 proves, the tail of GE´s configuration can reach the same blowdown concentration with less membrane area requirement since the average NDP is higher than that in conventional configurations.

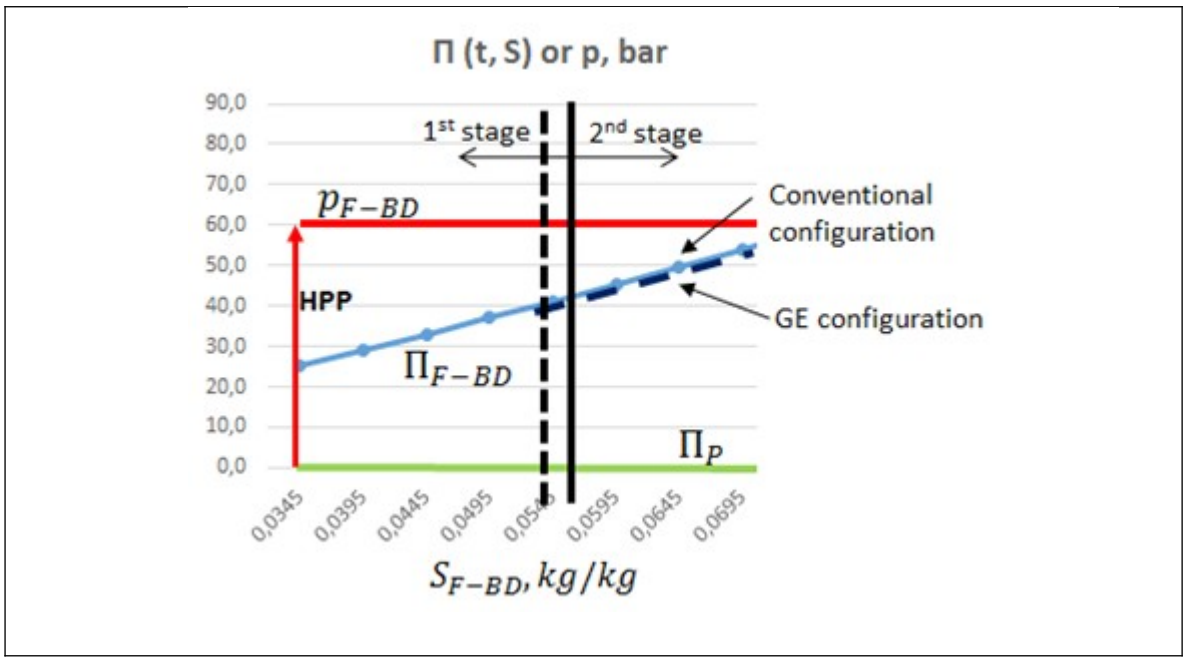


**Figure 5.18. Conceptual effect of GE configuration.**

Next table present an example of 1 PV with 10.17 $m^3/h$ of total feed flow with 4 $m^3/h$ of bypass flow. Recovery rate of 0.43 and product quality of 156 mg/L are obtained. The evolution of feed TDS shows the working conditions described in figure 5.18.

**Table 5.6. Results of a two-staged configuration with bypass (see Figure 5.18).**

| Stage 1 | Element | Recovery | Perm Flow ($m^3/h$) | Perm TDS (mg/l) | Feed Flow ($m^3/h$) | Feed TDS (mg/l) | Feed Press (bar) |
|---|---|---|---|---|---|---|---|
| | 1 | 0,15 | 0,91 | 75,26 | 6,17 | 37125,95 | 58,17 |
| | 2 | 0,14 | 0,72 | 107,98 | 5,26 | 43550,1 | 58,01 |
| | 3 | 0,12 | 0,54 | 160,26 | 4,54 | 50438,65 | 57,88 |
| | 4 | 0,1 | 0,38 | 244,45 | 4,00 | 57191,96 | 57,77 |
| **Stage 2** | **Element** | **Recovery** | **Perm Flow ($m^3/h$)** | **Perm TDS (mg/l)** | **Feed Flow ($m^3/h$)** | **Feed TDS (mg/l)** | **Feed Press (bar)** |
| | 1 | 0,08 | 0,61 | 133,54 | 7,62 | 49507,91 | 57,34 |
| | 2 | 0,07 | 0,5 | 174,54 | 7,01 | 53810,63 | 57,11 |
| | 3 | 0,06 | 0,39 | 230,61 | 6,51 | 57894,95 | 56,91 |
| | 4 | 0,05 | 0,31 | 307,2 | 6,12 | 61610,45 | 56,72 |

Therefore, this patent allows for both an increase of flow and a reduction of average feed concentration in the tail (second stage) in comparison to the conventional RO configuration, thus

in principle improving the working conditions of the tail membranes.

Increasing flow in the tail has in principle two advantages:

- The flow velocity also increases thus reducing the potential scaling since concentration polarisation decreases.
- Larger flow may allow for larger permeate production, attributable to the effect of concentration polarisation reduction if this effect is greater than the increase of pressure losses.

Reducing concentration in the tail has also in principle three advantages:

- The net driving pressure is increased thus permeate production is larger.
- The permeate quality increases due to the higher water passage.
- Less feed-blowdown average concentration also leads to reducing the potential scaling.

To sum up, in comparison to the conventional RO configuration, GE´s configuration may increase: i) Permeate production due to both, an increase of flow and a reduction of feed average concentration in the membranes of the tail, and ii) Permeate quality due to the increase of net driving pressure in the second stage. It also improves the behavior regarding potential scaling of the membranes due to both an increase of flow and a reduction of feed concentration in the tail of the pressure vessel (second stage).

However, the salinity of the brine outlet for a given recovery rate of the desalination process is the same. Besides, pressure losses may increase in comparison to conventional configuration. Moreover, considering a given permeate flow and recovery rate, increasing the flow in the tail of the pressure vessel requires similar decrease of feed flow in the front (first stage). Therefore, the higher permeate production of the tail should balance the lower permeate production in the front. Otherwise, if recovery rate increases the specific energy consumption would increase in comparison to conventional configuration.

Finally, this configuration has certain complexity when compared with the conventional RO configuration since requires more high pressure piping, connectors somewhere in the middle of the vessels, additional valves and space in the rack. All this additional complexity represents more CAPEX. Therefore, is not likely that the advantages of this configuration of less potential scaling and better permeate quality will justify the increase of CAPEX.

After this preliminary analysis, an assessment similar to that reported in section 3 is conducted. Next tables report on analysed performed on various cases with 10 PV´s in the first

and second stages and a bypass flow ranged between 0 $m^3/h$ and 40 $m^3/h$ split from a feed flow of 101.7 $m^3/h$. The case of bypass 0 $m^3/h$ corresponds to the conventional RO configuration with a single feed inlet in the front side. In table 5.6-5.8, white columns were obtained from ROSA software and those marked in blue show results of calculations performed from ROSA, namely, power saving attributable to ERI-PX energy recovery devices; net power consumption, $PW_{net}$; net specific energy consumption, $SEC_{net}$, and maximum flux. Configurations analysed in the respective tables are as follows:

- Table 5.7: 1st stage: 10 PV´s with 4 SW30HRLE-440i elements; 2nd stage: 10 PV´s with 4 SW30HRLE-440i elements. In this case, the second feed flow input is placed in the middle of the PV´s. Second feed flow ranges from 10 $m^3/h$ to 40 $m^3/h$.
- Table 5.8: 1st stage: 10 PV´s with 2 SW30HRLE-440i elements; 2nd stage: 10 PV´s with 6 SW30HRLE-440i elements. This case allows the comparative analysis concerning the position of the second feed-input. Similar range of the bypass flow of the previous case is analysed.
- Table 5.9: 1st stage: 10 PV´s with 2 SW30ULE-440i elements; 2nd stage: 10 PV´s with 6 SW30ULE-440i elements. This case allows the comparative analysis concerning the membrane element selected. The range of the bypass flow was expanded up to 60 $m^3/h$.

**Table 5.7. Results of a two-staged configuration. Both stages: 10 PV´s with 4 SW30HRLE-440i elements each. Operating conditions: feed pressure, 58.51 bar; permeate flow, 101.71 $m^3/h$.**

| 4 SW30HRLE-440i + 2nd stage: 4 SW3HRLE-440i | | | | | | | | | | | | | | |
|---|---|---|---|---|---|---|---|---|---|---|---|---|---|---|
| $p_F$, bar= 58,51 | | $q_{V,F}$, $m^3/h$ 101,71 | | | 10 PV´s in the 1st. st | | | Area= | 40,9 $m^2$ | | | | | |
| Bypass $m^3/h$ | SEC $kWh/m^3$ | Pw kW | Avg. flux $L/(m^2 \cdot h$ | Max. $q_{V,P}$ $m^3/h$ | Boron $TDS_P$ mg/L | Boron ($x10^2$) mg/L | r % | $q_{V,P}$ $m^3/h$ | $q_{V,BD}$ $m^3/h$ | $p_{BD}$ bar | (ERI-PX) kW | $PW_{net}$ kW | $SEC_{net}$ $kWh/m^3$ | Max. flux $L/(m^2 \cdot h$ |
| **0** | **4,52** | **206,7** | **14** | **0,98** | **145** | **90** | **45** | **45,8** | **56,0** | **57,1** | **-105,8** | **100,9** | **2,21** | **23,96** |
| **10** | 4,55 | 206,7 | 13,89 | 0,97 | 146,6 | 92 | 44,7 | 45,4 | 56,3 | 56,2 | **-104,7** | **101,9** | **2,24** | **23,72** |
| **20** | 4,60 | 206,7 | 13,75 | 0,96 | 149,0 | 93 | 44,2 | 45,0 | 56,7 | 56,3 | **-105,9** | **100,8** | **2,24** | **23,47** |
| **30** | 4,65 | 206,7 | 13,57 | 0,94 | 150,6 | 71 | 43,6 | 44,4 | 57,3 | 56,4 | **-107,2** | **99,5** | **2,24** | **22,98** |
| **40** | 4,74 | 206,7 | 13,33 | 0,91 | 155,8 | 97 | 42,9 | 43,6 | 58,1 | 56,6 | **-108,9** | **97,8** | **2,24** | **22,25** |

**Table 5.8. Results of a two-staged configuration: 10 PV´s with 2 SW30HRLE-440i elements + 10 PV´s with 6 SW30HRLE-440i elements. Operating conditions: feed pressure, 58.51 bar; permeate flow, 101.71 $m^3/h$.**

| 2 SW30HRLE-440i + 2nd stage: 6 SW3HRLE-440i | | | | | | | | | | | | | | |
|---|---|---|---|---|---|---|---|---|---|---|---|---|---|---|
| $p_F$, bar= 58,51 | | $q_{V,F}$, $m^3/h$ | 101,71 | | 10 PV´s in the 1st. st | | | Area= | 40,9 $m^2$ | | | | | |
| Bypass | SEC | Pw | Avg. flux | Max. $q_{V,P}$ | Boron $TDS_P$ | Boron ($x10^2$) | r | $q_{V,P}$ | $q_{V,BD}$ | $p_{BD}$ | (ERI-PX) | $PW_{net}$ | $SEC_{net}$ | Max. flu |
| $m^3/h$ | $kWh/m^3$ | kW | ) | $m^3/h$ | mg/L | mg/L | % | $m^3/h$ | $m^3/h$ | bar | kW | kW | $kWh/m^3$ | $L/(m^2 \cdot h$ |
| **0** | **4,52** | **206,7** | **14** | **0,98** | **145** | **90** | **45** | **45,8** | **56,0** | **57,1** | **-105,8** | **100,9** | **2,21** | **23,96** |
| **10** | 4,53 | 206,7 | 13,96 | 0,97 | 145,2 | 91 | 44,9 | 45,7 | 56,1 | 56,1 | **-104,2** | **102,5** | **2,25** | **23,72** |
| **20** | 4,54 | 206,7 | 13,93 | 0,96 | 145,9 | 91 | 44,8 | 45,6 | 56,2 | 56,2 | **-104,5** | **102,2** | **2,24** | **23,47** |
| **30** | 4,55 | 206,7 | 13,88 | 0,94 | 146,7 | 91 | 44,6 | 45,4 | 56,3 | 56,2 | **-104,9** | **101,8** | **2,24** | **22,98** |
| **40** | 4,57 | 206,7 | 13,82 | 0,91 | 145,9 | 91 | 44,4 | 45,2 | 56,5 | 56,3 | **-105,4** | **101,2** | **2,24** | **22,25** |

**Table 5.9. Results of a two-staged configuration: 10 PV´s with 2 SW30ULE-440i elements + 10 PV´s with 6 SW30ULE-440i elements. Operating conditions: feed pressure, 53.22 bar; permeate flow, 101.71 $m^3/h$.**

| 2 SW30ULE-440i + 2nd stage: 6 SW3ULE-440i | | | | | | | | | | | | | | |
|---|---|---|---|---|---|---|---|---|---|---|---|---|---|---|
| $p_F$, bar= 53,22 | | $q_{V,F}$, $m^3/h$ | 101,71 | | 10 PV´s in the 1st. s | | | Area= | 40,9 $m^2$ | | | | | |
| Bypass | SEC | Pw | Avg. flux | Max. $q_{V,P}$ | Boron $TDS_P$ | Boron ($x10^2$) | r | $q_{V,P}$ | $q_{V,BD}$ | $p_{BD}$ | (ERI-PX) | $PW_{net}$ | $SEC_{net}$ | Max. flux |
| $m^3/h$ | $kWh/m^3$ | kW | ) | $m^3/h$ | mg/L | mg/L | % | $m^3/h$ | $m^3/h$ | bar | kW | kW | $kWh/m^3$ | $L/(m^2 \cdot h$ |
| **0** | **4,11** | **188,0** | **14** | **1,18** | **311** | **151** | **45** | **45,8** | **55,9** | **51,1** | **-94,8** | **93,2** | **2,04** | **28,85** |
| **10** | 4,14 | **188,0** | 13,88 | 1,15 | 310,0 | 97 | 44,6 | 45,4 | 56,3 | 50,9 | **-95,0** | **93,0** | **2,05** | **28,12** |
| **20** | 4,15 | **188,0** | 13,84 | 1,13 | 311,5 | 98 | 44,5 | 45,3 | 56,5 | 50,9 | **-95,3** | **92,7** | **2,05** | **27,63** |
| **30** | 4,17 | **188,0** | 13,79 | 1,09 | 316,5 | 155 | 44,3 | 45,1 | 56,6 | 51,0 | **-95,7** | **92,3** | **2,05** | **26,65** |
| **40** | 4,19 | **188,0** | 13,73 | 1,05 | 315,5 | 101 | 44,1 | 44,9 | 56,8 | 51,1 | **-96,2** | **91,8** | **2,05** | **25,67** |
| **50** | 4,22 | **188,0** | 13,64 | 1,00 | 318,5 | 102 | 43,8 | 44,6 | 57,1 | 51,1 | **-96,8** | **91,2** | **2,05** | **24,45** |
| **60** | 4,25 | **188,0** | 13,51 | 0,93 | 322,3 | 103 | 43,4 | 44,2 | 57,5 | 51,2 | **-97,5** | **90,5** | **2,05** | **22,74** |

Results given in table 5.7 and 5.8 show that the proposed bypass slightly increases the $SEC_{net}$. Similar results were obtained for the two analysed positions of the second feed input. Besides that, the maximum flux (first membrane element) slightly decreases, thus lowering the fouling risk. Permeate quality is similar for all values of bypass flow analysed. The extra costs of implementing such configurations is not recommended due to the low influence on SEC and operating conditions. In addition, table 5.9 presents results with membrane modules of greater water permeability (ULE) and the second feed input between second and third positions of the PV´s. The $SEC_{net}$ is lower than for HRLE membranes but is similar for all bypass flows while the reduction of the maximum flux is greater. GE´s configuration with high bypass flow could be recommended in order to operate with the highest permeability elements (ULE) with an effective way of avoiding excessive fouling risk in the first membrane elements of the PV.

A complementary analysis is carried out in order to assess the usefulness of this patented configuration to develop extra-long PVs. To this end, table 5.10 gives results obtained by using

different design strategies based on including a third feed input. Thus, a three stage configuration is implemented within a single PV with 10-13 membrane elements. In table 5.10:

- The two first rows of corresponds to 10 PV´s consisting in 12 membrane elements, 3-6-3 SW30ULE-440i. A first trail (first row) with feed total flow of 101.7 $m^3/h$ was analysed. This resulted in too low average flux. Consequently, the following trails were performed with greater feed flow. Then, a total feed flow of 131.7 $m^3/h$ is set. In both rows feed flow is split by using a second and a third feed inlets with 10 $m^3/h$ and 20 $m^3/h$, respectively.
- The three following rows corresponds to 10 PV´s consisting eacch in 12, 11 and 10 SW30ULE-440i elements respectively. The three stages implemented are 2-7-3, 2-7-2 and 2-7-1, respectively. The total feed flow of 131.7 $m^3/h$ is split with 20 $m^3/h$ in the second feed inlet and 10 $m^3/h$ in the last one.
- Finally, in order to decrease the maximum flux, two membrane elements with lower water permeability are place in the front positions. Then, the three stages are composed by 2 SW30HRLE-440i + 7 SW30ULE-440i + 1 SW30ULE-440i. Total feed flow of 131.7 $m^3/h$ and bypass of 25 $m^3/h$ and 5 $m^3/h$ were considered.

**Table 5.10. Results of a three-staged configuration: 10 PV´s with 2 SW30HRLE-440i elements + 10 PV´s with 6 SW30HRLE-440i elements. Operating conditions: feed pressure, 53.22 bar. Feed flow: 101.71 $m^3/h$ for the first row and 131.71 $m^3/h$ in the rest.**

| 3 SW30ULE-440i + 2nd stage: 6 SW30ULE-440i + 3rd stage: 3, 2 or 1 SW30ULE | | | | | | | | | | | | | | | |
|---|---|---|---|---|---|---|---|---|---|---|---|---|---|---|---|
| $p_F$, bar= 53,22 | | $q_{V,F}$, $m^3/h$ 101,71 | | | 10 PV´s in the 1st. stag | | | Area= 40,9 $m^2$ | | | | | | | |
| Bypass $m^3/h$ | SEC $kWh/m^3$ | Pw kW | Avg. flux ) | Max. $q_{V,P}$ $m^3/h$ | $TDS_P$ mg/L | Boron ($x10^2$) mg/L | r % | $q_{V,P}$ $m^3/h$ | $q_{V,BD}$ $m^3/h$ | $p_{BD}$ bar | (ERI-PX) kW | $PW_{net}$ kW | $SEC_{net}$ $kWh/m^3$ | Max. flux $L/(m^2 \cdot h)$ | Elements per stage |
| **10+20** | **4,40** | **188,0** | **8,7** | **1,09** | **532** | **188** | **42** | **42,7** | **59,0** | **50,4** | **-98,6** | **89,4** | **2,1** | **26,7** | (3-6-3) ULE |
| **10+20** | 4,45 | **243,4** | 11,2 | 1,18 | 398,3 | 160 | 41,5 | 54,7 | 76,3 | 49,3 | **-124,7** | **118,7** | **2,2** | **28,9** | (3-6-3) ULE |
| **20+10** | 4,23 | **243,4** | 11,7 | 1,18 | 374,1 | 153 | 43,7 | 57,5 | 74,2 | 49,1 | **-120,6** | **122,8** | **2,1** | **28,9** | (2-7-3) ULE |
| **20+10** | 4,32 | **243,4** | 12,6 | 1,18 | 347,2 | 151 | 42,8 | 56,4 | 75,3 | 49,3 | **-123,0** | **120,4** | **2,1** | **28,9** | (2-7-2) ULE |
| **20+10** | 4,43 | **243,4** | 13,5 | 1,18 | 321,2 | 149 | 41,8 | 55,0 | 76,7 | 49,5 | **-125,9** | **117,5** | **2,1** | **28,9** | (2-7-1) ULE |
| **25+5** | 4,35 | **243,4** | 13,7 | 0,85 | 278,2 | 141 | 42,4 | 55,9 | 75,7 | 49,3 | **-123,7** | **119,8** | **2,1** | **20,8** | 2HRLE-(7-1) ULE |

Table 5.10 shows that no improvements were found attributable to enlarge the membrane series from 10 to 12 elements (see first to fifth rows). Besides that, the behaviour of permeate quality, $SEC_{net}$ and maximum flux is excellent in the last proposed configuration in which 10 elements are connected in series. In comparison to the last row of table 5.9, PVs with 10 elements may achieve:

- Similar $SEC_{net}$ with similar recovery rate, similar permeate TDS and low maximum flux. Therefore, similar OPEX is expected.

- Similar average flux and lower PVs and interconnection pipelines, thus resulting in lower CAPEX.

Otherwise, since recovery rate is similar to conventional configurations, scaling problems in the tail should be similar.

Finally, in order to draw conclusions on the most suitable number of membrane elements in a serial connection, a specific study is conducted. Table 5.11 reports on the study of variable number of membrane elements in the second stage, a single bypass of 20 $m^3/h$ is considered for a total feed flow of 101.7 $m^3/h$.

**Table 5.11. Results of simulations based on fig. 5.16, with 10 PV´s in each stage, feed flow of the first stage 101.7 $m^3/h$, bypass flow of 20 $m^3/h$ and variable number of membrane elements in the second stage, from 8 to 12.**

| HID (2 SW30HRLE-440i + 2 SW30ULE-440i )+ 2nd stage: # variable of SW30ULE-440i | | | | | | | | | | | | | | |
|---|---|---|---|---|---|---|---|---|---|---|---|---|---|---|
| $p_F$, bar= 54,25 | | $q_{V,F}$, 1stg, $m^3/h$= 101,71 | | 10 PV´s | | | | | Area= 40,9 $m^2$ | | Bypass 20 $m^3/h$ | | | |
| # mem 2nd stage | SEC kWh/$m^3$ | Pw kW | Avg. flux ) | Max. $q_{V,P}$ $m^3/h$ | TDS$_P$ mg/L | Boron (x$10^2$) mg/L | r % | $q_{V,P}$ $m^3/h$ | $q_{V,BD}$ $m^3/h$ | $p_{BD}$ bar | (ERI-PX) kW | $PW_{net}$ kW | $SEC_{net}$ kWh/$m^3$ | Max. flux L/($m^2$·h) |
| **8** | 4,57 | **229,3** | 15,3 | 0,88 | 240,5 | 129 | 41,2 | 50,2 | 71,6 | 51,1 | **-121,1** | **108,2** | **2,16** | **21,52** |
| **9** | 4,50 | **229,3** | 13,9 | 0,88 | 234,0 | 128 | 41,9 | 51,0 | 70,8 | 50,5 | **-118,5** | **110,8** | **2,18** | **21,52** |
| **10** | 4,24 | **229,3** | 13,2 | 0,88 | 296,0 | 146 | 44,4 | 54,1 | 67,6 | 50,7 | **-113,5** | **115,8** | **2,14** | **21,52** |
| **11** | 4,14 | **229,3** | 12,3 | 0,88 | 325,4 | 153 | 45,5 | 55,4 | 66,4 | 50,5 | **-111,0** | **118,3** | **2,14** | **21,52** |
| **12** | 4,13 | **229,3** | 11,3 | 0,88 | 322,0 | 154 | 45,6 | 55,6 | 66,2 | 49,9 | **-109,5** | **119,8** | **2,16** | **21,52** |

According to tables 5.10- 5.11, the concept presented in figures 5.16- 5.17 could be useful to significantly increase the serial connection due to suitable values of average flux, maximum flux, permeate quality and $SEC_{net.}$

To sum up, the proposed configuration by GE with high bypass flow could be recommended in order to operate with the highest permeability elements. This could be an effective way of avoiding excessive fouling risk in the front membrane elements. Moreover, the patented configuration allows to develop extra-long PV´s, thus decreasing CAPEX.

# 5. CONFIGURATION PATENTED BY DESALITECH

Figure 5.20 depicts the configuration referred to as Desalitech-CCD (Closed Circuit Desalination) [Stover, 2015]. This section deals with a thorough analysis of CCD in order to assess improvements in comparison to conventional RO layout. The CCD concept was identified in chapter 3 as a candidate option to dramatically reduce the SEC. This innovative configuration in principle might be operated either, as a stationary system or in batches. However, the CCD concept is only suitable to operate in batches.

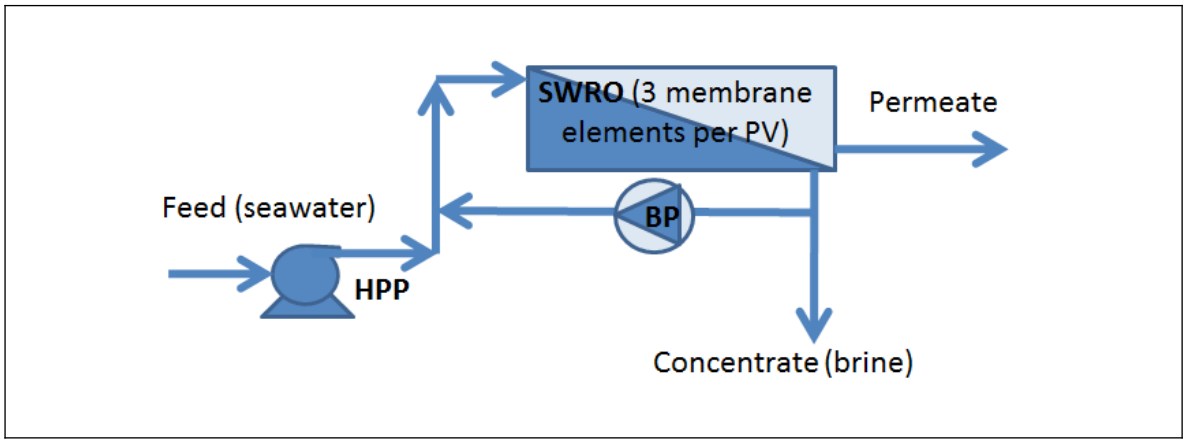


**Figure 5.20. Desalitech-CCD (Closed Circuit Desalination) concept. Energy recovery from the brine is not shown in the figure. HPP: High Pressure Pump; BP: Booster Pump; PV: Pressure Vessel.**

Concerning stationary operation of CCD, the seawater feed should reach at the high pressure pump (HPP) outlet a working pressure above the osmotic pressure of the concentrate (brine). Since the concentrate recycled after passing through the Booster Pump (BP) is mixed with the HPP outlet, the BP only compensates the pressure losses attributable to the circulation through the Pressure Vessel (PV). Therefore, the HPP consumption is similar to that of a single stage design. Also the brine flow and pressure are similar to those in conventional designs, but pressure losses within the PV are lower since it consists of only 3-4 membrane elements. The concentrate recycling by means of the BP results in higher osmotic pressure at the PV inlet than in conventional configuration. Thus the average Net Driving Pressure (NDP) goes down. The average flux should be similar to that of the tail elements in a conventional configuration the same recovery rate. Therefore, greater membrane area will be required, thus increasing the plant CAPEX. Therefore, in principle stationary operation is not useful for seawater desalination.

### 5.1. Batch mode

When analysing other innovative configurations we have seen that one of the main issues is that the net driving pressure is lower for the membranes in the tail of the PV. This is due to the combination of pressure decay and concentration increase as the feed water goes through the membranes in the PV. In addition, the highest risk of scaling corresponds to the tail element positions. In CCD configuration there are no membranes in the tail since it is based on PV with 3 to 4 elements. When operating in batch mode, the brine coming out of the PV is then recirculated to the head of the PV (as a first cycle), thus the same membranes have now feed water salinity similar to that in the middle of a conventional PV. Therefore a two cycles CCD should be equivalent to a conventional configuration in relation to salt concentration. However, the net driving pressure is increased by means of the recirculation pump. Therefore, the operation of two cycles as a whole is equivalent to two stages of 3-4 membrane elements with an interstage pump. Moreover, CCD allows to further recirculate and four cycles should then be equivalent to a conventional four stages RO desalination, thus increasing production and also recovery. The main positive effect of lowering the net driving pressure by means of multiple stages is the SEC decrease. However, product water quality decreases as a result of the corresponding lower water flux while salt passage remains unchanged.

Conceptual advantages of multi-stage configurations were analysed in chapter 3. Permeate is produced with relatively low net driving pressure according to figure 5.21. As a result, the SEC and the flux go down, thus decreasing the operation cost but increasing capital cost. The latter increases not only due the reduced flux but also due to capital costs of interstage pumps and additional piping and PV´s. For this reason, no more than two stages are implemented in seawater desalination industry. Other issue that should be taken into account is the effect of multistage configurations on permeate quality. Implementing more than two stages means that the net driving pressure became so low that may result in unsuitable balance between water flow and salt passage. Therefore, to obtain appropriate product quality may require a given minimum operation pressure.

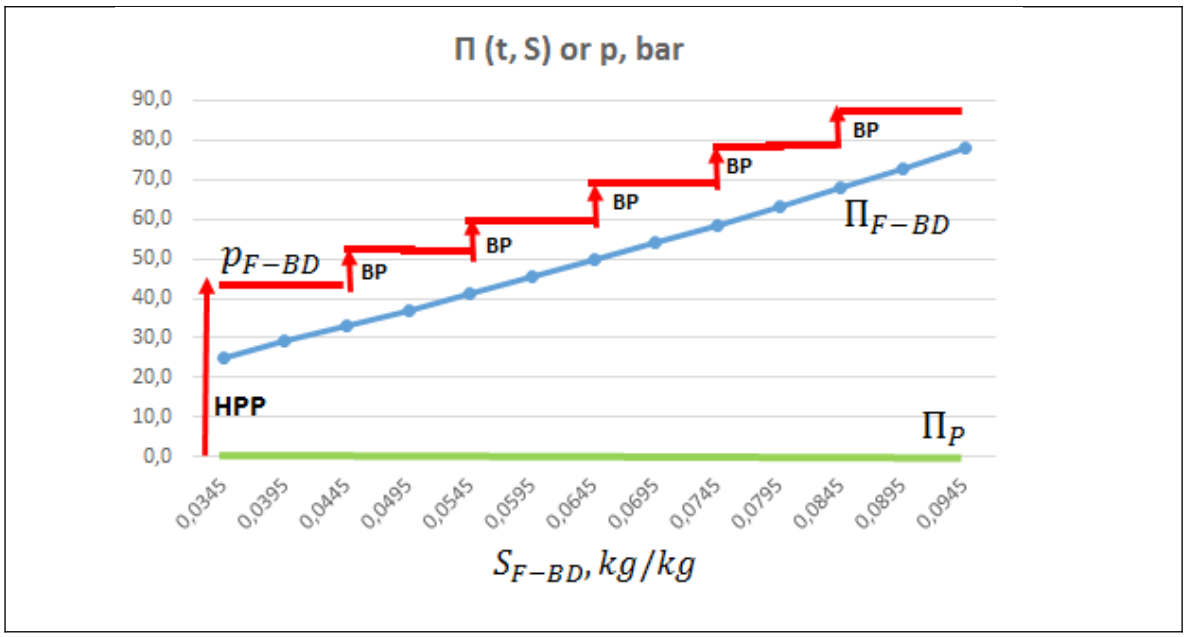


**Figure 5.21. Feed pressure and osmotic pressure in a theoretical SWRO desalination process with multiple stages with inter-stage Booster Pumps (BP´s).**

Considering the CCD configuration operating in batch mode, firstly a qualitative analysis is performed and after that, a quantitative assessment of specific issues is carried out. The hypothesis of brine energy recovery with similar efficiency of conventional configuration is assumed since the main aim is to carry out a theoretical analysis.

The feed water concentration will increase and a feed flow will reduce as the recirculation pump operates, thus the pressure can be adjusted for every cycle. In this way, the net driving pressure in each of the membranes could be maintained constant and equal to the design value (first cycle). However this will have a limit since the total pressure is also increasing in every cycle up to the selected design recovery rate (or maximum concentrate salinity). The permeate production and quality will then only depend on working pressure and concentration in every cycle.

Once the system has operated in closed circuit for a number of cycles, the brine has to be discharged and the PV fed with feed water, taking advantage of the brine pressure to pressurise the feed water (energy recovery). The first issue that comes is that the brine pressure after a number or cycles is higher than the feed pressure for the first cycle. This will add some complexity to the system if the brine pressure is to be completely recovered because. Moreover,

the conventional energy recovery devices are not designed to operate discontinuously. Operating CCD configuration in batch mode and adjusting the feed pressure every cycle allows maintaining the NDP constant in each membrane. The energy consumption will be the required by the high pressure and the recirculation pumps, thus also depend on the number of cycles (see Figure 5.21).

Table 5.12 analyses the effect of interstage pump pressure in conventional configuration consisting in two stages. The first stage comprises three SW30HRLE-440i elements in series and four of them are placed in the second stage. Results obtained for booster pressures ranged from 2 bar to 12 bar are depicted in the five first rows, being constant permeate flow and recovery rate. In order to allow a comparative assessment, the following row shows results for a conventional PV with 7 elements and same permeate flow. In addition, the behaviour of a similar two stage configuration, 4 SW30HRLE-440i + 3 SW30HRLE-440i, with booster pump pressure of 12 bar are also depicted in last row.

**Table 5.12. Configurations with two stages with different booster pump pressures, from 2 bar to 20 bar for 3 SW30HRLE-440i + 4 SW30HRLE-440i in comparison to 7 SW30HRLE-440i. Last two rows: 4 SW30HRLE-440i + 3 SW30HRLE-440i, booster pump pressure, 12 bar and 20 bar.**

| 3 SW30HRLE-440i + 2nd stage: 4 SW3HRLE-440i | | | | | | | | | | | | | |
|---|---|---|---|---|---|---|---|---|---|---|---|---|---|
| r, %= 45 | | $q_{V,P}$, $m^3$/ 4,01 | | | | Area= 40,9 $m^2$ | | | | | | | |
| Booster Pump bar | SEC kWh/$m^3$ | Pw kW | Avg. flux L/($m^2$·h) | Max. $q_{V,P}$ $m^3$/h | $TDS_P$ mg/L | Boron (x$10^2$) mg/L | r % | $q_{V,BD}$ $m^3$/h | $p_{BD}$ bar | (ERI-PX) kW | $PW_{net}$ kW | $SEC_{net}$ kWh/$m^3$ | Max. flux L/($m^2$·h) |
| 2 | 4,51 | 18,1 | 14,0 | 0,93 | 144 | 90 | 45 | 4,9 | 57,0 | -9,3 | 8,8 | 2,21 | 22,7 |
| 5 | 4,52 | 18,1 | 14,0 | 0,88 | 143 | 90 | 45 | 4,9 | 57,8 | -9,4 | 8,8 | 2,18 | 21,5 |
| 8 | 4,54 | 18,2 | 14,0 | 0,82 | 142 | 90 | 45 | 4,9 | 58,7 | -9,5 | 8,7 | 2,17 | 20,0 |
| 10 | 4,56 | 18,3 | 14,0 | 0,7 | 141 | 90 | 45 | 4,9 | 59,3 | -9,6 | 8,7 | 2,16 | 17,1 |
| 12 | 4,58 | 18,4 | 14,0 | 0,73 | 140 | 89 | 45 | 4,9 | 59,9 | -9,7 | 8,7 | 2,16 | 17,8 |
| 20 | 4,71 | 18,9 | 14,0 | 0,85 | 137 | 84 | 45 | 4,9 | 62,4 | -10,1 | 8,8 | 2,19 | 20,8 |
| 7 HRLE | 4,50 | 18,0 | 14,0 | 0,96 | 145 | 91 | 45 | 4,9 | 56,6 | -9,2 | 8,8 | 2,21 | 23,5 |
| Stg. 4-3 | 4,64 | 18,6 | 14,0 | 0,79 | 140 | 89 | 45 | 4,9 | 61,4 | -10,0 | 8,6 | 2,16 | 19,3 |
| Stg. 4-3 | 4,81 | 19,3 | 14,0 | 0,8 | 136 | 84 | 45 | 4,9 | 64,9 | -10,5 | 8,8 | 2,19 | 19,6 |

According to the conceptual figure 5.21, the SEC decreases as booster pump pressure goes up. This is attributable to the lower pressure required in the HPP. Besides that, two stages configurations with 4+3 and 3+4 elements are similar concerning product quality and SEC. However, the option consisting in 4+3 allows for lower maximum flux, which result in lower fouling in the first membrane elements.

Tables 5.13-5.14 provide results of an analogous analysis carried out with SW30XLE-440i and SW30ULE-440i membrane elements, respectively.

**Table 5.13. Configurations with two stages with different booster pump pressures, from 2 bar to 12 bar for 3 SW30XLE-440i + 4 SW30XLE-440i in comparison to 7 SW30XLE-440i. Last two rows: 4 SW30XLE-440i + 3 SW30XLE-440i, booster pump pressure, 12 bar and 20 bar.**

| 3 SW30XLE-440i + 2nd stage: 4 SW30XLE-440i | | | | | | | | | | | | | |
|---|---|---|---|---|---|---|---|---|---|---|---|---|---|
| r, %= 45 | | $q_{V,P}$, $m^3$/ | 4,01 | | | Area= 40,9 $m^2$ | | | | | | | |
| Booster Pump bar | SEC kWh/$m^3$ | Pw kW | Avg. flux L/($m^2$·h) | Max. $q_{V,P}$ $m^3$/h | $TDS_P$ mg/L | Boron (x$10^2$) mg/L | r % | $q_{V,BD}$ $m^3$/h | $p_{BD}$ bar | (ERI-PX) kW | $PW_{net}$ kW | $SEC_{net}$ kWh/$m^3$ | Max. flux L/($m^2$·h) |
| **2** | 4,30 | 17,2 | 14,0 | 1,01 | 172 | 153 | 45 | 4,9 | 54,2 | **-8,8** | **8,4** | **2,10** | **24,7** |
| **5** | 4,30 | 17,2 | 14,0 | 0,94 | 171 | 153 | 45 | 4,9 | 55,0 | **-8,9** | **8,3** | **2,07** | **23,0** |
| **8** | 4,31 | 17,3 | 14,0 | 0,87 | 169 | 153 | 45 | 4,9 | 55,8 | **-9,1** | **8,2** | **2,05** | **21,3** |
| **10** | 4,32 | 17,3 | 14,0 | 0,83 | 168 | 153 | 45 | 4,9 | 56,3 | **-9,1** | **8,2** | **2,05** | **20,3** |
| **12** | 4,34 | 17,4 | 14,0 | 0,78 | 167 | 153 | 45 | 4,9 | 56,8 | **-9,2** | **8,2** | **2,04** | **19,1** |
| **20** | 4,47 | 17,9 | 14,0 | 0,91 | 162 | 101 | 45 | 4,9 | 59,2 | **-9,6** | **8,3** | **2,08** | **22,2** |
| **7 XLE** | 4,29 | **17,2** | 14,0 | 1,05 | 173 | 108 | 45 | 4,9 | 53,9 | **-8,7** | **8,4** | **2,11** | **25,7** |
| **Stg. 4-3** | 4,40 | 17,6 | 14,0 | 0,83 | 166 | 107 | 45 | 4,9 | 58,3 | **-9,5** | **8,2** | **2,04** | **20,3** |
| **Stg. 4-3** | 4,57 | 18,3 | 14,0 | 0,85 | 161 | 101 | 45 | 4,9 | 61,7 | **-10,0** | **8,3** | **2,07** | **20,8** |

**Table 5.14. Configurations with two stages with different booster pump pressures, from 2 bar to 20 bar for 3 SW30ULE-440i + 4 SW30ULE-440i in comparison to 7 SW30ULE-440i. Last row: 4 SW30ULE-440i + 3 SW30ULE-440i, booster pump pressure, 12 bar.**

| 3 SW30ULE-440i + 2nd stage: 4 SW30ULE-440i | | | | | | | | | | | | | |
|---|---|---|---|---|---|---|---|---|---|---|---|---|---|
| r, %= 45 | | $q_{V,P}$, $m^3$/ | 4,01 | | | Area= 40,9 $m^2$ | | | | | | | |
| Booster Pump bar | SEC kWh/$m^3$ | Pw kW | Avg. flux L/($m^2$·h) | Max. $q_{V,P}$ $m^3$/h | $TDS_P$ mg/L | Boron (x$10^2$) mg/L | r % | $q_{V,BD}$ $m^3$/h | $p_{BD}$ bar | (ERI-PX) kW | $PW_{net}$ kW | $SEC_{net}$ kWh/$m^3$ | Max. flux L/($m^2$·h) |
| **2** | 4,11 | 16,5 | 14,0 | 1,10 | 310 | 108 | 45 | 4,9 | 51,9 | **-8,4** | **8,1** | **2,01** | **26,9** |
| **5** | 4,10 | **16,5** | 14,0 | 1,01 | 306 | 108 | 45 | 4,9 | 52,5 | **-8,5** | **7,9** | **1,98** | **24,7** |
| **8** | 4,11 | **16,5** | 14,0 | 0,93 | 303 | 107 | 45 | 4,9 | 53,3 | **-8,7** | **7,8** | **1,96** | **22,7** |
| **10** | 4,13 | **16,5** | 14,0 | 0,88 | 301 | 107 | 45 | 4,9 | 53,8 | **-8,7** | **7,8** | **1,95** | **21,5** |
| **12** | 4,14 | **16,6** | 14,0 | 0,87 | 298 | 107 | 45 | 4,9 | 54,3 | **-8,8** | **7,8** | **1,94** | **21,3** |
| **15** | 4,22 | **16,9** | 14,0 | 0,85 | 250 | 136 | 45 | 4,9 | 55,0 | **-8,9** | **8,0** | **2,00** | **20,8** |
| **20** | 4,27 | **17,1** | 14,0 | 0,99 | 288 | 144 | 45 | 4,9 | 56,4 | **-9,2** | **8,0** | **1,99** | **24,2** |
| **7 ULE** | 4,10 | **16,5** | 14,0 | 1,14 | 312 | 152 | 45 | 4,9 | 51,6 | **-8,4** | **8,1** | **2,02** | **27,9** |
| **Stg. 4-3** | 4,20 | **16,8** | 14,0 | 0,87 | 297 | 153 | 45 | 4,9 | 55,7 | **-9,0** | **7,8** | **1,94** | **21,3** |

Two stages configurations with SW30HRLE-440i, SW30XLE-440i and SW30ULE-440i analysed exhibit minimum SEC with booster pump pressure around 12 bar, with operating

conditions selected, recovery rate, 45%, and permeate flow, 4.01 $m^3/h$ . Results of additional configurations studied are given in tables 5.15-5.16. Tables 5.12-5.16 show that SEC decreases around 2.5-3.5% in configurations based on two stages, being negligible the effect of booster pump pressure. On the contrary, significant effect of two stages on the maximum flux is obtained, it decreases about a 30% for booster pump pressure of 12 bar. This effect would be relevant on fouling mitigation at membrane elements of the first positions of the PV.

**Table 5.15. Configurations with two stages with different booster pump pressures, from 2 bar to 12 bar for 3 SW30ULE-440i + 4 SW30XLE-440i in comparison to single stage configuration.**

| 3 SW30ULE-440i + 2nd stage: 4 SW30XLE-440i | | | | | | | | | | | | | |
|---|---|---|---|---|---|---|---|---|---|---|---|---|---|
| r, %= 45 | | $q_{V,P}$, $m^3$/ | 4,01 | | | | Area= | 40,9 $m^2$ | | | | | |
| Booster Pump bar | SEC kWh/$m^3$ | Pw kW | Avg. flux L/($m^2$·h) | Max. $q_{V,P}$ $m^3$/h | $TDS_P$ mg/L | Boron (x$10^2$) mg/L | r % | $q_{V,BD}$ $m^3$/h | $p_{BD}$ bar | (ERI-PX) kW | $PW_{net}$ kW | $SEC_{net}$ kWh/$m^3$ | Max. flux L/($m^2$·h) |
| 2 | 4,21 | 16,9 | 14,0 | 1,14 | 227,2 | 130 | 45 | 4,9 | 53,2 | -8,6 | 8,2 | 2,1 | 27,9 |
| 5 | 4,21 | 16,9 | 14,0 | 1,07 | 223,9 | 129 | 45,0 | 4,9 | 54,0 | -8,8 | 8,1 | 2,0 | 26,2 |
| 8 | 4,22 | 16,9 | 14,0 | 0,99 | 220,6 | 128 | 45,0 | 4,9 | 54,8 | -8,9 | 8,0 | 2,0 | 24,2 |
| 10 | 4,23 | 17,0 | 14,0 | 0,94 | 218,5 | 127 | 45,0 | 4,9 | 55,4 | -9,0 | 8,0 | 2,0 | 23,0 |
| 12 | 4,26 | 17,1 | 14,0 | 0,88 | 216,3 | 126 | 45,0 | 4,9 | 56,0 | -9,1 | 8,0 | 2,0 | 21,5 |

**Table 5.16. Configurations with two stages with different booster pump pressures, from 2 bar to 12 bar for 3 SW30XLE-440i + 4 SW3ULE-440i in comparison to single stage configuration.**

| 3 SW30XLE-440i + 2nd stage: 4 SW30ULE-440i | | | | | | | | | | | | | |
|---|---|---|---|---|---|---|---|---|---|---|---|---|---|
| r, %= 45 | | $q_{V,P}$, $m^3$/ | 4,01 | | | | Area= | 40,9 $m^2$ | | | | | |
| Booster Pump bar | SEC kWh/$m^3$ | Pw kW | Avg. flux L/($m^2$·h) | Max. $q_{V,P}$ $m^3$/h | $TDS_P$ mg/L | Boron (x$10^2$) mg/L | r % | $q_{V,BD}$ $m^3$/h | $p_{BD}$ bar | PW (ERI-PX) kW | $PW_{net}$ kW | $SEC_{net}$ kWh/$m^3$ | Max. flux L/($m^2$·h) |
| 2 | 4,18 | 16,8 | 14,0 | 0,97 | 255,9 | 134 | 45 | 4,9 | 52,7 | -8,6 | 8,2 | 2,0 | 23,7 |
| 5 | 4,18 | 16,8 | 14,0 | 0,89 | 254,1 | 135 | 45,0 | 4,9 | 53,4 | -8,7 | 8,1 | 2,0 | 21,8 |
| 8 | 4,19 | 16,8 | 14,0 | 0,82 | 252,1 | 135 | 45,0 | 4,9 | 54,1 | -8,8 | 8,0 | 2,0 | 20,0 |
| 10 | 4,20 | 16,8 | 14,0 | 0,77 | 250,9 | 135 | 45,0 | 4,9 | 54,5 | -8,9 | 8,0 | 2,0 | 18,8 |
| 12 | 4,22 | 16,9 | 14,0 | 0,72 | 249,6 | 136 | 45,0 | 4,9 | 55,0 | -8,9 | 8,0 | 2,0 | 17,6 |

Once studied the quantitative effect of using two stages, the CCD-Desalitech concept is assessed. Depending of the pressure at the HPP outlet the driving force is set, thus the corresponding permeate flow and salinity of the concentrate outlet is given. Therefore, HPP pressure can be selected in order to allow several stages up to achieve concentrate salinities

around that of conventional SWRO plants. A valve should be placed at the HPP outlet. When the valve is off, the booster pump operation results in recirculating the concentrate outlet of the PVs. When the concentrate salinity achieve the selected value is circulated through the energy recovery device instead of recirculated. Then, the PV is fed by seawater from the HPP.

Three options with 3 membrane elements (SW30ULE-440i) per PV are analysed, 2, 3 and 4 stages, all of them with same values of permeate flow and recovery rate, in order to allow a proper comparison between them. Tables 5.17-5.19 show respective results obtained by assuming constant value of the booster pump pressure in all stages. In order to show the behaviour of SEC detail values are given, however, only one decimal place may make sense. The booster pump pressure for minimum SEC is found in each case. The corresponding row is marked in blue in each table.

**Table 5.17. Simulation of CCD concept operated in bath mode, with one recirculation stage. Booster pump pressure ranges from 2 bar to 16 bar for 3 SW30ULE-440i placed within the pressure vessel. Last row shows results of conventional 7-element configuration (one stage).**

| 3 SW30ULE-440i + 2nd stage: 3 SW30ULE-440i | | | | | | | | | | | | | |
|---|---|---|---|---|---|---|---|---|---|---|---|---|---|
| r, %= 45 | | $q_{V,P}$, $m^3$/ 4,01 | | | | Area= 40,9 $m^2$ | | | | | | | |
| Booster Pump bar | SEC kWh/$m^3$ | Pw kW | Avg. flux L/($m^2$·h) | Max. $q_{V,P}$ $m^3$/h | $TDS_P$ mg/L | Boron (x$10^2$) mg/L | r % | $q_{V,BD}$ $m^3$/h | $p_{BD}$ bar | PW (ERI-PX) kW | $PW_{net}$ kW | $SEC_{net}$ kWh/$m^3$ | Max. flux L/($m^2$·h) |
| **2** | 4,27 | 17,13 | 16,4 | 1,17 | 267 | 135 | 45 | 4,9 | 54,15 | **-8,79** | **8,34** | **2,079** | **28,6** |
| **3** | 4,27 | **17,13** | 16,4 | 1,15 | 266 | 135 | 45 | 4,9 | 54,46 | **-8,84** | **8,29** | **2,067** | **28,1** |
| **4** | 4,28 | **17,15** | 16,4 | 1,12 | 266 | 135 | 45 | 4,9 | 54,78 | **-8,89** | **8,26** | **2,059** | **27,4** |
| **5** | 4,28 | **17,16** | 16,4 | 1,10 | 265 | 135 | 45 | 4,9 | 55,09 | **-8,94** | **8,22** | **2,049** | **26,9** |
| **6** | 4,28 | **17,18** | 16,4 | 1,08 | 264 | 135 | 45 | 4,9 | 55,41 | **-9,00** | **8,18** | **2,041** | **26,4** |
| **7** | 4,29 | **17,21** | 16,4 | 1,05 | 263 | 135 | 45 | 4,9 | 55,73 | **-9,05** | **8,16** | **2,041** | **25,7** |
| **8** | 4,30 | 17,24 | 16,4 | 1,03 | 262 | 134 | 45 | 4,9 | 56,06 | **-9,10** | **8,14** | **2,030** | **25,2** |
| **9** | 4,31 | **17,27** | 16,4 | 1,00 | 261 | 134 | 45 | 4,9 | 56,39 | **-9,15** | **8,12** | **2,024** | **24,4** |
| **10** | 4,32 | **17,31** | 16,4 | 0,98 | 260 | 134 | 45 | 4,9 | 56,72 | **-9,21** | **8,10** | **2,021** | **24,0** |
| **11** | 4,33 | **17,36** | 16,4 | 0,95 | 259 | 134 | 45 | 4,9 | 57,05 | **-9,26** | **8,10** | **2,020** | **23,2** |
| **12** | 4,34 | **17,41** | 16,4 | 0,93 | 258 | 134 | 45 | 4,9 | 57,39 | **-9,32** | **8,09** | **2,019** | **22,7** |
| **13** | 4,36 | **17,46** | 16,4 | 0,91 | 257 | 134 | 45 | 4,9 | 57,73 | **-9,37** | **8,09** | **2,022** | **22,2** |
| **14** | 4,37 | **17,52** | 16,4 | 0,88 | 256 | 133 | 45 | 4,9 | 58,07 | **-9,43** | **8,09** | **2,019** | **21,5** |
| **15** | 4,39 | **17,59** | 16,4 | 0,88 | 256 | 133 | 45 | 4,9 | 58,42 | **-9,48** | **8,11** | **2,027** | **21,5** |
| **16** | 4,40 | **17,66** | 16,4 | 0,9 | 255 | 133 | 45 | 4,9 | 58,77 | **-9,54** | **8,12** | **2,030** | **22,0** |
| **7 ULE** | 4,10 | **16,46** | 16,4 | 1,14 | 312 | 152 | 45 | 4,9 | 51,55 | **-8,37** | **8,09** | **2,017** | **27,9** |

**Table 5.18. Simulation of CCD concept operated in bath mode, with two recirculation stages. Booster pump pressure ranges from 2 bar to 16 bar for 3 SW30ULE-440i placed within the pressure vessel. Last row shows results of conventional 7-element configuration (one stage).**

| 3 SW30ULE-440i + 2nd stage: 3 SW30ULE-440i + 3rd stage: 3 SW30ULE-440i | | | | | | | | | | | | | |
|---|---|---|---|---|---|---|---|---|---|---|---|---|---|
| r, %= 45 | | $q_{V,P}$, $m^3$/ | 4,01 | | | Area= | 40,9 $m^2$ | | | | | | |
| Booster Pump | SEC | Pw | Avg. flux | Max. $q_{V,P}$ | $TDS_P$ | Boron (x$10^2$) | r | $q_{V,BD}$ | $p_{BD}$ | PW (ERI-PX) | $PW_{net}$ | $SEC_{net}$ | Max. flux |
| bar | kWh/$m^3$ | kW | L/($m^2$·h) | $m^3$/h | mg/L | mg/L | % | $m^3$/h | bar | kW | kW | kWh/$m^3$ | L/($m^2$·h) |
| 2 | 3,95 | 15,8 | 10,9 | 0,97 | 391 | 170 | 45 | 4,9 | 49,8 | -8,1 | 7,7 | 1,93 | 23,7 |
| 3 | 3,94 | 15,8 | 10,9 | 0,92 | 388 | 171 | 45 | 4,9 | 50,3 | -8,2 | 7,6 | 1,91 | 22,5 |
| 4 | 3,95 | 15,8 | 10,9 | 0,86 | 384 | 172 | 45 | 4,9 | 50,9 | -8,3 | 7,6 | 1,89 | 21,0 |
| 5 | 3,95 | 15,9 | 10,9 | 0,81 | 381 | 172 | 45 | 4,9 | 51,4 | -8,4 | 7,5 | 1,87 | 19,8 |
| 6 | 3,96 | 15,9 | 10,9 | 0,75 | 377 | 172 | 45 | 4,9 | 52,0 | -8,4 | 7,5 | 1,86 | 18,3 |
| 7 | 3,98 | 16,0 | 10,9 | 0,69 | 374 | 172 | 45 | 4,9 | 52,5 | -8,5 | 7,4 | 1,85 | 16,9 |
| 8 | 4,00 | 16,1 | 10,9 | 0,64 | 370 | 172 | 45 | 4,9 | 53,1 | -8,6 | 7,4 | 1,85 | 15,6 |
| 9 | 4,03 | 16,2 | 10,9 | 0,62 | 366 | 171 | 45 | 4,9 | 53,7 | -8,7 | 7,4 | 1,86 | 15,2 |
| 10 | 4,06 | 16,3 | 10,9 | 0,63 | 363 | 170 | 45 | 4,9 | 54,3 | -8,8 | 7,5 | 1,86 | 15,4 |
| 7 ULE | 4,10 | 16,46 | 16,4 | 1,14 | 312 | 152 | 45 | 4,9 | 51,55 | -8,37 | 8,09 | 2,017 | 27,9 |

**Table 5.19. Simulation of CCD concept operated in bath mode, with three recirculation stages. Booster pump pressure ranges from 2 bar to 16 bar for 3 SW30ULE-440i placed within the pressure vessel. Last row shows results of conventional 7-element configuration (one stage).**

| 3 SW30ULE-440i + 2nd stage: 3 SW30ULE-440i + 3rd stage: 3 SW30ULE-440i + 4th stage: 3 SW30ULE-440i | | | | | | | | | | | | | |
|---|---|---|---|---|---|---|---|---|---|---|---|---|---|
| r, %= 45 | | $q_{V,P}$, $m^3$/ | 4,01 | | | Area= | 40,9 $m^2$ | | | | | | |
| Booster Pump | SEC | Pw | Avg. flux | Max. $q_{V,P}$ | $TDS_P$ | Boron (x$10^2$) | r | $q_{V,BD}$ | $p_{BD}$ | PW (ERI-PX) | $PW_{net}$ | $SEC_{net}$ | Max. flux |
| bar | kWh/$m^3$ | kW | L/($m^2$·h) | $m^3$/h | mg/L | mg/L | % | $m^3$/h | bar | kW | kW | kWh/$m^3$ | L/($m^2$·h) |
| 2 | 3,82 | 15,3 | 8,2 | 0,86 | 515 | 196 | 45 | 4,9 | 48,0 | -7,8 | 7,5 | 1,87 | 21,0 |
| 3 | 3,82 | 15,3 | 8,2 | 0,78 | 507 | 200 | 45 | 4,9 | 48,8 | -7,9 | 7,4 | 1,84 | 19,1 |
| 4 | 3,82 | 15,3 | 8,2 | 0,69 | 499 | 202 | 45 | 4,9 | 49,5 | -8,0 | 7,3 | 1,82 | 16,9 |
| 5 | 3,84 | 15,4 | 8,2 | 0,60 | 491 | 203 | 45 | 4,9 | 50,2 | -8,2 | 7,2 | 1,80 | 14,7 |
| 6 | 3,86 | 15,5 | 8,2 | 0,5 | 482 | 203 | 45 | 4,9 | 50,9 | -8,3 | 7,2 | 1,80 | 12,2 |
| 7 | 3,90 | 15,6 | 8,2 | 0,48 | 473 | 202 | 45 | 4,9 | 51,7 | -8,4 | 7,3 | 1,81 | 11,7 |
| 8 | 3,95 | 15,8 | 8,2 | 0,50 | 465 | 199 | 45 | 4,9 | 52,4 | -8,5 | 7,3 | 1,83 | 12,2 |
| 9 | 4,02 | 16,1 | 8,2 | 0,55 | 456 | 195 | 45 | 4,9 | 53,2 | -8,6 | 7,5 | 1,86 | 13,4 |
| 10 | 4,09 | 16,4 | 8,2 | 0,6 | 446 | 188 | 45 | 4,9 | 54,0 | -8,8 | 7,6 | 1,90 | 14,7 |
| 7 ULE | 4,10 | 16,46 | 16,4 | 1,14 | 312 | 152 | 45 | 4,9 | 51,55 | -8,37 | 8,09 | 2,017 | 27,9 |

Table 5.19 shows that savings of 10% could be achieved by means of CCD concept implemented with 3elements per PV, applied to 4-stage operation with BP pressure of 6 bar. Besides that, 3-stage operation allows 7% of energy saving with booster pressure of 8 bar. The configuration operated with 2-stages results in negligible effect on SEC. Figures 5.22-5.25 depict

comparative results concerning SEC, maximum flux and permeate quality – i.e. TDS and boron concentration -.

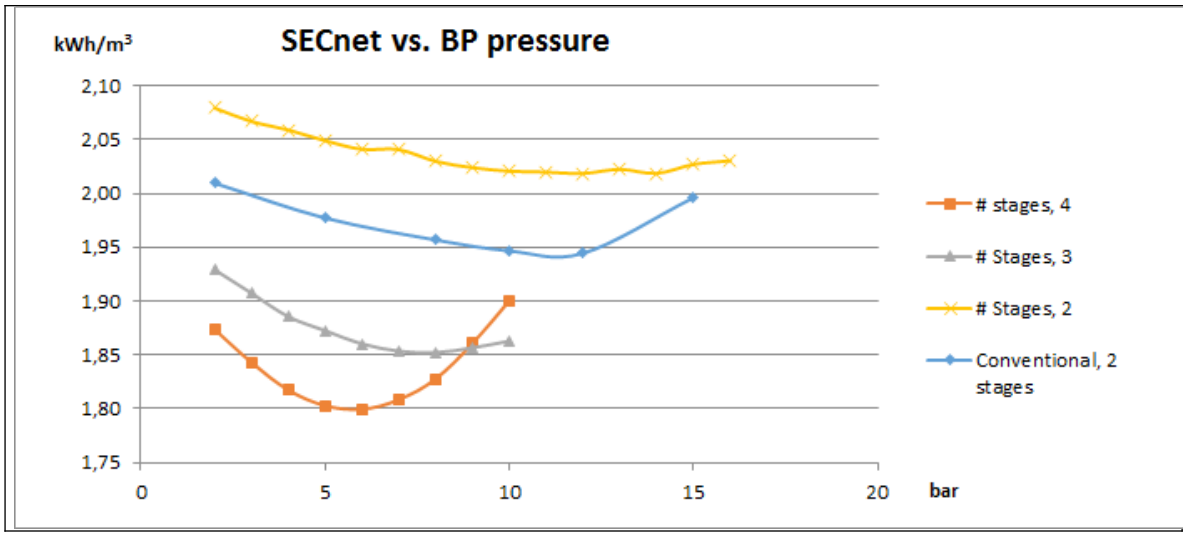


**Figure 5.22. Analysis of CCD concept operated in batches: Specific Energy Consumption versus Booster Pump (BP) pressure.**

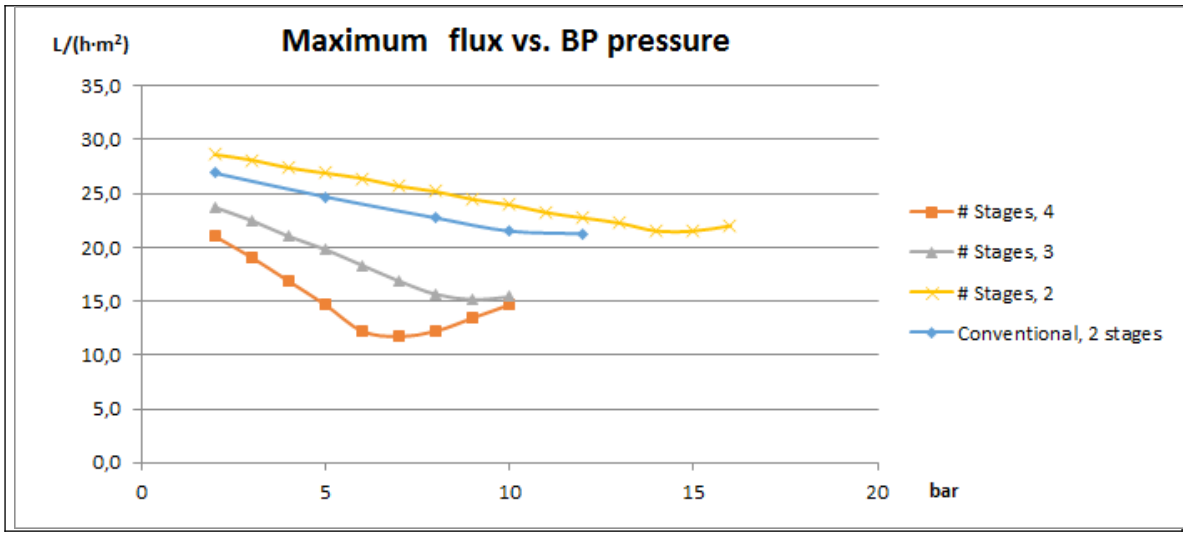


**Figure 5.23. Analysis of CCD concept operated in batches: Maximum flux as a function of BP pressure.**

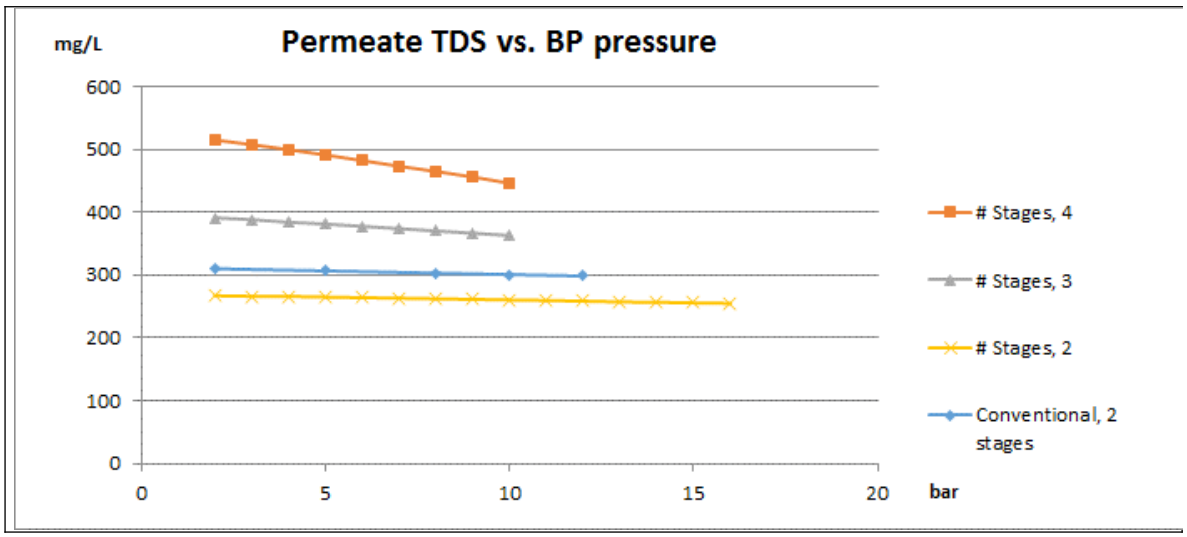


**Figure 5.24. Analysis of CCD concept operated in batches: Permeate TDS.**

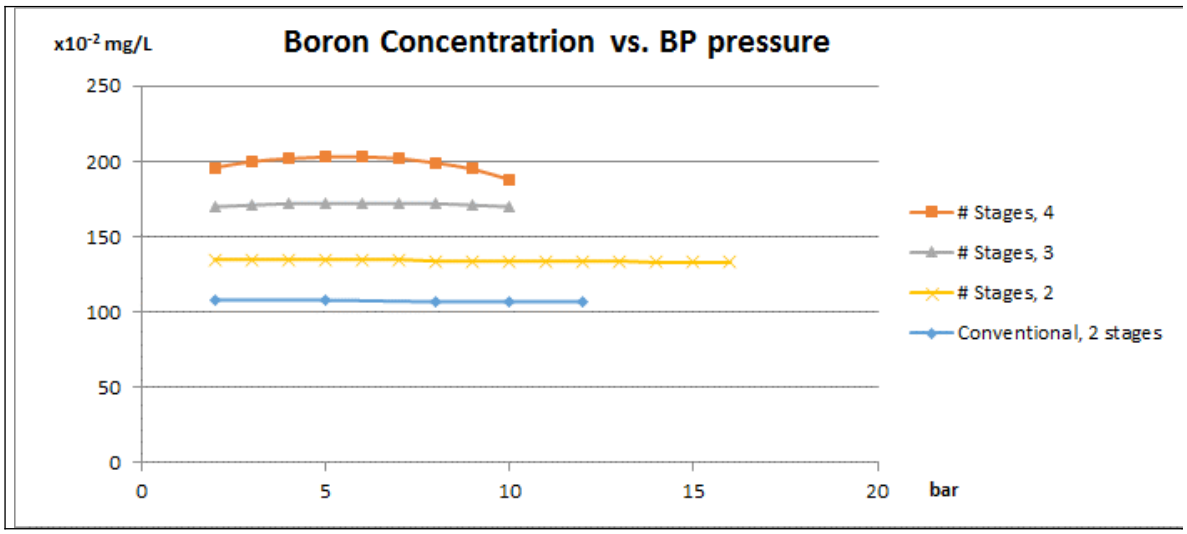


**Figure 5.25. Analysis of CCD concept operated in batches: Boron concentration in permeate.**

In order to avoid disconnections of HPP and BP if CCD concept is implemented, they could alternatively feed several groups of PVs. This avoids disadvantages associated to discontinuous operation, namely CAPEX and OPEX increase.

## 5.2. Semi-batch mode

A system based on CCD configuration can also be operated in semi-batch mode, that is, that the HPP is also adjusting the feed pressure in the same way as the recirculation pump and is feeding constantly with feed water in order to compensate for the permeate produced in every cycle.

If operating in semi-batch mode, the membranes will work at both constant NDP and feed flow. Moreover, the concentration of the feed water will increase from one cycle to the next one but not as much as in batch mode since the recirculated brine will mixt up with feed water at a lower concentration (see Fig.5.6).

Tables 5.20 and 5.21 allows to compare results of recovery rate 45% for conventional configuration with 7 membrane elements and semi-batch operation of CCD with 3 and 4 membrane elements. In addition, results obtained with same feed pressure and different values of recirculation flow are given. The configuration analysed exhibits no advantage in comparison to conventional configuration due to its higher SEC and salt concentration of permeate.

**Table 5.20. Simulation of CCD concept operated in semi bath mode. Recirculation flow from 1 to 7 $m^3/h$ for 3 SW30HRLE-440i placed within the pressure vessel.**

| 3 SW30HRLE-440i | | | | | | | | | | | | | | |
|---|---|---|---|---|---|---|---|---|---|---|---|---|---|---|
| $q_{V,F}$, $m^3/h$= | 8,91 | $p_{,F}$, bar= | 57,97 | | | | | | Area= | 40,9 $m^2$ | | | | |
| qrc | SEC | Pw | Avg. flux | Max. $q_{V,P}$ | $TDS_P$ | Boron ($x10^2$) | r | $q_{V,P}$ | $q_{V,BD}$ | $p_{BD}$ | (ERI-PX) | $PW_{net}$ | $SEC_{net}$ | Max. flux |
| $m^3/h$ | $kWh/m^3$ | kW | $L/(m^2 \cdot h)$ | $m^3/h$ | mg/L | mg/L | % | $m^3/h$ | $m^3/h$ | bar | kW | kW | $kWh/m^3$ | $L/(m^2 \cdot h)$ |
| **1** | 6,75 | 15,9 | 19,2 | 0,93 | 100 | 68 | 30 | 2,4 | 5,6 | 56,9 | **-10,5** | **5,4** | **2,29** | **22,7** |
| **2** | 6,35 | 13,9 | 17,8 | 0,86 | 112 | 74 | 32 | 2,2 | 4,7 | 56,9 | **-8,9** | **5,0** | **2,28** | **21,0** |
| **3** | 5,94 | 11,9 | 16,4 | 0,82 | 126 | 82 | 34 | 2,0 | 3,9 | 56,9 | **-7,4** | **4,6** | **2,28** | **20,0** |
| **4** | 5,64 | 10,0 | 14,5 | 0,7 | 149 | 95 | 36 | 1,8 | 3,1 | 56,9 | **-5,9** | **4,1** | **2,29** | **17,1** |
| **5** | 5,27 | 8,0 | 12,4 | 0,61 | 182 | 111 | 39 | 1,5 | 2,4 | 56,9 | **-4,5** | **3,5** | **2,31** | **14,9** |
| **6** | 5,05 | 6,1 | 14,0 | 0,48 | 241 | 139 | 41 | 1,2 | 1,7 | 56,8 | **-3,2** | **2,8** | **2,37** | **11,7** |
| **7** | 4,83 | 4,1 | 14,0 | 0,35 | 357 | 183 | 45 | 0,9 | 1,1 | 56,8 | **-2,0** | **2,1** | **2,48** | **8,6** |
| **7 HRLE** | 4,50 | **18,0** | 14,0 | 0,96 | 145 | 91 | 45 | 4,0 | 4,9 | 56,6 | **-9,2** | **8,8** | **2,21** | **23,5** |

**Table 5.21. Simulation of CCD concept operated in semi bath mode. Recirculation flow from 1 to 7 $m^3/h$ for 4 SW30HRLE-440i placed within the pressure vessel.**

| 4 SW30HRLE-440i | | | | | | | | | | | | | | |
|---|---|---|---|---|---|---|---|---|---|---|---|---|---|---|
| $q_{V,F}$, $m^3/h$= 8,91 | | $p_{,F}$, bar= | 57,97 | | | | | | Area= | 40,9 $m^2$ | | | | |
| qrc | SEC | Pw | Avg. flux | Max. $q_{V,P}$ | $TDS_P$ | Boron ($x10^2$) | r | $q_{V,P}$ | $q_{V,BD}$ | $p_{BD}$ | (ERI-PX) | $PW_{net}$ | $SEC_{net}$ | Max. flux |
| m3/h | $kWh/m^3$ | kW | $L/(m^2 \cdot h)$ | $m^3/h$ | mg/L | mg/L | % | $m^3/h$ | $m^3/h$ | bar | kW | kW | $kWh/m^3$ | $L/(m^2 \cdot h)$ |
| 1 | 5,65 | 15,9 | 17,2 | 0,91 | 100 | 68 | 36 | 2,8 | 5,1 | 56,7 | **-9,6** | **6,3** | **2,24** | **22,2** |
| 2 | 5,46 | 13,9 | 15,6 | 0,83 | 134 | 87 | 37 | 2,6 | 4,4 | 56,7 | **-8,2** | **5,7** | **2,24** | **20,3** |
| 3 | 5,18 | 12,0 | 14,1 | 0,75 | 153 | 97 | 39 | 2,3 | 3,6 | 56,7 | **-6,8** | **5,2** | **2,25** | **18,3** |
| 4 | 4,98 | 10,0 | 12,3 | 0,66 | 182 | 111 | 41 | 2,0 | 2,9 | 56,7 | **-5,4** | **4,6** | **2,27** | **16,1** |
| 5 | 4,85 | 8,1 | 10,1 | 0,55 | 231 | 134 | 42 | 1,7 | 2,3 | 56,6 | **-4,2** | **3,8** | **2,31** | **13,4** |
| 6 | 4,67 | 6,1 | 8,0 | 0,43 | 304 | 164 | 45 | 1,3 | 1,6 | 56,6 | **-3,0** | **3,1** | **2,38** | **10,5** |
| **7 HRLE** | 4,50 | **18,0** | 14,0 | 0,96 | 145 | 91 | 45 | 4,0 | 4,9 | 56,6 | **-9,2** | **8,8** | **2,21** | **23,5** |

# 6. INNOVATIVE REVERSE OSMOSIS DESALINATION PLANT

As a result of the deep analysis of RO technology carried out in chapters 3 and 4 and after the analyses of existing innovative configuration in this chapter 5, a patent pending configuration has been proposed. The thermodynamic approach to RO technology in this thesis and the understanding of the NDP as the driving force of the RO process, has led to the concept of counter-current flow RO and how to take advantage of this concept to propose an innovative RO desalination configuration (New Configuration).

Next figure depicts the conceptual diagram of a counter-current RO element in which there are two inputs (points 1 and 3 in fig. 5.26) – adapted from Gozálvez et al (2002) -.

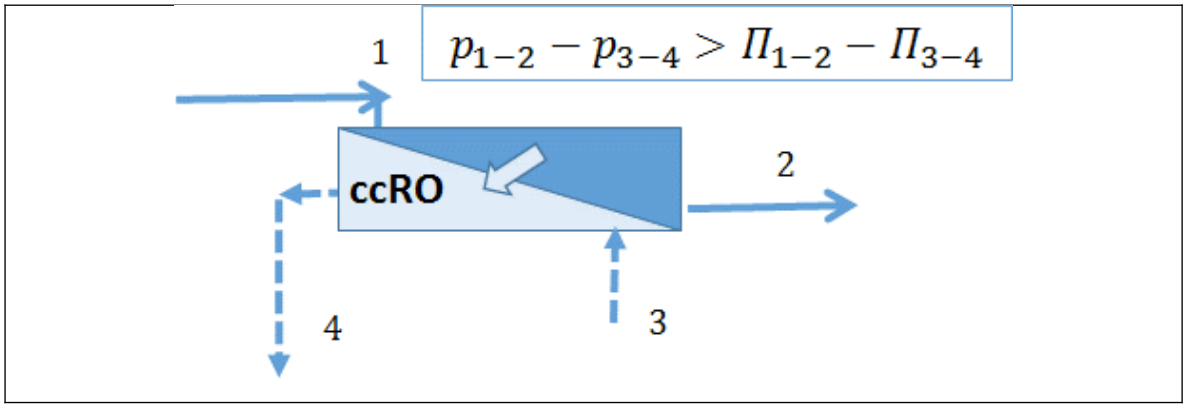


**Figure 5.26. Conceptual diagram of a counter-current membrane element (ccRO) and working conditions for allowing a permeate flow from 1-2 channel to 3-4 channel.**

In order to assess this New Configuration, operating conditions similar to those of conventional RO desalination have been considered and the comparison has been done in the same way as for the other innovative configurations in this Chapter.

The following tables (5.22-5.23) show results of the performance of the New Configuration when the tail differential pressure is set to 5 bar. Moreover, the considered efficiency for the HPP and its engine are 80% and 95% respectively and for the booster pump and its engine, 75% and 93% respectively, thus in the same way as in all previous analyses in this work.

Specific energy consumption of the New Configuration (SECnc) in comparison with the conventional configuration (SECc) are analysed as a function of seawater salinity ($S_{sw}$), temperature (T) and recovery rate (r). Table 5.22 shows the effect of salt concentration for a given recovery rate of 50%. Table 5.23 reports on the effect of using the New Configuration with the main aim of achieving high recovery rate.

**Table 5.22. Exemplary cases of energy savings of the New Configuration depending on the seawater salinity, $S_{sw}$.**

| $S_{sw}$ kg/kg | T °C | r % | $SEC_c$ kWh/m$^3$ | $SEC_{nc}$ kWh/m$^3$ | $SEC_{nc}$ - $SEC_c$ kWh/m$^3$ | Energy saving, % |
|---|---|---|---|---|---|---|
| 0.050 | 25 | 50.0 | 3.74 | 3.15 | -0.60 | 16 |
| 0.045 | 25 | 50.0 | 3.30 | 2.82 | -0.48 | 15 |
| 0.035 | 25 | 50.0 | 2.49 | 2.20 | -0.30 | 12 |

**Table 5.23. Study on the potential use of the New Configurations with the objective of increasing the overall plant recovery rate.**

| $S_{sw}$ kg/kg | T ºC | r % | $SEC_c$ kWh/m³ | $SEC_{nc}$ kWh/m³ | $SEC_{nc}$ - $SEC_c$ kWh/m³ | Energy saving, % |
|---|---|---|---|---|---|---|
| 0.035 | 25 | 64.8 | 3.51 | 2.74 | -0.77 | 22 |
| 0.035 | 25 | 60.5 | 3.10 | 2.49 | -0.61 | 20 |
| 0.035 | 25 | 57.0 | 2.87 | 2.38 | -0.48 | 17 |
| 0.035 | 25 | 54.0 | 2.68 | 2.22 | -0.46 | 17 |
| 0.035 | 25 | 50.0 | 2.49 | 2.20 | -0.30 | 12 |
| 0.035 | 25 | 45.0 | 2.31 | 2.14 | -0.17 | 7 |

The New Configuration shows for standard SWRO desalination operating conditions a specific energy consumption of 2,14 kwh/m$^3$. This means lower energy consumption than the corresponding conventional configuration (2,31 kwh/m$^3$), however the New Configuration shows limited energy savings (7%) when operating at recovery rates of 45%. This is not the case when operating at recovery rates of 65% allowing for energy savings up to 22%.

Therefore, the proposed New Configuration seems to be useful in applications of high salinity and high recovery rate.

Besides that, other patent pending configuration has been developed, which is related to brine treatments.

# 7. CONCLUSIONS

A few innovative configurations have been assessed in this chapter as follows:

- Conclusions from the assessment of Veolia´s configuration with respect to the conventional configuration:
    - Reduction of CAPEX by means of fewer membrane elements of the tail position does not improve main operation parameters.
    - Increasing the number of elements in the second stage improves SEC but increases the CAPEX.
    - The balance between CAPEX and OPEX seems to be better in conventional configuration. However, Veolia´s configuration might be useful in improving fouling and scaling performance or in allowing chemical dosing (or pH adjustment) at the first stage outlet.
    - Concerning scaling, to reduce the number of PV´s in the second stage could reduce the concentration polarisation since high feed flow promote turbulences.
    - In relation to fouling, in future development of RO membranes with high permeability this configuration may be essential to prevent excessive flux while maintain adequate average flux in order to achieve cost-effective configurations. Moreover, Veolia´s concept is useful if the compliance of product quality requires relatively high pressure due to either, high feed salinity or high temperature.

- The final conclusions from the assessment of GE´s configuration with respect to the conventional configuration are the following:
    - The patented bypass allows to reduce the fouling risk by reducing the maximum flux in the first membranes and average flux. It also allows to reduce the scaling risk by reducing the average feed salinity and the flow velocity in the tail membranes.
    - However, this configuration requires more high pressure piping, connectors somewhere in the middle of the vessels, additional valves and space in the rack. This represents higher CAPEX for GE´s configuration than for the conventional one if the same number of elements is considered.
    - Moreover, the energy consumption also increases slightly for GE´s configuration.
    - GE´s configuration could be recommended in order to operate with the highest permeability elements with an effective way of avoiding excessive fouling risk in the first membrane elements of the PV, but always with a CAPEX trade-off.
    - Besides that, GE configuration allows the implementation with high number of membrane elements, 12-14 elements per PV could achieve significant saving in CAPEX.

- CCD-Desalitech is analysed. Energy savings of 10% could be theoretically achieved by means of CCD concept implemented with three elements per PV, applied to 4-stage operation with BP pressure of 6 bar. However, operation in batches requires specific configurations for allowing energy recovery from brine.

- A patent pending configuration is proposed. This seems to be useful in applications of high salinity and high recovery rate. Main energy consumptions achieved by the New Configuration proposed are 3.15 kWh/$m^3$ with seawater salinity of 0.050 with recovery of 50%, and 2.74 kWh/$m^3$ for the case of salinity of 0.035 with recovery rate of 65%. This could be an opportunity to desalinate high concentration flows, as the brine outlet of distillation plants. Besides that, the configuration could be useful in order to achieve high recovery rate in plants with high auxiliary energy consumption.

## 8. REFERENCES


1. European Commission (EC): HORIZON 2020 WORK PROGRAMME 2014 – 2015: Leadership in enabling and industrial technologies ii. Nanotechnologies, Advanced Materials, Biotechnology and Advanced Manufacturing and Processing Revised. (https://ec.europa.eu/research/participants/data/ref/h2020/wp/2014_2015/main/h2020-wp1415-leit-nmp_en.pdf) Last visit: 22/09/2015.
2. ERI (Energy Recovery, Inc) (2006). Document Number 80074-01-00: ERI Technical Bulletin Flow in PX Arrays, 10/03/2006. http://www.energyrecovery.com/ (last visit 15/09/2011).
3. ERI (Energy Recovery, Inc) (2007). Document Number 80074-01-00: ERI Technical Bulletin Isobaric Device Mixing, 20/06/2007. http://www.energyrecovery.com/ (last visit 15/09/2011).
4. García Rodríguez, L. Chapter 2: Procesos de desalación mediante energía solar térmica. *In:* Estudio termoeconómico de los procesos de desalación de agua de mar mediante colectores solares cilindroparabólicos. Tesis Doctoral. Universidad de La Laguna, Junio, 1999. Sobresaliente cum laude.
5. Greenlee, F. L.; Desmond, F. L; Freeman, B. D.; Marrot, B., and Mouling, P. *Reverse osmosis desalination: Water sources, technology, and today's challenges.* Water Research, 43, 2009, pp. 2317-2348.
6. Kurihara M.; Maeda, K., and Yamamura, H.; *Method for multi-stage separation.* PT1161981 (E) – 2008-04-01. Applicants: TORAY INDUSTRIES
7. Leyendekkers, J. V. *Thermodynamics of Seawater.1st Part.* Marcel Dekker Inc. 1976.
8. Millero,F.J.; Feistel, R.; Wright, D. G., McDougall, T. J., *The composition of Standard Seawater and the definition of the Reference-Composition Salinity Scale.* Deep Sea Research

Part I: Oceanographic Research Papers, 55(1), 2008, pp. 50-72.

9. Peñate, B., and García-Rodríguez, L. *Reverse osmosis hybrid membrane inter-stage design: A comparative performance assessment.* Desalination, 281, 2011, pp. 354-363.
10. Safarov, J.; Berndt, S.; Millero, F. J.; Feistel, R.; Heintz, A., and Hassel, E. P., *(p,ρ,T) Properties of seawater at brackish salinities: Extensions to high temperatures and pressures.* Deep Sea Research Part I: Oceanographic Research Papers, 78, 2013, pp. 95-101.
11. Safarov, J.; Berndt, S.; Millero, F. J.; Feistel, R.; Heintz, A., and Hassel, E. P., *(p,ρ,T) properties of seawater: Extensions to high salinities.* Deep Sea Research Part I: Oceanographic Research Papers, 65, 2012, pp. 146-156.
12. Sadwani, J. J., and Veza, J. M., *Desalination and energy consumption in Canary Islands.* Desalination, 221, 2008, pp. 143-150.
13. Sharqawy, M. H.; Lienhard, J. H., and Zubair, S. M. *Thermophysycal properties of seawater: a review of existing correlation and data.* Desalination and Water Treatment, 16, 2010, pp. 354-380.
14. Slesarenko, V., and Shtim, A., *Determination of seawater enthalpy and entropy during the calculation of thermal desalination plants.* Desalination, 71, 1989, pp. 203-210.
15. Tu, K. I.; Nghiem, L. D., and Chivas, A. R. *Boron removal by reverse osmosis membranes in seawater desalination applications.* Separation and Purification Technology, 75, 2010, p. 87-101.
16. Viera Curbelo, O., *Pressure Vessel for sea water reverse osmosis and process that avoids scaling problems.* EP2576448(A1) – 2013-04-10. Applicant: GEN ELECTRIC (US).
17. Virgili, F.GWI DESALDATA. Desalination Market Update. Third quarter assessment. 26th Octiber 2016.
18. Voros, N. G; Maroulis, Z. B., and Marinos-Kouris, D., *Short-cut structural design of reverse osmosis desalination plants.* Journal of Membrane Science, 127, 1997, pp. 47-68.
19. Wilf, M., *The Guidebook to Membrane Desalination Technology. Reverse Osmosis, Nanofiltration and Hybrid Systems Process, Design, Applications and Economics.* Balaban Desalination Publications, 2007. ISBN 0-86689-065-3.
20. Wittmann, E.; Ventresque, C.; Lacaze-Eslous, F.; *Reverse osmosis water treatment plant including a first pass having multiple stages.* WO2013017628 (A1) – 2013-02-07. Applicants: VOELIA WATER SOLUTIONS & TECH.
21. Zhao, D.; Chen, S.; Guo, C. X.; Zhao, Q., and Lu, X., *Multi-functional forward osmosis draw solutes for seawater desalination.* Chinese Journal of Chemical Engineering, 24, 2016, pp. 23-30.
22. Zhou, Y.; *Reverse osmosis membrane pile system.* CN202237803 (U) – 2012-05-30. Applicants: CHANGZHOU CONNECT MACHINERY EQUIPMENT CO LTD.

23. European Commission (EC): HORIZON 2020 WORK PROGRAMME 2014 – 2015: Leadership in enabling and industrial technologies ii. Nanotechnologies, Advanced Materials, Biotechnology and Advanced Manufacturing and Processing Revised. (https://ec.europa.eu/research/participants/data/ref/h2020/wp/2014_2015/main/h2020-wp1415-leit-nmp_en.pdf) Last visit: 22/09/2015.

24. ERI (Energy Recovery, Inc) (2006). Document Number 80074-01-00: ERI Technical Bulletin Flow in PX Arrays, 10/03/2006. http://www.energyrecovery.com/ (last visit 15/09/2011).

25. ERI (Energy Recovery, Inc) (2007). Document Number 80074-01-00: ERI Technical Bulletin Isobaric Device Mixing, 20/06/2007. http://www.energyrecovery.com/ (last visit 15/09/2011).

26. García Rodríguez, L. Chapter 2: Procesos de desalación mediante energía solar térmica. *In:* Estudio termoeconómico de los procesos de desalación de agua de mar mediante colectores solares cilindroparabólicos. Tesis Doctoral. Universidad de La Laguna, Junio, 1999. Sobresaliente cum laude.

27. Gozálvez, J.M.; J. Lora, J.; Mendoza, J. A., and Sancho, M., Modelling of a low-pressure reverse osmosis system with concentrate recirculation to obtain high recovery levels, Desalination, 144 (1–3), 2002, pp. 341-345.

28. Greenlee, F. L.; Desmond, F. L; Freeman, B. D.; Marrot, B., and Mouling, P. *Reverse osmosis desalination: Water sources, technology, and today´s challenges.* Water Research, 43, 2009, pp. 2317-2348.

29. Kurihara M.; Maeda, K., and Yamamura, H.; *Method for multi-stage separation.* PT1161981 (E) – 2008-04-01. Applicants: TORAY INDUSTRIES

30. Leyendekkers, J. V. *Thermodynamics of Seawater.1st Part.* Marcel Dekker Inc. 1976.

31. Millero,F.J.; Feistel, R.; Wright, D. G., McDougall, T. J., *The composition of Standard Seawater and the definition of the Reference-Composition Salinity Scale.* Deep Sea Research Part I: Oceanographic Research Papers, 55(1), 2008, pp. 50-72.

32. Safarov, J.; Berndt, S.; Millero, F. J.; Feistel, R.; Heintz, A., and Hassel, E. P., *(p,ρ,T) Properties of seawater at brackish salinities: Extensions to high temperatures and pressures.* Deep Sea Research Part I: Oceanographic Research Papers, 78, 2013, pp. 95-101.

33. Safarov, J.; Berndt, S.; Millero, F. J.; Feistel, R.; Heintz, A., and Hassel, E. P., *(p,ρ,T) properties of seawater: Extensions to high salinities.* Deep Sea Research Part I: Oceanographic Research Papers, 65, 2012, pp. 146-156.

34. Sadwani, J. J., and Veza, J. M., *Desalination and energy consumption in Canary Islands.* Desalination, 221, 2008, pp. 143-150.

35. Sharqawy, M. H.; Lienhard, J. H., and Zubair, S. M. *Thermophysycal properties of seawater: a review of existing correlation and data.* Desalination and Water Treatment, 16, 2010, pp. 354-380.

36. Stover, R. *New high recovery reverse osmosis water treatment for industrial, agricultural and municipal applications.* The International Desalination Association (IDA) World Congress on Desalination and Water Reuse.

37. Slesarenko, V., and Shtim, A., *Determination of seawater enthalpy and entropy during the calculation of thermal desalination plants.* Desalination, 71, 1989, pp. 203-210.

38. Tu, K. I.; Nghiem, L. D., and Chivas, A. R. *Boron removal by reverse osmosis membranes in seawater desalination applications.* Separation and Purification Technology, 75, 2010, p. 87-101.

39. Viera Curbelo, O., *Pressure Vessel for sea water reverse osmosis and process that avoids scaling problems.* EP2576448(A1) – 2013-04-10. Applicant: GEN ELECTRIC (US).

40. Voros, N. G; Maroulis, Z. B., and Marinos-Kouris, D., *Short-cut structural design of reverse osmosis desalination plants.* Journal of Membrane Science, 127, 1997, pp. 47-68.

41. Wilf, M., *The Guidebook to Membrane Desalination Technology. Reverse Osmosis, Nanofiltration and Hybrid Systems Process, Design, Applications and Economics.* Balaban Desalination Publications, 2007. ISBN 0-86689-065-3.

42. Wittmann, E.; Ventresque, C.; Lacaze-Eslous, F.; *Reverse osmosis water treatment plant including a first pass having multiple stages.* WO2013017628 (A1) – 2013-02-07. Applicants: VOELIA WATER SOLUTIONS & TECH.

43. Zhao, D.; Chen, S.; Guo, C. X.; Zhao, Q., and Lu, X., *Multi-functional forward osmosis draw solutes for seawater desalination.* Chinese Journal of Chemical Engineering, 24, 2016, pp. 23-30.

44. Zhou, Y.; *Reverse osmosis membrane pile system.* CN202237803 (U) – 2012-05-30. Applicants: CHANGZHOU CONNECT MACHINERY EQUIPMENT CO LTD.

# Chapter 6. CONCLUSIONS

The main conclusions with regard to viable solutions for a potential market of solar thermal-powered desalination are reported in the first four conclusions, based on a comparative analysis of all desalination technologies. All of them, except Membrane Distillation (MD) are fully developed. Thus, only MD requires a thorough assessment of its technical limitations and potential improvements. A detailed thermodynamic analysis of seawater desalination based on MD technology has been carried out to understand the physical phenomena, the driving forces of the process and to identify and quantify the theoretical limits of the technology. Conclusions 4 and 5 summarise key points of the assessment performed. Reverse Osmosis (RO) is the most efficient desalination technology and the most suitable for both, conventional and renewable energy driven systems. The first question to answer is if a Specific Energy Consumption (SEC) of 1 kWh/$m^3$ is achievable. To this end a theoretical assessment of all potential options described in the literature are assessed. Besides that, a simulation model for preliminary design was developed. As a result of the thorough analysis of innovative configurations described so far, an innovative configuration is proposed that is patent pending. Points 6 to 12 report on conclusions related to SWRO desalination technology.

Main conclusions and recommendations are as follows:

1. Concerning solar desalination, conventional distillation processes for seawater desalination, namely multi-effect distillation and multi-stage flash distillation, exhibit too high solar energy consumption to compete with solar thermal-driven reverse osmosis. Moreover, discontinuous operation is not suitable for such technologies. Therefore, the use of conventional distillation processes is rejected in all cases, in particular when integrated into the thermal-cycle of a conventional solar power plant.

2. For market opportunities up to about 20.000 $m^3$/d, the only stand-alone solar thermal-powered desalination systems that may be considered are based on reverse osmosis driven by either:
   - Parabolic troughs or linear Fresnel concentrators by means of organic Rankine Cycles.
   - Dish concentrators coupled to micro gas turbines in case of limited water demand. A single unit could produce about 10 $m^3$/h of fresh water from seawater. Besides, several units could be coupled to drive the same desalination plant.

The main advantage of first option in comparison to stand-alone PhotoVoltaic (PV)-RO desalination is the possible use of thermal storage instead of batteries. Fire-boilers are not recommended as energy backup for solar organic Rankine Cycles due to the relatively low efficiency. Besides that, solar micro gas turbines have the advantage of the availability of heat rejection, which allows the Zero Liquid Discharge (ZLD) concept. Finally, they can be powered at night with conventional fossil fuels if necessary. Anyhow, for stand-alone desalination systems with energy backup, PV-RO desalination would always be more competitive than solar thermal-powered desalination systems.

3. Solar desalination for higher water demands require a large scale solar power plant and a reverse osmosis desalination plant. The concept of finding a global balance between consumption of electricity by the water production facility and the solar electricity generation is recommended, instead of the traditional concept of integrating both processes within the same plant. Besides that, the solar power plant technology, location and production should be adapted to the convenience of CAPital EXpenses (CAPEX) and OPEration EXpenses (OPEX). In addition, distributed fresh water production could also be considered if orography and distance between water demand locations make it necessary.

4. For medium and large seawater desalination systems, the low energy efficiency and limited production capacity of MD technology make it not competitive at all:
    - Temperature gradients across the membrane as low as 5ºC has been achieved, therefore increasing the efficiency up to PR of the order of 8-10 is possible – i.e. energy consumption greater than 230 kJ/kg -.
    - Limited production capacity of existing commercial products, as tested in commercial available modules with distillated fluxes in the range of 1 $L/(h \cdot m^2)$ to 6.5 $L/(h \cdot m^2)$, far away from other membrane seawater desalination technologies such as RO (with average permeate fluxes in the range of 14 $L/(h \cdot m^2)$.
    - High auxiliary energy consumption, as has been reported in literature and accordingly to high mass flow rate of seawater required to obtain unitary product flow.

5. On the other hand, the technology may be applied for small seawater desalination systems were the two handicaps of MD technology may be irrelevant compared to other advantages it has, such as simple pretreatment and process control, low maintenance requirements and its conceptual ability to be coupled with solar thermal energy. Thus, a specific application of MD technology would be small autonomous

solar thermal seawater desalination systems but competing with PV or wind powered RO seawater desalination systems.

6. Concerning modelling of SWRO desalination plants:
   - A simulation model with ERI-PX energy recovery device has been develop to carry out precise evaluation of the SEC considering only the productive core of a SWRO plant. The membrane skid is modelled with global parameters, namely, global pressure losses and net driving pressure at the tail of the membrane serial.
   - A thorough model of membrane series based on permeability coefficients of salt and water and empirical models of pressure losses and polarization effects was also developed Results on permeate flow, salinity and boron concentration along with recovery rate and pressure losses were validated by means of ROSA 9.1 software.

7. For RO Technology:

   - For a conventional SWRO configuration and working conditions of standard seawater at 25ºC and 48% of recovery rate, the SEC represents up to 2.3 kWh/m$^3$, considering 80% efficiency of the high pressure pump and 95% efficiency of the energy recovery. Around a 47% of the SEC in this case is attributable to the thermodynamic limit of the solvent extraction process and the other 53% to the configuration and real systems inefficiencies, being 0.38 and 0.86 kWh/m$^3$, respectively. Besides that, main inefficiencies are due to the high pressure pump, 0.53 kWh/m$^3$ (23%). Conventional configuration with ideal components represents 1.46 kWh/m$^3$, which corresponds to the technical limit with the current status.
   - The potential effect on the SEC of future improvements on membrane technology has been analysed and quantify to be lower than 0.19 kWh/m$^3$ (8%).
   - Regarding SWRO desalination with two stages, the benefits on the SEC have been analysed in this work for a wide range of temperatures, seawater salinities, recovery rates and pumping efficiencies. The influence of the second stage increases with recovery rate and feed salinity. For aforementioned conditions, the SEC goes down up to 1.97 kWh/m$^3$, being 0.34 kWh/m$^3$ (15%) the energy saving. Moreover, if operating with 60% of recovery rate is reliable, around 0.6-0.8 kWh/m$^3$ could be the energy saving attributable to a second stage (representing a reduction of 27 %).

   - Theoretically, PRO concept could be coupled to a conventional SWRO plant as an additional energy recovery device if an aqueous solution to be rejected is

available. Up to 0.45-0.55 kWh/m$^3$ (20%) of energy saving could be theoretically achievable.

8. Considering energy efficient high pressure pumps, plant configuration has the most relevant effect on SEC. Therefore innovative configurations with the best prospects to allow SEC decreasing were identified and analysed. These innovative configurations were proposed by Veolia, GE and Desalitech.

9. The balance between CAPEX and OPEX seems to be better in conventional configuration than in that proposed by Veolia. However, Veolia´s configuration might be useful in improving fouling and scaling performance. In relation to fouling, in future development of RO membranes with high permeability this configuration may be essential to prevent excessive flux while maintain adequate average flux in order to achieve cost-effective configurations. Moreover, Veolia´s concept is useful if the compliance of product quality requires relatively high pressure due to either, high feed salinity or high temperature.

10. The innovative configuration proposed by GE allows CAPEX decreasing if pressure vessels with 9 membrane elements or even more are implemented. Moreover, next generation of RO membranes with higher permeability than that of current technology could be adopted by using GE´s configuration since flux on the front positions can be limited by selecting suitable values of bypass flow.

11. The best innovative configuration to reduce the SEC is CCD-Desalitech, which allows up to 10% of SEC reduction in case of batch operation equivalent to with 4-stages. However, the adoption of this configuration results in very complex design of the energy recovery device, operation and control. Therefore, this configuration is not recommended for SWRO desalination plants.

12. A patent pending innovative configuration is proposed with interesting prospects of decreasing main and auxiliary energy needs. Main energy consumption for salinity 0.035 kg/kg and 25ºC could be:
    - 2.14 kWh/m$^3$ with recovery rate of 45%.
    - 2.74 kWh/m$^3$ for the case of salinity of 0.035 with recovery rate of 65%.

    They allow for energy saving of 7% and 22%, respectively. Besides, SEC of 3.15 kWh/m$^3$ would be achievable with seawater salinity of 0.050 with recovery of 50%. CAPEX goes up but the increase in complexity is limited. In addition, the proposed configuration is able to operate with seawater of high concentration as brine of distillation plants. There are no competing

technologies. This configuration could be adopted in SWRO plants with two-stages or PRO systems, thus resulting in additional energy saving.